ADVANCED ENERGY MATERIALS
www.advenergymat.de

Graphene-Based Nanocomposites for Energy Storage

Liwen Ji, Praveen Meduri, Victor Agubra, Xingcheng Xiao, and Mataz Alcoutlabi**

Since the first report of using micromechanical cleavage method to produce graphene sheets in 2004, graphene/graphene-based nanocomposites have attracted wide attention both for fundamental aspects as well as applications in advanced energy storage and conversion systems. In comparison to other materials, graphene-based nanostructured materials have unique 2D structure, high electronic mobility, exceptional electronic and thermal conductivities, excellent optical transmittance, good mechanical strength, and ultrahigh surface area. Therefore, they are considered as attractive materials for hydrogen (H_2) storage and high-performance electrochemical energy storage devices, such as supercapacitors, rechargeable lithium (Li)-ion batteries, Li–sulfur batteries, Li–air batteries, sodium (Na)-ion batteries, Na–air batteries, zinc (Zn)–air batteries, and vanadium redox flow batteries (VRFB), etc., as they can improve the efficiency, capacity, gravimetric energy/power densities, and cycle life of these energy storage devices. In this article, recent progress reported on the synthesis and fabrication of graphene nanocomposite materials for applications in these aforementioned various energy storage systems is reviewed. Importantly, the prospects and future challenges in both scalable manufacturing and more energy storage-related applications are discussed.

1. Introduction

The ever rising world population has led to increasing energy demand with the worldwide power consumption expected to double in the next several decades. Hence, it is imperative for scientists and researchers to develop sustainable, clean, and renewable energy technologies that are economical and environmentally benign to address the growing energy demands and challenges in our society.[1–6] The most common renewable energy sources such as the sun and wind are highly intermittent and thus, require to be coupled with viable high-performance energy storage devices.[2,4,5,7–16] Supercapacitors, high-performance rechargeable lithium (Li) batteries (including Li-ion, Li–S, and Li–air chemistries), sodium (Na) batteries (Na-ion, Na–S, and Na–air batteries), zinc (Zn)–air batteries, and vanadium redox flow batteries (VRFBs), are the most promising energy storage systems on account of their high specific energy, energy and/or power density, long cycle life, excellent rate performance, and design flexibilities.[2,4,5,7–18] Hydrogen (H_2) storage is another promising energy system that is considered as a critical area for its potential applications in sustainable energy without producing harmful byproducts.[19,20] Increased attention to the design and synthesis of nanostructured electrode materials in recent years has proven to be critical for the tremendous advancements in energy storage technologies.[21–24] Particularly, graphene and graphene-based nanocomposites have received great attention and have been extensively investigated as electrode materials for these various energy storage systems.[22–40]

Dr. L. Ji, Dr. X. Xiao
General Motors Global Research & Development Center
Chemical and Materials Systems Laboratory
Warren, MI 48092, USA
E-mail: liwenjiresearch@gmail.com
Prof. P. Meduri
Department of Chemical Engineering
Indian Institute of Technology Hyderabad
ODF Estates
Yeddumailaram, Medak, Telangana 502205, India
Dr. V. Agubra, Prof. M. Alcoutlabi
Department of Mechanical Engineering
The University of Texas Rio Grande Valley
Edinburg, TX 78539, USA
E-mail: mataz.alcoutlabi@utrgv.edu

DOI: 10.1002/aenm.201502159

1.1. What is Graphene?

Graphene is a new class of 2D "aromatic" monolayer of carbon atoms densely packed in a honeycomb crystal lattice. Graphene has attracted tremendous attention since its discovery in 2004,[41] as a promising material for next-generation energy storage devices owing to its superior properties.[22,25,42,43] Graphene offers a unique twofold advantage with remarkably high electron mobility at room temperature and fast heterogeneous electron transfer at the edges, with reported values in excess of 15 000 $cm^2\ V^{-1}\ s^{-1}$.[44,45] In addition, graphene has an ultrahigh surface area of ≈2630 $m^2\ g^{-1}$, which is significantly higher than its –1D (i.e., carbon nanotube, 1315 $m^2 g^{-1}$) and 3D (graphite, 10 $m^2\ g^{-1}$) counterparts.[42] Furthermore, graphene exhibits a high tensile strength with excellent flexibility, which is quite beneficial for building flexible devices.[46] Graphene also has outstanding optical transparency and transmittance, which leads to unexpectedly high opacity for an atomic monolayer,[47] and an intriguing thermal conductivity of 4.84×10^3 to 5.30×10^3 $W\ m^{-1}\ K^{-1}$ at room temperature.[48]

Several physical and chemical methods can be used to synthesize graphene including micromechanical cleavage (original scotch-tape method), chemical vapor deposition, liquid phase

exfoliation, thermal decomposition of silicon carbide (SiC), reduction of graphene oxide (GO), and un-zipping carbon nanotubes (CNTs).[49] The structure of graphene can be modified using various techniques to tune their properties and performance.[50] These methods include: (i) Direct assembly of graphene sheets into porous electrode materials; (ii) deposition and coating of metal, metal oxides, or other electrochemically active materials on graphene sheets; (iii) surface modification of graphene sheets with surfactant molecules; and (iv) self-assembly of ordered nanocomposites (**Figure 1**).[24] However, these modifications often present new challenges. For instance, the prevention of re-stacking is a key challenge in the direct assembly of graphene using a homogeneous dispersion that requires a proper balance between solvation and hydration forces of the solvent. The use of surfactants provides precise control of graphene dispersion, leading to the formation of new hybrid architectures through self-assembly. In the case of metal oxide deposition, it is important to control the surface defects and functional groups because they can serve as nucleation sites for crystal growth and dictate the deposition thickness.

Although these physical techniques used to synthesize graphene-based materials show promise for fundamental research on material properties and application testing, their applications in practical electronic and energy storage devices require the production of large quantities that demand further exploratory work. In this context, chemical methods including the reduction of graphene oxide (GO), electrochemical methods to treat graphite, non-covalent/covalent functionalization and solvothermal reactions of sodium and ethanol have been developed.[51–54] In addition, physical processes such as exfoliation/re-intercalation/expansion of graphite have been developed to produce graphene with fairly good conductivity and reasonable yield for mass production.[55] The as-synthesized graphenes can potentially be combined with other organic/inorganic materials to develop novel graphene nanocomposites, which include graphene/polymers,[56–61] graphene/metals,[62,63] graphene/metal oxides,[64–68] and graphene/CNTs,[69–71] for energy storage devices (Figure 1). Several techniques in the following discussion show promise for the large-scale production of graphene-based nanocomposites, which spark interest for fundamental investigation of graphene-based nanostructured materials in energy-related applications.[22–40] Our main thrust in this article is to review the field of energy storage systems and specifically discuss recent development on the use of graphene-based nanocomposites in these energy storage systems as well as various ways to improve the performance of these devices.

This review is organized as follows, we first discuss recent results reported in the literature on the application of graphene-based nanocomposites in H_2 storage, supercapacitors, Li-ion batteries, Li–S battery, Li–air battery, Na–ion batteries, Na–air batteries, Zn–air batteries, and VRFBs. We then discuss recent development efforts for the commercialization of graphene-based nanopcomposites in these energy storage systems. Finally, we discuss the challenges and issues facing this field followed by summary, conclusions as well as suggestions and perspectives for future research.

Liwen Ji is currently a Research Scientist II in the Energy & Power Group at Lynntech, Inc. Prior to that, he was a Contract Research Scientist at General Motors' Global Research & Development Center, and a Postdoctoral Fellow in the US Department of Energy (DOE)'s Pacific Northwest National Laboratory and the Lawrence Berkeley National Laboratory. He received his Ph.D. in Fiber and Polymer Science from North Carolina State University in 2009. His research focuses on fabrication of novel nanostructures for advanced energy storage and conversion systems, such as rechargeable batteries, supercapacitors, fuel cells, solar cells and solar water splitting cells.

Praveen Meduri is presently an Assistant Professor of Chemical Engineering at Indian Institute of Technology, Hyderabad focusing on materials for advanced energy storage systems. He was an independent researcher with the prestigiuos PSIEE fellowship at Pennsylvania State Unversity. He also worked as a post-doctoral researcher at the US Department of Energy (DOE)'s Pacific Northwest National Laboratory. He received his Ph.D. from the Department of Chemical Engineering at The University of Louisville in 2010 working on nanomaterials for Li-ion batteries. He received his M.S. in Chemical Engineering from The University of Akron in 2005.

Mataz Alcoutlabi currently is a RGV STARs Faculty-Assistant Professor in the Mechanical Engineering Department at The University of Texas Rio Grande Valley. Mataz received his B. S. degree in Mechanical Engineering from the University of Aleppo, Syria and M.S. degree in Mechanical Engineering from INSA, Toulouse, France. He obtained his Ph.D. degree in Materials Science and Engineering from INSA, Lyon, France. He then worked as a post-doctoral researcher at Laval University, Quebec city, Canada and at Texas Tech University in Lubbock, Texas. Mataz's research focuses on the design of nanomaterials with desirable properties for biomedical applications and energy storage systems.

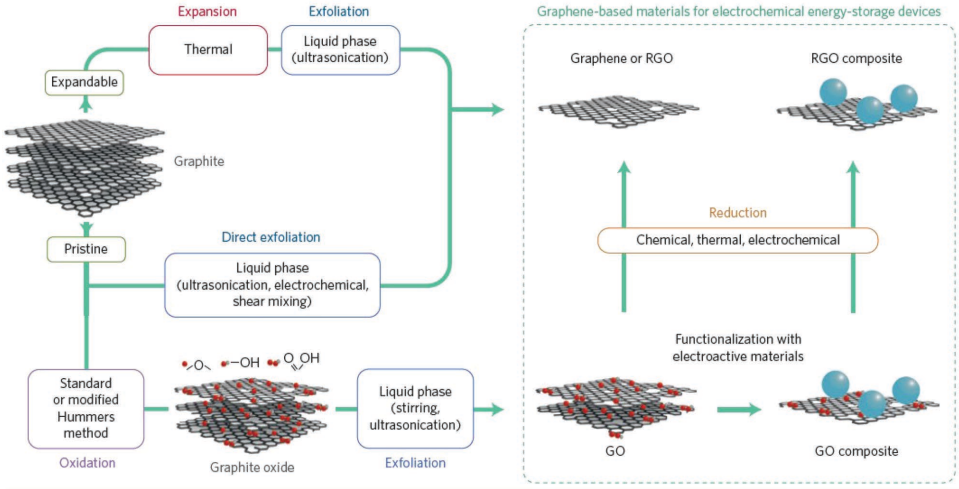

Figure 1. A typical synthetic pathways for producing GO, rGO, GO-, and rGO-based nanocomposites for use as electronic active materials for energy storage devices. Reproduced with permission.[24] Copyright 2015, Nature Publishing Group.

2. H_2 Storage

The abundance and environmental benignity of H_2 makes it an effective and efficient energy storage solution often termed as ''H_2 economy.''[19,20] However, it should be remembered that H_2 is not an energy source, but rather a secondary energy carrier.[19,20] The gravimetric energy density of H_2 is three times higher than that of gasoline, making it vital to understand, design, and execute for storage.[19,20] In light of this, selecting suitable materials for efficient H_2 storage assumes a primary importance. In addition to material dependence, the adsorption of H_2 also changes with both micropore volume and surface area of the material.[72–74]

The storage of H_2 has been realized in several solid systems including transition metal and light metal hydrides, which display a volumetric density between 0.08 and 0.15 kg m^{-3}.[75] Recently, several H_2 storage studies have focused on MgH_2, because of its relatively low cost and high weight storage capacity (7.6 wt%).[76] The MgH_2 power with the incorporation of 10 wt% of expanded natural graphite has been shown to enhance the thermal exchanges and improve the H_2 storage time.[77] Mg nanocrystals are another class of material with excellent H_2 storage ability, high volumetric storage capacity (i.e., 55 g L^{-1}) and rapid uptake (<30 min at 200 °C) greater than that of compressed H_2 gas.[78] In addition, $NaAlH_4$ has also been extensively explored as one promising solid-state H_2 storage material,[19] in particular, when doping with atoms such as Ti, Sc, Ce, and Pr (these cations can enhance the kinetic characteristics).[79] The main drawbacks of these systems are their relatively high weight and high activation barriers for both adsorption and desorption processes. In addition, it is a major challenge to simultaneously meet gravimetric, volumetric, thermodynamic and kinetic requirements for these transition metal hydrides, due to their strong binding energies for the metal hydride bonds, long diffusion path lengths, and oxidative instability of zero-valent metals.[19,80]

Amineborane-based materials (NH_3BH_3) have received a significant interest for H_2 storage given its stability and commercial availability.[81] There are still technical challenges to be addressed, which include enhancing the rate of H_2 release and the discovery of cheaper chemical processing pathways required to put the H_2 back on the top of dehydrogenated materials.[81]

Metal borohydrides are another class of materials that can be used for H_2 storage.[82] However, the major challenges facing these categories of materials are the high temperature of dehydrogenation, lack of reversibility of the dehydrogenation reaction, slow kinetics of dehydrogenation and hydrogenation, evolution of diborane during dehydrogenation, and high cost of borohydrides.[82]

A survey and discussion of the literature reported on H_2 storage systems show that compared to metal hydrides and other reported materials, graphene-based materials have some unique advantages which make them good candidates for H_2 storage.[75,83–85] The chemical versatility of carbon allows its switching from sp^2 to sp^3 hybridization and efficiently binding with H_2 atoms. In addition, the stability and robustness of graphene make it easy to transport for long distances. At the same time, it is mechanically flexible, thus enabling new charging/discharging strategies under room conditions that exploit the dependence of H_2-carbon binding on a local curvature. The flexibility of graphene and the unique electronic properties put it in a position where new design approaches for H_2 storage could be developed.[75,86] Mathematical models the adsorption of H_2 on graphene and graphene oxides (GOs) have been used to demonstrate enhanced performance that are approaching recommended DOE targets for H_2 storage. These mathematical models have been used to predict higher H_2 storage capacities for graphene-based nanocomposites (decorated with transition metal clusters or alkali/alkaline earth metals).

Graphene can be an ideal material for H_2 storage since it is lightweight, low cost, robust, chemically stable, highly porous and has high surface area to volume ratio.[75,87–92] Herein, we consider multilayers graphene, porous graphene, graphene-based 3D assemblies, and graphene nanocomposites because it is difficult to evaluate the H_2 storage potential for a single graphene layer.

H_2 can be stored in graphene-based materials in two ways: (i) physisorption through van der Waals (VdW) forces; and

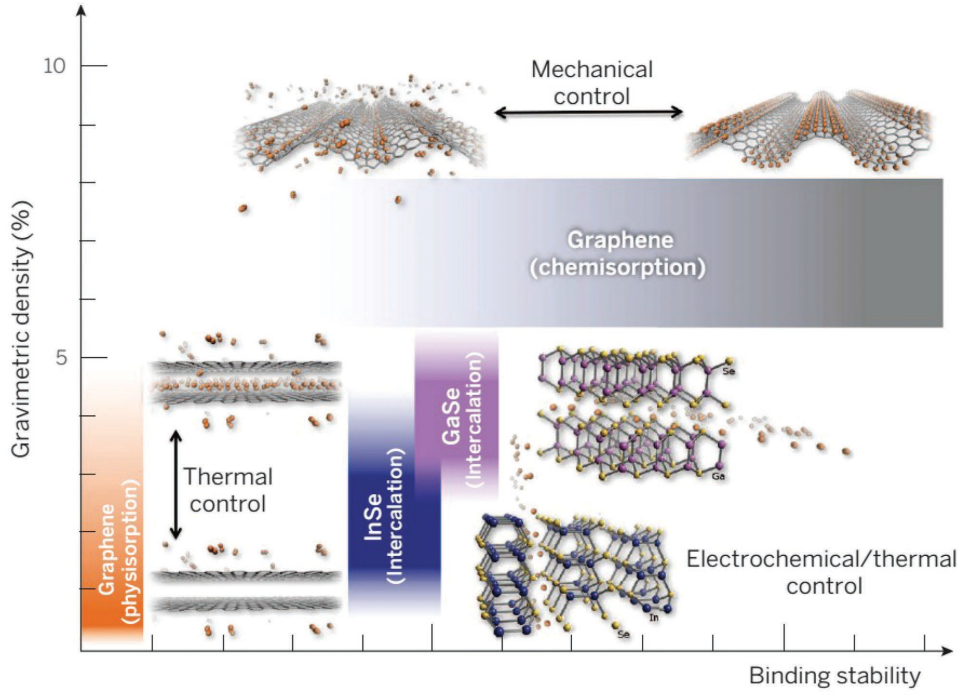

Figure 2. H_2 storage in graphene and graphene-based nanocomposites with bands showing gravimetric density and binding stability of different graphene and graphene-based nanocomposites and for physisorption or chemisorption mechanisms, with uptake/release controlled thermally and mechanically, respectively. Reproduced with permission.[83] Copyright 2015, American Association for the Advancement of Science.

(ii) chemisorption via forming a chemical bond with the C or other functional groups on graphene-based nanocomposite surfaces.[75,85,86] H_2 inherently undergoes a reversible weak physisorption on pure graphene sheets, which has been observed by using extensive experimental and theoretical work (**Figure 2**).[83] This results in a low capacity retention that is well below the required capacity for practical applications as outlined by the department of energy (DOE).[93]

Recent results reported in the literature show that H_2 uptake can be enhanced by using novel graphene nanostructures with engineered nanospaces,[94–97] surface modification of functionalized graphene,[93,98,99] and heteroatom-doping of graphene for H_2 polarization.[100,101] Using KOH activation procedure, Talyzin et al. fabricated highly porous graphene scaffold materials with surface area up to 3400 m^2 g^{-1} and a pore volume up to 2.2 cm^3 g^{-1} for H_2 storage. The maximal excess H_2 uptake of 7.5 wt% could be obtained at 77 K after additional activation by H_2 annealing with a H_2 storage value as high as 4 wt% observed at 193 K (120 bar H_2).[96] Ab initio and density functional theory (DFT) calculations showed that an artificial 3D pillared graphene with an interlayer spacing of 1.2 nm stabilized by perpendicularly inserted CNTs can lead to tunable pore sizes and high surface areas. Further doping with Li cations can store ≈41 g H_2 L^{-1} under ambient conditions which is close to DOE's target.[102] Similarly, Li-doped pillared GO with a gravimetric H_2 capacity of >10 wt% and a volumetric H_2 capacity of 55 g L^{-1} at 77 K and 100 bar, which also meets DOE's targets.[103] However, high Li coverage on graphene might possibly lead to strong electrostatic interactions between Li cations, which can weaken the H_2 adsorption ability. Recently, theoretical modeling showed that the adsorption of H_2 on Li-decorated porous graphene was as high as 12 wt%.[95] In comparison to Li-doped graphene, Li doping in porous graphene is expected to lower electrostatic interactions, leading to enhanced adsorption of H_2. The porous architecture itself can also lead to additional H_2 storage.[95,97,104,105]

Figure 3 illustrates a brief overview on the various possibilities of H_2 interaction with Li-decorated graphene.[95] In addition to Li, theoretical simulations and/or experimental evidences showed that Al,[106,107] B,[108] Ni,[109] Ni–B alloy,[110] Fe,[111] Ca,[101,112–114] Pd,[115] Ti,[116,117] Co,[118] Na,[119] and Mg,[120] doped graphene can also exhibit excellent H_2 storage capabilities. The favorable H_2 binding to these transition metals is attributed to Kubas-type interactions between the metal and H_2, which are stronger than static coulombic interactions among metal atoms.[113] Transition metals also tend to form clusters due to the high cohesive energy and thus, lowering the H_2 storage capability. The coupling of graphene with pure transition metals can hinder these cohesive forces, prevent their agglomeration and lead to enhanced H_2 storage.[121] A key challenge in H_2 storage is the chemisorb/desorb H_2 at room temperature without having to use high temperatures and pressures. Particularly, the desorption of atomic H_2 is associated with high energy barriers, which requires a thorough understanding of these systems. The use of catalytic transition metals can lead to the reduction of these energy barriers for better desorption.

Using first-principles calculations, Wang et al. investigated Ti anchoring on GO that consists of sp^2 C with one —O— and two —OH groups as basic building blocks.[116] The calculated Ti-O binding energies were as high as 450 kJ mol^{-1}, strong enough to prevent the clustering but still low enough to adsorb

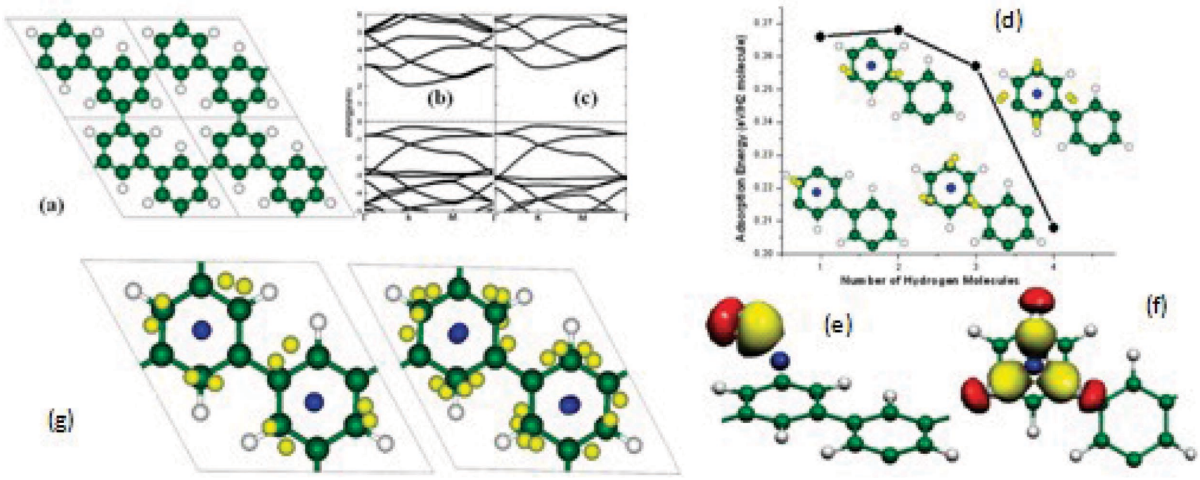

Figure 3. Illustration of a theoretical study of Li-decorated porous graphene and their potential applications for H_2 storage: a) Optimized geometry. b,c) Band structure based on the local density approximation. d) Adsorption energies and optimized geometries for the first, second, third, and fourth H_2 molecules around the Li atom on porous graphene. e,f) Charge density variations for Li-decorated porous graphene with one and three H_2 molecules. g) Top view of optimized geometries for 6 and 12 H_2 molecules adsorbed on two and four Li-decorated porous graphene. Green, white, blue, and yellow balls represent C, H, Li, and physisorbed H_2 molecules, respectively. Reproduced with permission.[95] Copyright 2010, American Chemical Society.

H_2. These GO–Ti nanocomposites were estimated to have theoretical gravimetric and volumetric capacities of about 4.9 wt% and 64 g L^{-1}, respectively. DFT calculations have shown that Al-doped graphene has an uptake of 13.79 wt% H_2 at temperature of 300 K, surpassing DOE's target.[107] In the same vein, first-principles study showed that Ca-decorated zigzag graphene nanoribbons can store ≈5 wt% H_2.[101]

The B-doping was found to form an electron-deficient structure that can help enhance the H_2 interaction energy.[122,123] The energy surface seems to extend over several graphene carbon sites, making the surface more heterogeneous.[122,123] B-doping in graphene could also help enhance the Li and Ca bonding strengths on the graphene. Lu and co-workers reported that Li- and Ca-decorated B-doped porous graphene showed improved H_2 adsorptions of 6.4 and 6.8 wt%, respectively.[124] The Ca adsorption on zigzag edge, porous or covalent-bonded graphenes (CBGs) is also reported.[101,125] CBGs further doped with B and decorated with Ca clusters show up to 6 wt% of H_2 adsorption.[114] The beryllium adsorbed on B-doped graphene could have a high H_2 uptake up to 15 wt%.[126] Recently, the H_2 adsorption capacity of 2.4 wt% was also reported in Si-doped graphene.[127]

The Sc decorated on either armchair of zigzag edges of graphene nanoribbons show >9 wt% of H_2 absorption.[128] Ni atomic dispersion on graphene yields about 3 wt% of H_2 but it is expected to reduce experimentally due to clusterization and nanoparticle formation.[109] In addition to graphene/pure metal nanocomposites, graphene/metal sulfide, such as graphene/Co_9S_8,[129] has been prepared for H_2 storage. Compared with the traditional metal decorated graphene, the graphene/Co_9S_8 nanocomposites show a much higher H_2 storage capacity and better stability.

As mentioned above, graphene has high specific surface area, high surface-to-volume ratio and is lightweight with good mechanical properties. In addition, fascinating architectures of graphene, such as porous, hollow, multilayer graphene nanostructures, heteroatom-doped graphene structures, and different types of graphene-based composites with larger cavities can be obtained, which are indispensable to the physisorption or chemisorption of H_2. As a result, graphene-based systems are among the best nanomaterials for long-term H_2 storage.[92]

Although these studies have shown good H_2 storage capabilities, the main challenge here is the synthesis of well-ordered structures on a large scale. Simulations do indicate the advantages of graphene but it has always been a challenge to synthesize the materials with the best properties and low defects.[130,131] In addition, graphene-based nanocomposites for H_2 storage still suffer from metal crystal oxidization and relatively low kinetics under ambient conditions.[75,120] The synthesis of graphene flakes with a variety of functionalization techniques and the fabrication of graphene nanocomposites and the development of new techniques for possible bulk production of H_2 storage devices have been explored, yet there remain major challenges for H_2 storage.[75,120] Another key issue is how to store H_2 in a small space using minimum energy. Currently, H_2 storage in numerous graphene-based materials with a high energy density form has energetic barriers whose theoretical estimations range in the order of several eV. Seeking suitable catalysts to desorb/separate the molecular H_2 from graphene is still a major challenge that needs further investigations before these materials can be used in practical applications.[132]

3. Supercapacitors

Supercapacitors also known as ultracapacitors or electrochemical capacitors offer a promising approach to meet the ever increasing power demand.[133–137] Supercapacitors can be classified into three main groups: electrical double-layer capacitors (EDLC), pseudo-capacitors, and hybrid/asymmetric capacitors. In EDLC,

the capacitance arises due to pure electrostatic charge accumulation at the electrode/electrolyte interface (non-Faradaic process where charges are distributed by physical absorption) resulting in a double layer (**Figure 4**).[83] In the case of pseudo-capacitors, fast and reversible faradaic processes such as redox reactions take place due to the electro-active species that result in storing the charges as shown in Figure 4.[83] In hybrid capacitors, a combination of both non-Faradaic and Faradaic processes is present.[133–136,138,139]

Carbon-based materials including carbon particles, carbon nanotubes, carbon nanofibers, graphite, and graphene have been used as electrodes for EDLCs owing to their exceptional properties, such as high surface area, porous structure, chemical inertness, and good electrical conductivity that promote a nanoscopic charge separation at the electrode/electrolyte interface.[43,135,140–144] In addition to carbon, both conducting polymers[145–150] and transition metal oxides such as manganese oxides (MnO, Mn_2O_3, Mn_3O_4, MnO_2),[151–153] RuO_2,[154,155] Fe_3O_4,[156–158] SnO_2,[159–161] NiO,[162–164] Fe_2O_3,[165–167] TiO_2,[168–170] MoO_2,[171] MoO_3,[172,173] CuO,[174,175] Co_3O_4,[176–179] $NiCo_2O_4$,[180–182] ZnO,[183–185] Bi_2O_3,[186] Nb_2O_5,[187–189] etc.,[190] have been used as electrode materials in pseudocapacitors due to their electrochemically active nature and the ability to carry out the Faradaic redox reaction.[191,192] The electron transfer between the electrodes and the electrolytes comes from the reversible electrochemical doping–redoping with conductive polymers and fast Faradaic redox reactions in transition metal oxides, respectively. In addition, various graphene-based nanostructures have been synthesized as electrodes for supercapacitors due to their special properties.[190,191,193–204] In the ensuing sections, we discuss recent results reported on the performance of graphene and graphene-based composites in supercapacitors.

3.1. Graphene

Graphene and graphene-based nanocomposites have been proposed as attractive and alternative nanostructured electrode materials for supercapacitors owing to their excellent chemical stability, and superior electrical and thermal conductivities.[190,191,193–205] The large open pores in graphene and graphene composites facilitate the fast transport of hydrate ions that can lead to high double-layer capacitance in different electrolytes.[25,42,142,190,193,200,206–211] Ruoff et al. have shown that the specific capacitance of graphene-based supercapacitors can reach 135 F g^{-1} in aqueous KOH electrolyte, 117 F g^{-1} in aqueous H_2SO_4 electrolyte, 99 F g^{-1} in organic electrolytes and 75 F g^{-1} in ionic liquid (IL)-based electrolytes.[212,213] Graphene synthesized using gas-based hydrazine reduction of GOs has shown a maximum specific capacitance of 205 F g^{-1} and a power density of 10 kW kg^{-1} at 28.5 Wh kg^{-1} energy density in an aqueous medium.[214] The highly active edge planes in graphene can cause restacking in graphene leading to loss of surface access (low surface areas and tortuous paths) and lower capacitance. Several approaches have been explored to keep the graphene sheets dispersed. One such example is to keep the electrode hydrated, this can greatly increase the specific capacity, and more impressively, the cycle stability at a high current density of the supercapacitor (**Figure 5**).[215]

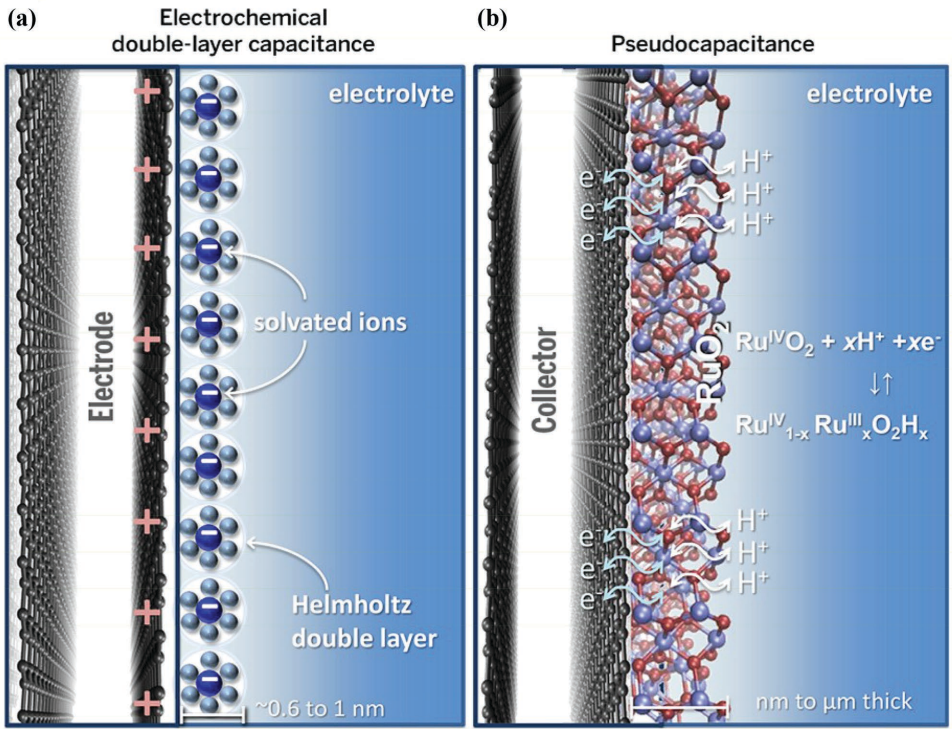

Figure 4. Schematic diagram showing charge storage in supercapacitors. a) Ion adsorption at the electrode surface (EDLC). b) Charge transfer near the surface of the electrode (pseudo-capacitance). Reproduced with permission.[83] Copyright 2015, American Association for the Advancement of Science.

The transformation of graphene from sheet architecture to a crumbled ball has also shown high specific capacitance and better rate performance. This is attributed to the special crumbled structure that prevents graphene aggregation and preferentially aligns them in a beneficial way for electron/ion transport.[216–218] The performance of graphene-based supercapacitors can be further enhanced by:[208,219–222] (i) Design and synthesis of porous structured graphene; (ii) surface modification of the graphene with heterogeneous atoms; and (iii) combining graphene with electrically conductive polymers, transition metal oxides, transition metal nitrides (or sulfide), secondary nanostructured carbon phases or others to develop hybrid architectures with controlled pore distributions, densities, and optimized morphologies and microstructures.

The fabrication of graphene with porous structure and large surface area is an effective strategy to further increase their electrochemical performance in supercapacitors, because the torosity in porous graphene can lead to well-defined pathways for efficient ionic and electronic transport, higher electrochemically accessible surface area to electrolyte, shorter ion diffusion lengths, and efficient electrode access for electrolytes.[223–234] All of these can be beneficial for the capacitance improvements. In addition, these pore structures could show a high adaptability when used as supercapacitor (EDLC) electrodes.[223–234] Zhang et al. designed a cell using freestanding, flexible, ultrahigh surface area (3100 m^2 g^{-1}), conductive (≈500 S m^{-1}), porous graphene films as electrodes with a specific capacitance of 120 F g^{-1} at a current density of 10 A g^{-1} in a $TEABF_4$/AN electrolyte.[225] The idea of using freestanding porous graphene films is great. However, the high ordering with huge spacing between the layers of graphene leads to low material tap density (density per unit volume). The low material loading per unit volume is a major concern, which can lead to low volumetric density. Li and co-workers used the process of capillary compression to form dense and porous graphene with high ion accessibility and low transport resistance.[235] Capacitors based on these chemically converted graphene electrodes yield a high volumetric capacity of 59.9 Wh L^{-1} along with a power density of ≈75 kW L^{-1}, additionally, a 95% capacity retention was seen after holding the device at 3.5 V for 300 h in a $EMIMBF_4$-based IL electrolytes.[235] It is therefore imperative to think of graphene synthesis with a dense 3D nanostructure, which can overcome the problems associated with the low tap density. Recently, Huang and co-workers fabricated a 3D hierarchical porous graphene carbon-based supercapacitors that exhibited a high reversible specific capacitance of about 300 F g^{-1} and ultrahigh specific

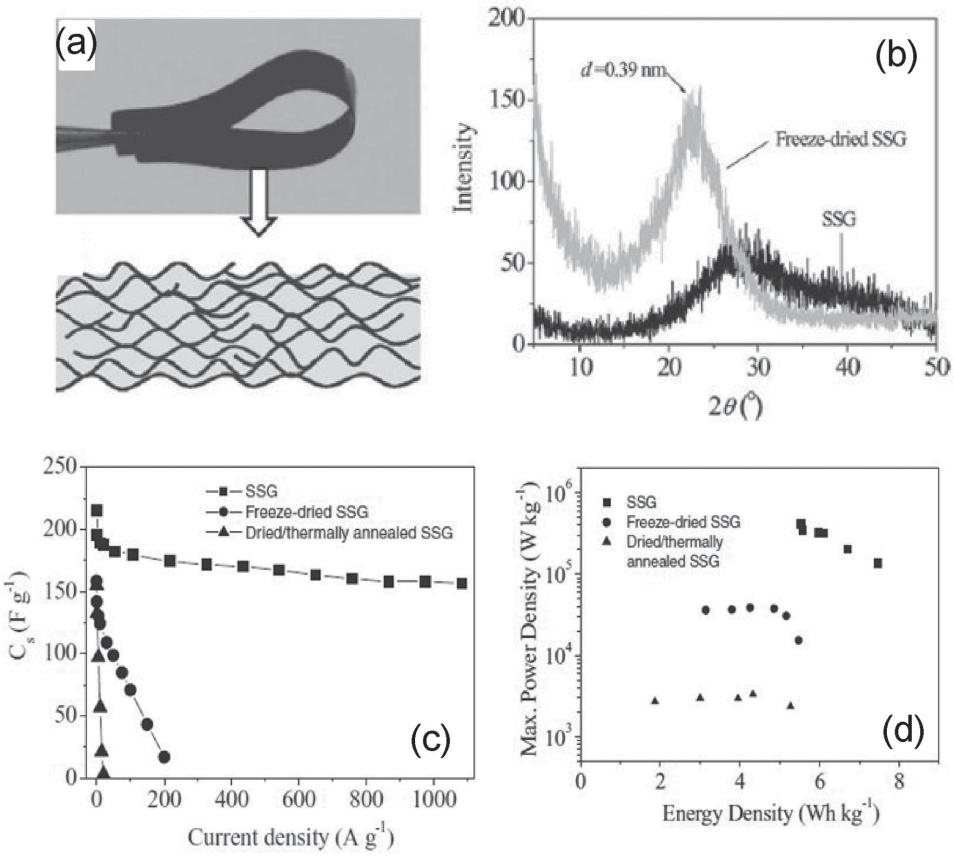

Figure 5. Structure of the self-stacked, solvated graphene (SSG) film and electrochemical characterization of the SSG film-based supercapacitors. a) A digital image and the cross-section of the SSG film. b) XRD spectra of wet and freeze dried SSG films with large spacing between graphene sheets. c) Gravimetric capacitances measured at various charge/discharge currents show high specific capacitance at high current density without drying. d) Ragone plots of the SSG films-based supercapacitors showing improved power and energy density for un-dried SSG film. Reproduced with permission.[215] Copyright 2011, Wiley.

energy/energy density/specific power of 67 Wh kg^{-1}, 54 Wh L^{-1}, and 60 kW kg^{-1}, respectively.[229]

A weakness of the porous graphene design for supercapacitor is that the high porosity may lead to a high electrolyte uptake that can lower the specific capacitance in a practical cell. The tortuosity inside porous graphene can also lead to a high irreversible capacity at the initial few charging/discharging cycles since the charge transport inside these channels slows down. In addition, porous graphene structures still suffer from the stacking disadvantages.[229]

3.2. Graphene-Based Nanostructures

Graphene modified with functional groups containing oxygen (O),[236–240] nitrogen (N),[222,241–247] sulfur (S),[248–250] boron (B),[251–254] silicon (Si)[255] have shown improved performance when used as supercapacitor electrodes. For example, reduced graphene oxides (rGOs) showed a specific capacitance of 264 F g^{-1}.[256] Graphene-based electrode made from electrochemically reduced GO displayed a capacitance of ≈165 F g^{-1} and excellent durability of over 1000 cycles in an aqueous electrolyte.[257] Partially reduced GO has capacitances of 348 and 158 F g^{-1} in aqueous and IL electrolytes, respectively. The performance improvement in modified graphene is due to synergistic effects of the electrical double-layer capacitance and pseudocapacitance. Kaner et al. used a standard lightscribe DVD optical drive to synthesize rGO with high electrical conductivity (1738 S m^{-1}) and high surface area (1520 m^2 g^{-1}).[258] This particular study presents a simple approach for graphene synthesis that is shown chronologically in **Figure 6**a–g.[258] These materials could be directly used as electrodes without the need of additional binders, carbon black, and current collectors, which could help improve the energy density of the devices. Figure 6h clearly indicates similar stack resistances using both aqueous and polymer electrolytes. Figure 6i shows that the resulting device exhibited ≈97% capacitance retention for over 10 000 cycles. The high mechanical flexibility is indicated by 95% capacitance retention for over 1000 cycles even upon bending (Figure 6j). The excellent mechanical flexibility is ascribed to the interconnected network architecture of the material along with the gel electrolyte.

N-doped sites at graphene basal planes can further enhance the electronic conductivity of the electrodes, leading to capacitance improvement.[241] N-doped graphene exhibits outstanding specific capacitance of 151 F g^{-1} at 5 A g^{-1} in KOH aqueous electrolyte. Additionally, these N-doped graphene electrodes exhibit superior rate capacity and excellent cycle performance of more than 5000 cycles.[259] In a study by Jeong and co-workers, N-doped graphene-based ultracapacitors showed higher capacitance of ≈280 F $g^{-1}_{electrode}$, which was four times larger than that for pristine graphene.[241] Another reported N-doped graphene containing hollow spheres can even deliver a high capacitance of 381 F g^{-1} at a current density of 1 A g^{-1}, which was attributed to the synergistic effects of the hollow nanostructure and N-doping.[242]

Results reported by Han et al. showed that the high surface area of B-doped graphene can lead to a high performance of supercapacitor electrodes.[260] Peng et al. also demonstrated that electrodes made of B-doped porous graphene exhibited three times higher capacitance and 5–10 times higher energy density than those for electrodes prepared from undoped graphene.[261]

The doping of heteroatoms in graphene can change the electronic structure and density of state significantly, thus modifying the quantum capacitance, leading to higher interfacial capacitance values.[262]

Although the presence of functional groups on the surface improved the capacities, the fabrication of these materials does require precise control and advanced synthesis techniques, which can lead to high fabrication costs. This can also lead to low loading because of the surface groups, hence limiting their practical applications. Moreover, controlling the density, order and the type of functional groups on the graphene surface still remains a challenge.

3.3. Graphene-Conducting Polymer Nanocomposites

Hybrid structures of graphene and electrically conducting polymers such as polyaniline (PANi), polypyrrole (PPy), poly(thiophene) (PTh), poly(hexylthiophene) (PHTh), and poly(3,4-ethylenedioxythiophene) (PEDOT) are often employed to further improve the performance of graphene-based electrodes for supercapacitors. Conductive polymers are promising owing to their high energy storage capacity, good electrical conductivity, low cost, and environmental stability.[263] However, conductive polymers inherently have low mechanical stability and break upon mechanical stress during cycling. Hence, efficient Faradaic charge-transfer mechanism across the electrode–electrolyte interface can significantly boost the charge storage capacity of pseudocapacitors when graphene is combined with these conductive polymers.

Graphene–PANi nanocomposites have been studied as potential supercapacitor electrodes[264–267] and show clearly improved electrochemical performance. Graphene–PANi nanocomposites, synthesized by in situ oxidation polymerization of aniline in the presence of functionalized graphene, show high specific capacitance of 863.6 F g^{-1} at 0.2 A g^{-1} and excellent rate capability of 581.6 F g^{-1} at 5 A g^{-1}.[266] Another reported graphene–PANi composite synthesized by in situ polymerization showed a high specific capacitance of 1046 F g^{-1} when compared to the value of 115 F g^{-1} for pure PANi.[268] Flexible graphene–PANi nanocomposites synthesized by in situ polymerization–reduction/dedoping–redoping process could deliver a specific capacitance of 1126 F g^{-1} and capacitance retention of 84% after 1000 cycles.[269] Xu et al. introduced a facile method to construct hierarchical nanocomposites by combining 1D PANi nanowires with 2D GO nanosheets.[270] The specific capacitance of the nanocomposite can be more than 550 F g^{-1} at 0.2 A g^{-1} current density along with excellent cycle life.[270]

The use of other hybrid materials, including flexible graphene–PANi nanofibers,[271] graphene–PANi flakes,[272] PANi-embedded holey graphene nanoribbons,[273] hierarchical graphene@PANi@graphene sandwich containing hollow structures,[274] 3D porous graphene/PANi,[275] freestanding hierarchical CNF/GO/PANi,[276] and PANi-grafted rGO,[277] has also been considered as potential materials for supercapacitors.

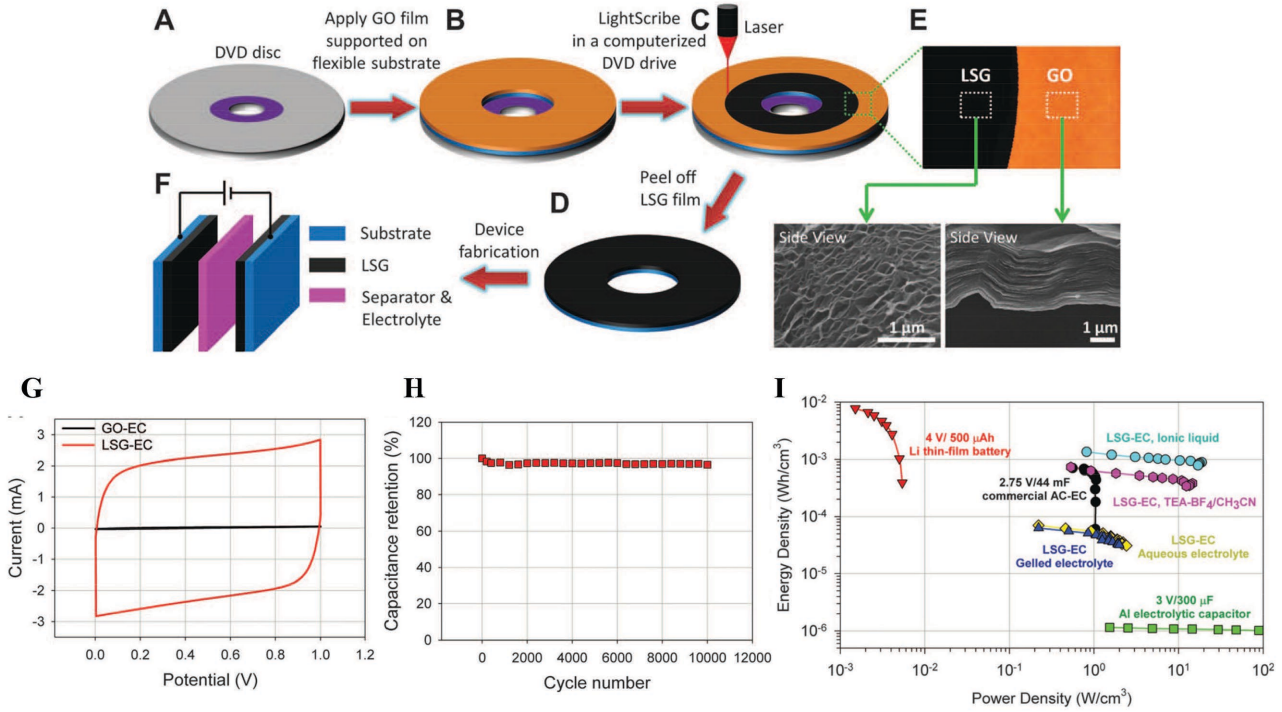

Figure 6. A flow diagram showing the construction of laser-scribed graphene (LSG)-based electrochemical capacitors (LSG-EC) and their associated electrochemical performance. a–d) Fabrication processes for the LSG-based electrodes for electrochemical capacitors on DVD media disc. e) The color of GO changes from golden brown to black, while layer structure of GO changes from stacked sheets to well-exfoliated few-layered LSG film. f) Fabrication of a symmetric EC using two identical LSG as electrodes. g) CV curve at a scan rate of 1000 mV s^{-1}. h) Cyclic stability at a high current density of 10 A g^{-1}. I) Comparison the energy and power densities of LSG-EC with other energy storage systems. Reproduced with permission.[258] Copyright 2012, American Association for the Advancement of Science.

PPy is another conductive polymer used with graphene for supercapacitors. Polymerized PPy with graphene showed a high specific capacitance of 482 F g^{-1} at a current density of 0.5 A g^{-1} in 1 M H_2SO_4. Sulfonated graphene (SG) and PPy composite films with ≈40 wt% of SG exhibited a specific capacitance of 285 F g^{-1} at a discharge rate of 0.5 A g^{-1}.[278] Hierarchical graphene–PPy nanosheet nanocomposites delivered a capacitance of 318.6 F g^{-1} at a scan rate of 2 mV s^{-1} with 95% capacity retention after 1000 cycles at a scan rate of 100 mV s^{-1}.[279] Composite films consisting of PPy and GO were electrochemically synthesized and directly used as an electrode for supercapacitors where the GO/PPy composite exhibited a high specific capacitance of 424 F g^{-1} in 1 M H_2SO_4-based electrolytes at a current density of 1 A g^{-1}.[280] The 3D framework of PPy wrapped on the graphene hydrogel nanocomposites displayed a high specific capacitance of 375 F g^{-1} at a scan rate of 10 mV s^{-1} along with excellent capacitance retention for more than 4000 cycles.[281] Recently, a freestanding CNT/graphene/PPy was used as hybrid electrodes in supercapacitors, which exhibited a specific capacitance of 453 F g^{-1} with ultrahigh energy and power density of ≈63 Wh kg^{-1} and ≈567 W kg^{-1}, respectively, at a scan rate of 5 mV s^{-1}.[282] Other hybrid graphene–PPy nanostructures such as nanowires,[283] nanotubes,[284] freestanding graphene/PPy film,[285] 3D graphene/bacterial cellulose/PPy composites,[286] freestanding TiO_2/graphene/PPy composite,[287] PPy/SG composite,[288] and PPy/rGO-CTAB[289] have also been considered as promising electrodes for supercapacitors.

Graphene–PTh nanocomposites[290,291] and graphene–PTh derivatives have also been reported as pseudocapacitor materials.[291–293] graphene–PEDOT and graphene–PHTh nanocomposites have showed specific capacitances of 800–1100 F g^{-1} at a current density of 0.1 A g^{-1}.[292] The composite films consisting of PEDOT and rGO exhibit better capacitive properties than pure PEDOT and rGO with a good specific capacitance retention up to 90% of the initial value even after 2000 cycles.[294]

Although conductive polymers are attractive, their inherently low conductivity compared to metals can lead to slow electron/ion diffusion characteristics and low rates of charge/discharge.

The orientation of polymer chains in graphene/conductive polymer nanocomposites can help improve the electron transport and enhance the charge/discharge rates in supercapacitors. The other important advantage of using graphene/polymer nanocomposites in supercapacitors is to create a tortuous path for ions in the graphene composite structure that can lead to irreversible specific capacitance losses. However, the key limitation for conducting polymers in supercapacitors is their low cycling stability that arises due to the structural breakdown of conducting polymers during the intercalation/de-intercalation process. From this viewpoint, the synthesis and fabrication of these nanocomposites are challenging and this requires further structure optimization and performance improvement.

3.4. Graphene/Carbon Nanocomposites

Different types of graphene/carbon nanocomposites can be prepared by mixing nanostructured carbons with graphene via chemical and physical methods, hence combining the material properties can lead to improved electrolyte–electrode accessibility and enhanced electrical conductivity of electrode.[295–298] Monolayer graphene sheets tend to form agglomerates and may even undergo stacking to form graphite,[299,300] which can be prevented by incorporating other carbon materials (carbon nanotubes, porous carbon spheres, activated carbon spheres, carbon black, etc.) to fabricate different graphene/carbon nanocomposites. For instance, self-assembly of multiwalled carbon nanotubes (MWCNTs) and polyethylenimine (PEI)-modified graphene sheets leads to the formation of hybrid interconnected nanocomposite carbon films with well-defined nanopores. This nanocomposite electrode exhibited rectangular cyclic voltammograms (CV) with a specific capacitance of 120 F g^{-1} at a scan rate of 1 V s^{-1}.[301] Graphene/MWCNT composites synthesized via layer-by-layer-assembly can have a large volumetric capacitance of ≈160 F cm^{-3} in 0.5 M H_2SO_4 electrolyte.[302] CNTs inserted between rGO sheets show enhanced cycleability and rate performance,[302,303] because 1D CNTs could physically separate 2D graphene sheets, preserving their high surface area and creating new pores. CNTs–graphene composite materials synthesized by CVD have shown good performance as supercapacitors.[304] In another study, hybrids of porous carbon materials with graphene showed outstanding stability for over 1000 cycles with 94% capacitance retention.[305] rGO-activated carbon nanocomposites were also reported to have high specific capacities of about 400 F g^{-1} at a current density of 1 A g^{-1} in KOH and 287 F g^{-1} at a current density of 0.5 A g^{-1} in an IL electrolyte.[306] A hierarchical nanostructured functionalized carbon spheres/graphene hybrids enhanced the specific capacitance of graphene by >70%.[307] The incorporation of carbon black (CB) into graphene sheets has been shown to improve the overall electrode conductivity and increase planar spacing between graphene sheets, leading to rapid diffusion paths for more edge plane participation in double-layer capacitance.[308]

Although the idea of using carbons to separate graphene sheets is promising and novel, further engineering of graphene synthesis is required to reduce the production cost of nanocomposites. In addition, the selection of dense carbons, such as CNT, CNF, should be an ideal choice for these architectures, because they can help lower the overall tap density and increase electrolyte uptake, which might be helpful for practical applications.

3.5. Graphene/Transition Metal Oxides (or Hydroxide) Nanocomposites

Transition metal oxides including MnO_2, Mn_3O_4, RuO_2, Co_3O_4, Fe_3O_4, SnO_2, NiO, Nb_2O_5, and ZnO have been widely used as electrode materials for supercapacitors. For example, MnO_2 is a promising material for supercapacitor owing to its superior electrochemical performance, environmental friendliness, and low production cost.[130,131] RuO_2 (including hydrous and amorphous RuO_2) has exceptionally high charge storage capacity due to its high electronic and protonic conductivities as well as high degree of redox process reversibility taking place over a wide potential range (up to 1.4 V).[309,310] However, pure metal oxide-based electrodes suffer from relatively low power performance and poor cyclability because of their relatively low electrical conductivities and serious agglomeration, leading to incomplete reactions during the electrochemical redox processes. In order to limit these obstacles and achieve improved electrochemical properties, many transition metal oxide/carbon composite electrodes have been investigated.[142,311–313] Carbon-based nanocomposites can take full advantage of double-layer capacitance and pseudocapacitance, leading to increased energy density and extended cycle life.[142] A particularly attractive option is to design and develop hybrid films based on graphene–metal oxide nanocomposites. Among these graphene-transition metal oxide nanocomposites, the graphene phase with high surface area governs the specific capacitance; while their high electronic conductivity is crucial to the improvement of rate capability and power density.[182,314–317] For example, the reduction of permanganate on graphene resulted in the formation of graphene–MnO_2 composite electrodes with a specific capacitance of 310 F g^{-1} at a scan rate of 2 mV s^{-1}.[318] Graphene–MnO_2 nanocomposites prepared by electrodeposition showed a specific capacitance of ≈315 F g^{-1}.[319] Asymmetric capacitors with graphene–MnO_2 textile and SWCNTs in an aqueous Na_2SO_4 electrolyte exhibit a maximum power density of 110 kW kg^{-1} and energy density of 12.5 Wh kg^{-1} with 95% capacitance retention for over 5000 cycles.[319]

Recently, Choi et al. fabricated 3D macroporous chemical modified graphene (named embossed-CMG (e-CMG) films) by using polystyrene colloidal particles as a sacrificial template.[224] Furthermore, a thin layer of MnO_2 was additionally deposited onto e-CMG (**Figure 7**a,b).[224] The 3D porous graphene structure with a large surface area facilitated fast ionic transport within the electrode while preserving decent electronic conductivity and thus endowed MnO_2/e-CMG composite electrodes with excellent electrochemical properties, such as a high specific capacitance of 389 F g^{-1} at 1 A g^{-1} and enhanced capacitance retention upon a current increase to 35 A g^{-1}. Moreover, when the MnO_2/e-CMG composite electrode was asymmetrically assembled with an e-CMG electrode, the cell showed improved reversible capacitance, excellent cycle life performance (Figure 7c) along with remarkable energy density of 44 Wh kg^{-1}, power density of 25 kW kg^{-1} (Figure 7d).[224]

New ternary composites of MnO_2 nanorods, PANi and GO were prepared by a two-step process. The 100 nm long MnO_2 nanorods with a diameter ≈20 nm were conformally coated with PANi layers and fastened between GO layers.[320] The ternary composite with 70% MnO_2 exhibited the highest specific capacitance of 512 F g^{-1} and outstanding cycling performance, with ≈97% capacitance retention over 5000 cycles, which was much higher than for PANi/GO binary composites.[320] On the other hand, ternary composites of MnO_2, PPy, and rGO hybrid composites delivered a maximum specific capacitance as high as 404 F g^{-1} with a capacitance retention over 91% after 5000 cycles.[321] In another study, Han and co-workers integrated MnO_x nanoparticles onto flexible graphite paper using an ultrathin CNT and rGO (CNT/rGO) layer as the supporting layer.[322] Supercapacitor electrodes employing the MnO_x/CNT/rGO

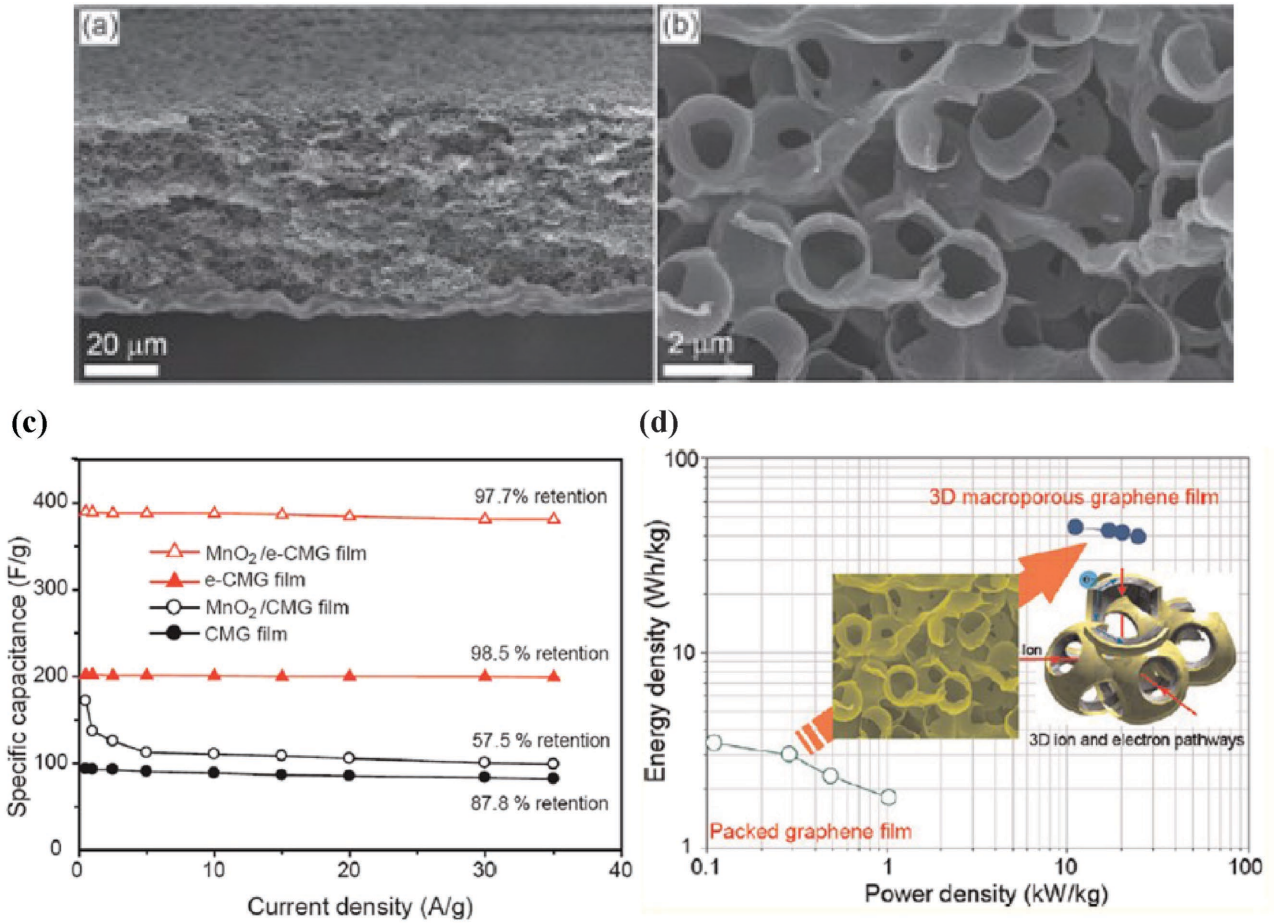

Figure 7. a) Low-magnified, and b) High-magnified cross-sectional SEM images of macroporous embossed chemically modified graphenes (e-CMG) film. c) The dependences of the specific capacitances of CMG, MnO_2/CMG, e-CMG, and MnO_2/e-CMG films on various current densities ranging from 0.5 to 35 A g^{-1}. d) The power density vs energy density of 3D macroporous graphene film and packed graphene film in a Ragone plot. Reproduced with permission.[224] Copyright 2012, American Chemical Society.

nanohybrids without any conductive additives or binders yielded a specific capacitance of 1070 F g^{-1} at 10 mV s^{-1}, which was among the highest values reported for a range of hybrid structures and it is close to the theoretical capacity of MnO_x. In addition, a further plasma treatment of the CNT/rGO supporting layer led to improved adhesion of MnO_x nanoparticles to the electrode surface, which resulted in improved cycling stability of the nanohybrid electrodes. These excellent performances were attributed to three factors: (i) Compared to single-phased MnO_2, MnO_x compounds (i.e., Mn atoms with multiple oxidation states and phases) usually contain both donor and acceptor sites in their microstructures as well as defects and mismatch induced by different phases, which can enable a higher charge storage capacity; (ii) the excellent structural features, including porous architecture, small and uniform size, and high electrical conductivity of both CNT and rGO; and (iii) the synergistic use of carbon nanomaterials and plasma-related effects.[322]

In addition, MnO_2 nanowires/graphene,[323] graphene nanoplate/MnO_2,[324] porous graphene/MnO_2,[224,325] graphene/MnO_2 composite and activated CNFs for asymmetric capacitors have also been investigated.[326] However, due to the insulating nature of MnO_2, the synthesis of nanocomposites requires high graphene amounts, which can once again affect the tap density and high electrolyte uptake. In order to overcome these problems and keep graphene to low composition, precise design and synthesis of these composites are required.

Graphene/RuO_2 nanocomposites have also has been designed in different electrolytes with improved electrochemical capacitance. Wu et al. synthesized hydrous graphene–RuO_2 composites for supercapacitor by a combination of sol–gel and low-temperature annealing processes, which delivered a specific capacitance of 570 F g^{-1} at 38.3 wt% Ru.[327] In the same vein, Deng et al. prepared graphene/RuO_2 nanocomposites using a solution-phase assembly for high-performance pseudocapacitors.[328] Since both RuO_2 and graphene nanosheets uniformly interlink with each other, these nanocomposites maintain good electrical conductivity and a high structural stability. This synergistic effect leads to a high specific capacitance of 479 F g^{-1}, a high energy density of 20.28 Wh kg^{-1} at a power density of 600 W kg^{-1} along with excellent cyclic performance. Ozkan et al. reported a simple and scalable way to prepare 3D RuO_2/graphene/CNT hybrid nanocomposites with graphene foam conformally covered with hybrid networks of RuO_2 nanoparticles and anchored CNTs for high-performance supercapacitor

electrodes. This tri-component nanocomposites showed superior gravimetric, per-area capacitive performance and exceptionally high energy and power density, demonstrating that hybrid RuO_2/graphene/CNT nanocomposites are promising materials for future energy storage applications.[329] In another study, Zhang et al. prepared quasi graphene nanosheet (QGN)/RuO_2 by GO modification along the longitudinal direction of MWCNTs with RuO_2 nanoparticles uniformly dispersed on the surface. The as-synthesized graphene/RuO_2 nanocomposites exhibited good capacitive properties compared to pure RuO_2 and pure QGN in both acidic and alkaline electrolytes. QGN/RuO_2 composites achieved a high voltage window of 1.6 V with excellent energy and power densities.[330] Nevertheless, Ru is a rare metal and quite expensive, therefore, the feasibility of using Ru for daily applications is highly improbable.

In addition to MnO_2 and RuO_2, other graphene/transition metal oxide (or hydroxides)-based nanocomposites, such as graphene–Co_3O_4,[331,332] graphene–Fe_3O_4,[333,334] graphene–SnO_2,[335] graphene–NiO,[336] graphene–Fe_2O_3,[165–167] graphene–ZnO,[335,337] graphene–TiO_2,[168–170] graphene–Mn_3O_4,[338,339] graphene–CuO,[174,175] graphene–NiO–MnO_2,[340] graphene–VO_2,[341] graphene–V_2O_5,[342] graphene–Nb_2O_5,[188,189,202] graphene–CeO_2,[343] graphene–ZnO,[184] graphene-mixed-valent MnO_x,[344] graphene–α–MoO_3,[345] graphene–$NiFe_2O_4$,[346] graphene–$NiCo_2O_4$,[180–182] graphene–$Co(OH)_2$,[347,348] graphene–$Ni(OH)_2$,[349,350] graphene–MnO_2–PANi,[320] etc. have been also used as potential supercapacitor materials with good performance. For example, a 3D graphene–Co_3O_4 composite was found to be capable of delivering a high specific capacitance of about 1100 F g^{-1} at a current density of 10 A g^{-1} with excellent cycling stability.[351] The graphene–Fe_3O_4 nanocomposite exhibited a high specific discharge capacitance of 220.1 F g^{-1} at 0.5 A g^{-1} and remains stable for more than 3000 cycles.[158] This good performance was attributed to the chemical interaction between graphene and Fe_3O_4, lower agglomeration and smaller particle size of Fe_3O_4. The optimized graphene–Fe_3O_4 paper even displayed a high specific capacitance of 368 F g^{-1} at 1 A g^{-1} and remained 245 F g^{-1} at 5 A g^{-1} for more than 1000 cycles.[352] Dong et al. reported results on the synthesis of ultrathin scale-like $NiCo_2O_4$ nanosheets (NSs) supported on N-doped rGO (N-rGO) for use in high-performance supercapacitors.[353] The $NiCo_2O_4$ NSs@N-rGO nanocomposite delivered a specific capacitance of 1540 F g^{-1} after 1000 cycles at 10 A g^{-1}.

Recently, a facile strategy was utilized to synthesize a graphene/$Co(OH)_2$ nanocomposite for supercapacitors by depositing $Co(OH)_2$ nanoparticles on the graphene sheets in a water–isopropyl alcohol system[354] The graphene/$Co(OH)_2$ nanocomposite exhibited a specific capacitance of 960 F g^{-1} at high current density of 10 A g^{-1}, demonstrating a significant improvement in performance compared to each individual counterpart. In addition, after 5000 cycles of charge/discharge, the $Co(OH)_2$/graphene composite maintained 93.4% of its initial specific capacitance value at a current density of 30 A g^{-1}.[354] In the same line, Dai and co-workers fabricated graphene–$Ni(OH)_2$ nanocomposites, in which $Ni(OH)_2$ hexagonal nanoplates were grown on low-oxidation graphene sheets that resulted in a high specific capacitance of ≈1335 F g^{-1}.[349] The metal oxides in conjunction with graphene acted as hybrid materials that contributed to the high capacity of these materials.

More recently, Dubal et al. designed a hybrid energy storage devices using hybrid electrodes based on rGO and pseudocapacitive $Ni(OH)_2$ and $Co(OH)_2$ deposited on the skeleton of 3D macroporous sponge support (**Figure 8**).[348] In this fascinating design, the authors first coated rGO onto the bare sponge substrate by "dip and dry" method using rGO ink in an aqueous solution and, subsequently depositing nanostructured $Ni(OH)_2$ and $Co(OH)_2$ by the chemical bath deposition (CBD) strategy (Figure 8a).[348] The 3D macroporous conducting framework uniformly covered with aggregates of rGO sheet with high surface area could be formed, which provided enough space for the further heavy and uniform deposition of $Ni(OH)_2$ and $Co(OH)_2$ onto the skeleton of the sponge.[348] A schematic of this hybrid device is sketched in Figure 8b, the characteristic of hybrid electrode is hybridization of pseudocapacitive component $Ni(OH)_2$ and $Co(OH)_2$ and nonfaradic component rGO in a single electrode so that energy can be stored through both mechanism (Figure 8b,c).[348]

Finally, long cycling-life tests were carried out for the rGO/rGO@$Ni(OH)_2$ and rGO/rGO@$Co(OH)_2$ hybrids by repeating the CV test at a scan rate of 100 mV s^{-1} for 2000 cycles (Figure 8d,e).[348] In that work, the specific capacitance was decreased suddenly after the initial 50 cycles, which was probably related to the pulverization and loss of electrical contact between the active materials and the current as well as to wettability issues.[348] After 2000 cycles, the rGO/rGO@$Ni(OH)_2$ and rGO/rGO@$Co(OH)_2$ hybrid devices displayed an excellent long cycle life with 90% and 87% retention of the initial values, respectively (Figure 8d,e).[348] Such a stable and connecting structure helped alleviate the structure damage caused by volume expansion during cycling process, which resulted in an enhanced stability.[348] More importantly, the excellent stability confirmed the proper hybridization of two different (pseudocapacitive and non-faradic) materials. Figure 8f shows the Ragone plot of the rGO/rGO@$Ni(OH)_2$ and rGO/rGO@$Co(OH)_2$ hybrid devices. The as-assembled SP@rGO//SP@rGO@Ni hybrid device with a cell voltage of 1.5 V delivered a high specific energy of 42.02 Wh kg^{-1} with a maximum specific power of 11 kW kg^{-1} while the SP@rGO//SP@rGO@Co cell exhibited 33.01 Wh kg^{-1} with a specific power of 8 kW kg^{-1}.[348] Furthermore, these devices can retain an energy density >10 Wh kg^{-1} even at a high power density.[348] The energy density reported in this work was significantly higher than those obtained for other carbon-based symmetric capacitors in aqueous electrolytes.[348]

We took notice of the facts that the electrochemical signatures (e.g., cyclic voltammogram and charge/discharge curve) of nickel oxide/hydroxide and cobalt oxide/hydroxide are analogous to that of a "battery" and they should be considered Faradaic electrodes,[355] because they do not display an electrochemical behavior typical of that observed for a capacitive carbon electrode in mild aqueous electrolyte (as shown in traditional supercapacitor electrode materials such as MnO_2, etc.).[355] Based these facts, nickel oxide/hydroxide and cobalt oxide/hydroxide are usually not considered supercapacitors materials. This information has been reported by Brousse et al.[355] and supported by Gogotsi et al.[16] which shed light to this topic and help the authors correctly address the description of the electrodes.

However, just as Brousse described, the behaviors of many electrochemical capacitor-relevant materials are more complex

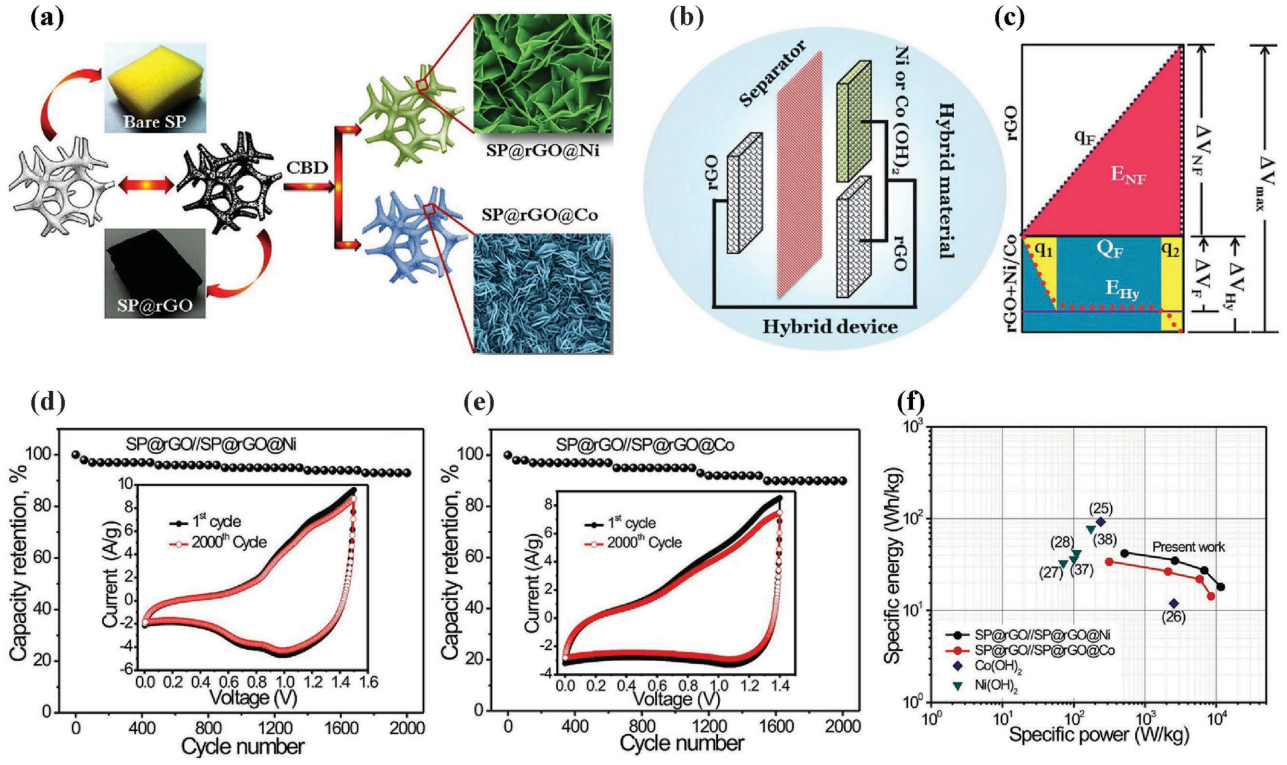

Figure 8. a) Schematic representation of the fabrication of hybrid materials based on rGO and transition metal hydroxides ($Ni(OH)_2$ and $Co(OH)_2$) onto skeleton of 3D macroporous sponge. b,c) Schematic representation of hybrid device of hybrid electrode (supercapacitor (SP)@rGO@$Ni(OH)_2$ or SP@rGO@$Co(OH)_2$) and SP@rGO electrode with propylene carbonate paper as separator along with charge-potential profile. Variation of capacity retention of d) SP@rGO//SP@rGO@$Ni(OH)_2$, and e) SP@rGO//SP@rGO@$Co(OH)_2$ hybrid devices with number of cycles at 100 mV s^{-1} scan rate and the corresponding CV curves (inset) at first and 2000th cycles. f) The power density versus energy density of SP@rGO//SP@rGO@$Ni(OH)_2$, and SP@rGO//SP@rGO@$Co(OH)_2$ hybrid devices in a Ragone plot. Reproduced with permission.[348] Copyright 2014, Nature Publishing Group.

than that described by a single term.[355] Some compounds exhibit both mechanisms with a pseudocapacitive contribution coming from the surface properties and faradaic contribution coming from other mechanisms.[355] Because of these reasons, many more papers continually report nickel oxide/hydroxide and cobalt oxide/hydroxide as supercapacitor materials. In this manuscript, we also have described these materials as pseudocapacitive electrodes.

3.6. Graphene/Transition Metal Nitrides (or Sulfide) Nanocomposites

In addition to transition metal oxide (or hydroxides) nanocomposites, transition metal nitrides (e.g., TiN, VN, Mo_3N_2, etc.),[356–361] and transition metal sulfides (CoS_2, NiS, $CoMoS_4$, MoS_2, CuS, MnS, etc.),[362–366] are also promising materials for use in supercapacitors due to their high specific capacitance, exceptional electrochemical properties, and excellent electrical conductivity. However, pure transitional metal nitride or metal sulfide electrodes suffer from irreversible oxidation reactions, which lead to poor cycleability.[356–361] Hence, metal nitrides or metal sulfide in conjunction with conductive carbon, such as graphene, can prevent the oxidation reaction and improve the cycleability of these materials.[367–371] For example, an asymmetrical solid state supercapacitor constructed from graphene–TiN cathode, graphene–Fe_2N anode, and poly(vinyl alcohol) (PVA)/LiCl-based solid electrolyte delivered an irreversible capacitance of about 58 F g^{-1} at 4 A g^{-1}.[372] This capacitance was relatively stable for up to 20 000 cycles.[372] Moreover, both high volumetric energy density and power density can be achieved at a high current density of 8 A g^{-1}.[372] A CoS/graphene hydrogel composites exhibited a maximum specific capacitance of 435.7 F g^{-1} at a current density of 0.5 A g^{-1} in 6 M KOH electrolyte, which was significantly higher than that of CoS and graphene. Furthermore, the graphene/CoS nanocomposites also showed excellent cycling stability with 82.3% a capacitance retention over 3000 cycles, which is higher than that of pure CoS. The enhanced electrochemical properties exhibited by the graphene/CoS composite highlight the special hydrogel structure and synergistic effects between CoS and graphene.[368] In the same line, Huang and co-workers synthesized MoS_2/rGO nanocomposites for use as electrodes in supercapacitors.[366] A capacitance of 243 F g^{-1} was reported at a current density of 1 A g^{-1} with energy density of 73.5 Wh kg^{-1} at a power density of 19.8 kW kg^{-1}.

3.7. Graphene/Layer Hydroxides Nanocomposites

Layered double hydroxides (LDHs) are in the form of $[M^{2+}{}_{1-x}\ M^{3+}{}_x(OH)_2][An^-{}_{x/n}.mH_2O]$ with M representing metal

cations and A representing the interlayer anion of n-valency. Xu and co-workers fabricated a hierarchical 3D composite composed of graphene layers with LDH nanosheet arrays grown on both sides.[373] It was found that the NiAl–LDH nanosheet arrays grow perpendicularly and uniformly on both sides of the graphene sheets, constructing a hierarchical 3D nanocomposite with an interesting sandwich structure. Dong and co-workers fabricated multilayer films of Co–Al LDH nanosheets and GO using layer-by-layer (LBL) assembly.[374] These films exhibited a high specific capacitance of 880 F g^{-1}, an area capacitance of 70 F m^{-2} at a scan rate of 5 mV s^{-1} and good cycleability for over 2000 cycles. The reduction of these films in H_2 resulted in increased specific capacitance and area capacitance of up to 1204 F g^{-1} and 90 F m^{-2}, respectively, due to the partial reduction of GO. Several LDH/graphene nanocomposites were also prepared using different synthesis techniques showed improved specific capacitance and area capacitance.[186–190]

Transition metal oxides (hydroxides), transition metal nitrides, transition metal sulfides, layer hydroxides have been widely used as pseudo-capacitive materials. Due to their chemical charge storage mechanism, pseudocapacitors show higher energy density and storage capacity, but usually exhibit a slow charge storage and limited lifetime. Increasing the energy density of supercapacitor electrodes without losing their power density and rate capability is a challenge that can be addressed by a rational design of the electrodes and producing carbon-metal oxide hybrid structures. Supercapacitors with graphene-based nanocomposites can store much higher charge than the conventional capacitors. However, their energy density is still low in comparison to Li-ion batteries and fuel cells. Asymmetric supercapacitors with enhanced energy density are considered as good alternatives to replace supercapacitors in high specific power applications.[200,375] The following section is focused on the design of graphene nanocomposites and their use in asymmetric supercapacitors.

3.8. Graphene Nanocomposites for Asymmetric Supercapacitors and Microsupercapacitors

Asymmetric supercapacitors primarily combines Faradic electrode (as energy source) and capacitive electrode (as power source) to increase the operation voltage thus enhancing their energy density while retaining their intrinsic high specific power.[339,350,376,377] The different graphene and graphene-based nanocomposites with high surface area can store charges electrostatically via reversible ion absorption at the electrode/electrolyte interface. The addition of transition metal oxides or redox conducting polymers, which use fast and reversible redox reactions at the surface of the electroactive materials for charge storage, can lead to high pseudo-capacitance. In recent study, Cheng and co-workers designed a high-voltage asymmetric supercapacitor using pure graphene as a negative electrode and graphene/MnO_2 nanocomposites as a positive electrode.[323] Na_2SO_4 aqueous electrolyte-based hybrid supercapacitors that can be cycled reversibly in high voltage region have high energy density and high power density. Similarly, Yu and co-workers fabricated asymmetric electrochemical capacitors with graphene/MnO_2-textile as the positive electrode and SWNTs-textile as the negative electrode in an aqueous Na_2SO_4 electrolyte solution.[319] These devices exhibit promising characteristics with maximum power density of 110 kW kg^{-1}, energy density of 12.5 Wh kg^{-1}, and excellent cycling performance with ≈95% capacitance retention for over 5000 cycles. In another study, Wang et al. developed both $Ni(OH)_2$ nanoplates and RuO_2 nanoparticles on high-quality graphene sheets to pair up a $Ni(OH)_2$/graphene electrode with battery characteristics and a RuO_2/graphene electrode with capacitor characteristics. The asymmetrical supercapacitor exhibited better energy density than symmetrical supercapacitors with RuO_2 and also better than asymmetrical supercapacitors based on individual electrode pairs.[378] A novel Li-ion hybrid capacitor based on 3D VN–rGO composite and porous carbon nanorods as the anode and cathode, respectively, can have an ultrahigh energy density of 162 Wh kg^{-1} at 200 W kg^{-1}, which remained at around 64 Wh kg^{-1} even at a high power density of 10 kW kg^{-1}.[371]

In addition to the above-mentioned reports, graphene/graphene–MnO_2 nanoflowers,[379] CNFs/graphene–MnO_2,[326] $MnFe_2O_4$/graphene as anode and MnO_2/CNTs as cathodes,[380] activated graphene–PANi/graphene/CNTs,[381] NiOOH/Ni_3S_2/3D graphene as an anode and Fe_3O_4/graphene composite as a cathode,[382] among others,[383] have been employed in asymmetric capacitors with high energy density as well as power density paving the way for further development in this area.

Recently, graphene-based fibers[384–386] and graphene-based composite fibers[301,387–391] have also been used for microsupercapacitors. However, the increase in volumetric energy density leads to a decrease in both power density and cycle life. The important factors affecting the performance of microsupercapacitors are the intrinsic properties of electrode materials and electrolyte, architectural design of the device and the fabrication methods.[392] Dai et al. synthesized hierarchical carbon microfibers with interconnected network of aligned SWNTs and mesoporous nitrogen-doped rGO sheets with high specific surface area and ultrahigh electrical conductivity.[393] The as-synthesized composite electrode exhibited a high volumetric capacity of ≈300 F cm^{-3} in PVA/H_3PO_4 electrolyte. This PVA/H_3PO_4 electrolyte-based supercapacitors were free of binder, current collector, and separator with a high volumetric energy density of 6.3 mWh cm^{-3}, stable cycling and excellent power density.[393]

Flexible solid-state supercapacitors have attracted considerable interest as mobile power supply sources in the future. Graphene-based thin films have been used for flexible solid-state supercapacitors with high gravimetric specific capacitance.[394] Recently, 3D graphene hydrogel films,[394] PANi–graphene nanoribbons/CNTs,[395] graphene/PPy composite fibers,[391] MnO_2/graphene and CNT/graphene composites,[396] and PANi–rGO/CF composite[397] have been used for flexible supercapacitors with reasonable capacitance and cycling stability. **Table 1** summarizes more of the various types of graphene-based nanocomposites that have been employed in supercapacitor electrodes.

As discussed earlier, the results reported on the use of graphene and graphene-based nanocomposites for supercapacitors are promising. However, there are several issues that need to be addressed. First, despite the significant advancements

Table 1. Examples of different graphene-based nanocomposites for supercapacitors reported in the literature.

Materials	Electrolyte	Electrochemical performance
MnO_2 nanorods–graphene oxide–PANi ternary composites[320]	1 M Na_2SO_4	Capacitance can be 512 F g^{-1}, cycle life > 5000 cycles
α-MnO_2/GO nanocomposites[399]	1 M Li_2SO_4	Capacitance can be 280 F g^{-1}, energy density: 35 Wh kg^{-1}, power density: 7.5 kW kg^{-1}, cycle life > 1000
Graphene/NiO–MnO_2 nanocomposite[340]	6 M KOH	Capacitance can be 242.15 F g^{-1}
Ag/MnO_2/rGO[400]	3 M KOH	Capacitance can be 467.5 F g^{-1}, cycle life > 1000
Co_3O_4/graphene nanocomposite[401]	6 M KOH	Specific capacitance of 415 F g^{-1}
Co_3O_4 nanoplates/graphene composites[402]	2 M KOH	Specific capacitance of 667.9 F g^{-1}
Needle-like Co_3O_4/graphene[178]	2 M KOH	Specific capacitance of 157.7 F g^{-1}, cycle life > 4000
Fe_3O_4/rGO nanocomposite[403]	2 M KOH	Specific capacitance of 220.1 F g^{-1}, cycle life > 3000
Fe_3O_4/rGO composite[404]		Specific capacitance of 350.6 F g^{-1}
Graphene/Fe_3O_4 nanocrystals[405]	1 M KOH	Specific capacitance of 169 F g^{-1}, cycle life > 1000
Fe_2O_3/graphene composite[406]	1 M KOH	Specific capacitance of 908 F g^{-1}
Fe_2O_3/graphene nanocomposite[407]	1 M Na_2SO_4	Specific capacitance of 226 F g^{-1}
Fe_2O_3 nanoparticles/N-graphene[167]	1 M KOH	Specific capacitance can be 618 F g^{-1}, cycle life > 5000
SnO_2/graphene nanocomposites[408]	1 M KOH	Specific capacitance can be 363.3 F g^{-1}
ZnO@rGO[409]	2 M KOH	Specific capacitance can be 314 F g^{-1}
NiO nanoflake/3D graphene[410]	1 M NaOH	Specific capacitance ≈1829 F g^{-1}, energy density: 138 Wh kg^{-1}, power density: 5.25 kW kg^{-1}
Graphene/WO_3[411]	1 M H_2SO4	Specific capacitance can be 143.6 F g^{-1}
Graphene/TiO_2[412]	1 M Na_2SO_4	A high specific capacitance of 165 F g^{-1}

in supercapacitors, it is worth mentioning that the current graphene-based supercapacitors still have lower (than expected) energy density for advanced energy storage applications. Second, transition metal oxides (hydroxide), transition metal nitrides (or sulfide), and conductive polymers incur higher costs than the commercial carbon-based materials for supercapacitors.

More research efforts are needed to address the above issues including the fabrication of novel graphene hybrids with higher specific surface area, controlled porosity and high electrochemical activity to make supercapacitors a viable option for storing energy comparable to that of Li-based batteries.[139,398] In the following section, the discussion will be centered on the progress made on the synthesis of graphene and graphene nanocomposites for Li ion batteries and the associated challenges.

4. Li-Ion Batteries

Li-ion batteries have received extensive attention from the scientific community as one of the most popular energy storage systems for applications in different areas due to their several important advantages, such as high energy density, no memory effect, long cycle life, and low self-discharging.[10,413,414] A Li-ion cell consists of four functional components, e.g., the anode (negative electrode), cathode (positive electrode), electrolyte, and separator.[10,413,414] During charging, an external electrical power source forces the current to pass in the reverse direction and enables the migration (diffusion) of Li ions from the cathode to the anode through the electrolyte. During the discharging process, Li ions move from back to the anode through the non-aqueous electrolyte, carrying the current (**Figure 9**).[83]

Graphene and graphene-based nanocomposites have attracted tremendous attention for use in rechargeable Li-ion batteries due to their superior properties.[208,415–419] Theoretically, graphene has good Li-storage ability, since Li can be bound on both sides of graphene sheets, sheet edges, and different types of defect sites. Graphene can also significantly enhance the electron conduction on contact with electrochemically active materials in Li-ion batteries when used as conductive matrix and effectively prevent aggregation of materials during lithiation/delithiation processes.[419,420] Hence, graphene and graphene-based nanostructured materials offer an exciting solution to the current limitations and issues related to gravimetric energy density. High surface area graphene allows for two fundamental improvements over conventional flat electrode design: (i) Higher Li uptake leads to increased storage capacity; and (ii) increased rate capability due to faster interfacial kinetics.[208,415–418] In the following sections, we discuss the experimental results reported on using graphene and graphene nanocomposites as anodes and cathodes for Li-ion batteries.

4.1. Anodes

4.1.1. Graphene-Based Anodes

In Li-ion batteries, the anode is considered to be a crucial component affecting the battery performance.[421–423] Nanostructured materials have been extensively used as anodes in Li-ion

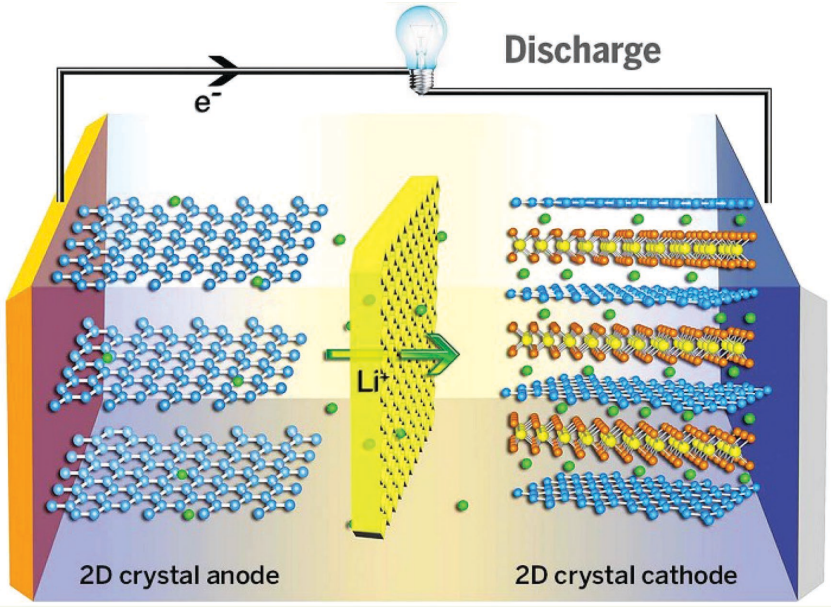

Figure 9. Schematic of showing the working principle of graphene-based electrodes for Li-ion batteries. With the anode composed of graphene flakes, the cathode is a hybrid graphene–Li compound (such as $LiCoO_2$ or $LiFePO_4$). The graphene-based electrode can help enhance electron transport kinetics compared with graphene-free Li compounds. Reproduced with permission.[83] Copyright 2015, American Association for the Advancement of Science.

batteries due to their high surface area and fast Li^+ diffusion and therefore their high ability of storing more Li^+ than that for bulk materials.[421,424–428] Li storage in graphene has been extensively explored to better understand its electrochemical properties.[429–433] Guo et al. used chemically prepared graphene as anode for rechargeable Li-ion batteries with charge and discharge capacities of 1233 mAh g^{-1} and 672 mAh g^{-1}, respectively, and a coulombic efficiency of 54.5% at the first cycle.[433] The reversible capacity retention after 30 cycles was about 502 mAh g^{-1}. In fact, the electrolyte interaction with oxygen-based functional groups and electrolyte penetration into graphene leads to SEI formation in nanocavities/defects of graphene and hence gives rise to the high irreversible capacity.[429–433] Graphene can produce high specific Li-storage capacity, but the lack of a distinct discharge plateau, high discharge potential, large first cycle capacity loss due to high graphene surface reactivity, high cost of graphene, and low packing density may limit their applications as anodes for Li-ion batteries. In addition, single sheets of graphene with defects are quite reactive which can contribute to electrolyte decomposition and reaction leading to SEI formation after the first cycle. More works and new strategies are required to help make graphene an ideal and practical anode material for Li-ion batteries.

Recent research studies show that Li ions are difficult to stabilize and diffuse in the pure graphene without defects. The performance of pure graphene-based electrodes normally suffers from severe graphene aggregation, which would inevitably hinder inferior ionic accessibility.[429,434–437] Therefore, a better design of a graphene electrode material is essential to further boost the performance of graphene in Li-ion batteries.[429,434–437] Nowadays, researchers focus on the fabrication of high performance anode materials comprising of porous graphene, doped graphene and graphene/electrochemically active material-based nanocomposites for Li-ion battery anodes.

4.1.2. Porous Graphene

Compared with pure graphene sheet, porous graphene has a larger specific surface area and a larger number of additional defects, which increases the number of electrochemically active Li-storage sites.[231,438–441] In addition, porous graphene with well-defined pores can further accelerate the Li-ion diffusion kinetics and minimize the Li-ion insertion/extraction distance because of the interconnected channels that connect the interior active sites.[231,438–441] It was reported that the specific capacities of these 2D porous graphene nanosheets can reach an extraordinary high level, e.g., 1040 mAh g^{-1} at 100 mA g^{-1} and 255 mAh g^{-1} at 5 A g^{-1}.[439] Another reported 3D hierarchical porous graphene aerogel with tunable mesopores on graphene nanosheets exhibited superior electrochemical performance including a high reversible specific capacity of 1100 mAh g^{-1} at a current density of 0.1 A g^{-1}, outstanding cycling stability and excellent rate performance. Even at a large current density of 20 A g^{-1}, the reversible capacity was approximately 300 mAh g^{-1}, which is larger than many porous carbon-based anodes reported elsewhere.[434] However, the outstanding electrochemical performance of porous graphene still suffers from possible aggregation and the restacking of individual graphene nanosheets.

4.1.3. Heteroatom-Doped Graphene-Based Anodes

N-doped graphene (N-graphene),[435,442–444] B-doped graphene (B-graphene),[442] P-doped graphene (P-graphene),[445] and S-doped graphene (S-graphene)[446] can also lead to improved performance when used as anodes for Li-ion batteries. For example, the reversible discharge capacity of N-graphene is almost double compared to the pristine graphene due to the additional surface and structural defects induced by N-doping.[435] Long-term cycling of N-graphene delivered a specific capacity of 684 mAh g^{-1} after 500 cycles, indicating both higher capacity and excellent capacity retention are possible.[443] A higher rate testing showed that N-graphene and B-graphene delivered capacities of about 199 and 235 mAh g^{-1} at 25 A g^{-1}, respectively.[442] P-graphene also exhibit significantly enhanced electrochemial properties in comparison to undoped one. The reversible capacity can be more than 460 mAh g^{-1} (this value is about 280 mAh g^{-1} for undoped graphene) for over 80 cycles along with excellent rate capability.[445] The effects of S doping on the electrochemical properties of graphene for use as Li-ion battery anodes were also studied. S doping in graphene contributes to the high specific capacity by providing more Li storage

sites due to the Faradaic reactions and improved electrical conductivity. In addition, good cyclic stability of S-graphene is maintained even after 500 cycles at a high current rate of 4C.[446] P and N dual-doped porous graphene were also reported as anode for Li-ion batteries. The fabricated electrode exhibited high reversible capacity (2250 mAh g^{-1} at 50 mA g^{-1}, excellent rate capability (750 mAh g^{-1} at 1000 mA g^{-1}), and satisfactory cycling stability (>1500 cycles), which are much better compared to the undoped graphene.[447] The excellent electrochemical performance of doped graphene could be attributed to the doping induced surface disorders, defects, increased electronic conductivity and increased interplanar distance which lead to fast ion/electron transports. Recently, Wang and co-workers constructed a highly conductive network, hierarchically porous graphene electrode doped with heteroatom.[436] The novel electrodes delivered high energy density and power density of 322 Wh kg^{-1} and 116 kW kg^{-1}, respectively, at a high current density of 80 A g^{-1}. Furthermore, the optimized electrodes exhibited long-cycling capability with nearly no capacity loss for 3000 cycles.[436] This strategy provided a couple of advantages, such as the porous structure can accommodate more Li ions, hierarchical designing can overcome the problem of graphene sheet aggregation and the large interfacial resistance of loosely stacked graphene sheets. In addition, the doping of heteroatoms can improve the ability of graphene to intercalate more Li ions, enhance the conductivity of graphene, and facilitate the transport of electrons and Li-ions.

4.1.4. Graphene Paste

A Li-ion battery provides capacities through Li intercalation with an active electrode material, and therefore, its high-rate performance is largely governed by Li^+ diffusivity and electron conductivity.[448–450] However, using a traditional procedure to prepare the electrode usually leads to a low electrical conductivity caused by many factors such as the poor contact resistances by random pore structures, poor adhesion to the current collector, etc. This can result in poor rate capabilities for practical Li-ion battery applications.[448–450] Recently, N- and B-doped graphene pastes with conductive binders were reported to have ultrahigh electrical conductivity, leading to a good rate capability of ≈178 mAh g^{-1} at 5.4C when used as Li-ion battery anodes.[442] In another study, the use of photoflash and laser-reduced free-standing graphene paper-based anodes with micrometer-scale pores, cracks, and intersheet voids facilitated efficient Li ions intercalation kinetics even at ultrafast charge/discharge rates of more than 100C.[451] This photothermally reduced graphene anode delivered a steady capacity of ≈156 mAh g^{-1} over 1000 cycles at high rates of ≈40C.[451] More recently, a reported monolithically structured rGO anode, prepared from a conductive rGO paste, delivered outstanding cycling stability and ultrahigh reversible capacity at ultrafast charge/discharge rates.[450] These excellent electrochemical performance could be attributed to the numerous large surface areas and the open pores that facilitated the Li ion diffusion and decreased the contact resistance between the graphene layers in the 3D structure.[450] The excellent electrochemical properties reported in this study on the graphene paste-based anodes are novel and very promising. The graphene paste anode is considered as a good candidate for future development needed to design ultrafast, high energy/power Li-ion battery anodes for practical applications.

4.1.5. Different Types of Graphene Nanocomposite-Based Anodes

Graphene has also been used to anchor electrochemically active transition metal oxides (TiO_2,[67,452–455] SnO_2,[68,456–460] Fe_3O_4,[461,462] Co_3O_4,[463–465] Fe_2O_3,[466–468] FeO,[469] Mn_3O_4,[65,470] MnO_2,[471,472] MnO,[473–475] CuO,[476–478] NiO,[479–481] NiO/SiO_2,[482] MoO_2,[483] CoO,[484] SiO_2,[485] $ZnCo_2O_4$,[423,486,487] CeO_2,[488] Cr_2O_3,[489] etc.), transition metal sulfides (MoS_2,[490–492] SnS_2,[493–496] CoS,[497] FeS,[498] Co_3S_4,[499] and NiS,[500,501] etc.), transition metal nitrides (FeN,[502] CoN,[502] NiN,[502] TiN,[503,504] VN,[505] etc.), transition metal phosphide (Co_2P,[506] CoP,[507] Ni_2P,[508,509] etc.), elements with alloying/dealloying mechanism, such as semiconductors, metals, and other elements (Si,[510–516] Ge,[517,518] Sn,[519–522] Sn-Sb,[523,524] P,[525] etc.) and others,[526] to fabricate graphene-based nanocomposite anodes for Li-ion batteries with improved performance.

The improvement in electrochemcial performance of graphene-based nanocomposites can be ascribed to three factors: (i) Flexible graphene layers suppress the large volume expansion of these electrochemically active materials during continuous charge/discharge processes and alleviate the aggregation/pulverization problems; (ii) graphene has excellent electrical conductivity ensuring good electrical contact between adjacent heterogeneous particles. As mentioned earlier, graphene has high surface area, surface defects and high porosity giving rise to high Li storage capability, enhanced electrolyte accessibility and rapid Li-ion diffusion; and (iii) confining electrochemically active nanoparticles between graphene layers can mitigate the restacking of graphene sheets and consequently keep their high surface area activity. These synergistic effects of both graphene and nanoparticles can combine the best merits of both materials. **Table 2** summarizes more of the various types of graphene-based nanocomposites for Li-ion battery anodes.

Graphene/Transmission Metal Oxide Nanocomposite-Based Anodes: Paek et al. synthesized SnO_2–graphene nanocomposites by introducing SnO_2 nanoparticles into graphene nanosheets.[456] The graphene nanocomposite-based anodes exhibited a high reversible capacity of 810 mAh g^{-1} at 50 Ma g^{-1} and relatively good capacity retention of 70% for over 30 cycles (570 mAh g^{-1}). Wang et al. used anionic sulfate surfactants to stabilize functionalized graphene sheets (FGS) and facilitate in situ growth of rutile and anatase TiO_2 on graphene surface (**Figure 10**a).[67] Amphiphilic surfactant plays an important role in interacting with both FGS and Ti oxide precursors, leading to the formation of homogeneously dispersed nanostructured TiO_2 on FGS surfaces.[67] Rutile phase TiO_2–FGS consist of oriented rod-like TiO_2 architectures randomly coated on FGS and parallel to the FGS surface (Figure 10b),[67] while anatase TiO_2–FGS composites with 5 nm spherical nanocrystallites homogeneously spread on FGS (Figure 10c).[67] Both nanocomposites showed enhanced Li-ion insertion/extraction kinetics, especially at high current rates, which can be attributed to the increased electrical conductivity (Figure 10d,e).[67] In addition, TiO_2–FGS

Table 2. Examples of different graphene-based nanocomposites for Li-ion batteries reported in the literature.

Materials	Electrochemical performance
Graphene/SnO_2[527]	The initial discharge capacity is 1996 mAh g^{-1} at the current density of 1 A g^{-1}, the reversible discharge capacity can remained at 1545.7 mAh g^{-1} at 40 cycles
Graphene/SnO_2[528]	The reversible discharge capacity is 1027 mAh g^{-1} at 0.1 A g^{-1} after 165 cycles, cycle life is > 600 cycles
Graphene/Co_3O_4[529]	A capacity of 910 mAh g^{-1} is retained after 100 cycles
Co_3O_4/rGO[530]	The discharge capacity is 860 mAh g^{-1} after 120th cycle at 40 mA g^{-1} current density
Graphene/Fe_3O_4[531]	The capacity is 785 mAh g^{-1} at 1C rate, the cycle life is > 500 cycles, the rate performance is good even at 60C
Graphene/Fe_3O_4[532]	The discharge capacity is 1148 mAh g^{-1} after 50 cycles at 0.2C
Graphene/Fe_2O_3[533]	The capacities are 946 and 634 mAh g^{-1} at a current density of 200 and 2000 mAg^{-1}, respectively, the cycle life is > 450 cycles
Fe_2O_3–graphene sheet-on-sheet sandwich-like nanocomposites[534]	The reversible capacity is 662.4 mAh g^{-1} at 1000 mA g^{-1}, the cycle life is > 100 cycles
Mn_3O_4/N-doped graphene[535]	The reversible capacity is 828 mAh g^{-1}after 40 cycles
Graphene/MnO[536]	The reversible capacity is 2014.1 mAh g^{-1} after 150 cycles at 200 mA g^{-1}, the cycle life is > 400 cycles
Graphene/MnO[537]	The initial charge capacity is 747 mAh g^{-1}, the cycle life is >100 cycles
Graphene/NiO[538]	The capacity is 646, 509, 369 mAh g^{-1} after 35 cycles at a current densities of 100, 400 and 800 mA g^{-1}, respectively
rGO/NiO[539]	The initial discharge capacity is 845 mAh g^{-1}, after 300 cycles

anodes used in conjunction with $LiFePO_4$ cathodes delivered a high capacity of about 170 mAh g^{-1} along with excellent capacity stability.[453]

Although metal oxides show huge improvements in capacities, they have high volume changes during the charge–discharge processes. This can lead to the development of high residual stresses and hence causing mechanical problems at the interface of metal oxides and graphene, which can ultimately cause their detachment from the surface leading to poor cyclability and total failure.

Wang et al. also adopted a ternary self-assembly approach to fabricate ordered transition metal oxide-FGS nanocomposites (**Figure 11**).[68] Anionic surfactants lead to the dispersion of hydrophobic domains on the FGS surface. Surfactant micelles along with the FGS are the fundamental building blocks which bind to the metal cations, forming ordered nanocomposites. The final structure consists of crystallized metal oxides between FGS, which upon self-assembly form multilayered nanostructures. Alternatively, metal cations can self-assemble into hexagonal mesophases on the FGS surface if using a nonionic block copolymer surfactant. SnO_2–FGSs nanocomposites synthesized using the above technique form freestanding, robust films after vacuum filtration.[68] SEM images in Figure 11a,b of a polished cross-section reveals parallel, layered architectures, while cross-sectional TEM in Figure 11c–g shows alternating layers of nanocrystalline SnO_2 and FGSs spanning the entire film.[68] SnO_2–FGS nanocomposite electrodes without binders and current collectors showed extraordinary charge/discharge reversibility and excellent cycle performance as anodes for rechargeable Li-ion batteries (Figure 11h).[68] FGS decorated with SnO_2 through thermal annealing showed a large reversible specific capacity of ≈1026 mAh g^{-1} after 30 cycles at 35 mA g^{-1} current density and 580 mAh g^{-1} after 100 cycles at 700 mA g^{-1} current density (Figure 11i).[68] In another study, Ji et al. synthesized Fe_3O_4 nanoparticles/rGO using chemical co-precipitation and subsequent high temperature reduction processes.[540] The as-synthesized material showed homogeneity of Fe_3O_4 nanoparticles on rGO surfaces with a reversible capacity 2.5 times that of graphite and enhanced reversible capacity of ≈200 mAh g^{-1} at a 10C rate (9260 mA g^{-1}). Most importantly, full cells assembled using these novel nanostructures as anodes and $LiNi_{1/3}Mn_{1/3}Co_{1/3}O_2$ as cathodes showed exceptional capacity retention at various current rates. Results reported by Zhang et al. on graphene–Fe_3O_4 nanocomposite anode delivered a high reversible specific capacity exceeding 1000 mAh g^{-1} at 90 mA g^{-1} and remained at 704 mAh g^{-1} at 2700 mA g^{-1}, with excellent rate capability and improved cycle stability.[541]

N-graphene–transition metal oxide nanocomposites, such as N-graphene–SnO_2,[542] N-graphene–Fe_2O_3,[543] N-graphene–MnO,[544] were also reported as promising anodes with high specific capacity, high rate capability, and excellent cycling stability. Zhou and co-workers synthesized N-graphene/SnO_2 nanocomposites that delivered high reversible capacity and good cycle performance due to the fact that the SnO_2 nanoparticles were pinned on the graphene sheets by Sn-N-C bonds which prevented the aggregation of SnO_2 nanoparticles.[545] The N-graphene provided an undisturbed supply of the electrons that enhanced the conductivity and stabilized the reversible storage process of Li-ion.[546–548] In fact, the use of nanoscale materials with graphene shows high capacity retention. However, the high surface areas of graphene can also lead to SEI formation with high irreversible capacities. Therefore, more work is needed to design the materials at a large scale with the aim to overcome this particular challenge.

Graphene/Transmission Metal Sulfide Nanocomposite-Based Anodes: Anodes prepared from graphene with transitional metal sulfides also show good electrochemcial performance. Transitional metal sulfides are considered as promising anode materials for Li-ion batteries due to their high theoretical capacities, low cost, and ease of availability. However, capacity fading, low conductivity, and poor cycle performance are drawbacks to their potential applications.[549–552] Recent studies have demonstrated that graphene can enhance the surface area and provide conductive pathways, thereby improving the cycling stability

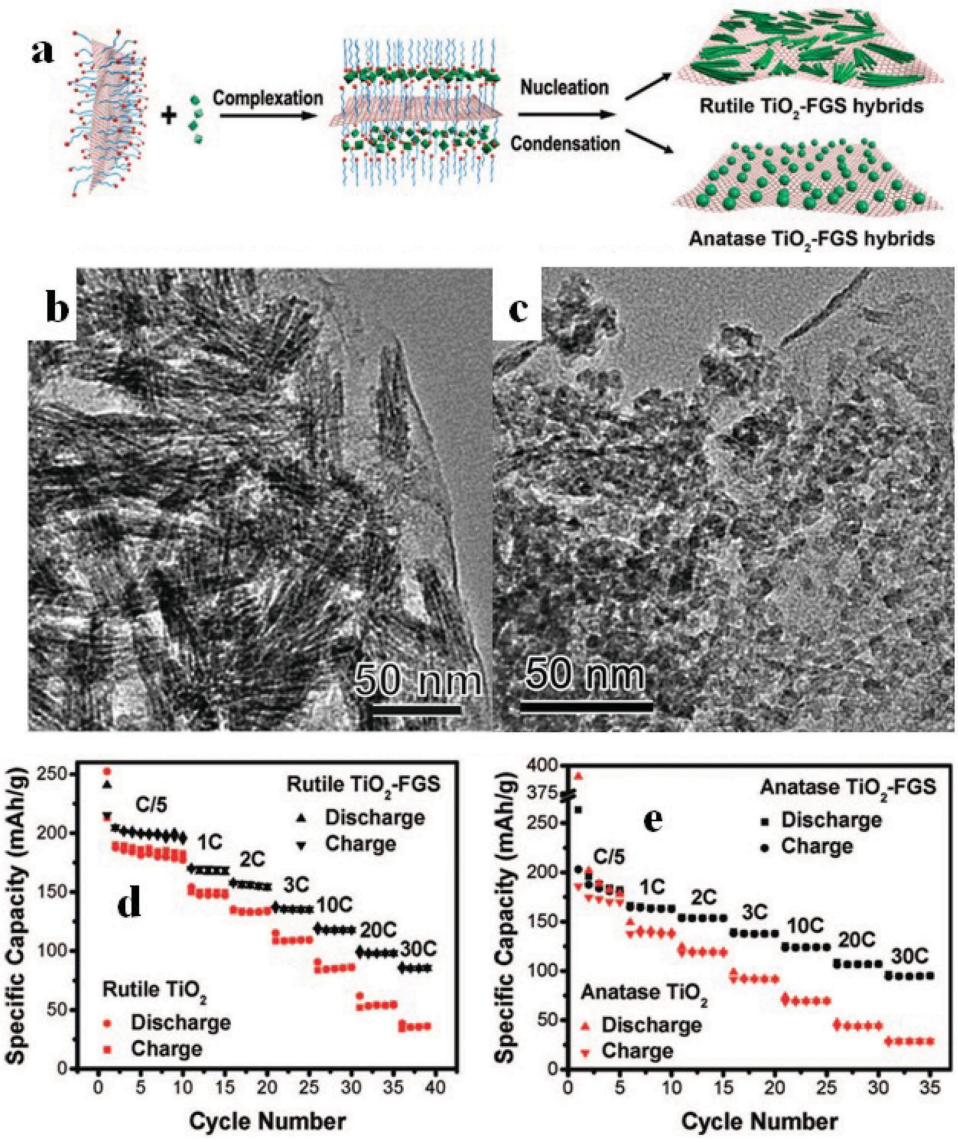

Figure 10. a) A schematic diagram showing the deposition of TiO_2 on functionalized graphene sheets (FGS): Anionic sulfate surfactant mediated stabilization of graphene self-assembly of TiO_2–FGS hybrid nanostructures. TEM image of b) rutile TiO_2–FGS, and c) Anatase TiO_2–FGS. Specific capacity of d) Rutile TiO_2–FGS, and e) Anatase TiO_2–FGS at various charge/discharge rates. Reproduced with permission.[67] Copyright 2009, American Chemical Society.

of the transition metal sulfide-based electrodes.[497,553–555] For example, Chang and co-workers synthesized MoS_2/graphene composites by a one-step in situ solution phase.[490] When assembled as an anode for Li-ion batteries, these composites exhibited improved reversible capacity of 1290 mAh g^{-1} at a current density of 100 mA g^{-1} and the capacity retained up to 50 cycles, which was almost a little more than double for pristine MoS_2 electrode. In addition, the composites exhibited good rate performance where a high specific capacity of 1040 mAh g^{-1} was reported at a high current density of 1000 mA g^{-1}, which is much higher than that for free MoS_2 and graphene.[490] Similarly, the same group also prepared single-layer MoS_2/graphene composites dispersed in amorphous carbon.[556] It was found that the nanocomposites at (1:1) ratio delivered very high reversible capacity of 1116 mAh g^{-1} with excellent cyclic stability and high-rate capability. The superior electrochemical performance of the composites was attributed to their robust composite structure, the synergistic effect between MoS_2 and graphene layers in the nanocomposites as well as the addition of amorphous carbon.

In a work reported by Mahmood and co-workers, the authors were able to synthesize N-doped graphene/Ni_3S_4 nanocomposites for use as anodes in Li-ion batteries (**Figure 12**).[557] The synthetic scheme used is illustrated in Figure 12a, which shows that Ni_3S_4 nanoparticles were anchored by the functional groups on the graphene sheet surface. Further annealing

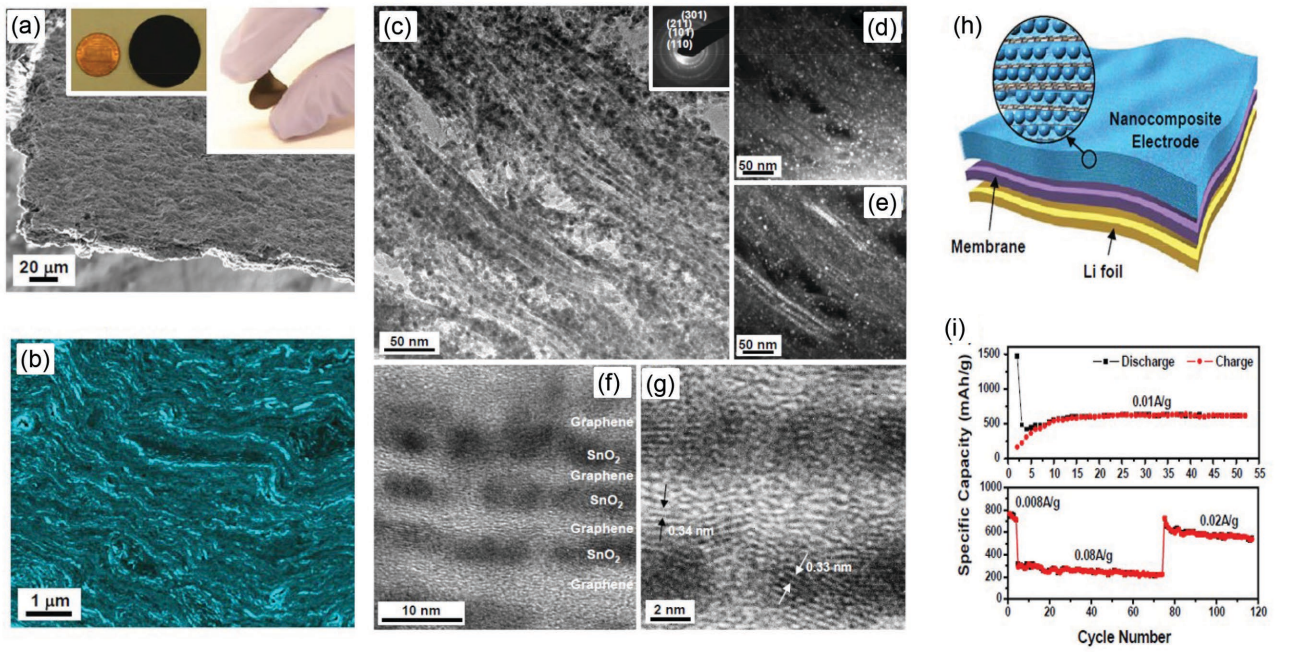

Figure 11. a,b) Self-assembled SnO_2–FGS nanocomposites: a) Side-view of freestanding film. b) Cross-sectional SEM of the layered structure. c) TEM image indicating of layered structure of the hybrid. d) Dark field image showing well-dispersed SnO_2 nanoparticles. e) Cross-sectional dark field image showing both SnO_2 nanoparticles and layered structure; f,g) High-resolution TEM image of the SnO_2–FGS layers with clear marking of both the materials. h) Li-ion cell configuration using freestanding SnO_2–FGS film as anode. i) Cycling life of the cell at 0.01 A g^{-1} (top) and rate capability (bottom). Reproduced with permission.[68] Copyright 2010, American Chemical Society.

at high temperature showed to increase the electrochemical coupling between graphene and Ni_3S_4 nanoparticles. Figure 12b,c shows that these materials can deliver high reversible capacity, stable capacity retention, and excellent rate capability as a result of the synergetic effect of N-doped graphene and Ni_3S_4 nanoparticles.[557]

Graphene/Transmission Metal Nitride Nanocomposite-Based Anodes: Results reported by Yue et al. on the in situ synthesis of graphene/TiN hybrid showed that graphene/TiN hybrid anode delivered a high initial reversible capacity of about 646 mAh g^{-1} at 20 mA g^{-1} with the initial coulomb efficiency of 75%.[503] At a current density of 2000 mA g^{-1}, the hybrid anode still retained a high capacity of more than 320 mAh g^{-1}.[503] The G/TiN hybrids displayed superior electrochemical performance as a result of the highly efficient mixed (electron and Li^+) conducting network. The internal defects between graphene layers, induced by N-doping in graphene/TiN, led to improved reversible Li storage. The catalytic sites on the surface of graphene, that are related to the decomposition of electrolyte, were occupied by TiN, leading to a decreased irreversible capacity. AC impedance also confirmed that both the solid electrolyte interface and charge-transfer resistance were decreased after the anchoring of TiN nanoparticles.[503]

Graphene/Si Nanocomposite-Based Anodes: Si is another promising anode material for rechargeable Li-ion batteries, but it suffers from significant capacity loss due to a 400% volume expansion. To overcome this problem, a 3D graphene scaffold/Si nanocomposite has been designed with a reversible capacity of about 3200 and 1100 mAh g^{-1} at 1 and 8 A g^{-1}. This architecture retained 99.9% of the capacity for over 150 cycles.[558] In another study, Si nanoparticles were wrapped by crumpled graphene using a capillary technique giving rise to capsule architectures. These Si-graphene capsules showed high capacity retention, good cyclic stability, and high columbic efficiencies compared to bare Si nanoparticles (NPs).[559]

Multilayered structures with alternating graphene and Si thin films were also fabricated using liquid-phase exfoliated graphene film and subsequent plasma-enhanced chemical vapor deposition (PECVD) coating of amorphous Si film (**Figure 13**a–c).[512] The multilayered nanocomposite films (Figure 13a) fabricated directly on copper foil showed four times higher than the capacities of graphite even after 30 cycles (Figure 13c).[512] A Si/graphene nanocomposite, with nano-Si particles tightly wrapped and connected by graphene nanosheets, was synthesized using discharge-plasma-assisted milling (P-milling). When used as Li-ion battery anodes, the nanocomposite with 50 wt% Si delivered a discharge capacity of 866 mAh g^{-1} with a coulombic efficiency above 99.0% even after 200 cycles. The capacity loss above 200 cycles was only ≈0.07% per cycle. In addition, this anode was coupled with a $LiMn_2O_4$ cathode to assemble a full coin-type cell, which could cycle with stable capacities at practical working voltages between 3.2 and 4.2 V, indicating that these nanocompsoites are very promising for use in practical applications.[560]

Recently, Son and co-workers directly grew graphene over Si NPs. The graphene layers anchored onto the Si surface accommodated the volume expansion of Si via a sliding process between adjacent graphene layers. When paired with a commercial $LiCoO_2$ cathode, the Si/graphene nanocomposite allowed the full cell to reach volumetric energy densities of 972

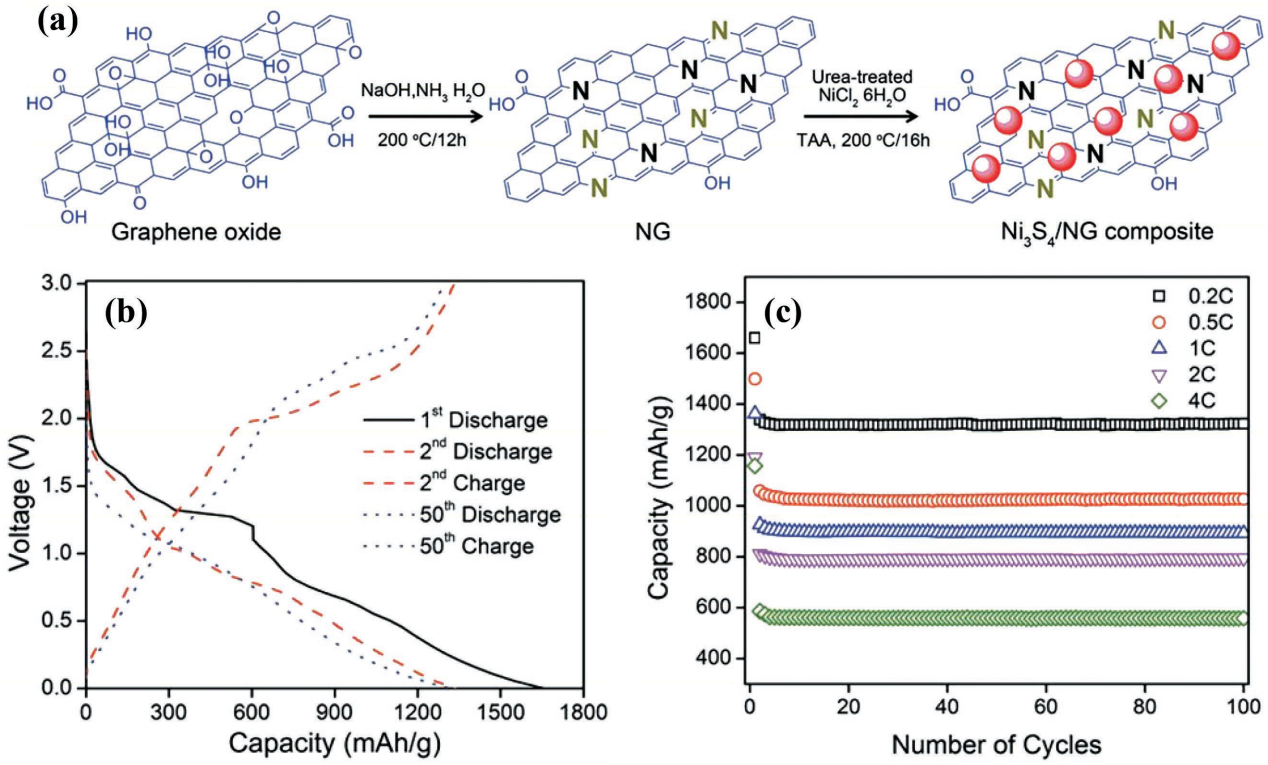

Figure 12. a) A schematic diagram illustrating the preparation of the Ni_3S_4/N-doped graphene nanocomposites. b) Charge–discharge curves of Ni_3S_4/N-doped graphene nanocomposite anodes at 0.2C in the range of 0–3 V. c) Cycle performance of Ni_3S_4/ N-doped graphene nanocomposite anodes at different C rates. Reproduced with permission.[557] Copyright 2013, Wiley.

and 700 Wh L^{-1} at first and 200th cycles, respectively, which are 1.8 and 1.5 times higher than those of current commercial Li-ion batteries.[561] A 3D mesoporous Si@graphene nanocomposites was also synthesized and used as anodes for Li-ion batteries.[562] These materials exhibited superior electrochemical performance including a high specific capacity of 1200 mAh g^{-1} at 1 A g^{-1}, excellent high rate capabilities, and outstanding cyclability. The synergistic effects arising from the combination of mesoporous Si nanospheres and graphene foam nanoarchitectures can prevent the intractable pulverization of Si electrode after repeated charge/discharge cycles.[562]

More recently, the more excellent performance of graphene/Si-based nanocomposites for Li-ion battery anodes was also reported by Cho and co-workers (**Figure 14**).[563] In this novel design, island-shaped amorphous Si nanoparticles with <10 nm size were strongly anchored and well distributed over the entire graphene backbone (a-SBG). The Si nanoparticels effectively relieved the induced strain and stress and prevented the interference between adjacent particles during the volume expansion due to the existence of the graphene phase in the nanocomposite. In addition, the highly flexible graphene yielded a synergetic elastic behavior and provided an unprecedented decrease in electrode thickness after cycling as a result of self-compacting (Figure 14a).[563] Hence, the novel nanocomposite-based electrodes exhibited outstanding merits in mitigating the detrimental effects of the Si volume changes and improving electronic conductivity, charge transfer and Li-ion diffusion. As a result, a high specific reversible capacity (>1000 mAh g^{-1} at 14 A g^{-1}), excellent power capability and extraordinary cycling stability for more than 1000 cycles were achieved (Figure 14b–d).[563]

Si has a volume expansion of 300%–400%, which can lead to the development of residual stress/strain at the interface and eventually contact problems with graphene. The high volume change can also lead to continuous formation/degradation of the SEI layer, which can cause the solvent in the electrolyte to be totally consumed before the materials start degrading. These are some of the challenges that still need to be addressed for these graphene/Si-based nanocomposites.

Graphene/Sn Nanocomposite-Based Anodes: Sn is another important and promising anode materials for Li-ion batteries with high theoretical capacity (≈1000 mAh g^{-1}) owing to the Li alloy formation. Similar to Si, the practical application of Sn-based anodes is hampered by its poor cyclability because of the huge volume changes. The incorporation of graphene can effectively accommodate the volume change of Sn and thus improve its cycling performance. Recently, Ji et al. fabricated graphene/Sn-nanopillar multilayered anodes for Li-ion batteries (Figure 13b).[519] The rationale for this sandwich design was to provide ample spaces to accommodate Sn volume changes during continued alloying/dealloying processes and to enhance Li-ion insertion by allowing easy electrolyte penetration and hence, reducing internal resistance. High electrical conductivity of both graphene and Sn along with distinctive structures offer fast reaction kinetics and short diffusion pathways for efficient Li^+ and e^- transfers.

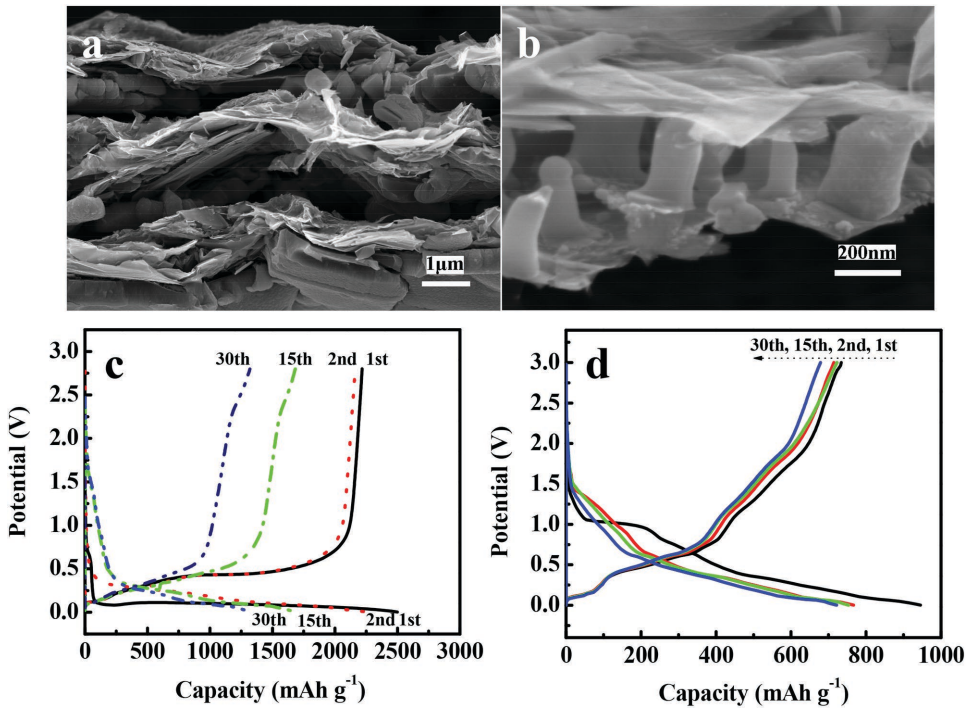

Figure 13. a,b) The morphology of cross-sectional SEM images of: a) Multilayered graphene/Si, and b) Graphene/Sn-nanopillar/graphene multilayer nanostructure. c,d) The corresponding galvanostatic charge/discharge profiles of: c) Five-layer graphene/Si multilayer structures at 100 mA g^{-1} current density between 2.8 V to 0.002 V, and d) Graphene/Sn nanopillars structures at 50 mA g^{-1} current density between 3.0 V to 0.002 V. Panels a,c) reproduced with permission.[512] Copyright 2012, Elsevier. Panel b,d) reproduced with permission.[519] Copyright 2011, Royal Society of Chemistry.

The use of polymer binders and conductive additives can also be avoided in these integrated electrodes, which improve the overall energy density of the batteries (Figure 13d). Wang and co-workers synthesized a novel Sn nanoparticle-decorated 3D foothill-like graphene architecture as Li-ion battery anode.[564] Electrochemical measurements demonstrated that the 3D Sn–graphene anode delivered a reversible capacity of 466 mAh g^{-1} at a current density of 879 mA g^{-1} after over 4000 cycles and 794 mAh g^{-1} at a current density of 293 mA g^{-1} after 400 cycles. The capacity at a current density of 293 mA g^{-1} was 200% higher than that of conventional graphite anodes, suggesting that the 3D Sn–graphene structure enabled a significant improvement in the overall performance of a Li-ion battery in terms of capacity, cycle life, and rate capacity.[564] Similarly, Qin et al. investigated Sn@graphene core–shell structures for Li-ion batteries anodes. This 3D hybrid anode exhibited very high rate performance (1022 mAh g^{-1} at 0.2C, 780 mAh g^{-1} at 1C, 459 mAh g^{-1} at 5C, and 270 mAh g^{-1} at 10C where 1C = 1 A g^{-1}) and extremely long cycling stability even at high rates (a high capacity of 682 mAh g^{-1} was achieved at 2C with a capacity retention of 96.3% after 1000 cycles).[565] Other various novel structures, including Sn-based nanoparticles encapsulated in a porous 3D graphene network,[566] 3D hollow Sn@C-graphene hybrids,[567] hierarchical Sn@ foam-like graphene composite,[568] and graphene-Sn/SnO_2-based nanocomposites,[569] etc., have also been reported to show improved electrochemical performance due to compensating for the volume expansion of graphene phase during long-term cycling.

Graphene/Ge, Sb, P Nanocomposite-Based Anodes: In addition to Si and Sn, other alloying–dealloying reaction mechanism-based elements such as Ge,[570–572] Sb,[573,574] P,[525] have also been combined with graphene to fabricate novel graphene-based nanocomposite-based anodes with improved performance for Li-ion batteries. The graphene phase can effectively accommodate the volume expansion of these inorganic nanomaterials, leading to markedly improved cycle performance and rate capability. For example, a first discharge capacity of 1034 mA g^{-1} was obtained for graphene-/Sb-based nanocomposites.[573] A designed Ge/graphene/CNT composite electrode exhibited outstanding energy capacity up to 863.8 mAh g^{-1} at a current density of 100 mA g^{-1} after 100 cycles and good rate performance at a current density up to 3200 mA g^{-1}.[575] A carbon-coated Ge nanoparticles/rGO sandwich structures exhibited superior performance with a capacity of 1332 mAh g^{-1} at 0.2C and with a high-rate capability over hundreds of cycles.[571] A red P-graphene nanosheet hybrid anode material for Li-ion batteries delivered a high gravimetric specific capacity of 2362 mAh g^{-1}, based on mass of P, and excellent capacity retention within 300 cycles.[525]

4.2. Cathodes

Commercially available Li-ion battery cathodes are almost exclusively limited to "lithiated transition metal oxides" such as $LiCoO_2$, $LiNiO_2$, $LiMn_2O_4$, mixed metal oxides with spinel structure and polyanion materials with olivine structure such

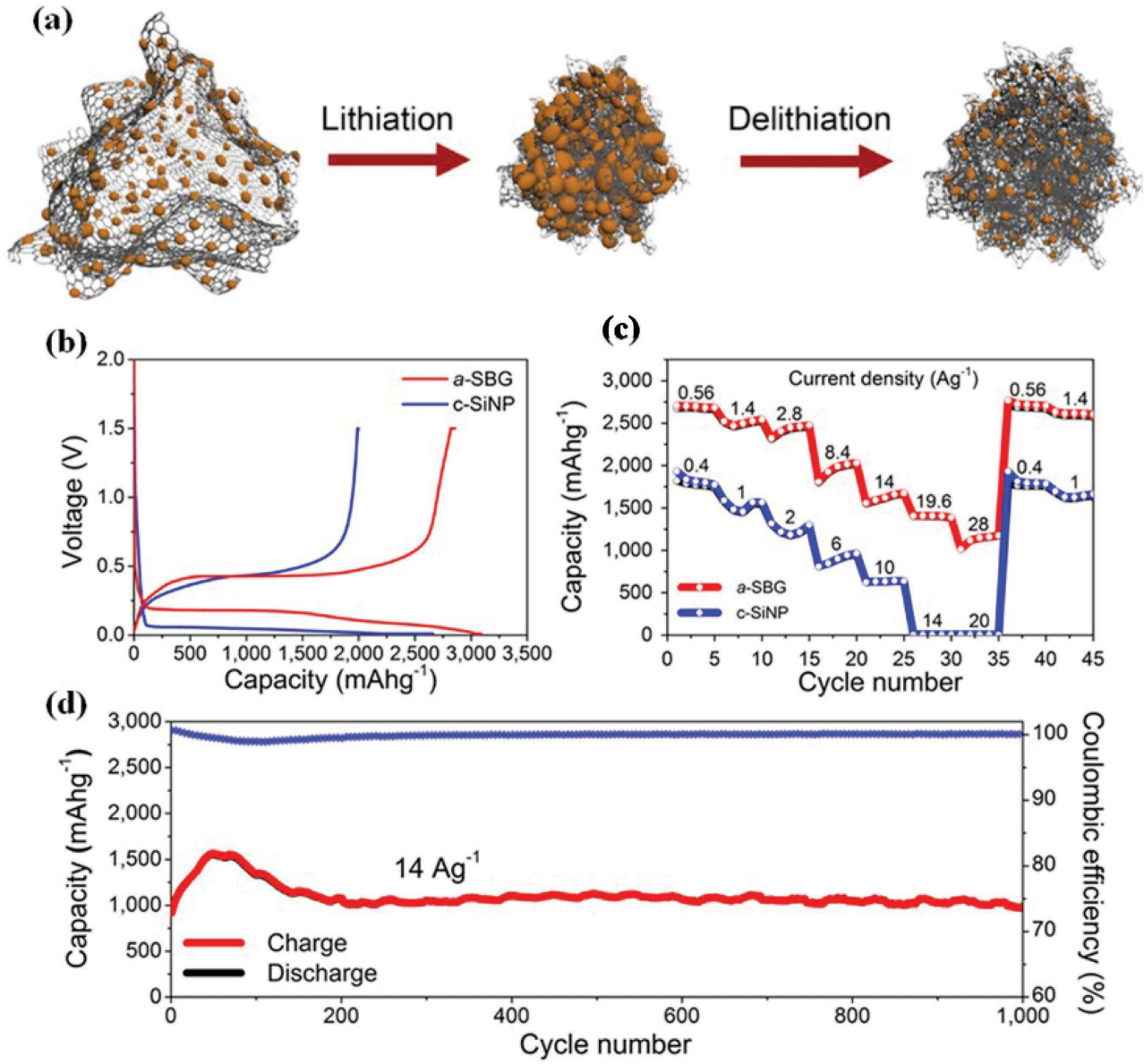

Figure 14. a) A Schematic diagram of amorphous Si nanoparticles backbonded-graphene (a-SBG) nanocomposite anode before and after electrochemical cycling. b) Galvanostatic charge/discharge profiles of a-SBG and crystalline Si nanopowder (c-SiNP) electrodes at a current density of 56 mA g^{-1} in the potential range of 1.5–0.01 V. c) Typical Capacities of a-SBG and c-SiNP anodes at various charge current densities from 0.56 to 28 A g^{-1} for a-SBG and from 0.4 to 20 A g^{-1} for c-SiNP, respectively. d) Cycling performance of the a-SBG nanocomposite electrode at a charge current density of 14 A g^{-1} and a discharge density of 2.8 A g^{-1} over 1000 cycles. Reproduced with permission.[563] Copyright 2014, American Chemical Society.

as $LiFePO_4$ and V_2O_5.[576–581] The practical limitations of these cathodes are their slow process kinetics due to slow Li-ion and electron diffusion and severe structural degradation during continuous charge/discharge processes. Hence, a considerable attention has been focused on graphene-based conductive and flexible nanocomposites to alleviate the stress/strain, improve the electrical conductivity and preserve material integrity.[582,583]

Graphene has been widely used to improve the electrochemcial properties of $LiFePO_4$ cathode for Li-ion batteries.[584–586] For example, graphene nanosheets were used as additives to prepare spherical $LiFePO_4$/graphene composites with ≈100 nm average particle sizes through co-precipitation, which delivered a specific capacity of 160 mAh g^{-1} at 0.2C and improved cycling stability.[587] Graphene/$LiFePO_4$ nanocomposites were synthesized via spray-drying in which $LiFePO_4$ primary nanoparticles were embedded in spherical micron-sized secondary particles with homogeneous graphene wrapping giving rise to 3D networks. This architecture facilitates electron diffusion throughout the secondary particles, while Li-ions occupy the abundant voids between $LiFePO_4$ nanoparticles and graphene sheets. As a result, the nanocomposites showed a capacity of 70 mAh g^{-1} even at 60C discharge rate. When cycled at

10C charge and 20C discharge rates for 1000 cycles, the capacity decay was only ≈15%.[588] Nanosized $LiMn_2O_4$ spinel/rGO hybrid cathode was also synthesized via a microwave-assisted hydrothermal reaction with nanosized $LiMn_2O_4$ particles evenly dispersed on rGO template without agglomeration. The inherent high active surface area of $LiMn_2O_4$ nanoparticles in the hybrid cathode to play a vital role in faster Li-ion diffusion as was reported based on the CV data.[589]

In a work reported by Wang et al., single-crystal $LiMn_{0.75}Fe_{0.25}PO_4$ nanorods@rGO nanocomposites were synthesized through hydrothermal reactions with a $LiMn_{0.75}Fe_{0.25}PO_4$ nanorod length of 50–100 nm and diameter of 20–30 nm (**Figure 15**a,b).[66] These $LiMn_{0.75}Fe_{0.25}PO_4$@rGO nanocomposites exhibited excellent capacity retention for more than 100 cycles at 0.5C (Figure 15c). In addition, these materials displayed high reversible capacities of about 153, 132, 107, 65 mAh g^{-1} even at high discharge rates of 2C, 20C, 50C, and 100C, respectively, indicating excellent rate capability (Figure 15d).

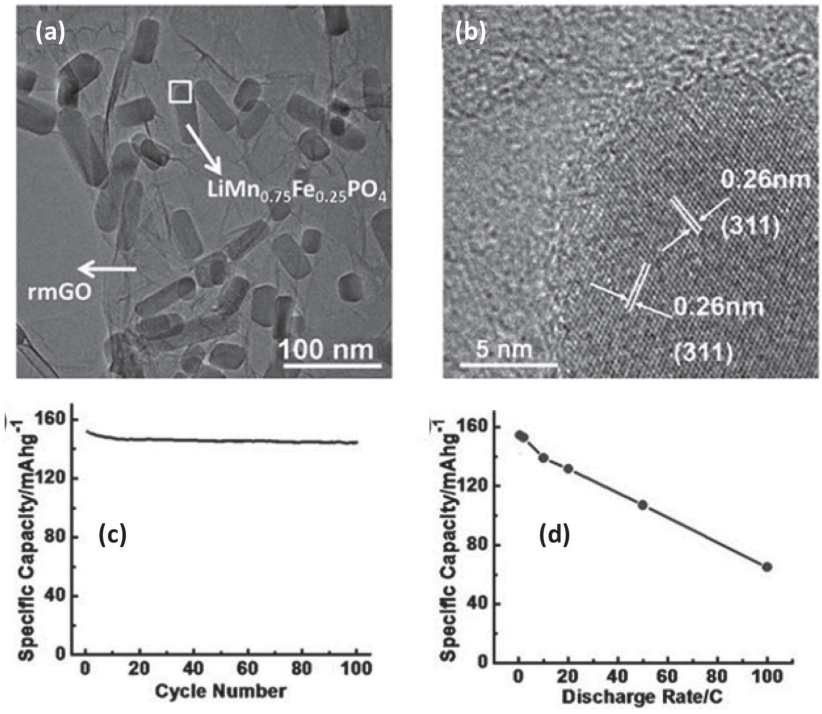

Figure 15. a) TEM image, and b) HRTEM image of the $LiMn_{0.75}Fe_{0.25}PO_4$ nanorods on rGO. c) Cycle performance at 0.5C rate (1C = 170 mA g^{-1}), and d) Rate capability of $LiMn_{0.75}Fe_{0.25}PO_4$-rGO nanocomposite-based cathodes in Li-ion batteries. Reproduced with permission.[66] Copyright 2011, Wiley.

Similarly, graphene/$LiMn_2O_4$,[590–592] graphene/$LiMnPO_4$,[593–595] graphene/$Li_3V_2(PO_4)_3$,[596–598] graphene/$Li_3T_2(PO4)_3$,[599] graphene/Li_2FeSiO_4,[600–603] graphene/Li_2MnSiO_4,[604–606] graphene/V_2O_5,[607,608] graphene/$FePO_4$,[609,610] graphene/FeF_3,[611–613] and graphene/$LiNi_{1/3}Co_{1/3}Mn_{1/3}O_2$[614] have been explored as possible cathodes for rechargeable Li-ion batteries. For instance, FeF_3/graphene composites delivered a charge capacity of 155, 113, and 73 mAh g^{-1} at 104, 502, and 1040 mA g^{-1}current density, with stable cyclability for over 100 cycles, which was attributed to the buffering effect and lowered resistance from the graphene.[615]

Liu et al. prepared a novel composite of 1D single-crystalline V_2O_5 nanowires/graphene nanocomposites through a green approach as described in **Figure 16**a.[608] In such a hybrid structure, the simultaneous assembly of V_2O_5 nanowires can helped prevent the restacking of graphene layer. While the presence of graphene with a high electrical conductivity is beneficial to the electron transport, in that, once the electrons reach the graphene, they can quickly access the V_2O_5 nanowire active materials (Figure 16b).[608] Because of these unique properties, these assembled nanostructure hybrids exhibited excellent performance as Li-ion battery cathodes.

It should be mentioned here that although the use of graphene enhances the electrochemical properties of Li-ion battery systems, the rates are still limited to mobile applications and require further advances for vehicular applications. Moreover, the synthesis of these nanocomposites does require unique processing techniques and significant graphene percentages, which drive up the cost of fabrication. The challenges that need to be addressed here are the large electrolyte uptake resulting from the graphene porosity and the first cycle reversible capacity losses caused by the SEI formation. The primary design goal is to use low graphene amounts to minimize the problems mentioned above. In addition, architectures where graphene is not exposed to the electrolyte can be developed to prevent these problems but this requires significant efforts in terms of synthesis.

Polymer/graphene nanocomposites have attracted great interest as cathode materials since polymers are sustainable, environmentally benign ("green" cathodes), have inherently faster kinetics and an electrochemically stable backbone, and can be paired with electrochemically active functional groups.[60,616,617] Specifically, researchers have focused on poly(anthraquinonyl sulfide) and polyimide composites with graphene using in situ polymerization.[60] The homogeneous dispersion of graphene sheets in the polymer matrix is evident in **Figure 17**a,b,[60] and their ultrafast charge/discharge kinetics of up to 100C with a capacity retention of 100 mAh g^{-1} is evident in Figure 17c,d.[60] However, polymer-based cathodes suffer from two major problems: (i) The inherent low specific capacity which will be even lower on mixing with graphene; and (ii) the low electrode potential (compared to traditional inorganic cathodes). These problems reduce the overall electrochemical performance the batteries (e.g., specific energy, energy density, and power density), limiting their practical applications.

Current Li-ion batteries using graphene or graphene-based nanocomposites as electrodes still operate on traditional faradaic reactions with higher energy density than supercapacitors but suffer from slow solid-state Li diffusion, leading to limited power density. Hence, a novel material and/or electrode design

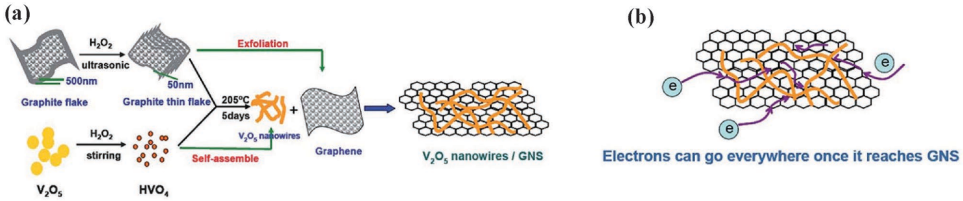

Figure 16. a) An illustration of the synthesis routes of V_2O_5–graphene nanocomposites. b) The ideal electron transfer pathway for V_2O_5–graphene nanocomposite-based cathodes in Li-ion batteries. Reproduced with permission.[608] Copyright 2011, Royal Society of Chemistry.

that can be a hybrid of both supercapacitors and Li-ion batteries should be helpful in attaining both high energy and power density.[541,618–621] In this regard, Jang et al. reported a novel strategy to design hybrid devices in which graphene modified electrode surfaces directly contact with electrolyte and can rapidly and reversibly capture Li ions through surface adsorption and/or surface redox reactions.[622] These devices based on randomly selected materials and configurations, delivered a high energy density of 160 Wh kg^{-1}per cell (30 times higher than traditional supercapacitors) and an excellent power density of ≈100 kW kg^{-1} per cell, ≈100 times higher than Li-ion batteries (**Figure 18**),[622] indicating that this new design can combine the advantages of both Li-ion batteries and supercapacitors. The further modifications of this novel design may lead to graphene-based hybrid energy storage devices for practical applications.

Recently, flexible half and full cells were fabricated using a 3D flexible, and conductive interconnected graphene foam as the current collector (**Figure 19**a).[623] $Li_4Ti_5O_{12}$ (LTP) and $LiFePO_4$ (LFP) loaded into the 3D graphene foam as the anode (LTP/GF) (Figure 19b,c) and cathode (LFP/GF), respectively.[623] The full cells were flexible with high capacity retentions for up to 10C for 100 cycles (Figure 19d). Similarly, the half cells retain high capacities up to 200C for 500 cycles (Figure 19e).[623] These architectures with high conductivity, flexibility, porosity and low weight hold great promise for the commercialization of flexible Li-ion batteries with high power density.

Li-ion batteries are now leading the portable electronics market. However, they face an uphill task in storing sufficient energy specifically for the extended driving range required by electric vehicles. Therefore, it is necessary to find alternative energy storage systems with higher energy/power density, which brings up Li-S and Li-air batteries as viable options due to their high theoretical capacity, high specific energy, facile handling/processing, and environmental benignity. However, theses batteries still face many challenges, which will be further discussed in the following sections.

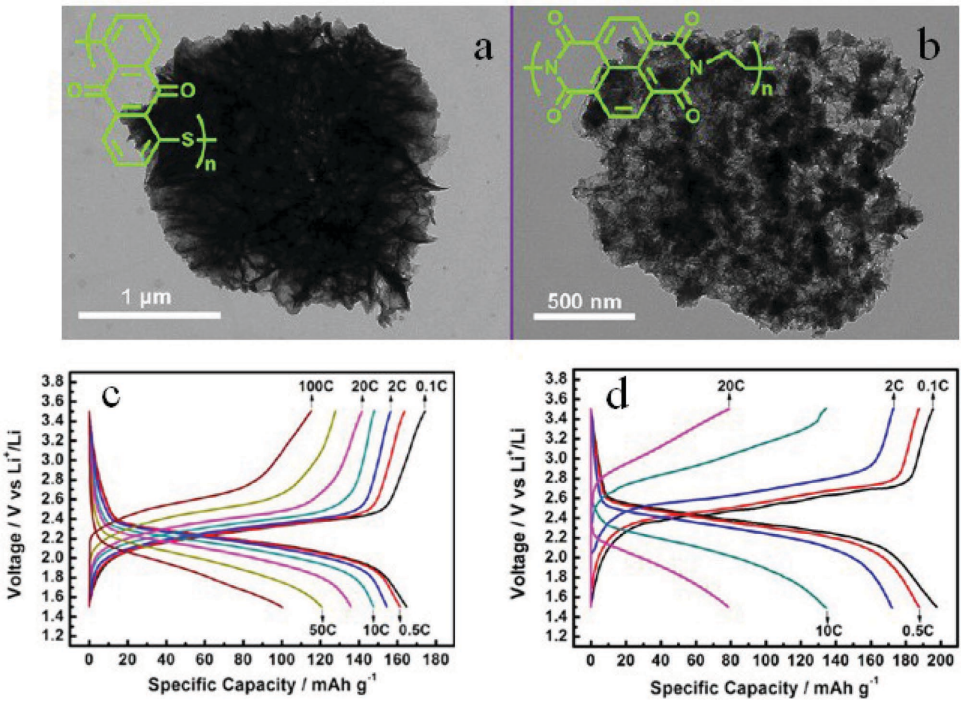

Figure 17. TEM images of: a) Poly(anthraquinonyl sulfide) (PAQS)–FGS, and b) Polyimide (PI)–FGS. The charge/discharge curves of: c) PAQS–FGS, and d) PI–FGS, at various C-rates. Reproduced with permission.[60] Copyright 2012, American Chemical Society.

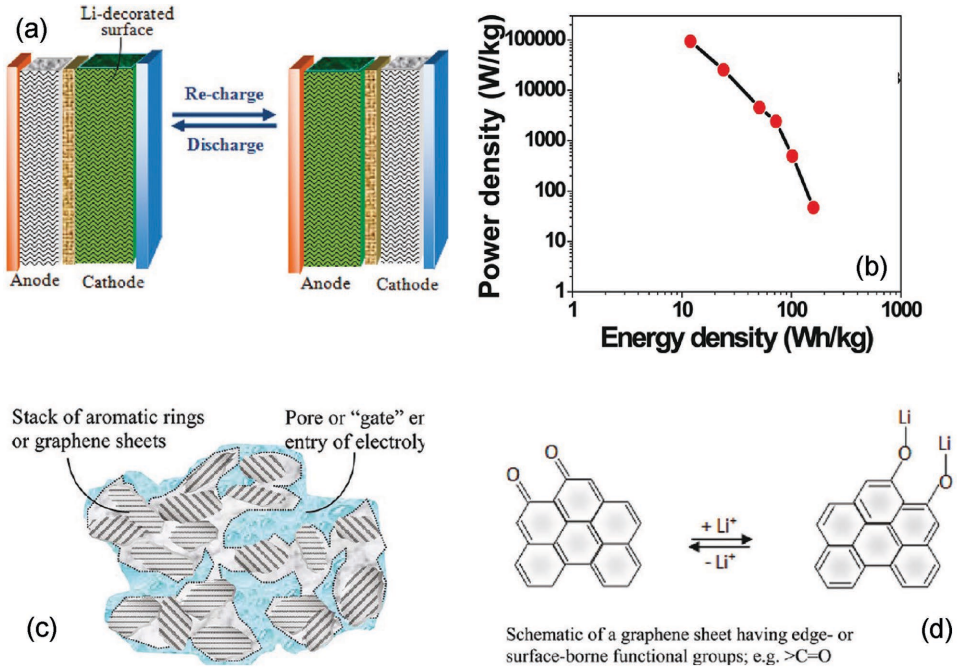

Figure 18. a) The cell structure with massive graphenes on both cathode and anode after the first discharge/charge processes. The graphene surfaces in direct contact with liquid electrolyte are able to rapidly and reversibly capture Li-ions through surface adsorption and/or surface redox reaction, leading to both high energy density (Li-ion batteries) and high power density (supercapacitor). b) Ragone plot of graphene surface-mediated cell. The graphene is from chemically reduced GO. c,d) A schematic drawing of the internal structure of a treated carbon black particle with pores or gates opened structure to provide accessibility to liquid electrolyte in such a manner that the functional groups attached to the edge or surface of graphene sheet can readily reach with Li ions. Reproduced with permission.[622] Copyright 2011, American Chemical Society.

5. Li–S Batteries

The high specific energy of the Li–S chemistry is the direct result of combining two relatively light elements as the primary active materials: a Li metal anode (theoretical specific capacity: 3860 mAh g^{-1}) and an elemental S cathode (theoretical specific capacity: 1675 mAh g^{-1}).[624–635] During the discharging process of the Li–S cell, the anodic reaction (at the negative electrode) is

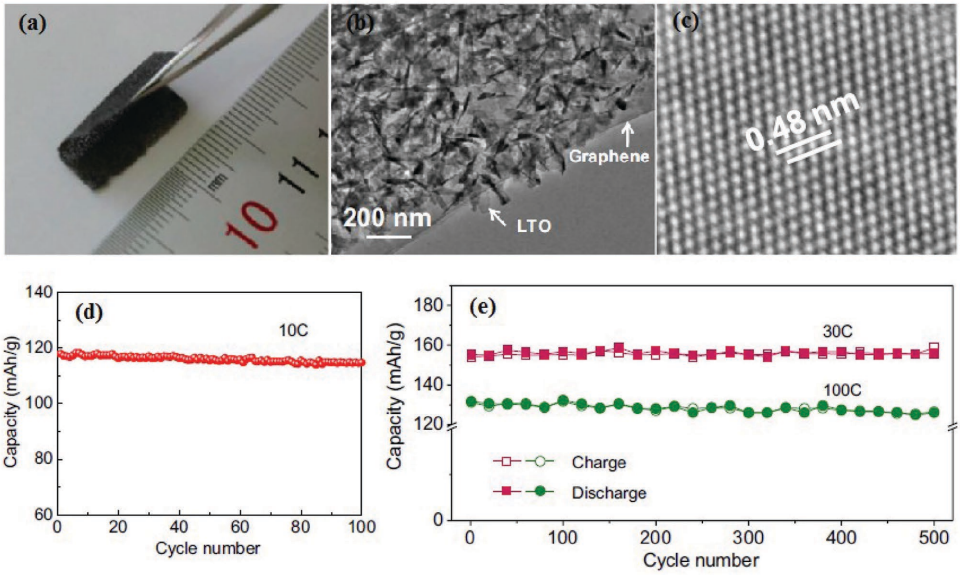

Figure 19. a) Photograph of a freestanding flexible LTO/GF being bent. b) TEM image of the LTO/GF. c) HR-TEM image of an LTO nanosheet showing lattice fringes with a spacing of 0.48 nm. d) Cyclic performance of a flexible LTO/GF//LFP/GF full cell charged/discharged at a constant 10C rate for 100 cycles; and e) Capacities of the LTO/GF charged/discharged at constant 30C and 100C rates for 500 cycles. Reproduced with permission.[623] Copyright 2012, United States National Academy of Sciences.

the oxidation of Li: $Li \rightarrow Li^+ + e^-$ (i), while the cathodic reaction (at the positive electrode) is the reduction of S: $S + 2e^- \rightarrow S^{2-}$ (ii). The overall cell reaction is $2Li + S \rightarrow Li_2S$ (iii). However, elemental S exists as octasulfur (S_8) rings, which adopts a stable orthorhombic crystal structure, so that equation (iii) is modified to: $16Li + S_8 \rightarrow 8Li_2S$ (**Figure 20**).[636]

Assuming an equivalent amount of Li for the negative electrode and S for the positive electrode, a complete reaction of Li and S to form Li_2S with an average discharge potential of 2.2 V per cell. The theoretical specific energy and energy density for Li-S batteries can be as high as 2600 Wh kg^{-1} and 2800 Wh L^{-1}, respectively.[624–635] In addition, S is highly abundant, nontoxic, and environmentally benign.[624–635] Because of these unique properties, Li–S batteries have attracted significant attention.

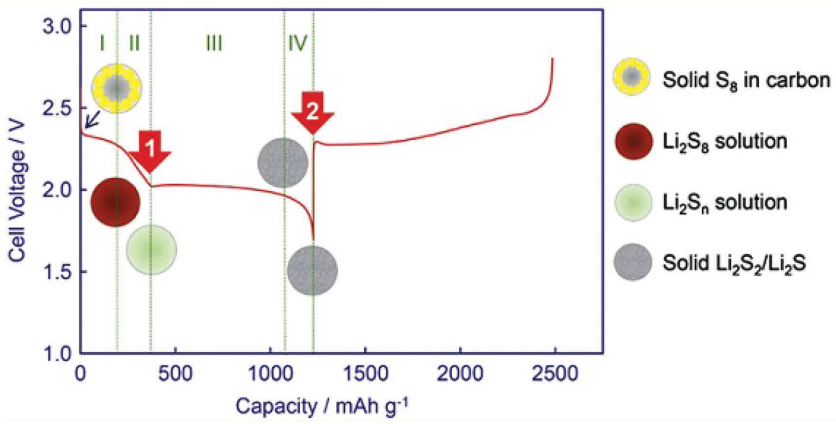

Figure 20. A typical discharge/charge voltage profile at the first cycle in a Li–S cell. Reproduced with permission.[636] Copyright 2013, Elsevier.

However, the Li–S chemistry faces several major challenges (**Figure 21**),[637] which include:[638–643] (i) Elemental S is highly insulating, necessitating S to be supported on a conductive skeleton to improve their utilizations. (ii) The intermediate polysulfide ions formed during the discharge/charge processes are very easy to dissolve in the organic-solvent-based electrolytes. These soluble polysulfide species can migrate from the cathode to Li anode through the battery separators where they are reduced to the insoluble Li_2S_2/Li_2S and low-ordered soluble polysulfides. Once there are concentrated on the Li anode side, the low-ordered polysulfides can diffuse back to the cathode side and will be re-oxidized into the original long-chain polysulfide species with repeated discharge/charge cycles, thus creating a so-called shuttle effect. The shuttle mechanism has been directly implicated as the cause for the loss of S following the initial discharge, which is exacerbated in subsequent discharge/charge cycles. Eventually, it results in low utilization of active materials, poor Coulombic efficiency, rapid capacity fading and degradation of the Li anode. This polysulfide shuttle effect is considered one of the greatest challenges of the Li–S battery; (iii) There are very large volume changes of S during extended electrochemical processes; and (iv) Current Li–S batteries still use pure Li as anode. There are some side-reactions between pure Li and dissolved polysulfide intermediates and the pure Li always experiences uneven deposition/stripping processes during extended cycling which form Li dendrites, inducing some safety issues.[624–635]

Hence, significant efforts have been focused on the fabrication of S composites with porous carbon and conducting polymers to improve electrode conductivity, effectively adsorb soluble polysulfide intermediates from dissolving into organic electrolytes, and accommodate S volume changes.[624–630,644–649] Ionic liquid electrolytes, electrolyte additives and new binders have shown to reduce polysulfide dissolution.[627,642,650–657] The use of nanostructured carbon (e.g., CNTs, graphene, CNFs, etc.) and carbon-based nanocomposites in Li–S batteries has shown improvement in their electrochemical performance.[638,658–661] Carbon-based nanomaterial such as graphene is a useful nanoscale building block to produce composite materials with element S. Recently, several groups have reported the use of graphene sheets to confine sulfur compounds for use in Li–S batteries.[192,415,662,663] The ensuing sections discuss recent

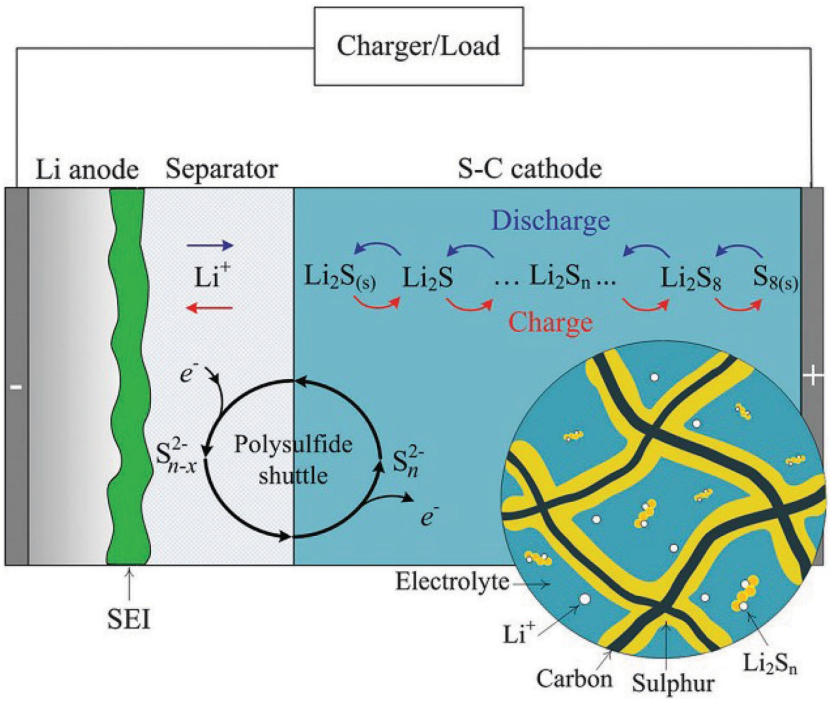

Figure 21. An illustration of the effects of polysulfide dissolution, shuttle phenomenon, effect on the cathode upon discharge/charge process in Li–S batteries. Reproduced with permission.[637] Copyright 2015, Royal Society of Chemistry.

results reported in the literature on the use of graphene and graphene-based nanocomposites in Li–S batteries.

5.1. Graphene/S

Graphene can ideally trap S, restrict polysulfide dissolution and accommodate S volume change and hence, is of great interest for Li–S batteries.[633,650,664–678] Cao et al. synthesized FGS-S multilayered 3D sandwich architectures with uniform S distribution on graphene surface. This material delivered a large reversible capacity of ≈505 mAh g^{-1} at a current density of 1C (1680 mA g^{-1}). To reduce the polysulfide dissolution and migration, the as-synthesized FGS-S composites was further coated with a thin layer of cation exchange nafion film. These materials exhibited a much improved cycle performance with 79.4% capacity retention for 50 cycles at a 0.1C rate, excellent rate performance for up to 1C and capacity retention over 100 cycles.[679]

Similarly, Wang and co-workers coated S particles with poly(ethylene glycol) (PEG), then wrapped it by graphene decorated with extra carbon black,[665] wherein, both graphene and PEG accommodate S volume changes, improve conductivity and restrict polysulfide dissolution. This structure was able to trap soluble polysulfides in the matrix, while allowing S particles to conduct electrical charge. As a result, the graphene-wrapped S particles delivered a high specific capacity of 750 mAh g^{-1} with a relatively stable capacity for about 140 cycles.

In another vein, S-impregnated graphene composites were also synthesized via heterogeneous crystal growth,[680] wet chemical oxidation,[681] impregnation,[682] and others.[683,684] It is also expected that optimizing the size and morphology of the S particles could help further improve the performance. Based on this concept, uniform graphene/S composite-based cathodes were fabricated, which delivered a high reversible capacity of more than 800 mAh g^{-1} after 80 cycles.[671] The high dispersion of the S on the graphene remarkably enhanced its utilization, while the unique 2D structure of graphene phase significantly facilitated the Li-ion and electron transports, thus improved the redox kinetics.[671] In addition, Park et al. demonstrated that HF-treated graphene could provide active nanopores for the controlled nucleation of S particles in an aqueous solution.[680] Zhang and co-workers adopted an oil–water system to fabricate saccule-like graphene/S nanocomposites. These novel synthetic strategies successfully produced size-controlled S particles and yielded unique graphene/S nanocomposite cathodes with high electrochemical performance for Li–S batteries.[666]

Nevertheless, the problem with this architecture is the slow diffusion of Li-ion since it has to diffuse through multiple layers. Although these approaches show promise, the rate capability of these synthesized materials is limited and an obvious concern is the huge loss in capacity during cycling.

As a typical 2D material, graphene itself is not considered as an effective substrate material to effectively confine S and polysulfide intermediates due to its intrinsic geometrical characteristics.[685–687] Hence, pure graphene cannot be directly used as cathode for Li–S batteries. Further performance improvement can be obtained using heteroatoms (e.g. O, N, B, P, etc.) doped graphene-S nanocomposites,[688–693] fabricating porous graphene-S nanocomposites,[663,694–704] and involving a second conductive phase to construct 3D graphene-based architectures.[705–710]

5.2. GO or rGO/S

Establishing strong physical interaction or even chemical bonding between graphene and S can help improve the electrochemical performance of Li–S batteries, since these interactions can trap S or polysulfide intermediates, decrease their dissolutions into the liquid electrolyte and minimize their migrations between cathode and anode.[229,650,685,711,712] Based on this fact, GO would be a suitable starting point to be used to immobilize S due to the ample functional groups on the surfaces.[229,650,685,711,712]

In Ji and co-workers's study, the authors incorporated nano-S into GO by chemical reaction in a microemulsion system (**Figure 22**a,b).[650,711] The heat treatment of the as-synthesized samples at low temperatures (155 °C) led to the removal of exposed unencapsulated S on GO. The GO with its large surface area and ubiquitous cavities can have intimate contact with S to prevent its aggregation and improve the electrical contact. In addition, heat-treated GO has hydrophilic groups that can strongly adsorb elemental S as well as polysulfides during discharge/charge processes (Figure 22c).[650] These nanostructured materials showed specific capacities of ≈950 mAh g^{-1} at 0.1C rate for up to 50 cycles (Figure 22d).[650]

Similar methods have been adopted to synthesize graphene–S nanocomposite cathodes with promising electrochemical performance.[227,231] Li et al. fabricated thermally exfoliated graphene nanosheet/S nanocomposites, then used rGOs to further coat the as-prepared nanocomposites.[667] These rGO/graphene@S nanocomposite cathode showed a high capability to restrain the diffusion of immediate polysulfides while delivering a large capacity at a high rate of 3.8C.[667]

Recently, Wang and co-workers reported a facile approach to synthesize high-performance graphene/S cathodes by covalently stabilizing the S and polysulfide intermediates on ethylenediamine (EDA)-functionalized rGO (EFG) (**Figure 23**).[687] The unique molecular structure of EDA with high reactivity can help crosslink polar Li polysulfides and nonpolar carbon (Figure 23b,c). The use of DFT calculations has verified strong affinity of Li polysulfides to EFG (Figure 23d–f). The strongly covalent stabilization of S and the polysulfides on EFG enabled a stable capacity retention of 80% for 350 cycles along with high reversible capacities and excellent rate performance (Figure 23g–i).[687] The authors reported that this two-electron-donating amine groups on the carbon aliphatic spacer covalently joined polar Li polysulfide and nonpolar carbon surface together, which prevents the loss of S active mass and promotes electrical contact.[687] In addition, the electron-donating effect of amine functional moieties could enhance the reactivity of aromatic carbon rings for S loading and favor the immobilization of S by complexation with them.[687] In another study, layers of amorphous S were tightly anchored on the graphene sheet via strong chemical bonding.[685] When employed as a cathode material in Li–S

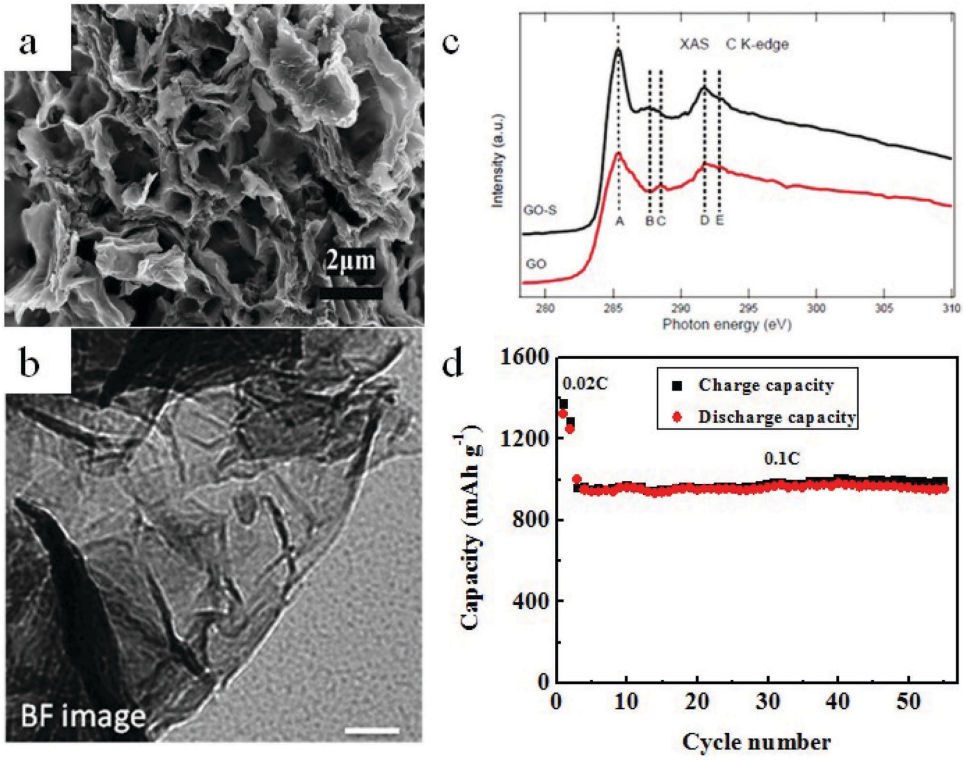

Figure 22. a) SEM and b) TEM images of thermally treated GO–S nanocomposites. c) The K-edge XAS spectra of pure GO and GO–S nanocomposites. d) The corresponding cycling performance at a constant current rate of 0.1C after initial activation processes at 0.02C for two cycles. Reproduced with permission.[650] Copyright 2011, American Chemical Society.

batteries, the as-synthesized composite delivered a high initial capacity of 1047 mAh g^{-1} and stable capacity retention for more than 70 cycles at 0.5C.[685]

5.3. Heteroatom-Doped Graphene/S

Although these strategies showed promises and consistently contributed to trapping intermediate polysulfides and partially reduce degradation of S cathode with substantial and encouraging advances, these approaches are fundamentally insufficient to suppress the polysulfide shuttle effect, which is considered as one of the major challenges of Li–S batteries. It was reported that N-doped carbon exhibits a strong chemisorption for polysulfides and Li_2S, and the electronegative N atoms in the carbon matrix are particularly effective in forming Li_xS••••N interactions via the lone-air electrons of N because of the strong interaction due to Lewis acid-based interaction between Li-ion cations in Li_2S_x and N atoms in the carbon matrix.[692,713–715] Alternatively, B atoms, as an electron-deficient alternative to N atoms, are electropositive in the carbon framework, thus leading to the chemisorption of polysulfide anions.[691,713] Accordingly, it was reported recently that a B-doped carbon host can also improve the performance of composite cathodes. Aside N and B, P, and S doped carbon have also been reported to be used for the fabrication of novel carbon/S nanocomposites for Li–S battery cathodes with enhanced electrochemical performance.[716]

Recently, N-doped graphene/S has been intruduced as a potential cathode for Li–S batteries.[717] Wang et al. reported work on the use of a porous 3D N-doped graphene for S cathodes (88% S loading), which delivered specific discharge capacity of about 800 mAh g^{-1} and stable capacity of 600 mAh g^{-1} after 145 cycles.[717] The N-doped graphene can facilite fast Li-ion transmission and simultaneously trap polysulfide and the porous 3D structures can accommodate the volume change while allowing electrolyte penetration, contributing to the electrochemical performance improvement.[717] Similarly, Zhang and co-workers prepared a carbon black-free N-doped graphene wrapped S cathode for Li–S batteries, which delivered high specific discharge capacities even at high rates.[692] Most importantly, the cells demonstrateed an ultralong cycle life for more than 2000 cycles with an extremely low-capacity-decay rate.[692] The X-ray spectroscopic analysis and ab initio calculation results indicated that the excellent performance was attributed to the well-restored C—C lattice and the unique Li polysulfide binding capability of the N-based functional groups in the graphene sheets.[692] Highly crumpled N-doped graphene/S nanocomposites were also fabricated.[693] The unique pore structure and N-doping induced strong polysulfide adsorption ability, Li–S battery cells using these wrinkled graphene sheets as both S host and interlayer achieved a high capacity of about 1000 mAh g^{-1} and exceptional cycling stability even at high S content (≥80 wt%) and S loading (5 mg cm^{-2}), which is higher compared to other recently developed sulfur cathodes and is

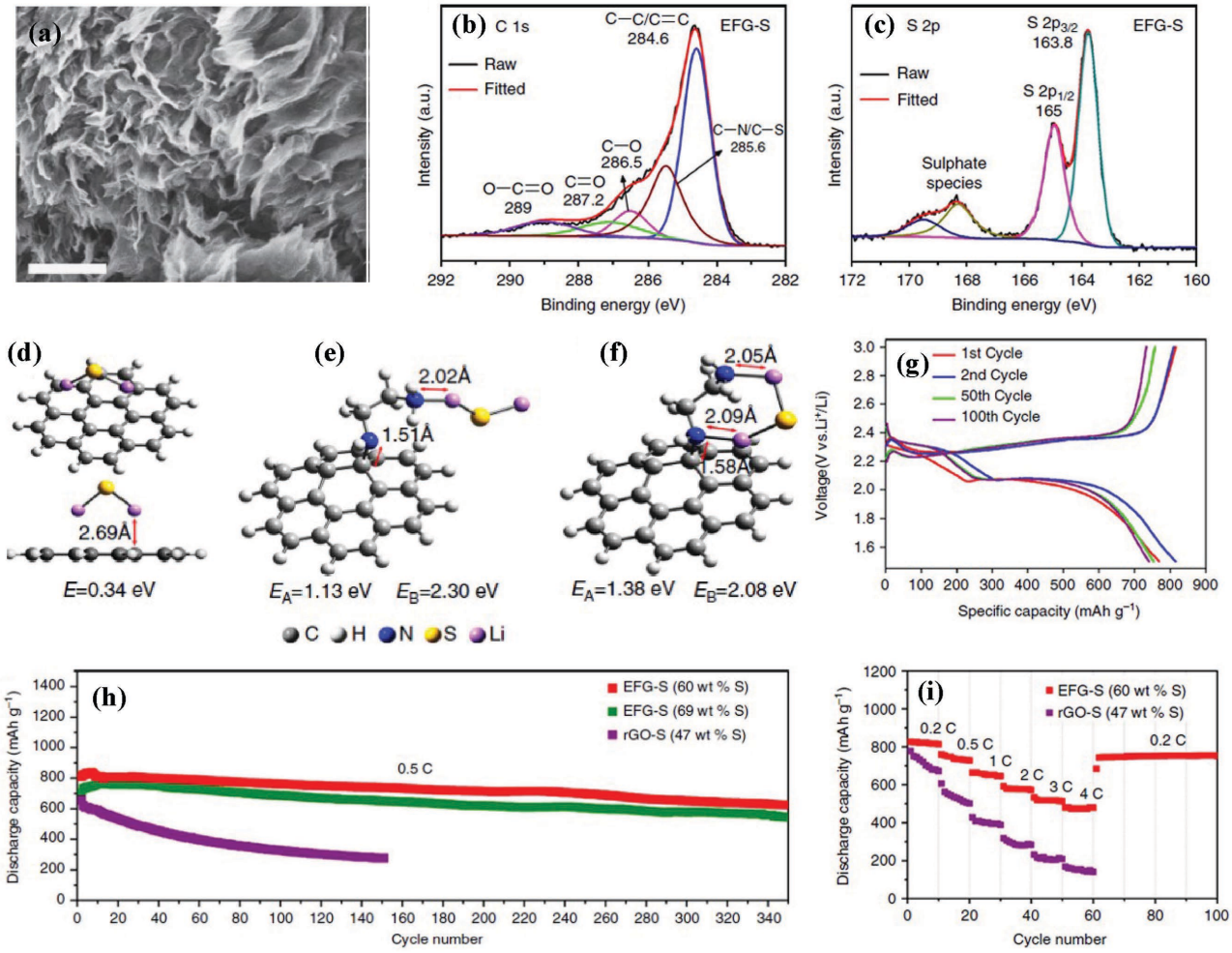

Figure 23. a) SEM of EFG–S nanocomposite. b,c) XPS analysis of EFG–S. d–f) DFT calculation showing the interaction between Li_2S cluster and graphene or EFG, models of C, H, N, S, and Li elements displayed as spheres in gray, white, blue, yellow, and pink, respectively. g) Discharge/charge voltage profiles at different cycles of EFG–S nanocomposite (60 wt% S). h) Long-term cyclability of EFG–S nanocomposite (60 and 69 wt% S) and rGO–S composite (47 wt% S). All these tests are conducted at 0.5C between 1.5 and 3.0 V. i) Rate capabilities of EFG–S and rGO–S nanocomposites at various current rates between 1.5 to 3.0 V. Reproduced with permission.[687] Copyright 2014, Nature Publishing Group.

ideal for practical applications.[693] In addition to N-doped graphene, 3D B-doped graphene aerogel/S nanocomposite was also reported where the results showed a higher capacity of 994 mAh g^{-1} at 0.2C after 100 cycles withan outstanding rate capability.[691] Yuan and co-workers presented a strategy to chemically bind S and its discharge products with a graphene-supported N/B co-doped carbon layer and employed it as the host to prepare the C/S composite cathode for Li–S batteries.[713] Due to the high conductivity and strong chemical bindings of N and B groups to Li polysulfides, the as-prepared electrodes with a 70 wt% S content display an ultralong cycling performance of more than 1500 cycles with a low decay rate of 0.035% per cycle at the rate of 2C and a high rate performance up to 3C.[713] Similarly, Gu and co-workers reported a conductive and porous N and P dual doped graphene layer/S nanocomposites.[689] The electrochemical evaluation results showed that the N and P dual doped graphene layer/S electrodes can deliver a superior initial capacity of more than 1158 mAh g^{-1} at 1C, excellent rate capability, and satisfactory cycling stability, which are better than those of the single N- or P-doped graphene.[689] More recently, Manthiram and co-workers presented an effective strategy to obtain Li/polysulphide batteries with high energy density and long-cyclic life using 3D N,S co-doped graphene sponge electrodes (**Figure 24**a,b).[718] The N,S co-doped graphene sponge electrode provided enough space for a high S loading, facilitated fast charge transfer and better immobilization of polysulfide ions (Figure 24c).[718] The heteroatom-doped sites demonstrated a strong binding energy and were capable of anchoring polysulfides based on the first-principles calculations. As a result, high specific capacity of 1200 mAh g^{-1} at 0.2C rate, high-rate capacity of 430 mAh g^{-1} at 2C rate and excellent cycling stability for 500 cycles with 0.078% capacity decay per cycle were achieved (Figure 24d–f).[718]

These promising results suggest that the synergetic combination of conductive and adsorptive confinement strategies induced by the multiheteroatom doping scheme is a promising approach for developing high performance Li–S batteries.[689]

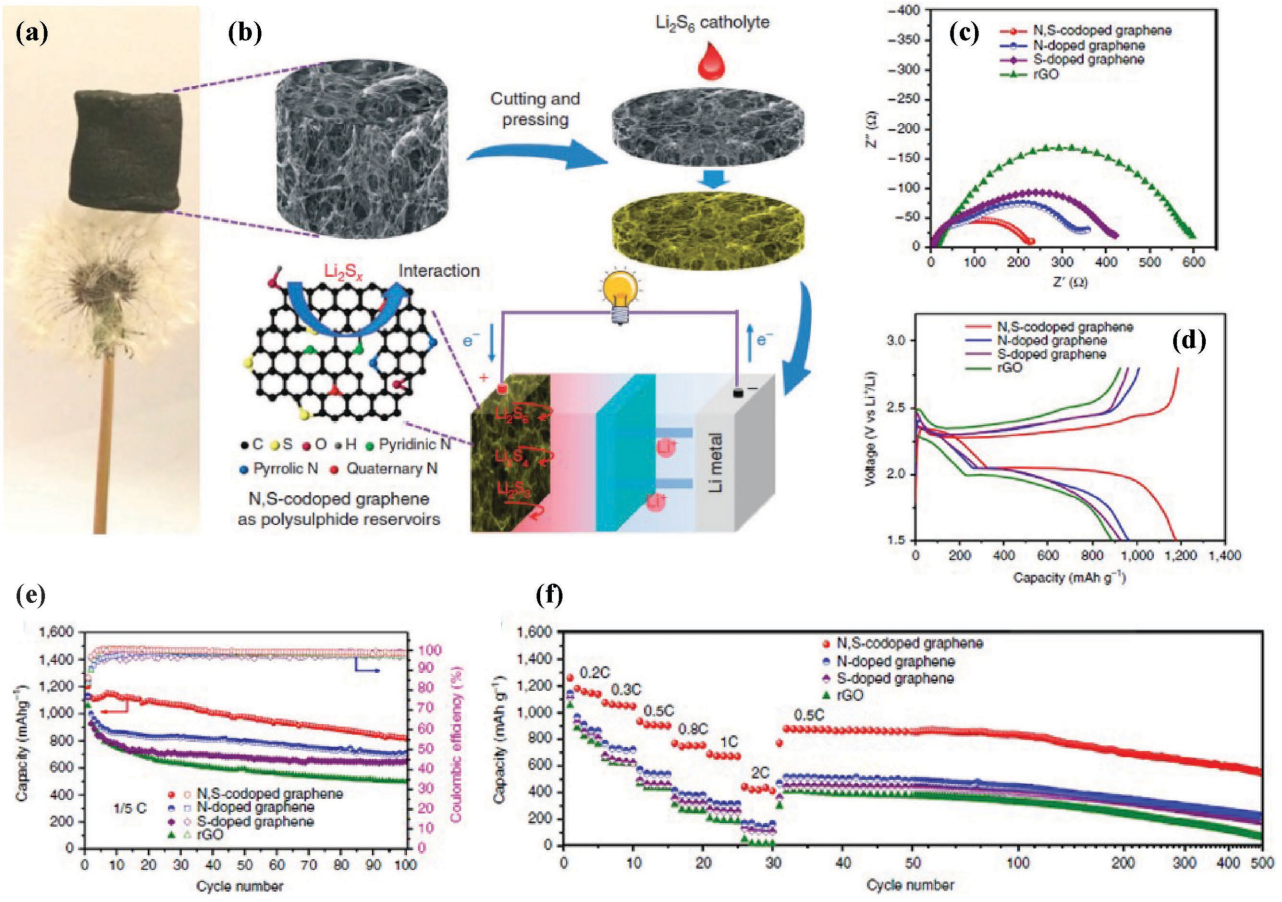

Figure 24. a) A lightweight N,S-co-doped graphene sponge standing on a dandelion. b) Illustration of the formation process of the N,S-co-doped graphene electrode and the fabrication of a Li/dissolved polysulfide cell with N,S-co-doped graphene electrode. c) Nyquist plots of the rGO, N-doped graphene, S-doped graphene, and N,S-co-doped graphene electrodes before cycling from 1 to 100 MHz at room temperature. d) The second galvanostatic discharge/charge profiles of the rGO, N-doped graphene, S-doped graphene, and N,S-co-doped graphene electrodes at 0.2C rate between 1.5 V and 2.8 V. e) Cycling performance of the Li polysulfide batteries with the rGO, N-doped graphene, S-doped graphene and N,S-co-doped graphene electrodes at 0.2C rate between 1.5 V and 2.8 V. f) Rate performance of the rGO, N-doped graphene, S-doped graphene, and N,S-co-doped graphene electrodes at different current rates and long-term cycle stability of the corresponding electrode at 0.5C for 500 cycles after 30 cycles at different current rates between 1.5 and 2.8 V. Reproduced with permission.[718] Copyright 2015, Nature Publishing Group.

Doping of heteroatoms into graphene not only changes the electronic distribution but also creates surface functional groups. These changes enhanced the chemical adsorption of carbon to polysulfide species, and have been intensively investigated to sequestrate soluble polysulfide intermediates in Li–S batteries.[716]

5.4. Graphene@Transition Metal Oxide/S

In a recent work by Nazar and co-workers, the authors reported the use MnO_2/graphene nanosheets as a cathode host to improve the performance of Li-S batteries.[719] The results showed that instead of the presence of a chemical interaction with surface affinity between the host materials (MnO_2) and Li polysulfides as existing in GO (or rGO)/S, doped (N, B, S, P, etc.) graphene/S nanocomposites, the thiosulfate species ($S_2O_3^{2-}$) were generated in situ on the surface of MnO_2 through the redox reaction with Li polysulfides.[719] The $S_2O_3^{2-}$ species were important to the retention of Li polysulfides within the positive electrode upon cycling. They may anchor "higher-order" S_x^{2-} polysulfides ($x \geq 4$) by further catenating them into the S—S bond in $[O_3S\text{-}S]^{2-}$ (thiosulfate) to create intermediate surface-bound polythionate complexes $[O_3S_2–(S)_{x-2}–S_2O_3]$, and converting them to insoluble "lower" polysulfide.[719] The polythionate complex formed on the surface is thus best described as a transfer mediator.[719] This process curtailed the active mass loss during the discharge/charge process and suppressed the polysulfide shuttle to result in high-performance cathodes with high S loading, capable of high-capacity retention after long time cycling up to 2000 cycles.[719] A follow-up comprehensive study by the same group on the ability of various transition metal oxides/graphene nanocomposites to chemically adsorb polysulfides showed that the interactions were directly correlated to the redox potentials of transition metal oxides.[720] Metal oxides with a redox potential that lies below ≈1.5 V (such as Co_3O_4, or Ti_4O_7) show no redox reaction with

Li polysulfides, and only strong beneficial surface polar and/or acid site interactions that mitigate polysulfides dissolutions.[720] Those with a redox potential in a target window (2.4 V < $E \leq$ 3.05 V) such as VO_2/graphene (2.79 V) and CuO/grahene can oxidize polysulfides to form thiosulfate/polythionate groups chemically bound to the reduced metal oxide surface (similar to that reported for graphene/MnO_2 nanosheets (3.05 V)).[720] On the other hand, metal oxides with a high redox potential (>3.05 V), such as V_2O_5/graphene and NiOOH/graphene can oxidize polysulfides to a mixture of sulfate and thiosulfate. This can repetitively oxidize polysulfides to electrochemically inactive sulfate groups, hence leading to a poor cycling performance as a result of the high redox potential (3.4 V) of these metal oxides.[720] This new outcome would allow for the design of Li–S batteries with a long cycle life by using new graphene-based nanocomposites with suitable redox potentials to form surface bound thiosulfate/polythionate mediators.

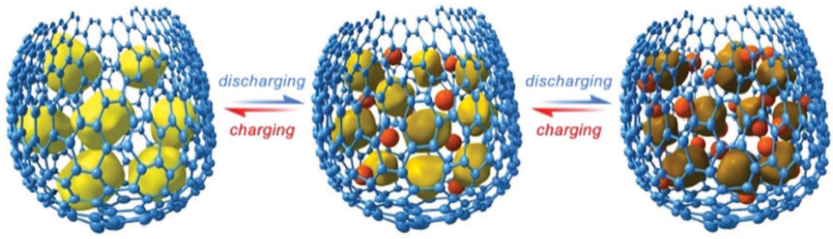

Figure 25. Schematic illustration of entrapment of S in hierarchical porous graphene support for Li–S batteries during the discharging/charging process. Reproduced with permission.[694] Copyright 2013, Elsevier.

5.5. Porous Graphene (or rGO)/S

A key performance index for graphene/S electrode lies in the fabrication of a well-designed nanostructure, in which the graphene framework acts not only as an electronic conduit for the encapsulated S but also have enough free space for the continuous electrochemical reaction.[721] Such entrapment ensures a more complete redox process and results in an enhanced utilization of S. From this point, the nanocomposites with S entrapped into different types of porous graphene can help further improve the electrochemical perforance in Li–S batteries.[663,694–704]

In one of these types of research, chemically activated rGO hydrogel has been used to uniformly confine elemental S in its nanopores with the aim to fabricate porous rGO–S nanocomposites.[695] Large pore volume and controlled nanopore size and distribution resulted in a high reversible capacity of up to 1379 mAh g^{-1} at 0.2C with excellent cycling stability for more than 50 cycles. Huang et al. fabricated hierarchical porous graphene–S nanocomposites with epoxyl and hydroxyl groups on the surface of graphene to enhance S binding.[694] In these nanostructures, graphene can also serve as a mini chamber for electrochemical reactions (**Figure 25**).[694] As a result, this novel nanostructured electrode can lead to a high discharge capacity of 1068 and 543 mAh g^{-1} at current densities of 0.5 and 10C, respectively. Hierarchically micro/mesoporous activated graphene with high surface area (up to 3000 m^2 g^{-1}) and large pore volume (up to 2.14 cm^3 g^{-1}) was also utilized as a superior carbon host material with high S loading for advanced Li–S batteries.[722] Freestanding hierarchically porous graphene-encapsulated S showed high rate capability (a reversible capacity of 1017 mAh g^{-1}, 865 mAh g^{-1}, and 726 mAh g^{-1} at 0.2C, 0.5C, and 1C, respectively) and excellent cycle stability for more than 300 cycles.[704] In addition, the electrode also exhibited a remarkable Li-storage ability at the bent state due to the excellent mechanical flexibility.[704]

5.6. 3D Porous Graphene (or rGO) Sponge/S

Although porous graphene can help further improve the electrochemical performance in Li–S batteries, the stacking of graphene is still not easily prevented, and the conductivity of chemically derived graphene materials decreases as more defects are introduced. The existence of curvatures and wrinkles on graphene can prevent the stacking of graphene to a certain extent and make the single-layer graphene thermally stable, but their presence is not sufficient to fully prevent the stacking. Fabrication of controllable 3D nanostructure and conductive scaffolds, as well as adding a second conductive phase to construct robust 3D frameworks may help avoid the stacking of graphene sheets, provide a 3D conductive network, reduce electron-transfer resistance, and further improve the electrochemical performance in Li–S batteries.[723–725]

The design of 3D graphene sponge/S structure produced a cathode with good electrochemical stability and high rate discharge capacity retention for up to 160 discharge/charge cycles at a high rate of 1C.[726] The most recently prepared 3D hierarchically interconnected porous graphene/S nanocomposites delivered a high initial specific discharge capacity of 914 mAh g^{-1} and a specific capacity of 486 mAh g^{-1} after 500 cycles at 1C. In addition, a high specific capacity of 467 and 162 mAh $g^{-1}$was obtained at a high rate of 10C with a Coulombic efficiency of over 90.0% at the first and 500th cycle, respectively.[727] Lu and co-workers reported an approach to assemble S/graphene sponge composites with S uniformly distributed into the pores of graphene sponge and directly used them as cathodes for Li–S batteries.[728] This 3D architecture electrode delivered high areal specific capacity and high retention ratio even at a large areal mass loading of ≈12 mg S cm^{-2}, approximately 6 to 12 times higher than that of most reports, with a slow decay rate at 0.1C (0.08% per cycle after 300 cycles).[728] In addition to the aforementioned 3D graphene/S design, other different type of 3D graphene sponge/S based electrode for Li–S batteries with promising electrochemical performance were also reported.[723–725]

In another study, the fabrication of graphene-based 3D hierarchical S cathodes through adding a second conductive phase has become a new strategy to tackle the intrinsic problems in Li–S batteries.[640] For instance, Li–S cells with high capacity and long cycle life with a dual-confined flexible cathode configuration by encapsulating S in N-doped double-shelled hollow carbon spheres followed by graphene wrapping has been reported.[729] In this design, S/polysulfides are effectively

immobilized in the cathode through physical confinement by the hollow spheres with porous shells and graphene wrapping as well as chemical binding between heteronitrogen atoms and polysulfides. This rationally designed freestanding nanostructured of S cathode provided a well-built 3D carbon conductive network without requiring binders, enabling a high initial discharge capacity of 1360 mAh g^{-1} at a current rate of C/5, excellent rate capability of 600 mAh g^{-1} at 2C rate, and sustainable cycling stability for 200 cycles with nearly 100% Coulombic efficiency.[729] In Chen and co-workers' work, they reported a graphene/MWCNT-based 3D hierarchical sandwich-type architecture for Li–S batteries.[730] The graphene–MWCNT@S composite exhibited a high initial capacity of 1396 mAh g^{-1} at a current density of 0.2C. A much improved cycling stability and rate capability were achieved for the graphene–MWCNT@S composite cathode compared with the composite without graphene or MWCNT. The superior electrochemical performance was mainly attributed to the synergistic effects of graphene and MWCNTs, which provided a 3D conductive network for electron transfer, open channels for ion diffusion, strong confinement of soluble polysulfides, and effective buffer for volume expansion of the S cathode during discharge.[730] The design of 3D nanoarchitectures of graphene/CNT@porous carbon resulted in interlinked hierarchical composites with good electrical conductivity and a robust framework, while the meso-/microporous carbon and the interlamellar compartment between the opposite graphene accommodated S and polysulfides.[731] Therefore, the nanocomposite cathodes showed an ultrahigh specific capacity of 1121 mAh g^{-1} at 0.5C, a favorable high-rate capability of 809 mAh g^{-1} at 10C, a very low capacity decay of 0.12% per cycle, and an impressive cycling stability of 877 mAh g^{-1} after 150 cycles at 1C.[731] In addition, as S loading increased from 50 wt% to 77 wt%, high capacities of 970, 914, and 613 mAh g^{-1} could still be obtained at current densities of 0.5, 1, and 5C, respectively.[731]

5.7. Graphene (or rGO)/S/Second Conductive Phase

The addition of another second conductive phase can also help improve conductivity, enhance the capacity retention, and cycle performance. In this context, CNFs, pyrolyzed polyacrylonitrile (PAN), and SWNT were used as a second conductive phase to synthesize rGO thermally exfoliated GNS–S nanocomposites,[667,732–735] pyrolyzed PAN–S/GNS (pPAN–S/GNS) composites,[668,736] graphene/SWNT-S hybrid material,[737,738] CNF/S/graphene,[739] and graphene/micro@mesoporous carbon/S,[740] respectively, showing improved electrochemical performance. Yin et al. prepared pyrolyzed PAN–S–graphene nanosheets tricomponents.[668] The electrochemical properties of the pyrolyzed PAN–S/GNS (pPAN–S/GNS) composite cathode exhibited a reversible capacity of 1500 mAh g^{-1} at the first cycle, corresponding to a S utilization of about 90%. Even up to 6C, a high capacity of 800 mAh g^{-1} was obtained. The superior performance of pPAN–S/GNS was attributed to the presence of GNS and the composite structure. The GNS in the composite materials exerted as a 3D nanocurrent collector, which provided not only as an electronically conductive matrix, but also as a framework, resulting in improved electrochemical performance.[668]

The same group also reported results on the design of a novel dual-mode S-based cathode material for Li–S batteries.[670] In this novel design, the S was embedded in both the pyrolyzed PAN nanoparticles (pPAN) and mildly reduced graphene oxide nanosheets (mGO).[670] The dual-mode pPAN–S/mGO–S composite delivered a high reversible capacity of 900–1400 mAh g^{-1} at 0.1C and a good cycling stability after initial 10 cycles due to the unique dual-mode structure of pPAN-S/mGO-S composite. In the same line, Xia and co-workers synthesized a leaf-like GO, which included an inherent carbon nanotube midrib in the GO plane, for preparing GO/S composites. Owing to the inherent high conductivity of carbon nanotube midribs and the abundant surface groups of GO for S-immobilization. The composite with a S-content of 60 wt% exhibited ultralong cycling stability for over 1000 cycles with a low capacity decay of 0.033% per cycle and a high rate up to 4C. Even with the high S-loading of 2.7 mg cm^{-2} on the electrode and the high S-content of 85 wt%, a promising cycling performance over 600 cycles was reported.[741] N-doped aligned CNT/graphene sandwiches were designed and in situ fabricated by a facile catalytic growth on bifunctional natural catalysts that exhibited a high-rate performance as scaffolds for Li–S batteries, with a high initial capacity of 1152 mAh g^{-1} at 1.0 C. A high capacity of 770 mAh g^{-1} was achieved even at 5C.[742]

Based on the above discussion, it is worthwhile to mention that the structure of graphene nanocomposite plays a central role in improving the electrochemical performance of Li–S cathodes. Recent work reported in the literature showed that graphene-based nanostructures can, to some extent, reduce the polysulfide dissolution in Li–S batteries and hence improve their capacity and cycle performance. The electrochemical performance of some of these graphene/S nanocomposite-based cathodes used in advanced Li–S batteries is summarized in **Table 3**.

5.8. Graphene (or rGO)-Modified Separators for Li–S Batteries

Although the above-mentioned strategies have consistently contributed to immobilize and trap the intermediate polysulfides and partially reduced the degradation of Li anodes, these approaches are fundamentally ineffective in avoiding polysulfide anions from migrating toward Li anode and eliminating the prevalent "shuttle effect" phenomenon. Because current Li–S batteries use Li metal as the anode, which is very reactive in most electrolyte solutions, therefore, leading to Li corrosion and dendrite formation, and hence causing deterioration in electrochemical performance, degradation/device failure and safety concerns. These problems can be further magnified in Li–S batteries because the Li surface and dendrite structures are also very reactive with the polysulfide species in the electrolyte, hence resulting in the deposition of insoluble Li sulfide coatings on the Li anode. These reactions can cause the removal of the active species from the system, and the loss of contact between the anode and the electrolyte which can lead to a serious capacity fading. In order to improve the electrochemical performance of Li–S batteries, the highly reactive Li must absolutely be isolated from contacting with the dissolved multiple intermediary sulfides during the

Table 3. Examples of different graphene-based nanocomposites for Li–S batteries reported in the literature.

Materials	S content [wt%]	Electrochemical performance
N-graphene/S[743]	80	1st cycle capacity: 1357 mAh g^{-1} at 0.1C Cycle life: 500 cycles at 1C
		Good rate capability
rGO/hair-derived carbon/S[744]	69	1st capacity: 1113.2 mAh g^{-1} at 0.2C
		Cycle life: 300 cycles at a 0.2C
		Rate capability: good
CNT–graphene/S[738]	53	1st cycle capacity: 912 mAh g^{-1} at 0.2C cycle life: 100 cycles at 0.2C
ZnO layer coated rGO/S[745]	55	1st cycle capacity: 998 mAh g^{-1} at 0.2C Cycle life: 100 cycles at 0.2C
Leaf-like GO/CNT/S[741]	60, 75, and 85	60% S-based composite cycle life >1000 cycles and high rate up to 4C
		75 wt% S-based composite cycle life >1000 cycles
		85 wt% S-based composite cycle life > 600 cycles
Amino-functionalized rGO/S[687]	69	1st capacity: >800 mAh g^{-1}
		Cycle life: 350 cycles
		Excellent high-rate response up to 4C
Vertically aligned S/graphene nanowalls[746]	66	1st cycle capacity:1261 mAh g^{-1} at 1/8C
		Cycle life > 120 cycles at 1/8C
		High-rate performance of over 400 mAh g^{-1} at 8C
Graphene/S[747]	70	1st cycle capacity:1080 mAh g^{-1} at 0.1 A g^{-1}
		Cycle life > 60 cycles at 0.1 A g^{-1}
		Good rate performance
Self-assembled graphene/S composite[748]	80	1st cycle capacity: 865.1 mAh g^{-1} at 0.5 mA cm^{-2}
		Cycle life > 50 cycles at 0.5 mA cm^{-2}
		Good rate performance
3D graphene/S hybrid sponges[728]	80	11th cycle areal specific capacitance: 6.0 mAh cm^{-2}
		Cycle life: 300 cycles

discharge/charge process. In this regard, a new design of a Li–S cell is necessary.[749–752]

Recently, rGO was used in sandwiched-like structure between S cathode and the separator to act as a shuttle inhibitor to the S and polysulfides.[753] This designed structure delivered large initial discharge capacity of 1260 mAh g^{-1} and excellent capacity retention of about 900 mAh g^{-1} even after 100 cycles. This improvement in performance was attributed to the strong absorption and strong interactions between rGO and the S and polysulfide, which can inhibit the shuttle phenomenon and promote the re-utilization of the electrochemically active materials during prolonged cycling.[753] Huang and co-workers proposed a unique Li–S battery configuration with an ultrathin GO membrane for high stability (**Figure 26**a).[754] The oxygen electronegative atoms modified GO into a polar plane, and the carboxyl groups acted as ion-hopping sites of positively charged species (Li^+) and rejected the transportation of negatively charged species (S_n^{2-}) as a result of the electrostatic interactions.[754] Such electrostatic repulsion and physical inhibition largely decreased the transference of polysulfides across the GO membrane in the Li–S system (Figure 26b).[754] Consequently, the GO membrane with highly tunable functionalized properties, high mechanical strength, low electric conductivity, and facile fabrication procedure was reported to be an effective permselective separator system in Li–S batteries (Figure 26c,d).[754]

Cheng and co-workers also designed a sandwich graphene-based structure for rechargeable Li–S batteries,[755,756] the graphene membrane was used as a current collector (GCC), while S was directly coated on it and acted as the active material.[755] An extra graphene membrane was coated on a commercial polymer separator surface.[755] In this way, both sides of S were coated by flexible and conductive graphene layers to enhance the electric conductivity, and accommodate the large volumetric expansion of S during lithiation.[755] In addition, these graphene layers acted as S reservoirs to store and reuse migrated polysulfides, hence alleviating the shuttling effect during continued discharging/charging (**Figure 27**a,b).[755]

As a result, this designed Li–S battery showed decreased interface impedance (Figure 27c) and delivered a very high reversible capacity up to 1200 mAh g^{-1} at 0.3 A g^{-1} current density. Even at increased current density to 1.5 and 6 A g^{-1}, high reversible capacities of 1000 and 750 mAh g^{-1}, respectively, were recorded which indicated an ultrafast charge/discharge capability and excellent rate performance.[755] Compared to the other configurations, the batteries with a GCC/S+G-separator exhibited improved capacity retention upon cycling for 300 times at 1.5 A g^{-1} current (Figure 27d).[755]

In Manthiram's work on 3D N/S-co-doped graphene sponge electrode research, with the help of a graphene-coated separator, further improvements of electrochemical performance in the Li–S battery system were obtained.[718] For example, even at high active material loading of 8.5 mg cm^{-2}, the unique structure enabled the battery to deliver a high capacity of 1070 mAh g^{-1} at 0.2C rate (**Figure 28**a),[718] and the reversible discharge capacity could reach 500 mAh g^{-1} at a large current rate of 2C rate (Figure 28b).[718] In addition, a long-term cyclic test at 0.5C rate was carried out and the initial specific capacity was 925 mAh g^{-1}, which stabilized at around 670 mAh g^{-1} after 200 cycles (Figure 28c).[718]

In addition to the aforementioned research, highly porous PAN/GO membrane separator,[757] TiO_2/graphene interlayer coated separator,[758] and janus separator of polypropylene(PP)-supported cellular graphene framework,[751] were also reported

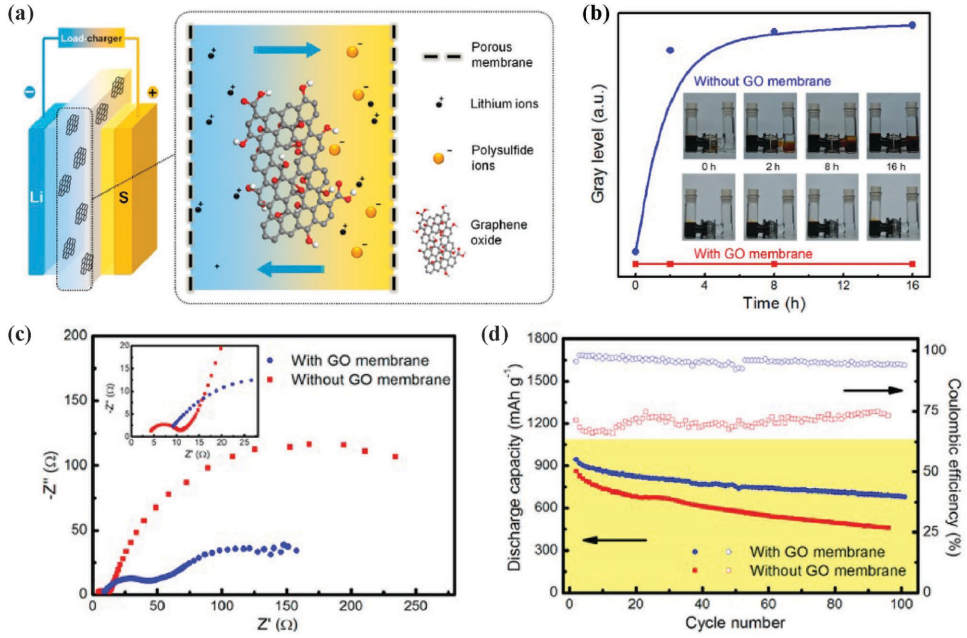

Figure 26. a) A schematic of a GO membrane in a Li–S cell. In this novel architecture, the GO membrane was sandwiched between cathode and anode, which can efficiently prohibit the shuttle of polysulfides through the GO membrane. b) Permselectivity of the GO membrane. Optical images indicated the diffusion of high-order polysulfides for H-type cell without (inset top) or with a GO membrane (inset bottom), and the dependence of the gray level in the right chamber as different diffusion times. c) The electrochemical impedance spectra (EIS) curves with/without GO membrane (inset is the enlarged EIS at high-frequency region). d) Cycling performance in Li–S batteries at a rate of 0.1C with/without a GO membrane. Reproduced with permission.[754] Copyright 2015, American Chemical Society.

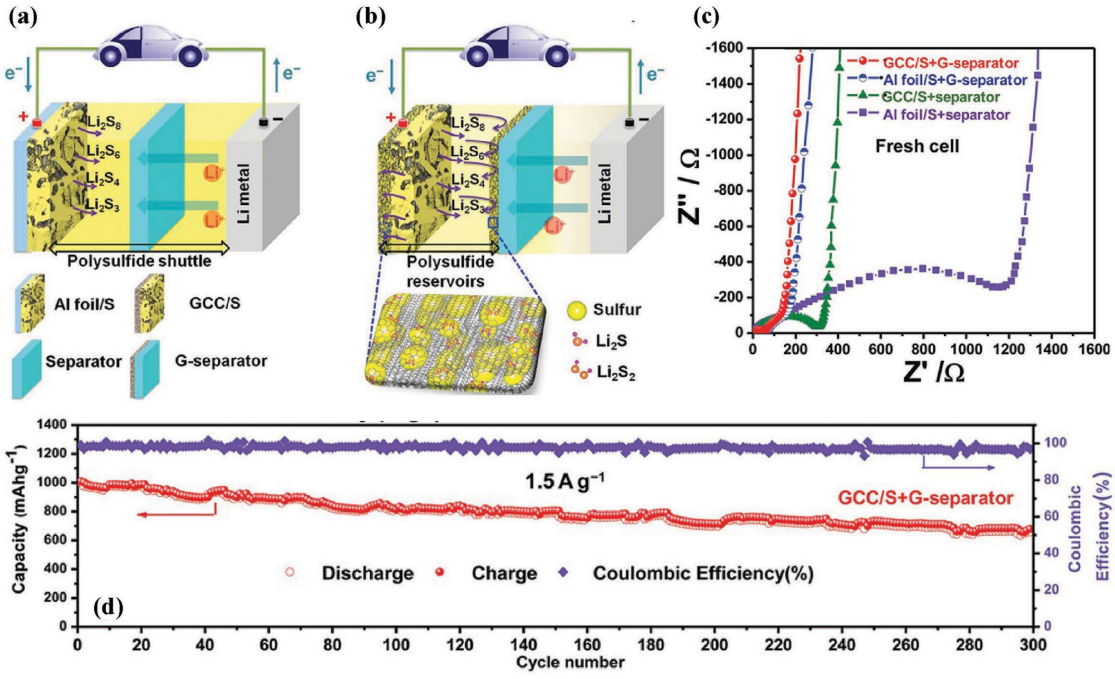

Figure 27. a) Schematic diagram of a Li–S battery with a common Al foil, S cathode, and commercial separator (Al foil/S+separator) configuration. b) Schematic of a Li–S battery with a graphene sponge as current collector (GCC), S cathode, and graphene separator (GCC/S+G separator). The paler yellow color represents the reduced shuttle effect. c) Nyquist plots of the impedance of the electrode for the different configurations. d) Cycling stability of the GCC/S+G separator cell at 1.5 A g^{-1} current for 300 cycles. Reproduced with permission.[755] Copyright 2014, Wiley.

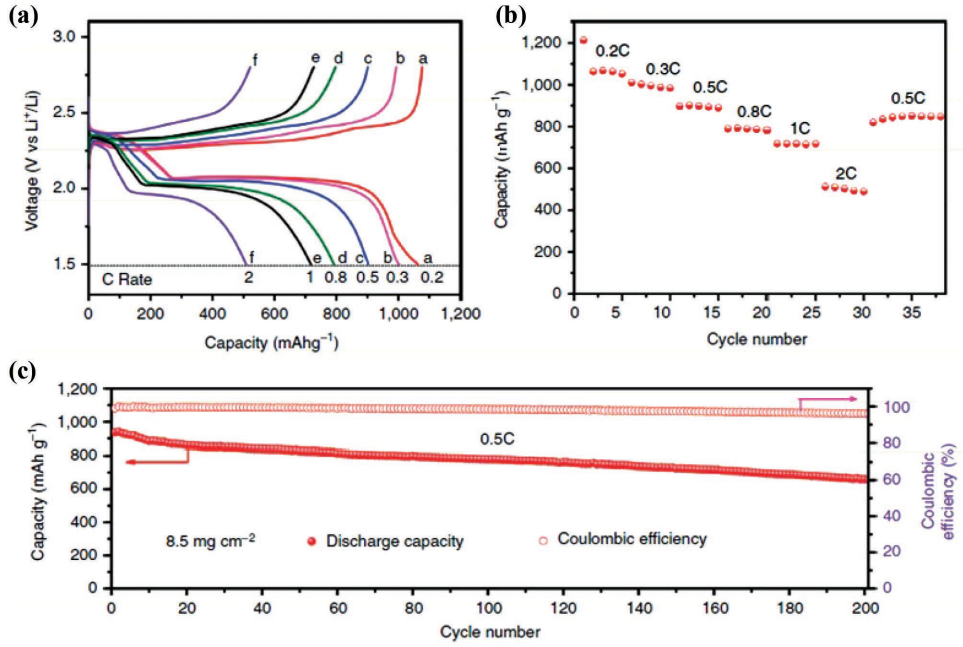

Figure 28. a) A galvanostatic discharge/charge profiles of the N,S-co-doped graphene electrode with graphene-coated separator at various rates. b) Rate performance of the N,S-co-doped graphene electrode with graphene-coated separator at different current densities. c) The cycling performance of the N,S-co-doped graphene electrodes with graphene-coated separator at 0.5C for 200 cycles. Reproduced with permission.[718] Copyright 2015, Nature Publishing Group.

as novel separators for Li–S batteries. The results discussed above show that incorporating graphene and graphene oxide into polymer membrane separators can lead to a significant performance improvement in the Li–S batteries.

5.9. Other Interesting Studies About Graphene (or rGO)-Based Materials in Li–S Batteries

Other novel research on the use of graphene-based materials for Li–S batteries also showed tremendous improvements in electrochemical performance. Among the methods used to prepare these graphene composites include, coating catalyst Pt on the surface of graphene to anchor soluble polysulfides,[759] using graphene to modify pure Li metal to protect Li anode and to minimize the shuttle phenomena,[760] and adding some inorganic nanoparticles, such as SiO_2,[761] ZrO_2,[762] into graphene phase to further trap polysulfides and minimize their dissolutions and prevent them from subsequent transportation between anodes and cathodes.

Based on our discussion in the Li/S section of this review, several issues including the safety, S utilization, rate capability, and cyclability still need to be addressed to advance the knowledge. Current Li–S batteries use pure Li metal as the anode, which can cause serious safety issues because Li metal is highly reactive in most electrolyte solutions where dendritic and mossy metals are very often formed during prolonged discharge/charge cycles. In addition, the pulverized and detached Li metal formed during cycling can result in explosion when exposed to air. These drawbacks can lead to serious problems including performance degradation, device failure, low Columbic efficiency, and safety concern.[441,636,760,763–769] In order to improve the overall electrochemical performance and safety of Li–S batteries, these problems must be tackled and minimized to the barest, which requires further insight at a more fundamental level.[760] One of the strategies used to address these issues is to use Li_2S as the cathode, which can be coupled with Li-free and safer anodes, such as nanostructured Si, Sn, and transition metal oxides to solve the Li dendrite problem.[770,771] However, two significant issues with the S cathode, e.g., the poor electrical conductivity and intrinsic polysulfide shuttle continue to exist in Li_2S cathode-based batteries.[770,771] The uniform dispersion of Li_2S phase into a conductive and flexible long-range 2D graphene framework to fabricate graphene/Li_2S-based nanocomposite cathodes, could be an effective way to realize a better utilization of Li_2S in Li–S batteries. For more details on this topic, we refer the reader to catch recent reported results on the use of graphene (or GO)/Li_2S nanocomposites for Li–S batteries.[772–776]

Another strategy that can be used is to directly protect Li anode using graphene-based materials. Recent work reported on the use of graphene composites in Li–S batteries showed that a graphene-modified Li anode with SEI induced by the polysulfide-containing electrolyte, demonstrated a superior dendrite-inhibition behavior and improved Coulombic efficiency to ≈97% for more than 100 cycles. The stable and efficient Li deposition could be maintained even after 2000 cycles.[760] Some other unique properties include rapid Li-ion transfer, high electron, and ionic conductivities, low polarization were also observed after using the graphene-modified Li anodes. These

fascinating results showed that the nanoscale interfacial electrode engineering combined with graphene-based materials could be a promising strategy to tackle the intrinsic problems of Li metal anodes, thus improving the performance and safety of Li–S cells.[760]

In addition, using advanced characterization techniques, such as X-ray diffraction (XRD), Raman spectroscopy, nuclear magnetic resonance (NMR), and establishing necessary theoretical models,[771,777–779] to fully understand the complex chemistry, such as the basic reaction mechanism, dissolution and precipitation of solid phases, and the detailed transport and migration of polysulfide species in Li–S batteries, are necessary to provide insight into the elementary and internal processes of the Li–S batteries.[637,778]

Finally, the potential utilizations of novel polymer or polymer composite-based solid-state electrolytes or gel electrolytes, inorganic solid-state electrolytes in Li–S batteries may also be very helpful to decrease the shuttle effect, prevent the Li dendrite formations and further improve the electrochemical performance.[6,639,780–785] Therefore, Li–S technologies are still far from commercialization and more efforts are needed to improve the electrochemcial performance of these promising battery systems. In the following section, we will discuss recent developments of graphene-based nanocomposites for use in Li–air batteries.

6. Li–Air Batteries

Li–air batteries that compose of Li metal anode, Li^+ conducting electrolyte, and porous air cathode have shown great promise as good candidates for high energy density energy storage devices.[786–796] A Li–air system is an integration chemistry in which the discharge process pertains to the electrochemical oxidation of Li metal at the anode and reduction of oxygen (O_2) from air at the cathode with the reaction between them leading to the formation of a series of products, Li peroxide (Li_2O_2), and Li oxide (Li_2O), which are generally referred to as "oxygen reduction reactions" (ORRs).[793,794,796–799] The charging process involves the electrochemical decomposition of Li_2O_2 (or Li_2O) to Li and O_2 and the related reaction is the so-called "oxygen evolution reaction" (OER) as illustrated in **Figure 29**.[792] In this system, metallic Li acts as the anode while the cathode (oxygen) is drawn from air which is the basis for high theoretical capacity and energy density, distinctly higher than that of conventional rechargeable battery systems (Ni-Cd, Ni-MH, and Li-ion). For example, the nonaqueous Li–air battery that operates based on a simple reaction chemistry between Li ions and oxygen ($2Li^+ + O_2 + 2e^- \leftrightarrow Li_2O_2$, $E = 2.96$ V) can have a high theoretical specific energy and energy density of about 3505 Wh kg^{-1} and 3436 Wh L^{-1}, respectively.

However, the current nonaqueous Li–air batteries still face many challenges, including:[793–795,797,800] (i) The lack of efficient electrocatalysts and air cathodes for both oxygen ORR and OER; (ii) isolation of electrolyte as well as Li metal to prevent reaction with H_2O and CO_2 from ambient air; and (iii) poor cycle life/reversibility of the chemistry and high overpotential due to the formation of irreversible Li_2O_2 products. The high reactivity of superoxide ions formed during discharge causes severe electrolyte degradation and catalyst poisoning, which require the design of multifunctional and stable electrocatalysts.

6.1. Graphene

Superior properties of graphene render pure graphene or graphene/catalyst nanocomposites as potential cathode materials and electrocatalysts for rechargeable Li–air batteries.[673,801,802] It was reported that a pure graphene cathode can form an ideal 3D structure with well-defined diffusion channels for both the electrolyte and O_2, which can increase the reaction efficiency. Graphene also have adequate active edge sites, which significantly contribute to the superior electrocatalytic activity toward ORR and lead to an excellent discharge capacity of 8706 mAh g^{-1} in nonaqueous electrolyte systems.[803] Sun et al. reported results on the use of graphene as a cathode catalyst for rechargeable Li–air batteries in an alkyl carbonate electrolyte, which showed higher catalytic activity than that of Vulcan XC-72 carbon-based cathode.[804] Similarly, Wang et al. drew a multi-layered graphene-based air electrode on the surface of a Li-ion conducting ceramic film-based electrolyte. These multilayered graphene-based cathode effectively catalyzed the ORR with capacity retention of 500–700 mAh g^{-1} for

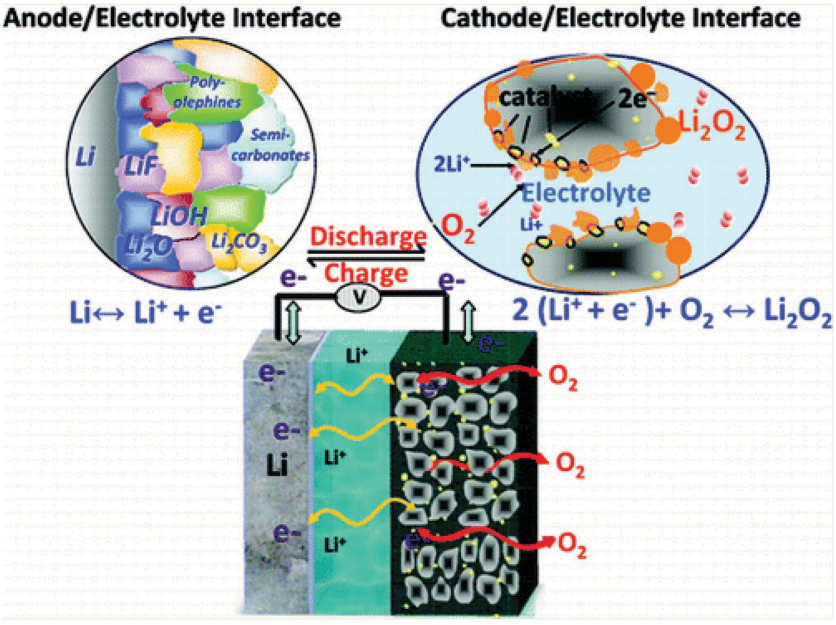

Figure 29. Schematic diagram showing the operations of a rechargeable aprotic Li–air battery. Reproduced with permission.[792] Copyright 2010, American Chemical Society.

over 15 cycles.[805] Graphene has also proved to be a promising constituent of air–cathode in hybrid Li–air systems composed of an aqueous electrolyte at the cathode side and an non-aqueous electrolyte at the anode side. In Yoo and co-workers' study, they examined graphene nanosheets (GNSs) for use as air–electrode in a hybrid Li–air system.[806] It was shown to significantly reduce the overpotential and a high capacity could be achieved in this hybrid battery systems. The presence of sp^3-hybridized carbon atoms at the edges of GNSs was suggested as the contributor for the reduction of overpotential. In additon, these GNS-based air electrodes exhibited a stable capacity retention up to 50 cycles.[806]

6.2. Porous Graphene

The structure of graphene electrode has a significant impact on the performance of Li–air batteries and a porous graphene electrode can help increase the performance because the pore size and pore volume can affect the discharge capacity in Li–air battery cathode.[807,808] For example, larger pore volume allows Li oxides to be accommodated during discharge process. On the other hand, the entrance of the pores clogs easily if the pore size is too small.[807,808] Therefore, the pore size should be optimized to prevent clogging, enhance effective diffusion of oxygen over the entire pore network in graphene and to maximize the pure volume to accommodate large amount of discharge products.[807,808]

Xiao and co-workers adopted colloidal microemulsion to fabricate hierarchically porous 3D graphene cathode with interconnected pore channels at both the micron and nanometer scales.[809] SEM images in **Figure 30**a,b clearly indicate the presence of porous architectures. In Figure 30c,d, the SEM images suggest that lattice defects on functionalized graphene play a critical role through hosting the small, nanometer-sized discharge products (Li_2O_2), which is also observed using DFT modeling as shown in Figure 30e,f. The combination of hierarchical pore structure and graphene surface defects produces an exceptionally high capacity of ≈15 000 mAh g^{-1} at the first discharge cycle as shown in Figure 30g.[809] The challenge here is to obtain a high density porous graphene material for an improved volumetric capacity and also to make the system rechargeable.

In Wang and co-worker's work, the authors found that a free-standing, hierarchically porous carbon derived from GO gel on Ni foam could serve as an effective air–electrode for Li–air batteries.[810] The Go nanocomposite delivered high capacities of 11060 mAh g^{-1} and 2020 mAh g^{-1} at high current density of 0.28 A g^{-1} and 2.8 A g^{-1}, respectively. The authors attributed these excellent performances to the synergistic effect of the loose packing of the carbon, the hierarchical porous structure, and the high electronic conductivity of the Ni foam.[810]

6.3. Heteroatom-Doped Graphene (or rGO)

Chemically doped graphene has been demonstrated as a catalyst with enhanced activity in Li-air battery electrodes.[811] Yoo et al. showed enhanced electrocatalytic activity of N-graphene cathode in acidic conditions.[812] According to DFT calculations, the presence of pyridine-type species in graphene (N-graphene) activates oxygen reduction due to oxygen bonding with the lone electron pair. In another study, Li et al. used N-graphene as a cathode for rechargeable Li-air batteries, which delivered a

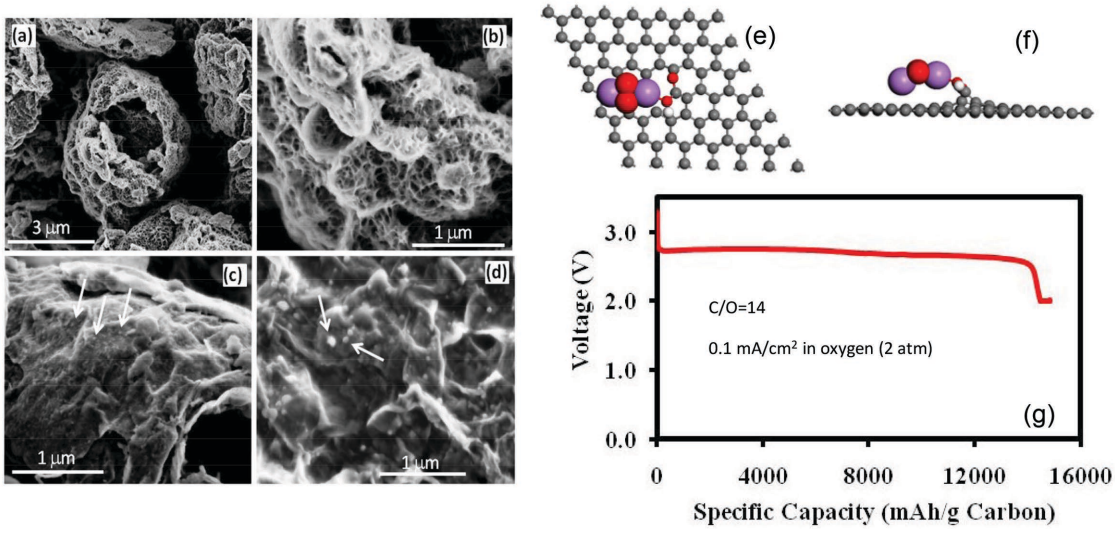

Figure 30. a) SEM of images of egg shell structured FGS with large pores. b) SEM image of the nanopores in FGS. c) Small Li_2O_2 nanoparticles produced on FGS with C/O = 14. d) Large Li_2O_2 nanoparticles of FGS with C/O = 100. e,f) Top and side views of optimized Li_2O_2 on the 5-8-5 defect graphene with COOH functional groups. g) Discharge curve for Li–air battery using FGS (C/O = 14). Reproduced with permission.[809] Copyright 2011, American Chemical Society.

large discharge capacity of 11 660 mAh g^{-1}, ≈40% higher than pristine graphene.[813] The electrocatalytic activity of N-graphene for ORR in a nonaqueous electrolyte was found to be 2.5 times higher than that of pristine graphene. However, the main challenge was the reversibility of oxide products formed after several cycles. The overpotential between the discharge/charge processes was still high due to the irreversible nature of Li_2O formation, which requires further investigation to be fully understood. Electrocatalytic materials for both ORR and OER in the same system have yet to be identified and studied. This requires both computational efforts using DFT modeling and experimental efforts to enable the development of novel low-cost materials.

Recently, Qiu and co-workers fabricated a 3D porous N-doped graphene frameworks made of interconnected nanocages for Li–O_2 batteries.[814] Benefiting from such a unique structure, the as-synthesized electrodes delivered a high specific capacity, an excellent rate capacity of 5978 mAh g^{-1} at 3.2 A g^{-1}, and long-cycle stability, especially at a large current density (54 cycles at 1 A g^{-1}). More importantly, based on the total mass of C and Li_2O_2, a high gravimetric energy density of 2400 Wh kg^{-1} was attained at a power density of 1300 W kg^{-1}. Similarly, N,S-co-doped graphene was also used as cathode for Li–O_2 batteries.[815] Due to the unique properties of these materials, such as large surface areas, good flexibility, coexistence of N and S atoms with tunable doping contents and positions, and high electrical conductivity, the obtained N,S-co-doped graphene sheets exhibited low discharge–recharge voltage gaps, high round-trip efficiencies as well as exceptional rate capability as cathode materials for Li–O_2 batteries.[815]

6.4. Graphene/Noble Metals or Transition Metal Oxides

To further reduce the discharge/charge over-potential and increase the energy efficiency and enhance cycle life stability of Li–air batteries, nanostructured noble metals, and transition metal oxides such as platinum nanoparticles (PtNP),[816] ruthenium (Ru),[817,818] RuO_2,[819,820] $CoMn_2O_4$,[821] $MnCo_2O_4$,[822,823] MnO_2,[824–826] Fe_2O_3,[827,828] Co_3O_4,[829,830] ZnO,[831] and C_3N_4,[832] have been incorporated on the surface of graphene or porous graphene and their electrochemical catalytic activities in Li–air batteries have also been investigaetd. For instance, PtNP–GNS hybrid materials synthesized by liquid phase pulsed laser ablation exhibited high capacity and good cycling performance.[816] α-MnO_2 nanorods on GNS showed excellent catalytic properties for ORR and OER in nonaqueous electrolyte.[826]

$MnCo_2O_4$ nanoparticles grown on graphene were also considered as a hybrid catalyst that showed better catalytic activity, comparable to that achieved using Pt/C system.[822] Moreover, a hybrid graphene/Co_3O_4 catalyst demonstrated an excellent catalytic activity toward ORR including a considerably more positive half-wave potential than that of pristine graphene. This catalyst showed better long-term durability than that of the commercial Pt/C catalyst in an alkaline solution.[833]

In Chen and co-workers' work, they developed a 3D nanoporous N-doped graphene/RuO_2 nanoparticle-based cathode for rechargeable Li–O_2 batteries.[834] The results showed that the encapsulated RuO_2 nanoparticles had significantly high catalytic activities and ultrahigh stability. The novel nanoporous N-doped graphene/RuO_2 based Li-O_2 batteries showed highly reversible cathodic reactions for up to 100 cycles at the cutoff capacity of 2000 mAh g^{-1} and low average charge potential of 3.7 V (excellent stability toward Li_2O_2 formation and decomposition), giving rise to low overpotentials for high-efficiency rechargeable Li–O_2 batteries.[834] Most importantly, this synthesis technique presents a general strategy to develop other transition metal oxide/graphene nanocomposites as multifunctional catalysts for Li-air batteries.

Noble metals/oxides show the best performance but their wide use is restricted by the high cost.[817] Transition metal oxides are inexpensive but show limited performance.[835] Therefore, a hybrid combination of both these types of materials is necessary to make the electrocatalysts work better for these systems. These can be designed by conducting modeling work and appropriate synthesis methods. Up to date, these attempts have resulted in low efficiency and poor rate performance, instability, and unwanted chemical reactions. Therefore, more work is needed to address these issues. The electrochemical properties of the various graphene/metal or metal oxide hybrid catalysts for Li–air batteries, including those discussed in this section, are summarized in **Table 4**.

6.5. Recent Breakthroughs

Recently, a team of researchers from the University of Cambridge have successfully used graphene-based cathodes to avoid the production of Li_2O_2 particles, and to overcome these problems in Li–air batteries (**Figure 31**).[843] The team engineered the negative electrode from a highly porous form of graphene, added water and used Li iodide as a "mediator." The synthesis technique also altered the chemical makeup of the electrolyte such that the battery created Li hydroxide (LiOH) at the cathode instead of relying on the Li_2O_2 used in other Li–air battery designs (Figure 31a). The products of the chemical reaction build up in the porous graphene cathode as the battery was discharged, and dissolved as the battery was recharged.[843] Combining the new chemical makeup of the electrolyte with the new, "fluffy" porous graphene electrode resulted in a battery that was far more stable, with an energy efficiency of 93%—which means that the amount of energy lost as heat was close to that of a Li-ion battery. The researchers claimed that their battery can be cycled for more than 2000 times with a relatively low capacity fading (Figure 31b,c).[843] This new approach is a significant advancement, but the researchers stressed that the development of the Li–air battery still has a long way to go, estimating a practical device is still a decade away. The main issue is that, unlike previous experimental Li–air batteries that are able to take their pure O_2 from the air, the Cambridge's battery is cycled in pure O_2.[843]

More recently, collaborative efforts of researchers at Argonne working on Li–air batteries, have led to the development of a novel Li–air battery that could avoid the problem of peroxide (Li_2O_2) build-up (**Figure 32**).[844] In their research published in the journal of Nature,[844] the Argonne team was able to produce a stable LiO_2 by using a rGO/iridium (Ir) nanopartricle-based cathode.[844]

Table 4. Examples of different graphene-based nanocomposites for Li-air batteries reported in the literature.

Cathode materials	Energy efficiency	Electrochemical performance
RuO_2•0.64H_2O/rGO hybrid[819]	75%	Good cycling performances for over 30 cycles at high current of 500 mA g^{-1}, high cutoff specific capacity of 5000 mAh g^{-1}
RuO_2/nanoporous N-doped graphene[836]	72%	Excellent cycle life for up to 100 cycles at the cutoff capacity of 2000 mAh g^{-1}
Graphene/Co_3O_4[833]	76.5%	Good cycling performances for over 50 cycles at a limited cutoff capacity of 200 mAh g^{-1} and a current rate of 160 mA g^{-1}
Fe_3O_4/graphene[837]	72%	Excellent discharge capacity of 1638 mAh g^{-1} at 50 mA g^{-1} current
Porous graphene/Ru[838]	78%	High reversible capacity of 17 700 mAh g^{-1} at 200 mA g^{-1} and a long cycle life up to 200 cycles under the cutoff capacity of 1000 mAh g^{-1} at the same current
Flexible binder-free graphene paper cathodes[839]	87%	Long cycle life up to 16 cycles under a cut-off capacity of 1000 mAh g^{-1} at a current density of 200 mA g^{-1}
Monodisperse MPd (M: Co, Ni, Cu) alloy nanoparticles/rGO[840]	–	High specific discharge capacities of 4407, 3158, and 2512 mAh g^{-1} for CuPd/rGO, Co_3Pd_7/rGO, and Ni_3Pd_7/rGO, respectively.The rGO/Ni_3Pd_7 has the highest capacity of 8175 mAh g^{-1} over 10 cycles
Freestanding, macroporous Graphene@g-C_3N_4[832]	–	High discharge capacity of about 17300 mAh g^{-1} and excellent cycling performance for more than 105 cycles at 1000 mAh g^{-1} cutoff capacity
$MnCo_2O_4$ nanowires/rGO[841]	–	High initial discharge capacity of 11092 mAh g^{-1} and excellent cycling performance for >35 cycles under a limited specific capacity of 1000 mAh g^{-1}
Co-Cu yolk–shell/graphene[842]	92%	High initial discharge capacity of 14821 mAh g^{-1} at 200 mA g^{-1}, 7955 mAh g^{-1} at 800 mA g^{-1}, long cyclability of more than 120 cycles at 200 mA g^{-1} at a cutoff capacity of 1000 mAh g^{-1}

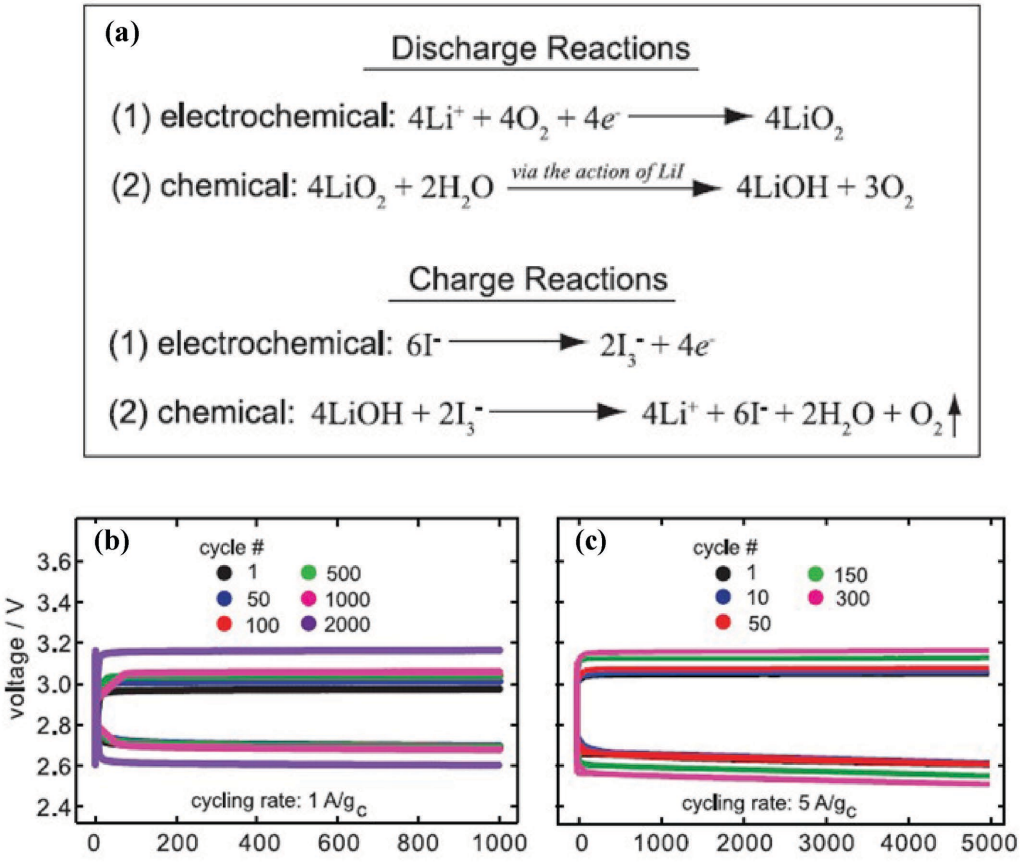

Figure 31. a) A schematic diagram showing mechanisms for the formation and removal of LiOH in iodide redox-mediated in Li-O_2 cells at the presence of water. The electron/LiOH molar ratios during discharge and charge are both equal to 1. b,c) Discharge/charge curves for Li-O_2 batteries using rGO electrodes and a 0.05 M LiI/0.25 M LiTFSI/DME electrolyte with capacity limits of b) 1000 mAhg_c^{-1} and c) 5000 mAhg_c^{-1}, respectively. The cell cycle rate is based on the mass of rGO. Reproduced with permission.[843] Copyright 2015, American Association for the Advancement of Science.

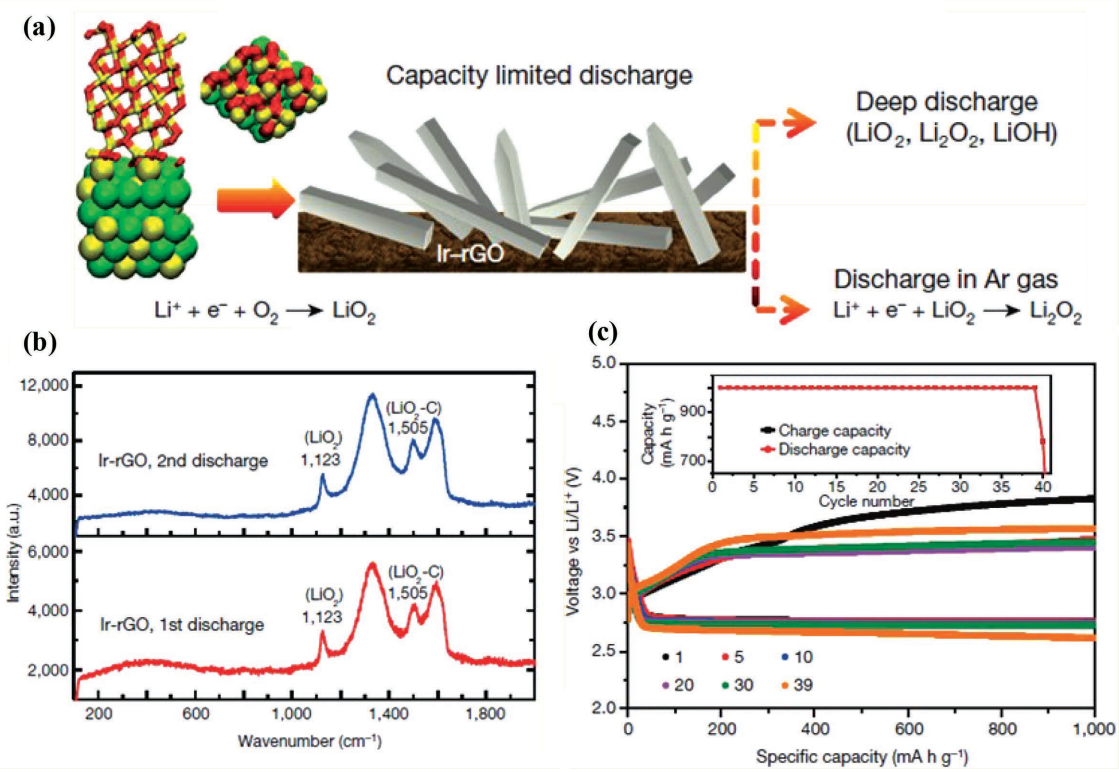

Figure 32. a) Schematic diagram showing lattice match between LiO_2 and Ir_3Li that may be responsible for the formation of LiO_2 found on the Ir–rGO cathode. The two structures at left are the side- and top-views representing epitaxial growth of crystalline LiO_2 in Ir_3Li (Li is yellow, O is red and Ir is green). The rod-like structures are schematic representations of the observed crystalline LiO_2 morphology. Two subsequent electrochemical reactions that the LiO_2 can undergo are shown on the right. b) Raman spectra of discharge product on Ir–rGO cathode for first and second discharge cycles, indicating the existence of LiO_2. c) Voltage profiles of the Ir–rGO cathode. Cycle number of voltage plot is given by the color of the plotting symbol. Inset shows capacity as a function of cycle number. Reproduced with permission.[844] Copyright 2016, Nature Publishing Group.

This approach avoided the presence of Li_2O_2, a solid precipitate in traditional Li–air batteries, which can clog the pores in the electrode, contaminate the cathode that could result in a total battery failure.[844] Additionally, the team found that the working principle of their batteries work relied on the fact that the spacing of the Ir catalyst nanoparticles in the rGO cathode favored the production of LiO_2 and inhibited Li_2O_2 generation.[844] The LiO_2 can easily dissociate back into Li and O_2. Avoiding the loss of O_2 tied up in Li_2O_2 enabled the development of a Li-air battery with a closed system, which would make the units safer and more efficient.[844]

Despite these developments and progresses, current Li–air batteries still suffer from low energy efficiency, poor cycling stability, and serious electrolyte decomposition due to many factors including the clogging of the porous air cathode by insoluble discharge products, contamination of the organic electrolyte and Li metal anode, and the decomposition of the electrolyte during cycling.[845] Li metal is one of the most challenging components in Li–air batteries, as it tends to roughen and form dendrites during cycling, which may also cause some safety issues.[763,764] Several methods exist to solve these problems that include: (i) using solid (inorganic or polymer) or hybrid electrolytes with high Li^+ conductivity, excellent chemical stability and reduced interface impedance,[769] (ii) introducing additives, and (iii) applying pressure on the whole cell to keep a tight contact between all the battery components.[845] Recently, some efforts have been focused on the use of novel graphene structures to increase the safety of Li metal anode.[441] This effective and fruitful pure Li anode protection strategy can help avoid the formation of Li dendrite, minimize electrolyte degradation at the Li anode surface and enhance the stability of Li metal-based batteries. In addition, such a protection strategy may extend the temperature range of the effective discharge of the battery down to negative temperatures.[441] The combination of these graphene-modified anodes with a well-designed graphene nanocomposite-based air cathode might be a promising solution to future practical applications of Li–air technologies. In addition to the electrode material-based research, a better understanding of the detailed reaction mechanisms at the cathode and electrolyte interface, the diffusion kinetics and the capacity limitation/voltage reduction in Li–air batteries are also necessary. Theoretical approaches and modeling studies are urgently needed to understand the relationship between the discharge time and the dimension of the pores that host the oxide precipitates.

Finally, the fabrication of novel polymer or polymer–inorganic nanofiller-based solid or gel electrolytes with improved ionic conductivities and mechanical/thermal properties coupled with graphene-based electrodes may be considered a good strategy to further improve the performance of Li–air systems.[846]

7. Na-Ion Batteries

Na-ion batteries have recently attracted a great interest among researchers as an important source to energy storage devices due largely to the fact that Na is environmentally friendly and inexpensive, and it is the sixth most abundant element in the earth's crust.[847–850] The working principle of Na-ion batteries is similar to that of Li-ion batteries where the transport and kinetic behaviors of Na^+ in the host materials are based on the intercalation or alloying type of the reaction, which is dependent on the host material itself.[847–850]

As shown in **Figure 33**, Na ions migrate back and forth in the Na ion-based electrolyte between the anode and cathode upon the application of a charge/discharge current.[851] The electron transmits through the outer electrical circuit, which counterbalances the ion flow within the electrode materials. Several materials have been used as electrodes for Na-ion batteries including graphitic carbon, hard carbons, Na alloys (e.g. Sn, Sb, SnSb, P, etc.) and some conversion materials (such as transition metal oxides, transition metal sulfide, etc) as anodes and layered oxides, polyanionic phosphates, and pyrophosphates as cathodes.[847–850] Organic compounds have also been proven to be good alternative and environmentally sustainable electrode materials for Na-ion batteries.[852] However, the search for the appropriate host materials for Na^+ is still ongoing. The relative larger ionic size of the Na ion compared to that of Li^+ limits the number of the available host materials.[853]

Graphene and graphene-based composites have been considered as promising electrode materials for Na-ion batteries due to the unique structure, excellent electrically conductive, and high surface area.[854,855]

7.1. Anodes

The anode is a crucial component in a Na-ion battery because it determines the safety and the cycle life of the Na-ion battery; therefore it is necessary to design anode materials that meet these requirements. Na metal cannot be directly used as anode in Na-ion batteries for practical applications due to its safety concern issues and the unstability of passive layer in most organic liquid electrolytes. Hence, it is necessary to use alternative anode materials with high capacity, appropriate voltage window and good structural integrity during prolonged charge/discharge cycles. The widely used graphite anode as Li^+ host could not be used as Na^+ host because of the larger ionic size of Na ion, which limits the total number of Na could be stored in graphite that has limited interlayer spacing.[856,857]

7.1.1. Pure Graphene-Based Anodes

Pure graphene has been rarely used as electrode material in Na-ion batteries due to the lack of defects in its layer structure and the low Na^+ adsorption to the graphene surface. In fact, the capacity of a single layer of pure graphene is very modest compared to hard carbon or to other carbonaceous materials.[858] Recent modeling work showed that the presence of defects in graphene can dramatically improve the electrochemical performance of graphene-based electrodes for Na-ion batteries due to the enhanced Na adsorption to the defective graphene rather than pristine graphene.[854,859]

The Na-storage properties of graphene-based materials can be further improved by creating hierarchically porous structure, carrying out heteroatom doping and/or fabricating different types of graphene-based nanocomposites.

7.1.2. Porous Graphene-Based Anodes

Porous graphene have recently shown promises as high capacity anodes for Na-ion batteries because the porous structure promotes fast Na^+ insertion and improves the electrical

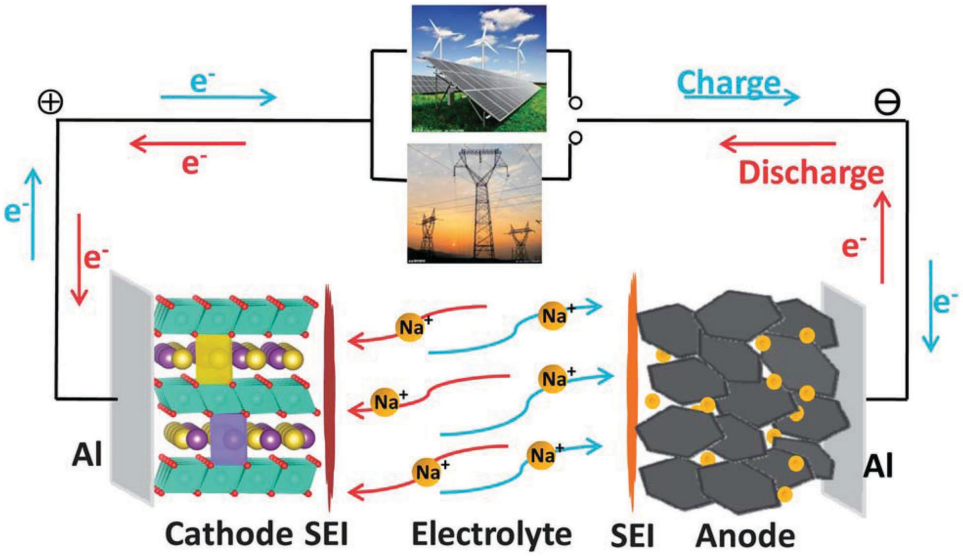

Figure 33. A schematic diagram which shows the working principle of the rocking chair type Na-ion batteries. Reproduced with permission.[851] Copyright 2013, Royal Society of Chemistry.

conductivity of graphene.[860–865] In fact, the porous graphene on both sides of graphene surface can enhance the Na^+ diffusion, thus improving the specific capacity and rate performance.[860,866] In the study conducted by Yan et al., a sandwich-like hierarchically porous carbon (HPC)/graphene composite was designed as a high-performance anode for Na-ion batteries.[867] The hierarchical porous carbon facilitated the Na-ion insertion while the graphene provided a high electronic conductivity for electrons supply. The sandwich-like graphene@HPC composite displayed a specific capacity of 400 mA g^{-1} at 1 A g^{-1} after 1000 cycles. However, a high irreversible capacity of the porous carbon/graphene composite anode was reported.[867] Substrates such as copper and nickel foam have been used to grow graphene oxides layers with common methods such as CVD, simple modified reduction process, and sintering. The porous hierarchical structure/architecture electrodes from these depositions often facilitate Na^+ diffusion while the graphene is beneficial for the fast electron transport.[868,869]

7.1.3. Heteroatom-Doped Graphene-Based Anodes

The heteroatom doping with O, N, B, P can significantly increase the electrode/electrolyte wettability, electronic conductivity, and also create abundant defects and active sites in the graphene structure.[859,866,870–873] Doped graphene composites have been recently used as anodes for Na-ion batteries due to the improved electron transfer efficiency caused by the increased amount of defects in the graphene structure after doping. In addition, the doping can help create more reactive site, preserve structure integrity of graphene during sodiation/desodiation, leading to improved electrochemical performance in Na-ion batteries.[874–876] Wang et al. was the first to report results on the use of rGO as anode in Na-ion batteries where a charge capacity around 150 to 200 mAh g^{-1} was reported.[877] The presence of defects in rGO results in improved capacity and rate performance but these defects had same drawbacks in terms of columbic efficiency for Na-ion batteries.[855,878–880] Similarly, Xu et al. developed a 3D graphene anode based on N-doped graphene (N-graphene) for Na-ion batteries.[871] The 3D N-graphene anode exhibited a high initial capacity of 852.6 mAh g^{-1} at 1C and the anode maintained a high capacity of 594 mAh g^{-1} with 70% capacity retention after 150 cycles. The outstanding electrochemical performance of the 3D N-graphene anode was attributed to the synergetic effects associated with the highly porous structure, high surface area, and the defects induced by the N-doping that facilitated the Na ion diffusion coupled with the low volume change of the porous structure after repeated charge/discharge cycles.[871] Recently, Ling et al. designed a B-doped graphene as promising anode for Na-ion batteries.[872] From the first-principle calculations, they demonstrated that the sodiation of B-doped graphene well preserve its structural integrity. These materials delivered a high reversible capacity which is more than 2.5 higher than that of hard carbon in a Na-ion battery. In addition, the high electronic mobility and Na mobility on this B-doped graphene also led to a high potential to reach good rate performance.

7.1.4. Graphene (or rGO)-Based Nanocomposites

Graphene or rGO-based nanocomposites,[881–892] also show excellent promise as good anode materials for Na-ion batteries due to their high specific capacity, excellent cycle performance, and enhanced rate capability.[879,880] Transition metal oxides (e.g., SnO_2, Co_3O_4, Fe_3O_4, Fe_2O_3, NiO, GeO_2,TiO_2, $MgFe_2O_4$), transition metal sulfides (such as SnS_2, SnS, MoS_2, NiS_2), metal or metal alloy (e.g. Sn, Sb, SnSb, P), and NASICON-type $NaTi_2(PO_4)_3$ were among the most popular materials added to graphene matrices, in the fabrication of fully functional nanocomposite-based anodes for Na-ion batteries.[496,856,873,886,893–913] The results showed that these graphene nanocomposite-based anodes enabled the development of Na-ion batteries with higher specific capacity, better rate capability and longer cycle life than bare graphene.[846,856,877,903,905,914–919]

Graphene (or rGO)/Transition Metal Oxide-Based Anodes: Transition metal oxide/graphene composites have shown a great interest as anodes for Na-ion batteries.[865,880] For example, SnO_2/graphene composite anode that was prepared by in situ hydrothermal method delivered a high capacity of 700 mAh g^{-1} after 100 cycles at 20 mA g^{-1} for Na-ion battery anode (**Figure 34**).[920]

Xie et al. investigated the effect of N-doping into graphene to improve the electrochemical performance of SnO_2/graphene composite-based anode for Na-ion batteries.[874] The SnO_2/N-graphene composite anode showed an enhanced electrochemical performance for Na-ion batteries compared to the SnO_2/graphene counterpart.[874] It was shown that N-doping could not only improve the Na^+ storage capacity within the graphene networks by increasing electro-active sites, but also improve the electron transfer efficiency within the electrode, leading to enhancement of the electro-activity in SnO_2/N-graphene nanocomposites.

Recently, Liu et al. synthesized Co_3O_4 mesoporous nanosheets/3D graphene networks (Co_3O_4MNSs/3DGNs) nanohybrids and investigated as anode materials for Na-ion batteries.[921] Results from this study showed that the Co_3O_4 MNSs/3DGNs nanohybrids exhibited better Na-storage performance with enhanced reversible capacity, good cycle performance, and rate capability as compared to single Co_3O_4 MNSs and Co_3O_4 nanoparticles. The improved electrochemical performance was attributed to the mesoporous nature of the products, the addition of 3DGNs, 3D assembled hierarchical architecture and the decrease in volume expansion during cycling.[921] In Fu and co-workers' study, they fabricated diamond-like Fe_3O_4 nanoparticle/graphene composites for Na-ion batteries.[908] The reported initial discharge capacity was 855 mAh g^{-1} at 100 mA g^{-1}, and after 40 cycles, the discharge capacity was stabilized at about 210 mAh g^{-1}. This value can remain relatively stable for more than 250 cycles.[908] The excellent performance was attributed to the greatly improved electrical conductivity, large surface area, and excellent stability of the electrode material.[908]

Graphene (or rGO)/Transition Metal Sulfide-Based Anodes: Transitional metal sulfide/graphene composites are also considered as good candidates for Na-ion batteries anodes.[353,865,896,916,922–928] Xu et al. reported results on the use of a freestanding SnS_2/graphene nanosheets as anodes for Na-ion batteries by using a two-step solvothermal reaction

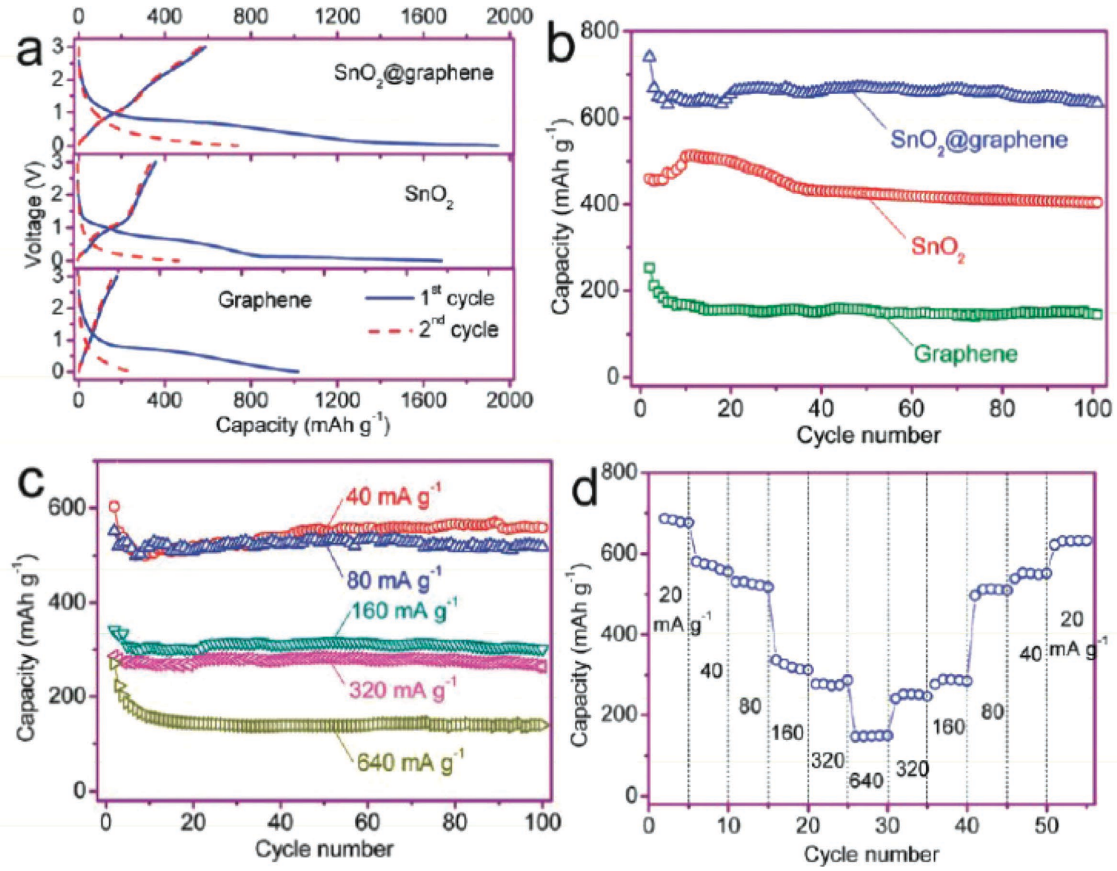

Figure 34. a) The charge and discharge profiles at the first and second cycles of bare graphene, bare SnO_2, and SnO_2@graphene nanocomposite-based anodes at 20 mA g^{-1} current density. b) Cycling performance of bare graphene, bare SnO_2, and SnO_2@graphene nanocomposites at 20 mA g^{-1} current density. c) Cycling performance of SnO_2@graphene nanocomposites at various current densities. d) Rate performance of SnO_2@graphene nanocomposites at varied current densities. Reproduced with permission.[920] Copyright 2013, Royal Society of Chemistry.

strategy.[900] The anode exhibited a capacity of 378 mAh g^{-1} after 200 cycles at a current density of 1200 mA g^{-1} with a good rate performance up to 3000 mA g^{-1}.[900] Similarly, SnS_2 restacked on graphene was developed by Liu et al. as an anode for Na-ion batteries where a high capacity of 650 mAh g^{-1} at a current density of 200 mA g^{-1} was reported, showing an excellent electrochemical performance.[496] This outstanding performance of the SnS_2/graphene composite anode was attributed to the synergetic effects between the ultra small SnS_2 and the highly conductive graphene network.[496] Results reported by Qu et al. on the design of a layered SnS_2/rGO composite anode for Na-ion batteries[929] showed that the SnS_2/rGO electrode delivered a high charge specific capacity of 630 mAh g^{-1} at 0.2 A g^{-1}, good rate performance and long cycle-life of 500 mAh g^{-1} at 1 A g^{-1} for 400 cycles (**Figure 35**).[929]

The good electrochemical performance was attributed to the SnS_2-layered structure where the increased interlayer spacing acted as a buffer for the high volume change during Na–Sn insertion and deinsertion; and also to the good conductivity and mechanical resilience of the rGO nanocomposite.[929] In a study involving exfoliated MoS_2 sheets and rGO synthesized by Sahu et al. and directly used as anode for Na-ion batteries,[896] a reversible specific capacity of 575 mAh g^{-1} at 100 mA g^{-1} and 218 mAh g^{-1} at 50 mA g^{-1} was reported.[896]

Similarly, a 3D MoS_2–GO microsphere was used as anode for Na-ion batteries.[930] The MoS_2/GO microsphere composite delivered a high charge/discharge capacity of 797 and 573 mAh g^{-1} at the first cycle at 0.2 A g^{-1}.[930] After 600 cycles, the discharge capacity was preserved at about 322 mAh g^{-1} at a current density of 1.5 A g^{-1}.[930] Aside the incorporation of the graphene oxide into the host material matrix, growing graphene directly on a suitable substrate has been demonstrated to deliver a better electrochemical performance.[869,924,931,932]

Metal sulfide/metal oxide graphene tri-composites have also been considered as suitable anodes for Na-ion batteries. For instance, SnO_2 has extensively been investigated as a potential anode for Na-ion batteries due to its high theoretical capacity (667 mAh g^{-1}) and abundance but it shows poor electronic conductivity and low initial columbic efficiency.[933,934] SnS has also attracted attention as good anode material for Na-ion batteries owing to its layered structure and high reversible capacity.[912,935] Hence, designing hetrostructures of metal oxides and metal sulfides can result in anodes with enhanced electronic conductivity, Na-ion diffusion capability, good cyclability, and performance.[936] In a study by Zheng et al., the authors developed a novel anode electrode with a good architecture for Na-ion batteries. In this design, an amorphous carbon covered SnS/SnO_2 heterostructures were further anchored by graphene

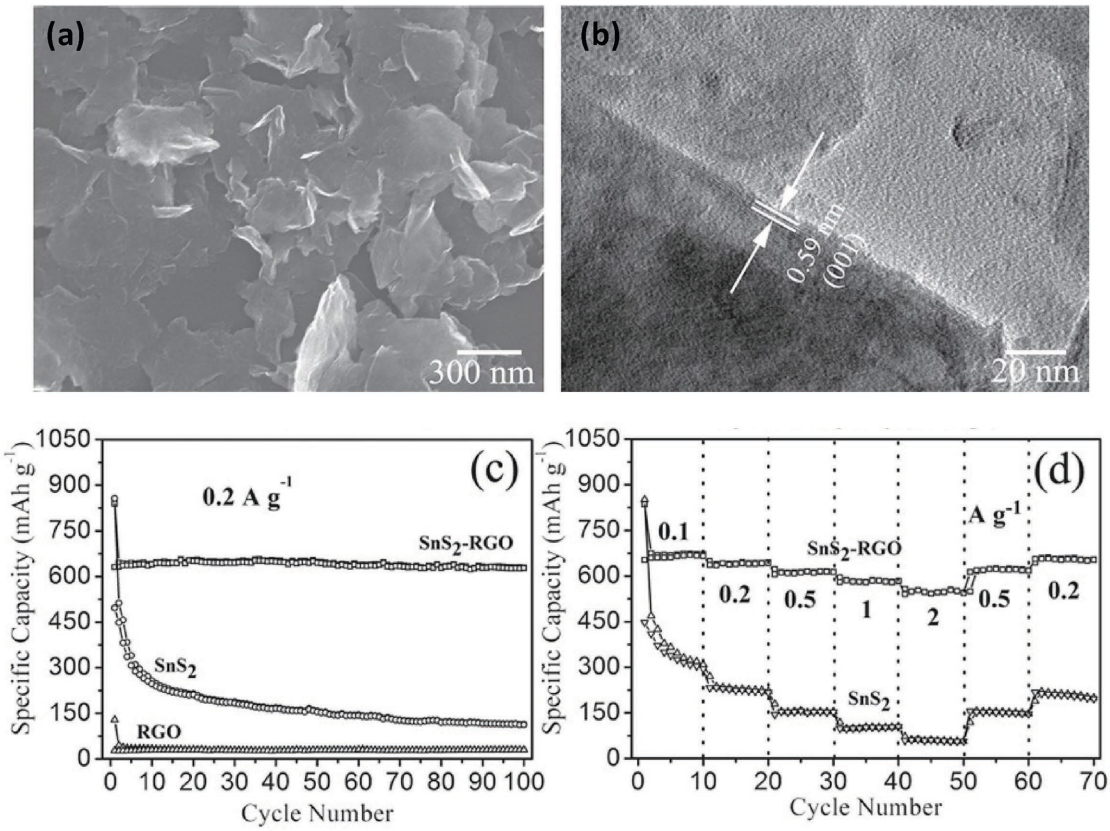

Figure 35. Representative a) FE-SEM and b) HR-TEM images of the SnS_2–rGO nanocomposites. c) Cycle performance of the SnS_2–rGO nanocomposite-, SnS_2-, and rGO-based anodes in Na-ion batteries at 0.2 A g^{-1} for 100 cycles. d) Rate performance of SnS_2–rGO nanocomposites and SnS_2-based anodes at various current densities. Reproduced with permission.[929] Copyright 2014, Wiley.

nanosheets and used as Na-ion battery anodes (**Figure 36**a).[936] The C@SnS/SnO_2@graphene composite anode delivered a capacity of 409 mAh g^{-1} after 500 cycles at 810 mA g^{-1} with a capacity retention of 73%, indicating an outstanding cycling stability (Figure 36d). At prolonged 500 cycles at 2430 mA g^{-1}, this graphene-based nanocomposite anodes still exhibited a reversible capacity of 360 mAh g^{-1} (Figure 36d).[936]

Graphene/Metal or P Nanocomposite-Based Anodes: Metal/graphene composites have also attracted interest as anodes for Na-ion batteries. In one study, a Sb/multilayer graphene hybrid anode delivered a high reversible sodium storage capacity of 452 mAh g^{-1} at 100 mA g^{-1} with a stable cycling performance (90% capacity retention after 200 cycles) and good rate capability up to 5000 mA g^{-1}.[937] In the same vein, Ding et al. fabricated NiSb/Sb hybrid nanostructures in situ grown in the interlayer between graphene and 3D nickel substrate by a graphene confined replacement strategy.[898] The graphene composite anode delivered a reversible capacity of 517 mAh g^{-1} at 50 mA g^{-1} and 315 mAh g^{-1} at 1000 mA g^{-1} with a capacity retention of 305 mAh g^{-1} after 100 cycles at 300 mAh g^{-1}, respectively.[898] Sb-C-graphene fibrous composites were also prepared by Li et al. using electrospinning technique and the subsequent carbonizaton processes and used as a binder, and carbon black-free anode for Na-ion batteries.[938] The Sb nanoparticles were well distributed in the C-graphene matrix where a good reversible specific capacity of 274 mAh g^{-1} was reported after 100 charge/discharge cycles at a current density of 100 mA g^{-1}.[938] A rGO loaded with SnSb nanocomposites was also investigated by Ji et al. as anode in Na-ion batteries.[895] The rGO–SnSb nanocomposites were synthesized through a hydrothermal reaction and subsequent thermal reduction treatments. The rGO–SnSb nanocomposite anode delivered a capacity of 407 mAh g^{-1} over 80 cycles with a good rate capability up to 30C.[895] Sun et al. reported interesting results on anode for Na-ion batteries composed of a few P layers sandwiched between graphene layers, which showed a specific capacity of 2440 mAh g^{-1} at a current density of 0.05 A g^{-1} with a capacity retention of 83% after 100 cycles.[939] In Zhang and co-workers study, they fabricated flexible paper made of N-doped graphene and amorphous P.[940] The nanostructured hybrid anode exhibits an ultrastable cyclic performance and excellent rate capability (809 mAh g^{-1} at 1500 mA g^{-1}). The excellent structural integrity of the novel anode was further visualized during cycling by using in situ experiments inside a HRTEM technique. A density functional theory (DFT) calculations confirmed that the N-doped graphene not only contributes to an increase in capacity for Na storage but also is beneficial in regards to improved rate performance of the anode.[940]

Graphene/NASICON-Type ($NaTi_2(PO4)_3$) (NTP): The NASICON-type $NaTi_2(PO_4)_3$ (NTP) has recently been used as electrode (anode and cathode) materials for Na-ion batteries due to its high theoretical capacity (133 mAh g^{-1}), high Na^+ conduction, and pronounced thermal stability.[862,941,942]

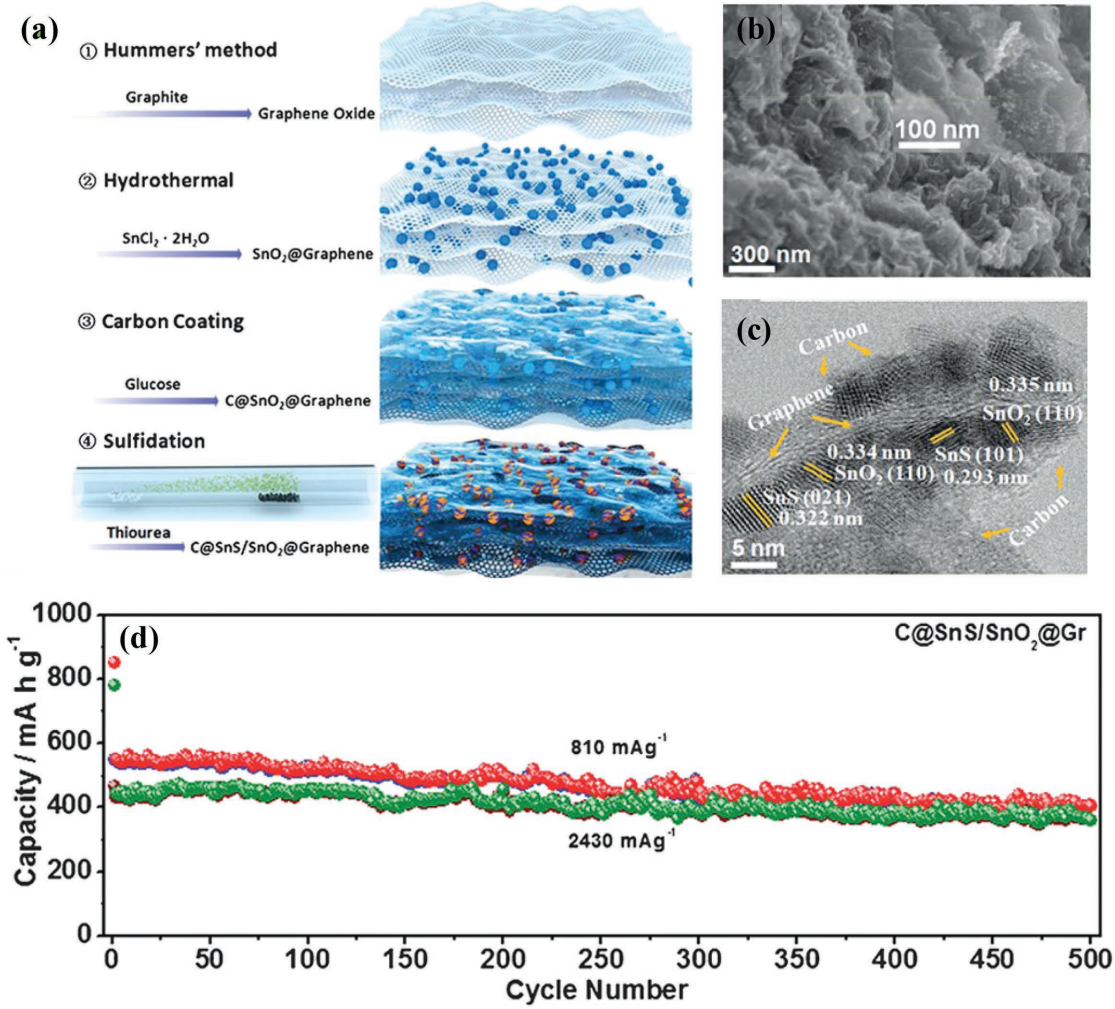

Figure 36. a) Schematic illustration of the formation of the C@SnS/SnO_2@graphene hybrid nanoarchitectures. b) SEM image, and c) TEM image of the fabricated C@SnS/SnO_2@graphene nanocomposites. d) Long-term cycling performance of the C@SnS/SnO_2@graphene nanocomposite-based anodes in Na-ion batteries at two different current densities. Reproduced with permission.[936] Copyright 2016, Wiley.

Owing to the moderate voltage range, NTP can be used as both anode and cathode in Na-ion systems.[862,941,942] Nevertheless, the electrochemical performance of the NASICON-type NTP electrodes suffer from strong polarization (large voltage difference between charge and discharge curves), low capacity release, and poor cycle stability due to its low electronic conductivity.[862,941,942] Combining NTP with electrically conductive materials, such as graphene, to synthesize graphene/NTP nanocomposites are suitable way to prevent these hurdles and improve the overall electrochemical performance of these promising electrodes in Na-ion systems.[862,941,942]

Recently, Pang et al. synthesized 2D graphene/NTP hybrid nanoarchitecture using a novel solvothermal strategy.[906] When used as anode materials for Na-ion batteries, this 2D hybrid nanocomposite-based electrode delivered high specific capacities of 110, 85, 65 mAh g^{-1} at 2, 5, and 10, respectively, and could preserve 90% of the initial capacity after 100 cycles at 2C.[906] Li and co-workers also synthesized graphene/NTP nanocomposites by a sol–gel and post heat-treatment approach.[943] These synthesized nanocomposites displayed a capacity of about 64 m hg^{-1} at 20C, and retained 71% of the initial capacity after 2000 cycles as Na-ion battery anodes.[943] In a recent study by Wu et al., the authors synthesized a novel graphene/NTP architecture that comprised embedded porous NTP nanoparticles in a 3D graphene network (0D-NTP⊂3D-GN).[862] When directly used as anodes in Na-ion batteries, the reversible capacities can be 117, 112, 105, 96, 85 mAh g^{-1} at current rates of 0.5, 1, 5, 10, 20C, respectively. Remarkably, even at a current rate as high as 50C, a reversible capacity of 67 mAh g^{-1} can be available. After 1000 cycles at 10C, it remains 80% retention of the initial charge capacity, outperforming the cycling-stability of the other reported NTP/carbon anodes.[862] In **Table 5**, the electrochemical performance of more of recent graphene-based anode materials for Na-ion batteries are summarized.

Recently, lots of research efforts have been made by many researchers to improve the electrochemical performance of graphene-based nanocomposite anodes for Na-ion batteries. The fabricated graphene nanocomposite-based anodes also enable Na-ion batteries with higher specific capacity, better rate capability, and longer cycle life than that of the corresponding

Table 5. Examples of different graphene-based nanocomposites as anodes for Na-ion batteries reported in the literature.

Materials	Electrochemical performance
SnS_2@graphene nanosheets[900]	A capacity 633 mAh g^{-1} with a current density of 1 A g^{-1} at 400 cycles
Graphene/TiO_2[907]	A capacity of 115 mAh g^{-1} with a current density of 1 A g^{-1} at 300 cycles
Graphene/TiO_2[883]	A capacity of 143 mAh g^{-1} with a current density of 33.5 A g^{-1} at 50 cycles
Sb/carbon/graphene[938]	A capacity of 274 mAh g^{-1} with a current density of 100 A g^{-1} at 100 cycles
Graphene/GeO_2[905]	A capacity of 330 mAh g^{-1} with a current density of 100 A g^{-1} at 50 cycles
Sb/graphene[937]	A capacity of 452 mAh g^{-1} with a current density of 100 A g^{-1} at 200 cycles
Hollow FeSex-decoreated rGO[944]	A discharge capacity of 434 mAh g^{-1} at the 200th cycle at current density of 0.3 A g^{-1}
$MgFe_2O_4$/graphene[793]	A capacity of 347 mAh g^{-1} with a current density of 50 Ag^{-1} at 70 cycles
SnO_2/graphene[920]	A capacity of 700 mAh g^{-1} with a current density of 20 Ag^{-1} after 100 cycles
N-doped graphene foams[871]	A capacity of 852.6 mAh g^{-1} at 1C after 150 cycles
SnSb@carbon nanocable/graphene nanocomposite[945]	A capacity of 360 mAh g^{-1} for up to 100 cycles
SnS/rGO composite[881]	A capacity of 407 mAh g^{-1} with a current density of 100 mA g^{-1} after 100 cycles
3D MoS_2–graphene microspheres[930]	A capacity of 573 mAh g^{-1} at a current density of 0.2 A g^{-1}; The 600th capacity at a current density of 1.5 A g^{-1} is 322 mAh g^{-1}
VS_4/rGO[946]	A reversible capacity of 362 mAh g^{-1} at 100 mA g^{-1} and a good rate performance

individual components. Nevertheless, there are still numerous unsolved issues and concerns that need to be addressed. These issues are often related to the high cost associated with the synthesis and the large-scale production of graphene-based nanocomposites for commercial applications of Na-ion batteries in large stationary energy storage and smart grids. Additionally, more work is needed to improve the safety and the first-cycle Coulombic efficiency of graphene nanocomposite-based anodes for Na-ion batteries.

7.2. Cathodes

Different types of materials with higher voltage than 2 V vs. Na^+/Na have been used as cathodes for Na-ion batteries. Those include but not limited to, Na-Mn-O, $NaMnO_2$, P_2-Na_xVO_2, $Na_2Fe_2(SO_4)_3$, P_2-$NaxCoO_2$, olivine $Na[Fe,Mn]PO_4$, and $Na_{5/8}MnO_2$.[947–952] Graphene-based composites have been investigated as potential cathode materials for Na-ion batteries due to their high electrical conductivity and the ability to prevent active materials from reuniting.[861,953–964] These include graphene or rGO with $NaFeF_3$, $NaMPO_4$, $Na_3M_2(PO_4)_2F_3$, $NaTi_2(PO_4)_3$ (NTP), $(Na_3V_2(PO_4)_2F_3)$, P_2-Na_xCoO_2, $VOPO_4$, and $Na_{5/8}MnO_2$. The $VOPO_4$ cathode displays a high reversible capacity of 11÷h g^{-1}, but it suffers from a slow charge transfer resulting from low electronic conductivity. Interestingly, by incorporating rGO with the above-mentioned conventional cathode materials, the capacity can be increased to a high value up to 150 mAh g^{-1} due to the synergetic effects of rGO on the cathode electrical conductivity.[965] Ruan et al. synthesized a graphene-modified $NaVPO_4F$ as a cathode material for Na-ion batteries.[955] The graphene composite cathode exhibited improved electrochemical performance compared to the pristine $NaVPO_4F$ cathode where a high capacity of 120 mAh g^{-1} and a capacity retention of 97.7% after 50 cycles at 0.05C can be obtained.[955] An FeF_3 hydrate/rGO composite was synthesized by a nonaqueous precipitation method and directly used as cathodes for Na-ion batteries.[956] The FeF_3/rGO composite cathode exhibited a higher discharge capacity of 266 mAh g^{-1} compared to 158 mAh g^{-1} for the pristine FeF_3 cathode. The improved capacity was attributed to the effect of the rGO layers on enhancing the electrical conductivity.[956]

In a recent investigation conducted by Goodenough and co-workers, a $Na_3V_2O_2(PO_4)_2F$/rGO sandwich structure was synthesized using a one-step solvothermal method and was directly used as cathode in a Na-ion battery.[957] The rGO composite cathode delivered a high reversible capacity of 120 mAh g^{-1} at a discharge rate of C/20 with a capacity retention of 100.4 mAh g^{-1} at 1C and excellent cyclic retention of 91.4% after 200 cycles.[957] The improved electrochemical performance of the $Na_3V_2O_2(PO_4)_2F$/rGO composite cathode was due to the sandwich structure of the nanocomposite and the high electrical conductivity the rGO phase.[957] Similar results are also reported by Rui et al. on the synthesis of carbon coated $Na_3V_2O_2(PO_4)_2$ (NVP) in a porous graphene network (from rGO) using a freeze-drying-assisted method (**Figure 37**).[864] The NVP@C@rGO nanocomposite cathode exhibited a long cycle life up to 10 000 cycles at a high rate of 100C (Figure 37).[864] The discharge capacity remained around 55 mAh g^{-1} after 10 000 cycles with a capacity retention of 64% of its initial capacity.[864]

In Wu and co-workers' recent study, the NASICON-type porous $NaTi_2(PO_4)_3$ (NTP) nanoparticles in a 3D graphene network (0D-NTP⊂3D-GN)-based nanocomposite was also used as cathode for Na-ion batteries.[862] The 0D-NTP⊂3D-GN electrode delivered improved electrochemical performance in terms of capacity, cycle life, and rate capability compared to the pristine NTP cathode (**Figure 38**).[862] The incorporation of NTP in the 3D graphene framework synergistically combines the advantages of a 3D graphene network and porous NTP nanoparticles. The macro/mesoporous network enabled the rapid ion transport and

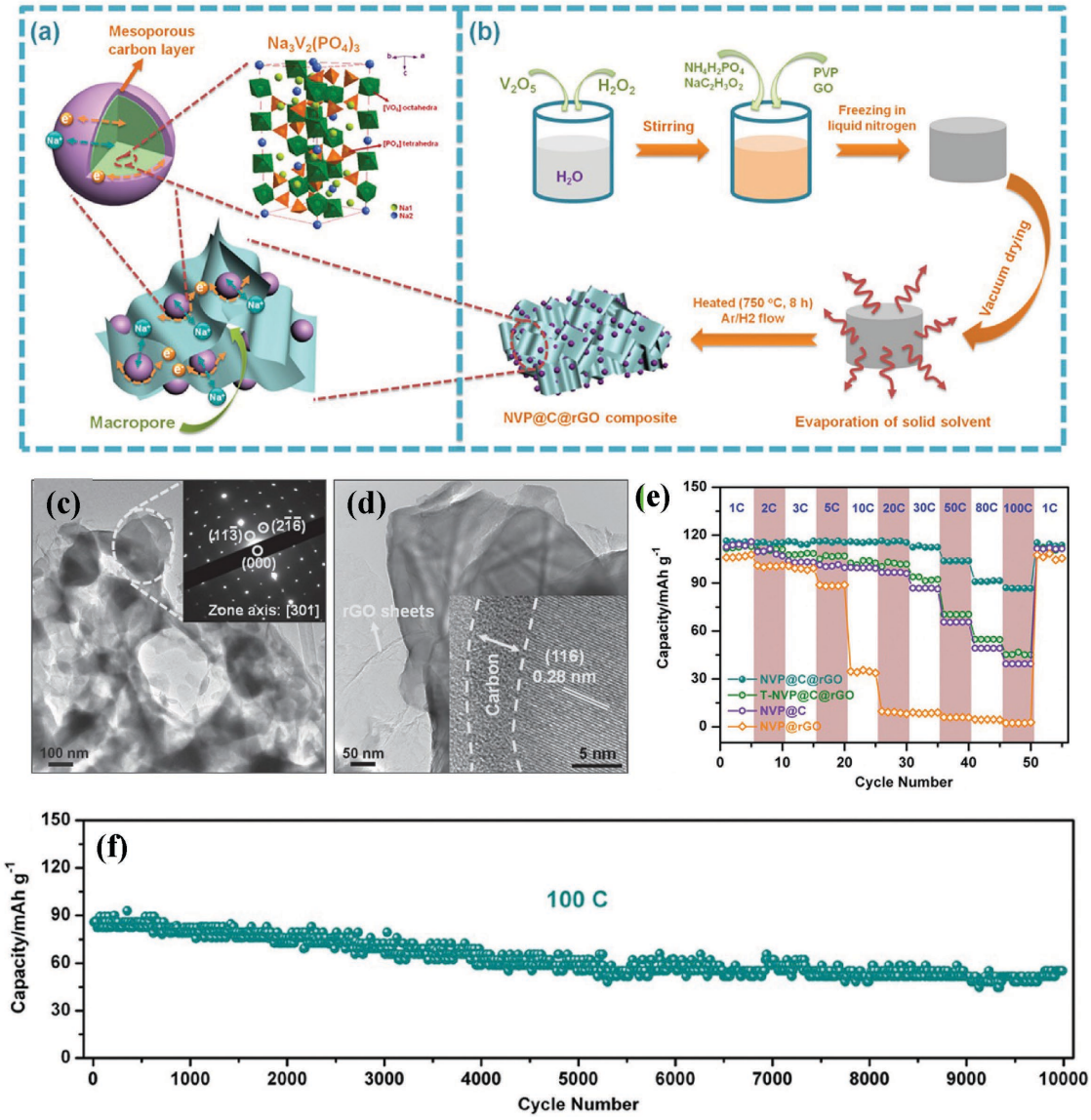

Figure 37. a) A schematic diagram of 3D hierarchical meso- and macroporous $Na_3V_2(PO_4)_3$ (NVP)@C@rGO cathode with pathways for both electrons and Na ions (the upper right corner shows the crystal structure of NASICON-type NVP). b) An illustration of freeze-drying-assisted strategy to prepare NVP@C@rGO nanocomposites. c,d) TEM images of the as-prepared NVP@C@rGO with different magnifications, SAED pattern of an individual particle marked by the circle is inserted in (c), HRTEM image is inserted in (d). e) Rate performance of NVP@C@rGO-based cathodes in Na-ion batteries at various current rates. f) Long-term cycle life of NVP@C@rGO-based cathodes in Na-ion batteries for 10 000 cycles at 100C. Reproduced with permission.[864] Copyright 2015, Wiley.

buffered the strain induced in the intercalation process.[862] This architecture could also greatly enhance the electron/ion transport kinetics and assured the electrode structure integrity, leading to improved electrochemical performance. In addition to NTP, the 3D conductive graphene network also restricted the aggregation of other cathode nanoparticles like, $Na_3V_2(PO_4)_3$, etc, helped improve their electrochemical behaviors as Na-ion battery cathodes.[910,966] In **Table 6**, the electrochemical performance of recent cathode materials used for Na-ion batteries is summarized. Typically the charge/discharge capacities of these cathode materials range between 110 mAh g^{-1} and 266 mAh g^{-1} over several charge/discharge cycles.

8. Na–Air Batteries

Recently, Na–air batteries have attracted a great interest due to their extremely high energy density of about 1600 Wh kg^{-1}. In addition, Na–air batteries are considered good alternatives to replace Li-ion or Li-air batteries due to their low material costs and the natural abundance of Na, which is 30 times cheaper than Li.[967–973] Unlike Li, Na is capable of reversibly forming a stable superoxide (NaO_2) in pure O_2 environment with low overpotentials during discharge process (**Figure 39**).[974]

This enables the Na–air battery to cycle with a charge efficiency of 80%–90% after the first cycle. The formation of

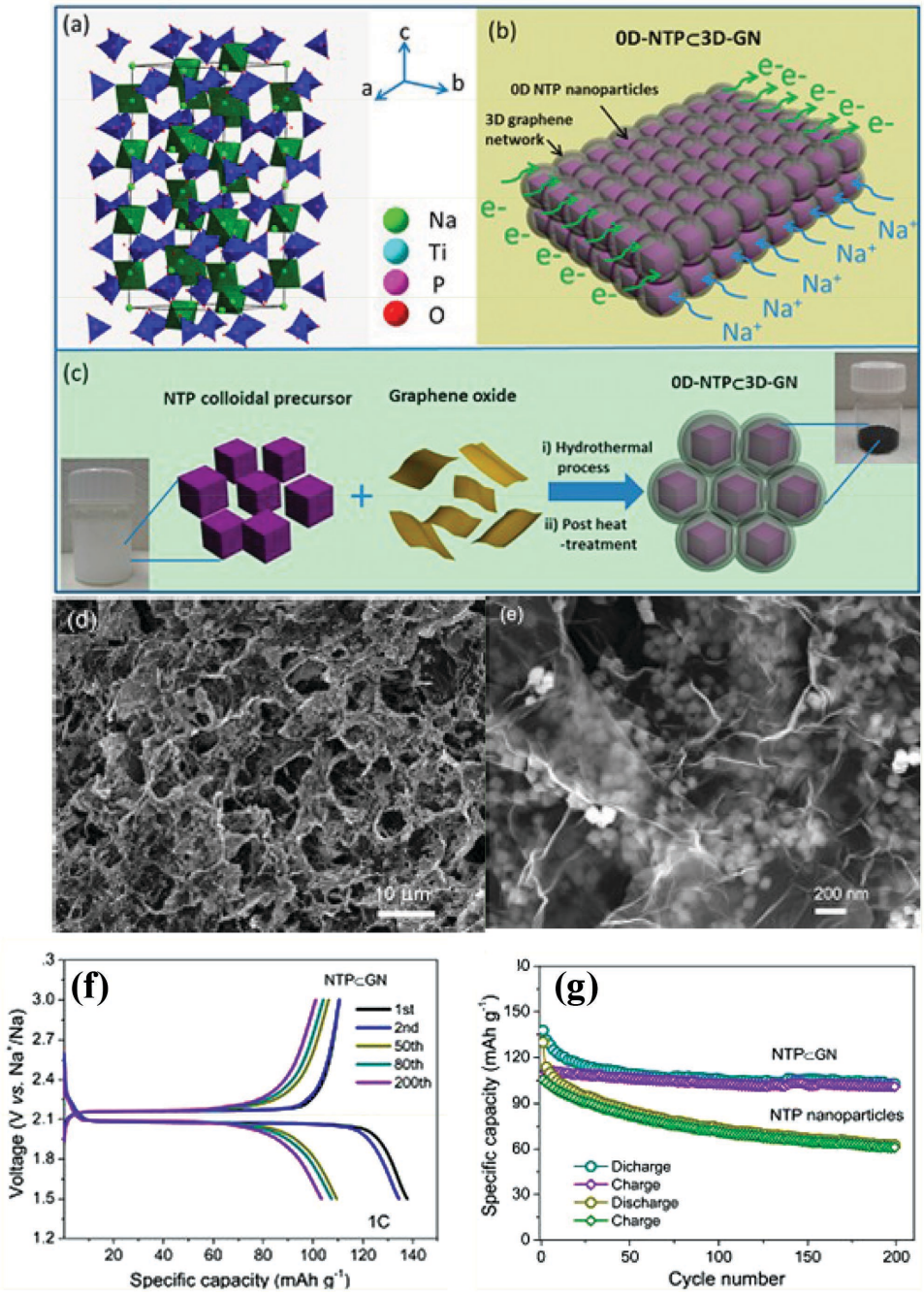

Figure 38. a) Crystal structure of the NASION-type NTP phase. b) Schematic illustration of 0D-NTP⊂3D-GN structure, showing that 0D porous NTP nanoparticles are embedded in 3D graphene network. c) Schematic synthesis processes of 0D-NTP⊂3D-GN, including the two steps of hydrothermal process and postheat treatment. d,e) SEM images of the NTP⊂GN. f) The charge/discharge profiles of the NTP⊂GN-based electrodes at 1C rate. Reproduced with permission.[862] Copyright 2015, American Chemical Society.

peroxide (Na_2O_2), however, is kinetically hindered as it requires a suitable catalyst. A major challenge that needs to be addressed in the Na–air battery technologies is the excessive discharge products that accumulate on the cathode surface. Most of these products have very low electrical conductivity, and thus tend to inactivate surface reaction sites and block O_2 diffusion channels, leading to the increase in polarization during charging and eventual termination of the OER.[967–973] Reducing the accumulation of discharge products, that lead to decreased charge potential and improved cycling performance, requires the morphological and structural properties of the cathode (e.g. surface area, pore volume, and pore size) to be tailored through employing different catalysts.[967–973]

Recently, Liu and co-workers demonstrated that the use of graphene nanosheets as cathodes in Na–air systems can deliver a high discharge capacity and maintain a stable cycle

Table 6. Examples of different graphene-based nanocomposites as cathodes for Na-ion batteries reported in the literature.

Materials	Electrochemical performance
$NaTi_2(PO_4)_3$ embedded in 3D graphene network[862]	A capacity of 112 mAh g^{-1} with a current density of 1 A g^{-1} at 1000 cycles
$Na_3V_2(PO_4)_3$/C nanoparticles[861]	A capacity of 76 mAh g^{-1} with a current density 40 mAh g^{-1} at 1500 cycles
$Na_{3/2}Fe_{1/2}Mn_{1/2}O_2$@graphene[953]	A reversible capacity of 156 mA g^{-1}
$VOPO_4$/rGO[337]	A capacity of 150 mAh g^{-1} at 0.05C
$Fe_2(MoO_4)_3$/rGO nanocomposite[954]	A specific capacity of 75.92 mAh g^{-1} after 50 cycles at 1.5C
$NaVPO_4F$/graphene[955]	A discharge capacity of 118 mAh g^{-1} after 50 cycles at 0.05C
FeF_3/rGO composite[956]	A discharge capacity of 266 mAh g^{-1} at 0.05C with a capacity retention of 86% after 100 cycles
$Na_3V_2O_2(PO_4)_2F$/rGO sandwich structure[957]	A reversible capacity of 120 mAh g^{-1} at a discharge rate of C/20 with a capacity retention of 100.4 mAh g^{-1} at 1C
GO wrapped $Na_3V_2(PO_4)_3$/C nanocomposite[958]	An initial discharge capacity of 106.5 mAh g^{-1} at 0.1C with a capacity retention of 92.5% after 200 cycles
GNS/VOx[959]	A capacity of 224 mAh g^{-1} after 50 cycles at 200 mA g^{-1}
NVP/C/rGO composite[960]	A specific capacity of 103 mAh g^{-1} after 200 cycles at 0.2C
$FeF_3.xH_2O$/graphene[961]	A reversible capacity of 101 mAh g^{-1} after 30 cycles at 0.1C
$Na_3V_2O_2(PO_4)_2F$@ carbon/graphene[962]	A reversible capacity of 112.1 mAh g^{-1} after 40 cycles at 1C
$Na_{6.24}Fe_{4.88}(P_2O_7)_4$@porous graphene composite[963]	A discharge capacity of 114 mAh g^{-1} after 50 cycles at 0.2C

performance for up to 10 cycles.[975] In addition, the rGO has shown remarkable catalytic properties toward the formation of Na_2O_2 under dry air conditions. However, the charge potential increased gradually during cycling, which is attributed to the accumulation of discharge product.[975] In Li and co-workers' study, the authors employed N-doped graphene nanosheets as Na–air battery cathodes.[976] The materials delivered a discharge capacity that was doubled of the value of the undoped graphene nanosheets, confirming the excellent electrocatalytic activity of N-doped graphene nanosheets for ORRs.[976] However, the charge potential was also increased during cycling.[976] Similarly, graphene nanosheets loaded with highly dispersed Pt nanoparticles (Pt@GNSs) were prepared and used as an air cathode material for Na–air batteries (**Figure 40**a,b).[977] These novel materials exhibited a very high initial discharge capacity of 7574 mAh g^{-1} at a current density of 0.1 mA cm^{-2} and delivered a stable cycling performance for 10 cycles (Figure 40).[977]

Despite these progresses, the development of Na–air batteries with graphene-based cathodes is still in a very early stage. Many challenges, such as dendrite formation, instability of electrolytes, by-product formation and poor cycle life still need to be addressed. Therefore, improving the overall electrochemical performance and overcoming the key challenges of the graphene-based cathode in Na–air batteries still requires innovative strategies and solutions.

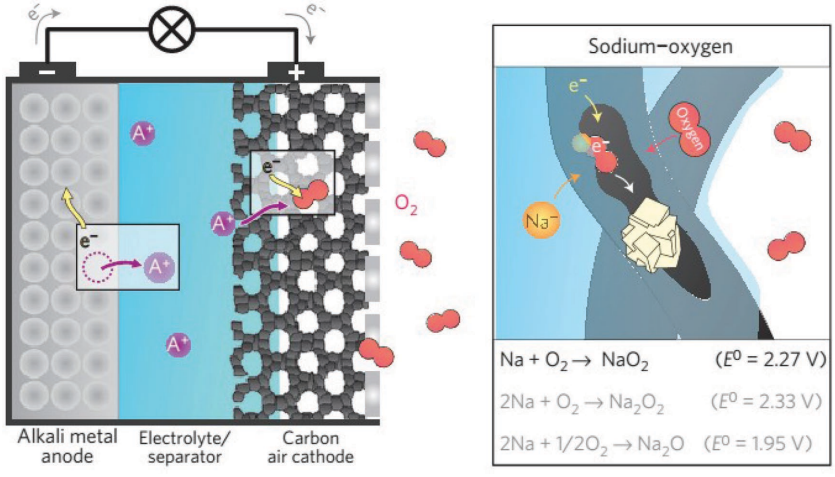

Figure 39. A schematic diagram showing the general working principle of an alkali metal-O_2 battery. During discharge, metal A is oxidized to a soluble A^+ cation at the anode side and the electron will be transferred to the outer circuit. At the cathode side, oxygen will be reduced to an O^{2-} species (superoxide radical) that may form an alkali metal superoxide (AO_2) with the available A^+ cations. In the case of Na, the same reactions may occur, but NaO_2 is thermodynamically more stable and is indeed found as main discharge product in a Na-O_2 cell. Reproduced with permission.[974] Copyright 2013, Nature Publishing Group.

9. Zn–Air Batteries

In rechargeable Zn–air batteries, O_2 from the atmosphere is mixed with Zn in a liquid alkaline electrolyte to create a charge (**Figure 41**).[978] The capacity produced from this reaction is about five times higher than that of the Li-ion batteries.[979–984] Zn–air batteries, with at a theoretical energy density around 1086 Wh kg^{-1}, are expected to be safer, lighter, cheaper, and durable than Li-ion batteries.[979–984] However, the current Zn–air batteries suffer from many challenges such as low cell voltage, carbonate formation in the air electrodes as well as slow kinetic of ORR and OER.[979–985] More research is urgently needed to develop more highly efficient, alternative novel

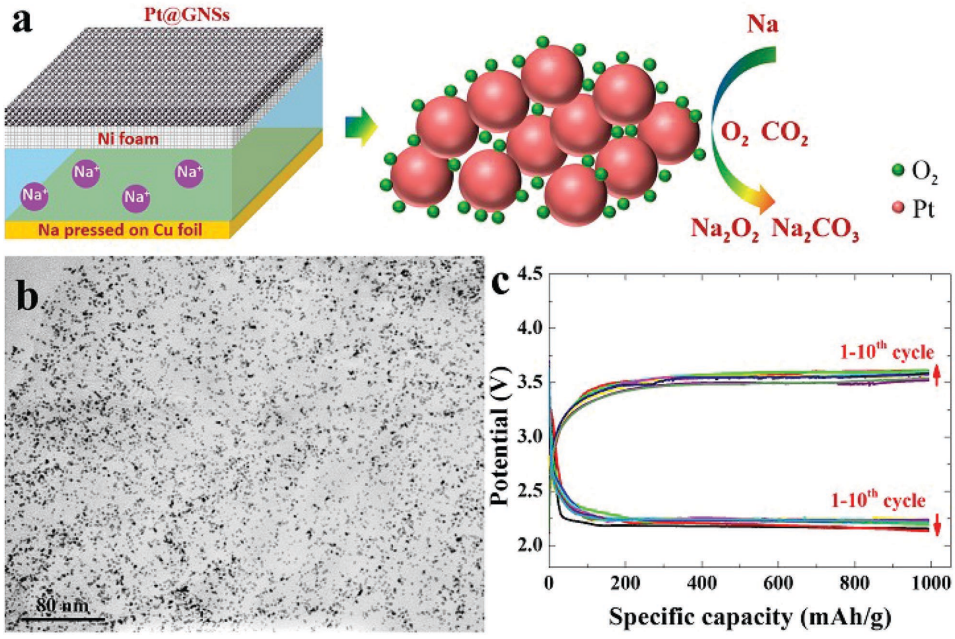

Figure 40. a) A schematic of the structure and proposed electrocatalytic mechanism of the Na–O_2 cell with graphene nanosheets loaded with Pt nanoparticles (Pt@GNSs) as air cathodes. b) TEM images of Pt@GNSs. c) Cycle performance of the initial 10 cycles of Pt@GNS-base air cathodes in a Na–O_2 cell with a capacity limitation of 1000 mAh g^{-1} at 0.1 mA cm^{-2} current. Reproduced with permission.[977] Copyright 2015, Royal Society of Chemistry.

bifunctional electrocatalysts that are effective for both ORR and OER processes.[979–984] The graphene nanosheet with a high specific surface area can provide an excellent substrate for hosting and growing functional nanomaterials for high-performance Zn–air batteries. In fact, novel graphene-based bifunctional air-breathing cathode materials have been considered as a promising electrocatalystic activity that would significantly reduce the overpotential and enhance the cyclic stability toward the realization of rechargeable Zn–air batteries.

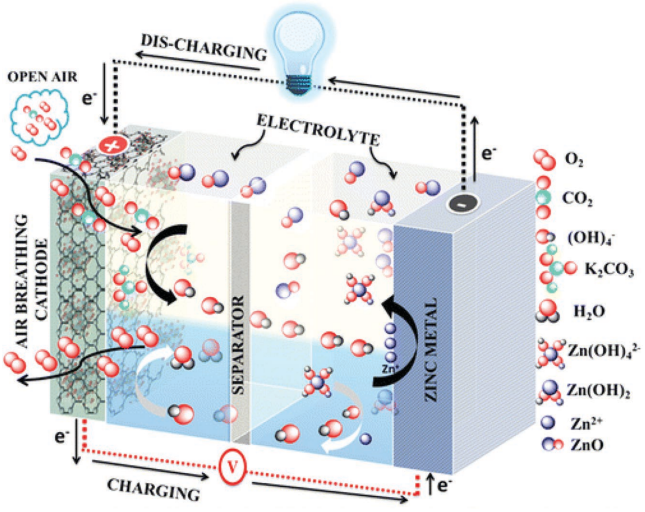

Figure 41. A schematic diagram shows the operation of rechargeable aprotic Zn–air battery. Reproduced with permission.[978] Copyright 2014, American Chemical Society.

In Lee and co-workers' study, integrated Mn_3O_4 nanoparticles were integrated with graphene sheets via a solution-based technique and utilized as effective electrocatalyst for the ORR in Zn–air batteries (**Figure 42**).[986] Figure 42a,b showed the uniform distribution of Mn_3O_4 nanoparticles in the graphene matrix. Figure 42c exhibited that the lattice spacing indeed corresponded to the crystalline Mn_3O_4. The combination of ionic liquid, Mn_3O_4 nanoparticles, and GNS enhanced the ORR electrocatalytic activity for Zn–air batteries as shown in Figure 42d,e, indicating their considerably high catalytic activity for Zn–air batteries.[986]

Recently, experimental observations and theoretical calculations revealed that heteroatoms (e.g., N or/and P, B, S)-doped carbon materials could serve as efficient metal-free electrocatalysts for ORR as the result of their unique electronic properties, which are derived from the heteroatom-induced charge transfer and delocalization.[987–990] Similar reports on N-graphene electrode showed 60% higher discharge current and voltage in a Zn–air system, as well as 42% capacity increase over pure carbon black cathodes in a Zn–air system.[991] In another study, Prabu and co-workers anchored $CoMn_2O_4$ nanoparticles on N-doped graphene sheets and used it as electrocatalyst for rechargeable Zn–air batteries.[992] The N-graphene/$CoMn_2O_4$ nanocomposites were reversibly discharged/charged for several cycles with a good capacity retention in pure O_2 environment.[992] The improved performance was assigned to the synergistic effect of covalently coupling between N-graphene and $CoMn_2O_4$ nanoparticles. Further explorations in ambient air environment also showed outstanding discharge and charge performance and maintained good cycle stability for over 200 cycles.[978] The unique structural, morphological, and electrocatalytic properties of

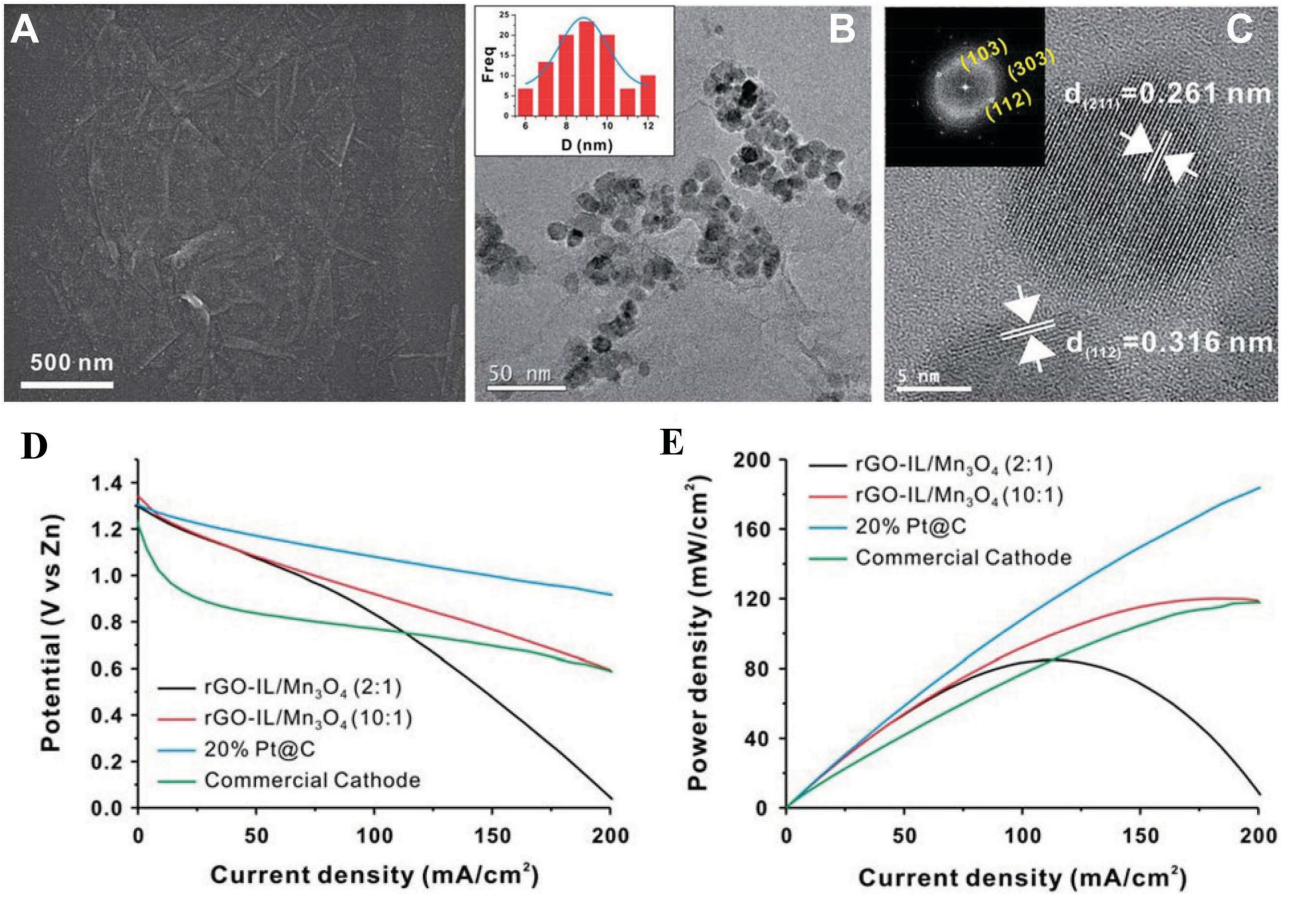

Figure 42. IL-modified rGO (rGO-IL) nanosheets anchoring Mn_3O_4 as efficient electrocatalysts for Zn–air batteries. a) SEM image, b) TEM image, and c) HR-TEM images of Mn_3O_4 nanoparticles with the inset showing the corresponding SAED pattern. d) Polarization curve in a zinc–air cell. e) Power density plot of (black) rGO–IL/Mn_3O_4 (2:1), (red) rGO–IL/Mn_3O_4 (10:1), (blue) 20% Pt/C, and (green) commercial cathode at current densities ranging from 0 to 200 mA cm^{-2}. Reproduced with permission.[986] Copyright 2011, Royal Society of Chemistry.

N-graphene/$CoMn_2O_4$ hybrid electrodes may be a promising candidate for future Zn–air battery applications.[978] Other graphene or graphene-based nanocomposites, such as highly active graphene,[993] N-graphene/Co_3O_4 nanoparticles,[994] N,S-co-doped graphene/CoS_2,[995] N/S-co-doped graphene microwires,[996] and graphene/$LaMn_{1-x}Co_xO_3$,[997] have also been synthesized and their electrocatalytic properties in Zn–air batteries were also evaluated.

Although these recent progresses, there are still several potential problems with these cathode compartments. Some of which include: (i) Mechanical breakdown generated on the catalyst from the air–cathode surface caused by oxygen evolution during charging; (ii) atmospheric CO_2 can react with hydroxyl ions to form carbonates; and (iii) formation of discharge product ZnO deposit on the surface can lead to a severe failure of the air cathode, which will limit the lifetime of Zn–air batteries with large overpotential. In the future, a better understanding of the structure and morphological changes that occur on a bifunctional air electrode will be necessary and helpful to further improve the performance.

10. Vanadium Redox Flow Battery

Vanadium redox flow battery (VRFB) technology has attracted tremendous attention due to their high storage capacity, high efficiency, high reliability, long cycle life, and cost effectiveness.[7,8,998–1005] The VRFB stores energy in the form of two dissolved redox pairs: V(II)/V(III) and V(IV)/V(V) contained in external electrolyte tanks. Energy is generated/stored when the redox species flow through the electrochemical cell anode and cathode chambers separated by an ion-exchange (cation or anion) or microporous membrane and undergo electron transfer reactions at inert electrodes (**Figure 43**).[8] Since the redox reactions are reversible, the VRFB can be classified as a secondary battery system.[7,8,998–1001,1006]

10.1. Electrodes

Graphene promotes a higher rate of ionic adsorption and thereby, enhances electrochemical properties in a VRFB

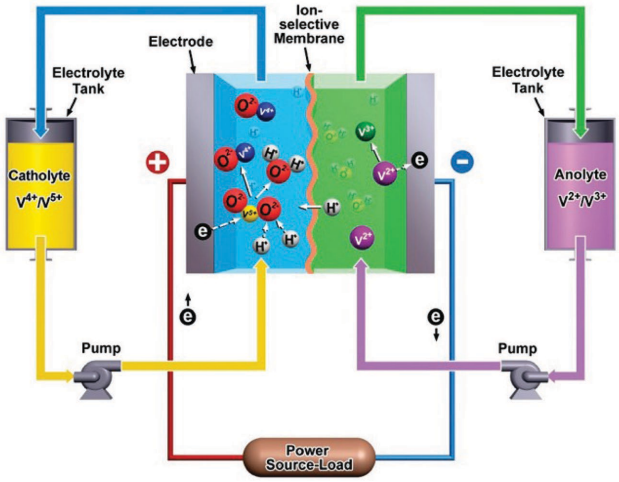

Figure 43. Schematic of an all VRFB as an example of redox flow batteries. Reproduced with permission.[8] Copyright 2011, American Chemical Society.

system.[1002,1007–1009] For example, graphene-based materials obtained from thermally reduced graphite oxides are used as active electrodes in the positive half-cell of VRFB with outstanding electrochemical performance in terms of peak current densities and reversibility.[1010,1011] The rGO composite that contains defects at both edges have been used to improve electrocatalytic activity towards vanadium redox couples (V^{2+}/V^{3+} and VO^{2+}/VO_2^+).[1012] GO with polymer binders also exhibited superior electrocatalytic activity for vanadium bromide RFB.[1013] Graphene-supported monometallic (Pt) and bimetallic ($CuPt_3$) materials have shown to improve the VO^{2+}/VO_2^+ redox process.[1014] RuSe/rGO can significantly alleviate the polarization and improve the reversibility of VO^{2+}/VO_2^+ redox couples in VRFB, by virtue of the excellent catalytic activity and electronic conductivity.[1015] Ir-decorated graphene in VRFB showed improved electrocatalytic activity and reversibility due to high surface area for electrolyte penetration and strong affinity of Ir/vanadium-oxygen ions facilitating ion and electron transport.[1016] N-graphene sheets have also been used as positive electrodes in VRFB.[1017] The N-doped graphene exhibited low electron transfer (ET) resistance and high reversibility indicating high catalytic activity. The N-doped rGO/Mn_3O_4 composites show significantly higher electrocatalytic activity for VO^{2+}/VO_2^+ electrochemistry than those of the individual components due to synergy between Mn_3O_4 and the carbonaceous support material.[1018] These results open new avenues for the fabrication of electrocatalysts using other heteroatoms such as P, B, or S with graphene.[1019]

The GO/MWCNT hybrid materials are synthesized using electrostatic spray technique have shown improved reversibility in VO^{2+}/VO_2^+ redox couples.[1020] A schematic of the electrospray process and material architecture are shown in **Figure 44**a,b.[1020] The fibrous architectures are clearly seen in the TEM images. Specifically, hybrid materials exhibited high anodic and cathodic current densities (Figure 44c) at a high current density ratio of 1.2 even at a 100 mV s^{-1} scan rate (Figure 44d).[1020] The hybrid architecture efficiently reduces the electrode/electrolyte interfacial resistance thereby improving both electron and ion transport kinetics.

In another study, 3D graphene nanowall-decorated carbon felts (CF) were synthesized via an in situ microwave plasma by enhanced CVD method and used as positive electrode for VRFB.[1021] The carbon fibers in CF were successfully wrapped by vertically grown graphene nanowalls, which not only increased the electrode specific area, but also exposed a high density of sharp graphene edges with good catalytic activities for the vanadium ions.[1021] As a result, the VRFB with this novel electrode showed three times higher reaction rate toward VO^{2+}/VO_2^+ redox couple and 11% increased energy efficiency over VRFB with an unmodified CF electrode.[1021] Additionally, the designed electrode architecture showed excellent stability in the battery operation. After 100 charging/discharging cycles, the electrode not only showed no observable morphology changes, but also can be reused in another battery and practically exhibited the same performance. It is believed that this novel structure including the synthesis procedure will provide a new direction for the VRFB electrode development.[1021]

10.2. Membrane Separators

In addition to be used as electrochemical catalysts, graphene nanostructured materials, including sulfonated polyimide (SPI) and zwitterionic polymer-functionalized GO (ZGO),[1022] sulfonated polyimide (SPI) with polyethyleneimine-functionalized rGO (PEI-rGO),[1023] sulfonated poly(ether ether ketone) (SPEEK)/GO,[1024] and GO/Nafion composite membrane,[1025] with tuned physicochemical properties (e.g., vanadium ion barrier and proton transport pathway), have also been used to fabricate hybrid membranes for VRFB. These graphene-based materials showed high ion selectivity and excellent chemical stability under the strong acidic and oxidizing conditions. For instance, the hybrid SPI/ZGO membrane reported higher cell efficiencies (CE: 92%–98%, EE: 65%–79%) than commercial Nafion 117 membrane (CE: 89%–94%, EE: 59%–70%) for VRB application at 30–80 mA cm^{-2} and displayed a stable cycling performance over 280 cycles.[1022] The novel acid-based hybrid SPI/PEI-rGO membranes exhibited higher coulombic efficiency (CE, 95%) and energy efficiency (EE, 75.6%) at 40 mA cm^{-2}.[1022] The self-discharge time of the VRB with SPI/PEI-rGO hybrid membrane (80 h) was longer than that of commercially available Nafion 117 membrane (26 h). After 100 charge/discharge cycles, SPI/PEI-rGO membrane exhibited good stability under strong oxidizing and acid condition.[1023] The VRFB assembled with the SPEEK/GO composite membrane exhibited highly improved cell parameters and strikingly long cycling stability compared with commercial Nafion 117 membrane.[1024] With the protection of porous PTFE substrate, the pore-filling SPEEK/GO composite membrane based on VRFB ran for 1200 cycles with relatively low capacity decline.

Although energy storage in VRFB is inexpensive and efficient and graphene-based materials also show brilliant perspective for VRFB application, they are still in the early stage of development. VRFB requires further advancement to improve the specific energy density as well as energy management of the entire system. It is also worthwhile to look at new materials,

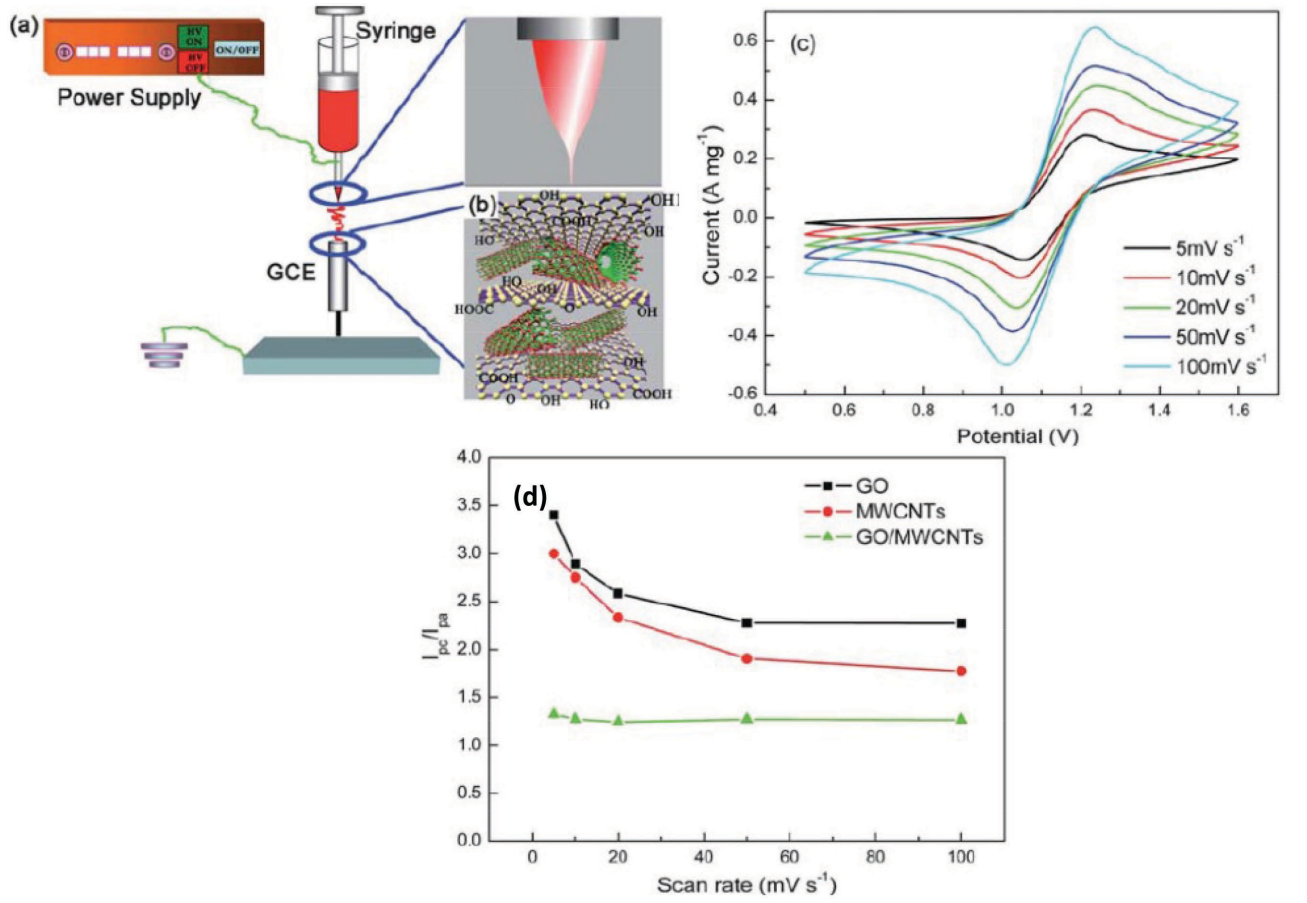

Figure 44. a) A schematic of the electro-spray technique used to fabricate e-sprayed GO/MWCNTs hybrid on a glass carbon electrode (GCE). b) E-sprayed GO/MWNTs hybrid on a GCE. c) CV curves of GO/MWCNTs hybrid at different scan rates in 2 mol L^{-1} $VOSO_4$ + 2 mol L^{-1} H_2SO_4; and d) Curves of I_{pa}/I_{pc} as a function of scan rate for VO^{2+}/VO_2^+ redox couples. Reproduced with permission.[1020] Copyright 2011, Royal Society of Chemistry.

electrolyte, and electrode designs for further progress of VRFB technology.

11. Conclusions and Perspectives

In this article, we have discussed the recent research progress in graphene and graphene-based nanocomposites for energy storage systems. Although a significant progress has been made, their tremendous potentials for practical applications in advanced energy storage systems still needs further explorations.[208,1026–1028] First, the development of graphene and graphene-based nanocomposites for different energy storage-related applications are still in early stage where fundamental gaps exist to understand the atomic and molecular level processes that govern operation, limitations and failure of the devices.[22–38,208,1027] Therefore, multidisciplinary approaches are necessary to better understand the correlation between electrochemistry, materials science, engineering, microstructures, properties, and interactions to overcome the significant challenges facing these energy storage systems. These approaches will lead to the efficient use of large but transient energy sources such as solar and wind necessary to solve the worldwide critical energy issues that are heading the list of global challenges.[22–38,1027]

Second, the high surface area of graphene-based materials plays an important role in supercapacitors and H_2 storage. Specifically, different types of graphene-based nanocomposites, such as graphene/transitional metal oxide (hydroxide), graphene/transition metal nitrides (or sulfide), and graphene–polymer nanocomposites can give rise to twofold advantages, due to the fact that the combination of high surface area of graphene (EDLC) and pseudocapacitative behavior of these polymers/metal oxides (hydroxides, nitrides or sulfides) can result in a tremendous improvement of the capacitance. Although graphene by itself cannot be utilized for H_2 uptake, the use of graphene-based nanocomposites and doped graphene can lead to a high H_2 uptake, much closer to the DOE targets. Despite the great advances in the development of H_2 storage and supercapacitor systems, there is still room for materials' structure and composition optimizations and for further performance improvements.

Li-based chemistries have high energy densities and are considered the primary choice for electronic energy storage. It is highly desirable to use graphene or graphene nanocomposites as potential electrode materials for rechargeable Li-ion batteries. Anode systems would benefit from graphene-based material due to its high conductivity, high surface area and 2D sheet-like architecture. Specifically, the high electronic

conductivity of graphene leads to improved rate performance and power density of the Li-ion battery anode. The high surface area of graphene can either accommodate more Li ions or host other materials when used in composites, which can help improve the capacity and energy density. The 2D architecture is very important since it can significantly improve the material tap density when the sheets are stacked parallel to each other and are more viable for commercialization. Graphene can also manage the interfacial instability when it is introduced as an interfacial layer between the current collector and the anode material, which can help improve the cycling capability of Li-ion batteries.[1029]

The use of graphene as an additive for cathode materials can also help improve the electrochemical performance of the Li-ion battery. Graphene can act as efficient electron transport pathways, hence improving the electron transport between the current collector and the cathode active material. This can help reduce the internal resistance of the battery and enhance the output power. Additionally, the excellent mechanical properties of graphene phases are of great benefit to the structure stability of cathode materials and this can lead to improved cyclic stability and rate capability.

Li–S and Li–air batteries have attracted great attention as potential successors to Li-ion batteries due to their exceptionally high specific energy and energy density compared to the state-of-the-art Li-ion technology. However, both of these new battery technologies suffer from poor cycle stability and low rate capability, which limit their practical applications. Graphene and graphene-based nanocomposites, with their high surface area and enhanced catalytic properties, are considered to be the key potential materials to advance Li–S and Li–air technologies and to achieve a long standing performance for practical applications. In fact, graphene serves as a porous backbone for supporting S to improve the conductivity and hold polysulfide products formed during the discharge process in Li–S batteries. Similarly, the graphene's porosity, conduction and defect sites can help promote oxygen diffusion and selective Li_2O_2 deposition during the discharge process in Li–air batteries.

However, the practical applications of Li–S/Li–air batteries are limited because pure Li metal anode is used in both systems, which can cause the corrosion of Li metal anode and can also promote dendrite formation, hence leading to performance degradation and/or device failure as well as safety issues. If a viable solution for the safe use of Li metal anode can be formulated, a high energy density can be achieved in rechargeable Li metal batteries including Li–S and Li–air systems.

A solution of the Li dendrite formation problem in Li-metal batteries may be the novel cell configurations reported by Jang and co-workers (**Figure 45**a).[1030] In their new designs, both the cathode and anode were coated with graphene sheets having ultra high surface areas. This graphene composite architecture dramatically increased the electrode surface areas and decreased the effective electrode current density. As a result, the dendrite initiation time is delayed and dendrite growth rate is significantly reduced. The "intercalation-free operation" enables a fast discharge/charge time with a high energy density and specific power of about 320 Wh Wkg^{-1} and 187 kW kg^{-1}, respectively, (Figure 45c) along with excellent long-term stability (Figure 45b).[1030] This innovative cell configuration and novel strategy open a new avenue to make good use graphene in a Li-metal batteries.

Graphene-based materials have also been used for coating PP membrane separators to stabilize the Li electrode in Li-metal batteries by effectively suppressing dendrite growth and maintaining a uniform ionic flux on the metal surface.[1031] It was reported that the unique graphene layers can effectively act as stable interfacial layers to stabilize pure Li metal anode due to the remarkable stability, mechanical strength, and flexibility of graphene.[1032] In addition, these coated uniform graphene layers also helped improve the dimensional stability of the polymer membrane separator at elevated temperatures.[1031]

The use of graphene and graphene-based nanocomposites has been also extensively explored as electrodes in Na-ion batteries. Graphene composites-based anodes have shown promising electrochemical behavior, good cycle life, and excellent rate capability. Such remarkable performance can be attributed to the presence of defects (e.g., residual oxygen-containing groups). However, the presence of defects represents a serious drawback in terms of Coulombic efficiency for Na-ion batteries. Similarly to Li-ion batteries, graphene-based nanocomposites enable Na-ion batteries with higher specific capacity, better rate capability, and longer cycle life than the pristine electrode. So far, only a few reports are available on the use of graphene-based composites as cathodes for Na-ion batteries. In all cases, the graphene or rGO matrix seems to enhance the electrical conductivity of the composite and improve the rate capability compared to the non-graphene contained cathode materials.

Graphene and graphene-based nanocomposites have also been used as air electrodes in Na–air, Zn–air batteries, and as active electrodes in VRFBs with aim to improve their electrochemical performance. Similar to Li–air batteries, Na–air and Zn–air batteries have several technical hurdles, which hamper their potential applications. Although VRFBs are very promising for practical applications, current electrodes and membranes do not exhibit satisfactory electrochemical properties and also suffer from relatively high costs. Graphene and graphene-based nanocomposites show remarkable catalytic properties towards ORR and OER processed in these metal–air battery systems though there are a few reports available on the use of graphene/composites in these systems. These technologies are in the very early stage of development and more work is needed for further explorations. Graphene-based materials can also be used to improve the electrical conductivity, kinetic reversibility, and electrocatalytic activity of electrodes in VRFBs. Additionally, GO and commercial graphene have recently been tested as additives in VRFB ion-exchange membranes, with the aim of reducing the vanadium permeation and preventing ionic cross-mixing. The results achieved so far seem to be promising when compared to those obtained with bare membranes. However, the development of a successful commercial VRFB containing graphene is still far away.

Unlike Li and Na, Mg and Al can be safely used as metallic anodes because their repetitive plating proceeds without dendrite formations, they are non-toxic, and do not degrade in air environment.[1033] Owing to these unique properties, rechargeable Mg-ion and Al-ion batteries have attracted great attentions

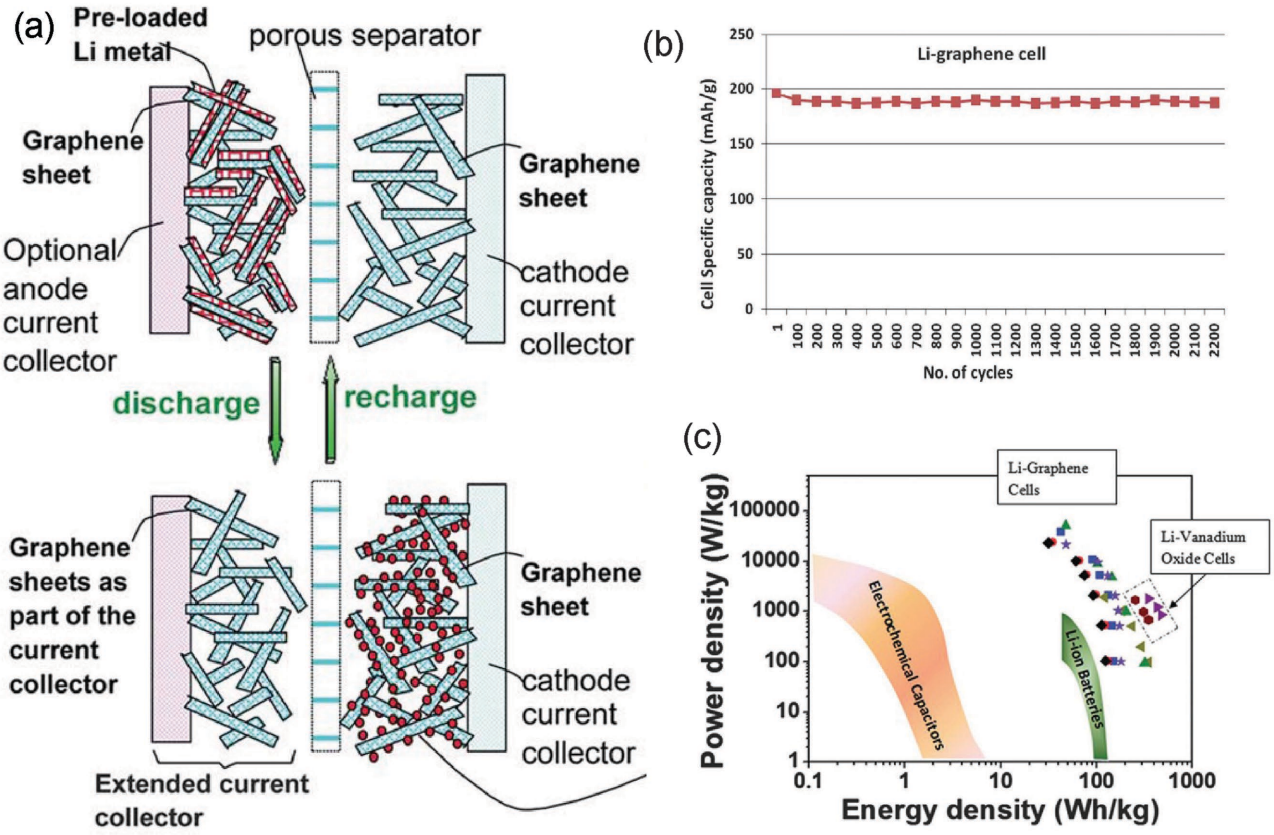

Figure 45. a) The upper portion shows the structure of a Li–graphene cell containing an optional anode current collector and a graphene layer acting as an extended current collector, a porous separator, a liquid electrolyte, and a porous graphene nanostructure acting as a cathode active material. The lower portion shows the structure of this cell after its first discharge. b) Cycling performance of a Li–graphene cell at 0.3C. c) Ragone plot of various Li–graphene cells (high power cells) and Li–vanadium oxide cells (high energy cells). Reproduced with permission.[1030] Copyright 2012, Royal Society of Chemistry.

as emerging low-cost and high energy density technologies for large-scale renewable energy storage applications.[1034] However, the development of these batteries is hindered by the limited choice of high-performance electrode materials.[1034] Recent developments of graphene-based nanocomposites may help open a new avenue for the design of new electrodes for Mg-ion and Al-ion batteries with high energy densities and improved electrochemcial behaviors. However, it remains a challenge to achieve such a goal at this time. Research efforts have been recently made to explore the use of graphene and graphene composites as electrode materials for Mg-ion batteries.[1035–1037] Although the results showed poor electrochemcial performance, they are considered the first attempts to use graphene composites in Mg-ion batteries.[1035–1037] We believe that graphene and graphene nanocomposites may find their true role as good composite electrodes for Mg and Al batteries. This needs consistent investigation and commitment from researchers to develop graphene-based electrodes with good electrochemcial stabilities. The research in the field of these two multivalent metal-ion batteries is still in the early stage and more work is needed for improvement.

In addition, a rechargeable battery that combines S or O_2 at the cathode and a multivalent metal (e.g., Mg or Al) at the anode could provide perhaps the most promising path to a rechargeable electrochemical storage device with high charge storage capacity and have the potential to further increase energy/power densities and reduce the associated costs. For example, the combination of Mg with S could offer a theoretical energy density of over 3200 Wh L^{-1}.[1038] Theoretically, Al–air battery contains approximately half specific energy (8100 Wh kg^{-1}) and three times energy density (21 870 Wh L^{-1}) of gasoline.[1039] Compared to the substantial progress made on Li–S and Li–air batteries, Mg–S, Mg–air batteries, and Al–S, Al–air batteries are still at the concept level of research and development. Recently, many efforts have been made to develop new electrolytes (for Mg and Al battery systems) that, are stable in contact with the electrode materials, do not form a blocking layer and have a wide electrochemical window. In addition, current multivalent metal-sulfur batteries also suffer from low utilization of active materials (S or transitional metal sulfides), low coulombic efficiency, and rapid capacity loss on repeated discharging/charging.[1040] These problems are traceable to the low electronic conductivity (insulating nature) of S and to the high solubility of the long-chain polysulfide ions in organic solvent-based electrolytes. The major challenges currently facing the widespread use of most multivalent metal–air batteries are the limited energy efficiency that results from the huge overpotential/polarization losses at the cathode during continued discharging/charging.[1041] The

use of graphene and graphene-based composites in these systems would solve some of the problems that limit their performance and stabilities. For example, the use of a graphene-S composite-based cathode, with high surface area, ubiquitous porous morphology, very high electronic conductivity and the presence of oxygen functional group, along with a non-nucleophilic Mg electrolyte, led to improved performance of Mg–S batteries.[1042] It is expected that graphene-based materials may also play vital roles in future Mg–air, Al–S and Al–air battery developments. In addition to the aforementioned energy storage applications, graphene-based nanocomposites may also be used in other energy storage systems such as rechargeable Na–S batteries,[1043] rechargeable potassium (K),[1044,1045] and rechargeable calcium (Ca) batteries.[1046,1047]

The main challenge facing the practical application of graphene may also arise from its superior properties. The high surface area and porosity of graphene can adversely affect its performance when used as electrode materials. For instance, a high surface area can lead to increased formation on the solid electrolyte interphase (SEI) layer, leading to a low first cycle coulombic efficiency, which can limit practical applications of graphene composites energy storage systems. Similarly, porous graphene can absorb a high amount of electrolyte, which can lead to higher consumption of expensive electrolyte as well as to graphene swelling during electrochemical processes.[1048–1050]

Furthermore, heteroatom-doped graphene can create disordered morphology, ubiquitous defects, improved electrical conductivity, and thermal stability, which are also beneficial for improving the electrochemical performance in advanced energy storage devices.[1051] Despite the many advances made so far, more attention should be paid to controlling doping levels, which is critical for improving the device performance . In addition, cost-effective, intelligent, and straightforward engineering solutions to the design of electrodes for industry-level applications must be considered in the future rather than focusing on the synthesis and fabrication of complicated nanostructured materials. Efforts should focus on more controllable and cost-effective methods for the fabrication of 3D architectures and transform research and development of heteroatom-doped graphene into practical applications.[1052]

The other challenge is the large-scale production of graphene and graphene-based composites, which requires tremendous efforts. The challenges are: (i) how to prevent the agglomeration of graphene in the matrix, (ii) how to control the surface defects; and (iii) how to tune the properties that are based on the applications. Although several synthesis techniques exist for graphene productions, only a few reports were reported so far on the commercialization of graphene-based energy storage devices. In order to overcome these challenges, new approaches and engineering solutions are needed to address these concerns that aim to improve the graphene properties and performance. Addressing the economic and environmental sustainability becomes a worldwide challenge shared by one and all. Nevertheless, this opens up a new opportunity for us to understand and utilize graphene to bridge the knowledge gaps.

A final thought is that graphene-based nanocomposites can also hold a great promise to capture or store CO_2 via physical/chemical processes,[1053] or transfer heat and store thermal energy.[1054] A large amount of work has been published in these areas and the details of these topics are beyond of the scope of this review and we refer the reader to the associated references. Nevertheless, strong emphasis is particularly necessary to the fundamental understanding of various composite materials for each specific application.

Acknowledgement

M.A. acknowledges the support from NSF PREM award (DMR-1523577): UTRGV-UMN Partnership for Fostering Innovation by Bridging Excellence in Research and Student Success.

Received: November 1, 2015
Revised: March 29, 2016
Published online:

[1] J. M. Tarascon, M. Armand, *Nature* **2001**, *414*, 359.
[2] D. Larcher, J. M. Tarascon, *Nat. Chem.* **2015**, *7*, 19.
[3] A. S. Arico, P. Bruce, B. Scrosati, J.-M. Tarascon, W. van Schalkwijk, *Nat. Mater.* **2005**, *4*, 366.
[4] B. Dunn, H. Kamath, J.-M. Tarascon, *Science* **2011**, *334*, 928.
[5] S. Chu, A. Majumdar, *Nature* **2012**, *488*, 294.
[6] K. Xu, *Chem. Rev.* **2014**, *114*, 11503.
[7] J. Liu, J.-G. Zhang, Z. Yang, J. P. Lemmon, C. Imhoff, G. L. Graff, L. Li, J. Hu, C. Wang, J. Xiao, G. Xia, V. V. Viswanathan, S. Baskaran, V. Sprenkle, X. Li, Y. Shao, B. Schwenzer, *Adv. Funct. Mater.* **2012**, *23*, 929.
[8] Z. Yang, J. Zhang, M. C. W. Kintner-Meyer, X. Lu, D. Choi, J. P. Lemmon, J. Liu, *Chem. Rev.* **2011**, *111*, 3577.
[9] J. Liu, G. Cao, Z. Yang, D. Wang, D. Dubois, X. Zhou, G. L. Graff, L. R. Pederson, J.-G. Zhang, *ChemSusChem* **2008**, *1*, 676.
[10] L. Ji, Z. Lin, M. Alcoutlabi, X. Zhang, *Energy Environ. Sci.* **2011**, *4*, 2682.
[11] X. Zhang, L. Ji, O. Toprakci, Y. Liang, M. Alcoutlabi, *Polym. Rev.* **2011**, *51*, 239.
[12] S. L. Candelaria, Y. Shao, W. Zhou, X. Li, J. Xiao, J.-G. Zhang, Y. Wang, J. Liu, J. Li, G. Cao, *Nano Energy* **2012**, *1*, 195.
[13] N.-S. Choi, Z. Chen, S. A. Freunberger, X. Ji, Y.-K. Sun, K. Amine, G. Yushin, L. F. Nazar, J. Cho, P. G. Bruce, *Angew. Chem.* **2012**, *51*, 9994.
[14] K. Xu, *Chem. Rev.* **2004**, *104*, 4303.
[15] R. C. Armstrong, C. Wolfram, K. P. de Jong, R. Gross, N. S. Lewis, B. Boardman, A. J. Ragauskas, K. Ehrhardt-Martinez, G. Crabtree, M. V. Ramana, *Nat. Energy* **2016**, *1*, 15020.
[16] Y. Gogotsi, *ACS Nano* **2014**, *8*, 5369.
[17] V. A. Agubra, L. Zuniga, D. De la Garza, L. Gallegos, M. Pokhrel, M. Alcoutlabi, *Solid State Ionics* **2016**, *286*, 73.
[18] V. A. Agubra, L. Zuniga, D. Flores, J. Villareal, M. Alcoutlabi, *Electrochim. Acta* **2016**, *192*, 529.
[19] L. Schlapbach, A. Zuttel, *Nature* **2001**, *414*, 353.
[20] S. A. Shevlin, Z. X. Guo, *Chem. Soc. Rev.* **2009**, *38*, 211.
[21] M. Pumera, *Chem. Soc. Rev.* **2010**, *39*, 4146.
[22] D. Chen, L. Tang, J. Li, *Chem. Soc. Rev.* **2010**, *39*, 3157.
[23] D. A. C. Brownson, D. K. Kampouris, C. E. Banks, *J. Power Sources* **2011**, *196*, 4873.
[24] R. Raccichini, A. Varzi, S. Passerini, B. Scrosati, *Nat. Mater.* **2015**, *14*, 271.
[25] Y. Sun, Q. Wu, G. Shi, *Energy Environ. Sci.* **2011**, *4*, 1113.
[26] F. Liu, S. Song, D. Xue, H. Zhang, *Adv. Mater.* **2012**, *24*, 1089.

[27] X. Huang, Z. Zeng, Z. Fan, J. Liu, H. Zhang, *Adv. Mater.* **2012**, *24*, 5979.
[28] S. Guo, S. Dong, *Chem. Soc. Rev.* **2011**, *40*, 2644.
[29] N. O. Weiss, H. Zhou, L. Liao, Y. Liu, S. Jiang, Y. Huang, X. Duan, *Adv. Mater.* **2012**, *24*, 5776.
[30] B. Luo, S. Liu, L. Zhi, *Small* **2012**, *8*, 630.
[31] S. Han, D. Wu, S. Li, F. Zhang, X. Feng, *Small* **2013**, *9*, 1173.
[32] F. Liu, C. W. Lee, J. S. Im, *J. Nanomater.* **2013**, DOI: 10.1155/2013/642915, 642915.
[33] Q. Ke, J. Wang, *J. Materiomics* **2016**, *2*, 37.
[34] I. V. Lightcap, P. V. Kamat, *Acc. Chem. Res.* **2012**, *46*, 2235.
[35] L. Grande, V. T. Chundi, D. Wei, C. Bower, P. Andrew, T. Ryhänen, *Particuology* **2012**, *10*, 1.
[36] D. A. C. Brownson, J. P. Metters, C. E. Banks, in *Nanotechnology for the Energy Challenge*, Wiley-VCH Verlag GmbH & Co. KGaA, (Ed.: Javier García-Martínez) Weinheim, Germany **2013**, pp. 133.
[37] L. Qu, C. Hu, L. Song, Z. Zhang, N. Chen, Z. Feng, *Energy Environ. Sci.* **2014**, *8*, 31.
[38] J. Zhu, D. Yang, Z. Yin, Q. Yan, H. Zhang, *Small* **2014**, *10*, 3480.
[39] Y. Yang, C. Han, B. Jiang, J. Iocozzia, C. He, D. Shi, T. Jiang, Z. Lin, *Mater. Sci. Eng., R* **2016**, *102*, 1.
[40] F. Bonaccorso, L. Colombo, G. Yu, M. Stoller, V. Tozzini, A. C. Ferrari, R. S. Ruoff, V. Pellegrini, *Science* **2015**, *347*, 1246501.
[41] K. S. Novoselov, A. K. Geim, S. V. Morozov, D. Jiang, Y. Zhang, S. V. Dubonos, I. V. Grigorieva, A. A. Firsov, *Science* **2004**, *306*, 666.
[42] M. Pumera, *Energy Environ. Sci.* **2011**, *4*, 668.
[43] C. N. R. Rao, A. K. Sood, K. S. Subrahmanyam, A. Govindaraj, *Angew. Chem. Int. Ed.* **2009**, *48*, 7752.
[44] A. K. Geim, K. S. Novoselov, *Nat. Mater.* **2007**, *6*, 183.
[45] F. Chen, N. J. Tao, *Acc. Chem. Res.* **2009**, *42*, 429.
[46] C. Lee, X. Wei, J. W. Kysar, J. Hone, *Science* **2008**, *321*, 385.
[47] A. B. Kuzmenko, E. van Heumen, F. Carbone, D. van der Marel, *Phys. Rev. Lett.* **2008**, *100*, 117401.
[48] A. A. Balandin, S. Ghosh, W. Bao, I. Calizo, D. Teweldebrhan, F. Miao, C. N. Lau, *Nano Lett.* **2008**, *8*, 902.
[49] V. Singh, D. Joung, L. Zhai, S. Das, S. I. Khondaker, S. Seal, *Prog. Mater. Sci.* **2011**, *56*, 1178.
[50] N. Saravanan, R. Rajasekar, S. Mahalakshmi, T. P. Sathishkumar, K. S. K. Sasikumar, S. Sahoo, *J. Reinf. Plast. Compos.* **2014**, *33*, 1158.
[51] X. Li, X. Wang, L. Zhang, S. Lee, H. Dai, *Science* **2008**, *319*, 1229.
[52] D. R. Dreyer, S. Park, C. W. Bielawski, R. S. Ruoff, *Chem. Soc. Rev.* **2010**, *39*, 228.
[53] Y. Zhu, S. Murali, W. Cai, X. Li, J. W. Suk, J. R. Potts, R. S. Ruoff, *Adv. Mater.* **2010**, *22*, 3906.
[54] Y. Zhu, D. K. James, J. M. Tour, *Adv. Mater.* **2012**, *24*, 4924.
[55] X. Li, G. Zhang, X. Bai, X. Sun, X. Wang, E. Wang, H. Dai, *Nat. Nano* **2008**, *3*, 538.
[56] J. R. Potts, D. R. Dreyer, C. W. Bielawski, R. S. Ruoff, *Polymer* **2011**, *52*, 5.
[57] H. Kim, A. A. Abdala, C. W. Macosko, *Macromolecules* **2010**, *43*, 6515.
[58] H. Kim, Y. Miura, C. W. Macosko, *Chem. Mater.* **2010**, *22*, 3441.
[59] V. Mittal, *Polymer-Graphene Nanocomposites*, Royal Society of Chemistry, Cambridge, CB4 0WF, UK **2012**, .
[60] Z. Song, T. Xu, M. L. Gordin, Y.-B. Jiang, I.-T. Bae, Q. Xiao, H. Zhan, J. Liu, D. Wang, *Nano Lett.* **2012**, *12*, 2205.
[61] S. Giri, D. Ghosh, C. K. Das, *Adv. Funct. Mater.* **2014**, *24*, 1312.
[62] C. Xu, X. Wang, J. Zhu, *J. Phys. Chem. C* **2008**, *112*, 19841.
[63] C. Tan, X. Huang, H. Zhang, *Mater. Today* **2013**, *16*, 29.
[64] Y. Zou, J. Kan, Y. Wang, *J. Phys. Chem. C* **2011**, *115*, 20747.
[65] H. Wang, L.-F. Cui, Y. Yang, H. Sanchez Casalongue, J. T. Robinson, Y. Liang, Y. Cui, H. Dai, *J. Am. Chem. Soc.* **2010**, *132*, 13978.
[66] H. Wang, Y. Yang, Y. Liang, L.-F. Cui, H. Sanchez Casalongue, Y. Li, G. Hong, Y. Cui, H. Dai, *Angew. Chem. Int. Ed.* **2011**, *50*, 7364.
[67] D. Wang, D. Choi, J. Li, Z. Yang, Z. Nie, R. Kou, D. Hu, C. Wang, L. V. Saraf, J. Zhang, I. A. Aksay, J. Liu, *ACS Nano* **2009**, *3*, 907.
[68] D. Wang, R. Kou, D. Choi, Z. Yang, Z. Nie, J. Li, L. V. Saraf, D. Hu, J. Zhang, G. L. Graff, J. Liu, M. A. Pope, I. A. Aksay, *ACS Nano* **2010**, *4*, 1587.
[69] C. Wu, X. Huang, X. Wu, L. Xie, K. Yang, P. Jiang, *Nanoscale* **2013**, *5*, 3847.
[70] J. Li, X. Cheng, J. Sun, C. Brand, A. Shashurin, M. Reeves, M. Keidar, *J. Appl. Phys.* **2014**, *115*, 164301.
[71] N. Jung, S. Kwon, D. Lee, D.-M. Yoon, Y. M. Park, A. Benayad, J.-Y. Choi, J. S. Park, *Adv. Mater.* **2013**, *25*, 6854.
[72] S. K. Bhatia, A. L. Myers, *Langmuir* **2006**, *22*, 1688.
[73] P. Kowalczyk, R. Holyst, M. Terrones, H. Terrones, *Phys. Chem. Chem. Phys.* **2007**, *9*, 1786.
[74] M. Jordá-Beneyto, F. Suárez-García, D. Lozano-Castelló, D. Cazorla-Amorós, A. Linares-Solano, *Carbon* **2007**, *45*, 293.
[75] V. Tozzini, V. Pellegrini, *Phys. Chem. Chem. Phys.* **2013**, *15*, 80.
[76] V. L. Blair, W. Clegg, A. R. Kennedy, Z. Livingstone, L. Russo, E. Hevia, *Angew. Chem. Int. Ed.* **2011**, *50*, 9857.
[77] B. Delhomme, P. de Rango, P. Marty, M. Bacia, B. Zawilski, C. Raufast, S. Miraglia, D. Fruchart, *Int. J. Hydrogen Energy* **2012**, *37*, 9103.
[78] K.-J. Jeon, H. R. Moon, A. M. Ruminski, B. Jiang, C. Kisielowski, R. Bardhan, J. J. Urban, *Nat. Mater.* **2011**, *10*, 286.
[79] B. Bogdanović, M. Felderhoff, A. Pommerin, F. Schüth, N. Spielkamp, *Adv. Mater.* **2006**, *18*, 1198.
[80] A. Züttel, *Mater. Today* **2003**, *6*, 24.
[81] M. E. Bluhm, M. G. Bradley, R. Butterick, U. Kusari, L. G. Sneddon, *J. Am. Chem. Soc.* **2006**, *128*, 7748.
[82] H.-W. Li, Y. Yan, S.-I. Orimo, A. Züttel, C. M. Jensen, *Energies* **2011**, *4*, 185.
[83] F. Bonaccorso, L. Colombo, G. H. Yu, M. Stoller, V. Tozzini, A. C. Ferrari, R. S. Ruoff, V. Pellegrini, *Science* **2015**, *347*, 1246501.
[84] S. Niaz, T. Manzoor, A. H. Pandith, *Renewable Sustainable Energy Rev.* **2015**, *50*, 457.
[85] S. Gadipelli, Z. X. Guo, *Prog. Mater. Sci.* **2015**, *69*, 1.
[86] K. Spyrou, D. Gournis, P. Rudolf, *ECS J. Solid State Sci. Technol.* **2013**, *2*, M3160.
[87] R. Balog, B. Jørgensen, J. Wells, E. Lægsgaard, P. Hofmann, F. Besenbacher, L. Hornekær, *J. Am. Chem. Soc.* **2009**, *131*, 8744.
[88] S. Patchkovskii, J. S. Tse, S. N. Yurchenko, L. Zhechkov, T. Heine, G. Seifert, *Proc. Natl. Acad. Sci. USA* **2005**, *102*, 10439.
[89] K. S. Subrahmanyam, P. Kumar, U. Maitra, A. Govindaraj, K. P. S. S. Hembram, U. V. Waghmare, C. N. R. Rao, *Proc. Natl. Acad. Sci.* **2011**, *108*, 2674.
[90] A. G. Klechikov, G. Mercier, P. Merino, S. Blanco, C. Merino, A. V. Talyzin, *Microporous Mesoporous Mater.* **2015**, *210*, 46.
[91] H. Wang, X. Yuan, in *Graphene-Based Energy Devices*, Wiley-VCH Verlag GmbH & Co. KGaA, (Ed.: A. Rashid bin Mohd Yusoff) Wiley-VCH, Weinheim, Germany **2015**, pp. 295.
[92] H. Wang, X. Z. Yuan, Y. Wu, H. J. Huang, X. Peng, G. M. Zeng, H. Zhong, J. Liang, M. M. Ren, *Adv. Colloid Interface Sci.* **2013**, *195*, 19.
[93] G. Srinivas, Y. Zhu, R. Piner, N. Skipper, M. Ellerby, R. Ruoff, *Carbon* **2010**, *48*, 630.
[94] Z. Jin, W. Lu, K. J. O'Neill, P. A. Parilla, L. J. Simpson, C. Kittrell, J. M. Tour, *Chem. Mater.* **2011**, *23*, 923.
[95] A. Du, Z. Zhu, S. C. Smith, *J. Am. Chem. Soc.* **2010**, *132*, 2876.

[96] A. Klechikov, G. Mercier, T. Sharifi, I. A. Baburin, G. Seifert, A. V. Talyzin, *Chem. Commun.* **2015**, *51*, 15280.
[97] C. X. Guo, Y. Wang, C. M. Li, *ACS Sustainable Chem. Eng.* **2013**, *1*, 14.
[98] F. D. Lamari, D. Levesque, *Carbon* **2011**, *49*, 5196.
[99] M. Seydou, K. Lassoued, F. Tielens, F. Maurel, F. Raouafi, B. Diawara, *RSC Adv.* **2015**, *5*, 14400.
[100] G. Kim, S.-H. Jhi, N. Park, *Appl. Phys. Lett.* **2008**, *92*, 013106.
[101] H. Lee, J. Ihm, M. L. Cohen, S. G. Louie, *Nano Lett.* **2010**, *10*, 793.
[102] G. K. Dimitrakakis, E. Tylianakis, G. E. Froudakis, *Nano Lett.* **2008**, *8*, 3166.
[103] E. Tylianakis, G. M. Psofogiannakis, G. E. Froudakis, *J. Phys. Chem. Lett.* **2010**, *1*, 2459.
[104] N. Kostoglou, V. Tzitzios, A. G. Kontos, K. Giannakopoulos, C. Tampaxis, A. Papavasiliou, G. Charalambopoulou, T. Steriotis, Y. Q. Li, K. Liao, K. Polychronopoulou, C. Mitterer, C. Rebholz, *Int. J. Hydrogen Energy* **2015**, *40*, 6844.
[105] Z. M. Ao, S. X. Dou, Z. M. Xu, Q. G. Jiang, G. X. Wang, *Int. J. Hydrogen Energy* **2014**, *39*, 16244.
[106] Z. M. Ao, Q. Jiang, R. Q. Zhang, T. T. Tan, S. Li, *J. Appl. Phys.* **2009**, *105*, 074307.
[107] Z. M. Ao, F. M. Peeters, *Phys. Rev. B* **2010**, *81*, 205406.
[108] H.-Y. Wu, X. Fan, J.-L. Kuo, W.-Q. Deng, *The J. Phys. Chem. C* **2011**, *115*, 9241.
[109] A. Sigal, M. I. Rojas, E. P. M. Leiva, *Int. J. Hydrogen Energy* **2011**, *36*, 3537.
[110] Y. Wang, C. X. Guo, X. Wang, C. Guan, H. Yang, K. Wang, C. M. Li, *Energy Environ. Sci.* **2011**, *4*, 195.
[111] M. Sterlin Leo Hudson, H. Raghubanshi, S. Awasthi, T. Sadhasivam, A. Bhatnager, S. Simizu, S. G. Sankar, O. N. Srivastava, *Int. J. Hydrogen Energy* **2014**, *39*, 8311.
[112] J. Jiang, Q. Gao, Z. Zheng, K. Xia, J. Hu, *Int. J. Hydrogen Energy* **2010**, *35*, 210.
[113] P. Reunchan, S.-H. Jhi, *Appl. Phys. Lett.* **2011**, *98*, 093103.
[114] G. Kim, S.-H. Jhi, *J. Phys. Chem. C* **2009**, *113*, 20499.
[115] C. I. Contescu, C. M. Brown, Y. Liu, V. V. Bhat, N. C. Gallego, *J. Phys. Chem. C* **2009**, *113*, 5886.
[116] L. Wang, K. Lee, Y.-Y. Sun, M. Lucking, Z. Chen, J. J. Zhao, S. B. Zhang, *ACS Nano* **2009**, *3*, 2995.
[117] S. Li, H.-m. Zhao, P. Jena, *Front. Phys.* **2011**, *6*, 204.
[118] Y. Chen, Q. Wang, C. Zhu, P. Gao, Q. Ouyang, T. Wang, Y. Ma, C. Sun, *J. Mater. Chem.* **2012**, *22*, 5924.
[119] F. D. Wang, F. Wang, N. N. Zhang, Y. H. Li, S. W. Tang, H. Sun, Y. F. Chang, R. S. Wang, *Chem. Phys. Lett.* **2013**, *555*, 212.
[120] E. S. Cho, A. M. Ruminski, S. Aloni, Y.-S. Liu, J. Guo, J. J. Urban, *Nat. Commun.* **2016**, *7*, 10804.
[121] W. G. Hong, B. H. Kim, S. M. Lee, H. Y. Yu, Y. J. Yun, Y. Jun, J. B. Lee, H. J. Kim, *Int. J. Hydrogen Energy* **2012**, *37*, 7594.
[122] H. An, C.-S. Liu, Z. Zeng, C. Fan, X. Ju, *Appl. Phys. Lett.* **2011**, *98*, 173101.
[123] C.-S. Liu, Z. Zeng, *Appl. Phys. Lett.* **2010**, *96*, 123101.
[124] R. Lu, D. Rao, Z. Lu, J. Qian, F. Li, H. Wu, Y. Wang, C. Xiao, K. Deng, E. Kan, W. Deng, *J. Phys. Chem. C* **2012**, *116*, 21291.
[125] P. Reunchan, S.-H. Jhi, *Appl. Phys. Lett.* **2011**, *98*, 093103.
[126] D. Li, Y. Ouyang, J. Li, Y. Sun, L. Chen, *Solid State Commun.* **2012**, *152*, 422.
[127] J. H. Cho, S. J. Yang, K. Lee, C. R. Park, *Int. J. Hydrogen Energy* **2011**, *36*, 12286.
[128] M. Wu, Y. Gao, Z. Zhang, X. C. Zeng, *Nanoscale* **2012**, *4*, 915.
[129] W. Qin, L. Han, H. Bi, J. Jian, X. Wu, P. Gao, *Nanoscale* **2015**, *7*, 20180.
[130] H. Jiang, X. L. Cheng, H. Zhang, Y. J. Tang, C. X. Zhao, *Comput. Theor. Chem.* **2015**, *1068*, 97.
[131] C. D. Wu, T. H. Fang, J. Y. Lo, Y. L. Feng, *J. Mol. Model.* **2013**, *19*, 3813.
[132] H. D. Yoo, E. Markevich, G. Salitra, D. Sharon, D. Aurbach, *Mater. Today* **2014**, *17*, 110.
[133] P. Simon, Y. Gogotsi, *Nat. Mater.* **2008**, *7*, 845.
[134] L. L. Zhang, X. S. Zhao, *Chem. Soc. Rev.* **2009**, *38*, 2520.
[135] G. Wang, L. Zhang, J. Zhang, *Chem. Soc. Rev.* **2012**, *41*, 797.
[136] M. Zhi, C. Xiang, J. Li, M. Li, N. Wu, *Nanoscale* **2013**, *5*, 72.
[137] Y. He, W. Chen, C. Gao, J. Zhou, X. Li, E. Xie, *Nanoscale* **2013**, *5*, 8799.
[138] Y. Gogotsi, P. Simon, *Sci. Mag.* **2011**, *334*, 917.
[139] P. Simon, Y. Gogotsi, B. Dunn, *Science* **2014**, *343*, 1210.
[140] A. G. Pandolfo, A. F. Hollenkamp, *J. Power Sources* **2006**, *157*, 11.
[141] E. Frackowiak, *Phys. Chem. Chem. Phys.* **2007**, *9*, 1774.
[142] D. Li, Y. R. Liu, B. P. Lin, Y. Sun, H. Yang, X. Q. Zhang, *Prog. Chem.* **2015**, *27*, 404.
[143] M. Agharkar, S. Kochrekar, S. Hidouri, M. A. Azeez, *Mater. Res. Bull.* **2014**, *59*, 323.
[144] P. Simon, Y. Gogotsi, *Acc. Chem. Res.* **2013**, *46*, 1094.
[145] M. Mastragostino, C. Arbizzani, F. Soavi, *Solid State Ionics* **2002**, *148*, 493.
[146] E. Frackowiak, V. Khomenko, K. Jurewicz, K. Lota, F. Béguin, *J. Power Sources* **2006**, *153*, 413.
[147] G. A. Snook, P. Kao, A. S. Best, *J. Power Sources* **2011**, *196*, 1.
[148] I. Shown, A. Ganguly, L.-C. Chen, K.-H. Chen, *Energy Sci. Eng.* **2015**, *3*, 2.
[149] P. Pieta, I. Obraztsov, F. D'Souza, W. Kutner, *ECS J. Solid State Sci. Technol.* **2013**, *2*, M3120.
[150] M. E. Roberts, D. R. Wheeler, B. B. McKenzie, B. C. Bunker, *J. Mater. Chem.* **2009**, *19*, 6977.
[151] J. Jiang, A. Kucernak, *Electrochim. Acta* **2002**, *47*, 2381.
[152] C.-C. Hu, T.-W. Tsou, *Electrochem. Commun.* **2002**, *4*, 105.
[153] W. Wei, X. Cui, W. Chen, D. G. Ivey, *Chem. Soc. Rev.* **2011**, *40*, 1697.
[154] C.-C. Hu, K.-H. Chang, M.-C. Lin, Y.-T. Wu, *Nano Lett.* **2006**, *6*, 2690.
[155] X. Zhao, B. M. Sanchez, P. J. Dobson, P. S. Grant, *Nanoscale* **2011**, *3*, 839.
[156] N.-L. Wu, S.-Y. Wang, C.-Y. Han, D.-S. Wu, L.-R. Shiue, *J. Power Sources* **2003**, *113*, 173.
[157] T. Qi, J. Jiang, H. Chen, H. Wan, L. Miao, L. Zhang, *Electrochim. Acta* **2013**, *114*, 674.
[158] Q. Wang, L. Jiao, H. Du, Y. Wang, H. Yuan, *J. Power Sources* **2014**, *245*, 101.
[159] K. R. Prasad, N. Miura, *Electrochem. Commun.* **2004**, *6*, 849.
[160] G. Chen, Q.-F. Lü, H.-B. Zhao, *J. Mater. Sci. Technol.* **2015**, *31*, 1101.
[161] Q. Zhao, L. Ma, Q. Zhang, C. Wang, X. Xu, *J. Nanomater.* **2015**, 850147.
[162] K.-W. Nam, W.-S. Yoon, K.-B. Kim, *Electrochim. Acta* **2002**, *47*, 3201.
[163] D. T. Dam, X. Wang, J.-M. Lee, *ACS Appl. Mater. Interfaces* **2014**, *6*, 8246.
[164] Y.-G. Zhu, G.-S. Cao, C.-Y. Sun, J. Xie, S.-Y. Liu, T.-J. Zhu, X. B. Zhao, H. Y. Yang, *RSC Adv.* **2013**, *3*, 19409.
[165] Z. Chen, V. Augustyn, J. Wen, Y. Zhang, M. Shen, B. Dunn, Y. Lu, *Adv. Mater.* **2011**, *23*, 791.
[166] H. Zhang, Q. Gao, K. Yang, Y. Tan, W. Tian, L. Zhu, Z. Li, C. Yang, *J. Mater. Chem. A* **2015**, *3*, 22005.
[167] Z. Ma, X. Huang, S. Dou, J. Wu, S. Wang, *J. Phys. Chem. C* **2014**, *118*, 17231.
[168] Q. Wang, Z. H. Wen, J. H. Li, *Adv. Funct. Mater.* **2006**, *16*, 2141.
[169] J. Kim, W.-H. Khoh, B.-H. Wee, J.-D. Hong, *RSC Adv.* **2015**, *5*, 9904.

[170] R. Kumar, R. K. Singh, P. Kumar Dubey, D. P. Singh, R. M. Yadav, R. S. Tiwari, *RSC Adv.* **2015**, *5*, 7112.
[171] J. Rajeswari, P. S. Kishore, B. Viswanathan, T. K. Varadarajan, *Electrochem. Commun.* **2009**, *11*, 572.
[172] T. Brezesinski, J. Wang, S. H. Tolbert, B. Dunn, *Nat. Mater.* **2010**, *9*, 146.
[173] J. Zhou, J. Song, H. Li, X. Feng, Z. Huang, S. Chen, Y. Ma, L. Wang, X. Yan, *New J. Chem.* **2015**, *39*, 8780.
[174] S. Zhu, M. Wu, M.-H. Ge, H. Zhang, S.-K. Li, C.-H. Li, *J. Power Sources* **2016**, *306*, 593.
[175] K. K. Purushothaman, B. Saravanakumar, I. M. Babu, B. Sethuraman, G. Muralidharan, *RSC Adv.* **2014**, *4*, 23485.
[176] G. He, J. Li, H. Chen, J. Shi, X. Sun, S. Chen, X. Wang, *Mater. Lett.* **2012**, *82*, 61.
[177] C. Xiang, M. Li, M. Zhi, A. Manivannan, N. Wu, *J. Power Sources* **2013**, *226*, 65.
[178] Q. Guan, J. Cheng, B. Wang, W. Ni, G. Gu, X. Li, L. Huang, G. Yang, F. Nie, *ACS Appl. Mater. Interfaces* **2014**, *6*, 7626.
[179] L. Ma, H. Zhou, X. Shen, Q. Chen, G. Zhu, Z. Ji, *RSC Adv.* **2014**, *4*, 53180.
[180] E. Umeshbabu, G. Rajeshkhanna, P. Justin, G. R. Rao, *RSC Adv.* **2015**, *5*, 66657.
[181] Y. Xu, L. Wang, P. Cao, C. Cai, Y. Fu, X. Ma, *J.Power Sources* **2016**, *306*, 742.
[182] S. Zhuiykov, in *Nanostructured Semiconductor Oxides for the Next Generation of Electronics and Functional Devices*, Woodhead Publishing, Sawston, Cambridge **2014**, Chap. 5, pp. 213.
[183] A. Ramadoss, S. J. Kim, *Mater. Chem. Phys.* **2013**, *140*, 405.
[184] Y.-L. Chen, Z.-A. Hu, Y.-Q. Chang, H.-W. Wang, Z.-Y. Zhang, Y.-Y. Yang, H.-Y. Wu, *J. Phys. Chem. C* **2011**, *115*, 2563.
[185] V. Sahu, S. Goel, R. K. Sharma, G. Singh, *Nanoscale* **2015**, *7*, 20642.
[186] F.-L. Zheng, G.-R. Li, Y.-N. Ou, Z.-L. Wang, C.-Y. Su, Y.-X. Tong, *Chem. Commun.* **2010**, *46*, 5021.
[187] V. Augustyn, J. Come, M. A. Lowe, J. W. Kim, P.-L. Taberna, S. H. Tolbert, H. D. Abruña, P. Simon, B. Dunn, *Nat. Mater.* **2013**, *12*, 518.
[188] L. Kong, C. Zhang, S. Zhang, J. Wang, R. Cai, C. Lv, W. Qiao, L. Ling, D. Long, *J. Mater. Chem. A* **2014**, *2*, 17962.
[189] L. Kong, C. Zhang, J. Wang, W. Qiao, L. Ling, D. Long, *ACS Nano* **2015**, *9*, 11200.
[190] J. Yan, Q. Wang, T. Wei, Z. Fan, *Adv. Energy Mater.* **2014**, *4*, 1300816.
[191] N. Mahmood, C. Zhang, H. Yin, Y. Hou, *J. Mater. Chem. A* **2014**, *2*, 15.
[192] Q. Li, N. Mahmood, J. H. Zhu, Y. L. Hou, S. H. Sun, *Nano Today* **2014**, *9*, 668.
[193] Y. B. Tan, J.-M. Lee, *J. Mater. Chem. A* **2013**, *1*, 14814.
[194] R. R. Salunkhe, Y.-H. Lee, K.-H. Chang, J.-M. Li, P. Simon, J. Tang, N. L. Torad, C.-C. Hu, Y. Yamauchi, *Chem. - Eur. J.* **2014**, *20*, 13838.
[195] F. Xiao, S. Yang, Z. Zhang, H. Liu, J. Xiao, L. Wan, J. Luo, S. Wang, Y. Liu, *Sci. Rep.* **2015**, *5*, 9359.
[196] G. Han, Y. Liu, L. Zhang, E. Kan, S. Zhang, J. Tang, W. Tang, *Sci. Rep.* **2014**, *4*, 4824.
[197] L. Chen, Y. Liu, Y. Zhao, N. Chen, L. Qu, *Nanotechnology* **2016**, *27*, 032001.
[198] A. K. Mishra, S. Ramaprabhu, *J. Phys. Chem. C* **2011**, *115*, 14006.
[199] X. Fan, B. D. Phebus, L. Li, S. Chen, *Sci. Adv. Mater.* **2015**, *7*, 1916.
[200] Y. Huang, J. Liang, Y. Chen, *Small* **2012**, *8*, 1805.
[201] Y. Gogotsi, *J. Phys. Chem. Lett.* **2011**, *2*, 2509.
[202] B. Anasori, M. Beidaghi, Y. Gogotsi, *Mater. Today* **2014**, *17*, 253.
[203] Z.-S. Wu, G. Zhou, L.-C. Yin, W. Ren, F. Li, H.-M. Cheng, *Nano Energy* **2012**, *1*, 107.
[204] M. Boota, K. B. Hatzell, M. Alhabeb, E. C. Kumbur, Y. Gogotsi, *Carbon* **2015**, *92*, 142.
[205] P. Thangavelu, B. Jong-Beom, *2D Mater.* **2015**, *2*, 032002.
[206] L. L. Zhang, R. Zhou, X. S. Zhao, *J. Mater. Chem.* **2010**, *20*, 5983.
[207] J. Hou, Y. Shao, M. W. Ellis, R. B. Moore, B. Yi, *Phys. Chem. Chem. Phys.* **2011**, *13*, 15384.
[208] K. F. Chen, S. Y. Song, F. Liu, D. F. Xue, *Chem. Soc. Rev.* **2015**, *44*, 6230.
[209] A. W. Anwar, A. Majeed, N. Iqbal, W. Ullah, A. Shuaib, U. Ilyas, F. Bibi, H. M. Rafique, *J. Mater. Sci. Technol.* **2015**, *31*, 699.
[210] Y. X. Xu, G. Q. Shi, X. F. Duan, *Acc. Chem. Res.* **2015**, *48*, 1666.
[211] A. Z. Shabi, H. S. Jae, in *Chemical Functionalization of Carbon Nanomaterials*, (Ed.: V. K. Thakur, T. M. Kumari) CRC Press, Taylor & Francis Group, 6000 Broken Sound Parkway NW, Suite 300, Boca Raton, FL 33487-2742, **2015**, pp. 844–867.
[212] M. D. Stoller, S. Park, Y. Zhu, J. An, R. S. Ruoff, *Nano Lett.* **2008**, *8*, 3498.
[213] S. Vivekchand, C. Rout, K. Subrahmanyam, A. Govindaraj, C. Rao, *J. Chem. Sci.* **2008**, *120*, 9.
[214] Y. Wang, Z. Shi, Y. Huang, Y. Ma, C. Wang, M. Chen, Y. Chen, *J. Phys. Chem. C* **2009**, *113*, 13103.
[215] X. Yang, J. Zhu, L. Qiu, D. Li, *Adv. Mater.* **2011**, *23*, 2833.
[216] J. Luo, H. D. Jang, J. Huang, *ACS Nano* **2013**, *7*, 1464.
[217] S. L. Zhang, N. Pan, *Adv. Energy Mater.* **2015**, *5*, 1401401.
[218] W. Q. Tian, Q. M. Gao, Y. L. Tan, Y. L. Zhang, J. D. Xu, Z. Y. Li, K. Yang, L. H. Zhu, Z. P. Liu, *Carbon* **2015**, *85*, 351.
[219] C. Li, X. Zhang, K. Wang, H. T. Zhang, X. Z. Sun, Y. W. Ma, *New Carbon Mater.* **2015**, *30*, 193.
[220] M. Mao, J. Y. Hu, H. T. Liu, *Int. J. Energy Res.* **2015**, *39*, 727.
[221] R. R. Salunkhe, Y. H. Lee, K. H. Chang, J. M. Li, P. Simon, J. Tang, N. L. Torad, C. C. Hu, Y. Yamauchi, *Chem.- Eur. J.* **2014**, *20*, 13838.
[222] T. Lin, I.-W. Chen, F. Liu, C. Yang, H. Bi, F. Xu, F. Huang, *Science* **2015**, *350*, 1508.
[223] Y. Zhu, S. Murali, M. D. Stoller, K. J. Ganesh, W. Cai, P. J. Ferreira, A. Pirkle, R. M. Wallace, K. A. Cychosz, M. Thommes, D. Su, E. A. Stach, R. S. Ruoff, *Science* **2011**, *332*, 1537.
[224] B. G. Choi, M. Yang, W. H. Hong, J. W. Choi, Y. S. Huh, *ACS Nano* **2012**, *6*, 4020.
[225] L. L. Zhang, X. Zhao, M. D. Stoller, Y. Zhu, H. Ji, S. Murali, Y. Wu, S. Perales, B. Clevenger, R. S. Ruoff, *Nano Lett.* **2012**, *12*, 1806.
[226] Z. Fan, Q. Zhao, T. Li, J. Yan, Y. Ren, J. Feng, T. Wei, *Carbon* **2012**, *50*, 1699.
[227] Z. Y. Xiong, C. L. Liao, W. H. Han, X. G. Wang, *Adv. Mater.* **2015**, *27*, 4469.
[228] J. L. Huang, J. Y. Wang, C. W. Wang, H. N. Zhang, C. X. Lu, J. Z. Wang, *Chem. Mater.* **2015**, *27*, 2107.
[229] J. Huang, J. Wang, C. Wang, H. Zhang, C. Lu, J. Wang, *Chem. Mater.* **2015**, *27*, 2107.
[230] X. Zhang, H. Zhang, C. Li, K. Wang, X. Sun, Y. Ma, *RSC Adv.* **2014**, *4*, 45862.
[231] S. Han, D. Wu, S. Li, F. Zhang, X. Feng, *Adv. Mater.* **2014**, *26*, 849.
[232] S. M. Jung, D. L. Mafra, C.-T. Lin, H. Y. Jung, J. Kong, *Nanoscale* **2015**, *7*, 4386.
[233] Y. Wang, J. Zhu, *Nanotechnology* **2015**, *26*, 055401.
[234] K. Yuan, Y. Xu, J. Uihlein, G. Brunklaus, L. Shi, R. Heiderhoff, M. Que, M. Forster, T. Chassé, T. Pichler, T. Riedl, Y. Chen, U. Scherf, *Adv. Mater.* **2015**, *27*, 6714.
[235] X. Yang, C. Cheng, Y. Wang, L. Qiu, D. Li, *Science* **2013**, *341*, 534.
[236] K. Zhang, L. Mao, L. L. Zhang, H. S. On Chan, X. S. Zhao, J. Wu, *J. Mater. Chem.* **2011**, *21*, 7302.

[237] L. Jiang, L. Sheng, C. Long, T. Wei, Z. Fan, *Adv. Energy Mater.* **2015**, *5*, 1500771.
[238] M. Wang, L. D. Duong, N. T. Mai, S. Kim, Y. Kim, H. Seo, Y. C. Kim, W. Jang, Y. Lee, J. Suhr, J.-D. Nam, *ACS Appl. Mater. Interfaces* **2015**, *7*, 1348.
[239] Q. Wang, N. Plylahan, M. V. Shelke, R. R. Devarapalli, M. Li, P. Subramanian, T. Djenizian, R. Boukherroub, S. Szunerits, *Carbon* **2014**, *68*, 175.
[240] J. Li, H. Xie, Y. Li, *J. Nanosci. Nanotechnol.* **2015**, *15*, 3280.
[241] H. M. Jeong, J. W. Lee, W. H. Shin, Y. J. Choi, H. J. Shin, J. K. Kang, J. W. Choi, *Nano Lett.* **2011**, *11*, 2472.
[242] W. Fan, Y.-Y. Xia, W. W. Tjiu, P. K. Pallathadka, C. He, T. Liu, *J. Power Sources* **2013**, *243*, 973.
[243] D. Li, C. Yu, M. Wang, Y. Zhang, C. Pan, *RSC Adv.* **2014**, *4*, 55394.
[244] T. Kesavan, R. Aswathy, I. A. Raj, T. P. Kumar, P. Ragupathy, *ECS J. Solid State Sci. Technol.* **2015**, *4*, M88.
[245] J. Wang, B. Ding, Y. Xu, L. Shen, H. Dou, X. Zhang, *ACS Appl. Mater. Interfaces* **2015**, *7*, 22284.
[246] D. Wang, Y. Min, Y. Yu, B. Peng, *J. Colloid Interface Sci.* **2014**, *417*, 270.
[247] P. Yu, X. Zhao, Y. Li, Q. Zhang, *MRS Proceedings* **2014**, *1644*, mrsf13-1644-dd06-05.
[248] T. Wang, L.-X. Wang, D.-L. Wu, W. Xia, D.-Z. Jia, *Sci. Rep.* **2015**, *5*, 9591.
[249] X. a. Chen, X. Chen, X. Xu, Z. Yang, Z. Liu, L. Zhang, X. Xu, Y. Chen, S. Huang, *Nanoscale* **2014**, *6*, 13740.
[250] A. Alabadi, S. Razzaque, Z. Dong, W. Wang, B. Tan, *J. Power Sources* **2016**, *306*, 241.
[251] Z.-S. Wu, A. Winter, L. Chen, Y. Sun, A. Turchanin, X. Feng, K. Müllen, *Adv. Mater.* **2012**, *24*, 5130.
[252] J. Han, L. L. Zhang, S. Lee, J. Oh, K.-S. Lee, J. R. Potts, J. Ji, X. Zhao, R. S. Ruoff, S. Park, *ACS Nano* **2013**, *7*, 19.
[253] D.-Y. Yeom, W. Jeon, N. D. K. Tu, S. Y. Yeo, S.-S. Lee, B. J. Sung, H. Chang, J. A. Lim, H. Kim, *Sci. Rep.* **2015**, *5*, 9817.
[254] K. Fujisawa, R. Cruz-Silva, K.-S. Yang, Y. A. Kim, T. Hayashi, M. Endo, M. Terrones, M. S. Dresselhaus, *J. Mater. Chem. A* **2014**, *2*, 9532.
[255] Z. Wang, Y. Chen, P. Li, J. He, W. Zhang, Z. Guo, Y. Li, M. Dong, *RSC Adv.* **2016**, *6*, 15080.
[256] W. Lv, D.-M. Tang, Y.-B. He, C.-H. You, Z.-Q. Shi, X.-C. Chen, C.-M. Chen, P.-X. Hou, C. Liu, Q.-H. Yang, *ACS Nano* **2009**, *3*, 3730.
[257] Y. Shao, J. Wang, M. Engelhard, C. Wang, Y. Lin, *J. Mater. Chem.* **2010**, *20*, 743.
[258] M. F. El-Kady, V. Strong, S. Dubin, R. B. Kaner, *Science* **2012**, *335*, 1326.
[259] K. Wang, L. Li, T. Zhang, Z. Liu, *Energy* **2014**, *70*, 612.
[260] J. Han, L. L. Zhang, S. Lee, J. Oh, K.-S. Lee, J. R. Potts, J. Ji, X. Zhao, R. S. Ruoff, S. Park, *ACS Nano* **2013**, *7*, 19.
[261] Z. Peng, R. Ye, J. A. Mann, D. Zakhidov, Y. Li, P. R. Smalley, J. Lin, J. M. Tour, *ACS Nano* **2015**, *9*, 5868.
[262] Y. Zhou, X. Xu, B. Shan, Y. Wen, T. Jiang, J. Lu, S. Zhang, D. P. Wilkinson, J. Zhang, Y. Huang, *Energy Storage Mater.* **2015**, *1*, 103.
[263] M. E. Abdelhamid, A. P. O'Mullane, G. A. Snook, *RSC Adv.* **2015**, *5*, 11611.
[264] D.-W. Wang, F. Li, J. Zhao, W. Ren, Z.-G. Chen, J. Tan, Z.-S. Wu, I. Gentle, G. Q. Lu, H.-M. Cheng, *ACS Nano* **2009**, *3*, 1745.
[265] H. Gómez, M. K. Ram, F. Alvi, P. Villalba, E. Stefanakos, A. Kumar, *J. Power Sources* **2011**, *196*, 4102.
[266] X. B. Liu, Y. Y. Zheng, X. L. Wang, *Chem. Eur. J.* **2015**, *21*, 10408.
[267] H.-P. Cong, X.-C. Ren, P. Wang, S.-H. Yu, *Energy Environ. Sci.* **2013**, *6*, 1185.
[268] J. Yan, T. Wei, B. Shao, Z. Fan, W. Qian, M. Zhang, F. Wei, *Carbon* **2010**, *48*, 487.
[269] H. Wang, Q. Hao, X. Yang, L. Lu, X. Wang, *Nanoscale* **2010**, *2*, 2164.
[270] J. Xu, K. Wang, S.-Z. Zu, B.-H. Han, Z. Wei, *ACS Nano* **2010**, *4*, 5019.
[271] Q. Wu, Y. Xu, Z. Yao, A. Liu, G. Shi, *ACS Nano* **2010**, *4*, 1963.
[272] F. Chen, P. Liu, Q. Zhao, *Electrochim. Acta* **2012**, *76*, 62.
[273] S. Grover, S. Goel, V. Sahu, G. Singh, R. K. Sharma, *ACS Sustainable Chem. Eng.* **2015**, *3*, 1460.
[274] X. Liu, N. Wen, X. Wang, Y. Zheng, *ACS Sustainable Chem. Eng.* **2015**, *3*, 475.
[275] K. Chi, Z. Zhang, J. Xi, Y. Huang, F. Xiao, S. Wang, Y. Liu, *ACS Appl. Mater. Interfaces* **2014**, *6*, 16312.
[276] D. Xu, Q. Xu, K. Wang, J. Chen, Z. Chen, *ACS Appl. Mater. Interfaces* **2014**, *6*, 200.
[277] N. A. Kumar, H.-J. Choi, Y. R. Shin, D. W. Chang, L. Dai, J.-B. Baek, *ACS Nano* **2012**, *6*, 1715.
[278] A. Liu, C. Li, H. Bai, G. Shi, *J. Phys. Chem. C* **2010**, *114*, 22783.
[279] C. Xu, J. Sun, L. Gao, *J. Mater. Chem.* **2011**, *21*, 11253.
[280] H.-H. Chang, C.-K. Chang, Y.-C. Tsai, C.-S. Liao, *Carbon* **2012**, *50*, 2331.
[281] F. Zhang, F. Xiao, Z. H. Dong, W. Shi, *Electrochim. Acta* **2013**, *114*, 125.
[282] A. Aphale, K. Maisuria, M. K. Mahapatra, A. Santiago, P. Singh, P. Patra, *Sci. Rep.* **2015**, *5*, 14445.
[283] S. Biswas, L. T. Drzal, *Chem. Mater.* **2010**, *22*, 5667.
[284] J. Liu, J. An, Y. Ma, M. Li, R. Ma, *J. Electrochem. Soc.* **2012**, *159*, A828.
[285] H. P. de Oliveira, S. A. Sydlik, T. M. Swager, *J. Phys. Chem. C* **2013**, *117*, 10270.
[286] Y. Liu, J. Zhou, J. Tang, W. Tang, *Chem. Mater.* **2015**, *27*, 7034.
[287] L.-L. Jiang, X. Lu, C.-M. Xie, G.-J. Wan, H.-P. Zhang, T. Youhong, *J. Phys. Chem. C* **2015**, *119*, 3903.
[288] C. Bora, J. Sharma, S. Dolui, *J. Phys. Chem. C* **2014**, *118*, 29688.
[289] X. Fan, Z. Yang, N. He, *RSC Adv.* **2015**, *5*, 15096.
[290] F. Alvi, P. A. Basnayaka, M. K. Ram, H. Gomez, E. Stefanako, Y. Goswami, A. Kumar, *J. New Mater. Electrochem. Syst.* **2012**, *15*, 089.
[291] F. Alvi, M. K. Ram, P. Basnayaka, E. Stefanakos, Y. Goswami, A. Hoff, A. Kumar, *ECS Trans.* **2011**, *35*, 167.
[292] F. Alvi, M. K. Ram, P. A. Basnayaka, E. Stefanakos, Y. Goswami, A. Kumar, *Electrochim. Acta* **2011**, *56*, 9406.
[293] J. Cherusseri, K. K. Kar, in *Polymer Nanocomposites Based on Inorganic and Organic Nanomaterials*, John Wiley & Sons, Inc., Smita Mohanty, Beverly MA, USA **2015**, pp. 229.
[294] S. Lehtimäki, M. Suominen, P. Damlin, S. Tuukkanen, C. Kvarnström, D. Lupo, *ACS Appl. Mater. Interfaces* **2015**, *7*, 22137.
[295] G. H. Jeong, I. Lee, J. G. Kang, H. Lee, S. Yoon, S. W. Kim, *RSC Adv.* **2015**, *5*, 73119.
[296] D. C. Lv, J. L. Shen, G. C. Wang, *RSC Adv.* **2015**, *5*, 24599.
[297] Y. X. Wang, Y. F. Song, Y. Wang, X. Chen, Y. Y. Xia, Z. Z. Shao, *J. Mater. Chem. A* **2015**, *3*, 773.
[298] J. Ma, Q. Guo, H. L. Gao, X. Qin, *Fullerenes, Nanotubes, Carbon Nanostruct.* **2015**, *23*, 477.
[299] S. Stankovich, D. A. Dikin, G. H. B. Dommett, K. M. Kohlhaas, E. J. Zimney, E. A. Stach, R. D. Piner, S. T. Nguyen, R. S. Ruoff, *Nature* **2006**, *442*, 282.
[300] Y. Liang, D. Wu, X. Feng, K. Müllen, *Adv. Mater.* **2009**, *21*, 1679.
[301] D. Yu, L. Dai, *J. Phys. Chem. Lett.* **2009**, *1*, 467.
[302] H. R. Byon, S. W. Lee, S. Chen, P. T. Hammond, Y. Shao-Horn, *Carbon* **2011**, *49*, 457.

[303] L. Qiu, X. Yang, X. Gou, W. Yang, Z.-F. Ma, G. G. Wallace, D. Li, *Chem. - Eur. J.* **2010**, *16*, 10653.
[304] Z. Fan, J. Yan, L. Zhi, Q. Zhang, T. Wei, J. Feng, M. Zhang, W. Qian, F. Wei, *Adv. Mater.* **2010**, *22*, 3723.
[305] Z. Lei, N. Christov, X. S. Zhao, *EnergyEnviron. Sci.* **2011**, *4*, 1866.
[306] K. Zhang, B. T. Ang, L. L. Zhang, X. S. Zhao, J. Wu, *J. Mater. Chem.* **2011**, *21*, 2663.
[307] C. X. Guo, C. M. Li, *Energy Environ. Sci.* **2011**, *4*, 4504.
[308] J. Yan, T. Wei, B. Shao, F. Ma, Z. Fan, M. Zhang, C. Zheng, Y. Shang, W. Qian, F. Wei, *Carbon* **2010**, *48*, 1731.
[309] P. Soudan, J. Gaudet, D. Guay, D. Bélanger, R. Schulz, *Chem. Mater.* **2002**, *14*, 1210.
[310] X. Wu, W. Xiong, Y. Y. Chen, D. N. Lan, X. L. Pu, Y. Zeng, H. R. Gao, J. S. Chen, H. Tong, Z. H. Zhu, *J. Power Sources* **2015**, *294*, 88.
[311] R. R. Salunkhe, J. J. Lin, V. Malgras, S. X. Dou, J. H. Kim, Y. Yamauchi, *Nano Energy* **2015**, *11*, 211.
[312] Z. J. Han, D. H. Seo, S. Yick, J. H. Chen, K. Ostrikov, *NPG Asia Mater.* **2014**, *6*, e140.
[313] M. M. Liu, J. Sun, *J. Mater. Chem. A* **2014**, *2*, 12068.
[314] C.-C. Wang, H.-C. Chen, S.-Y. Lu, *Chem. - Eur. J.* **2014**, *20*, 517.
[315] H.-C. Chen, C.-C. Wang, S.-Y. Lu, *J. Mater. Chem. A* **2014**, *2*, 16955.
[316] B. Mu, W. Zhang, S. Shao, A. Wang, *Phys. Chem. Chem. Phys.* **2014**, *16*, 7872.
[317] D. Mhamane, A. Suryawanshi, S. M. Unni, C. Rode, S. Kurungot, S. Ogale, *Small* **2013**, *9*, 2801.
[318] J. Yan, Z. Fan, T. Wei, W. Qian, M. Zhang, F. Wei, *Carbon* **2010**, *48*, 3825.
[319] G. Yu, L. Hu, M. Vosgueritchian, H. Wang, X. Xie, J. R. McDonough, X. Cui, Y. Cui, Z. Bao, *Nano Lett.* **2011**, *11*, 2905.
[320] G. Han, Y. Liu, L. Zhang, E. Kan, S. Zhang, J. Tang, W. Tang, *Sci. Rep.* **2014**, *4*, 4824.
[321] G. Han, Y. Liu, E. Kan, J. Tang, L. Zhang, H. Wang, W. Tang, *RSC Adv.* **2014**, *4*, 9898.
[322] Z. J. Han, D. H. Seo, S. Yick, J. H. Chen, K. Ostrikov, *NPG Asia Mater.* **2014**, *6*, e140.
[323] Z.-S. Wu, W. Ren, D.-W. Wang, F. Li, B. Liu, H.-M. Cheng, *ACS Nano* **2010**, *4*, 5835.
[324] H. Huang, X. Wang, *Nanoscale* **2011**, *3*, 3185.
[325] X. Zhao, L. Zhang, S. Murali, M. D. Stoller, Q. Zhang, Y. Zhu, R. S. Ruoff, *ACS Nano* **2012**, *6*, 5404.
[326] Z. Fan, J. Yan, T. Wei, L. Zhi, G. Ning, T. Li, F. Wei, *Adv. Funct. Mater.* **2011**, *21*, 2366.
[327] Z.-S. Wu, D.-W. Wang, W. Ren, J. Zhao, G. Zhou, F. Li, H.-M. Cheng, *Adv. Funct. Mater.* **2010**, *20*, 3595.
[328] L. Deng, J. Wang, G. Zhu, L. Kang, Z. Hao, Z. Lei, Z. Yang, Z.-H. Liu, *J. Power Sources* **2014**, *248*, 407.
[329] W. Wang, S. Guo, I. Lee, K. Ahmed, J. Zhong, Z. Favors, F. Zaera, M. Ozkan, C. S. Ozkan, *Sci. Rep.* **2014**, *4*, 4452.
[330] C. Zhang, H. Zhou, X. Yu, D. Shan, T. Ye, Z. Huang, Y. Kuang, *RSC Adv.* **2014**, *4*, 11197.
[331] J. Yan, T. Wei, W. Qiao, B. Shao, Q. Zhao, L. Zhang, Z. Fan, *Electrochim. Acta* **2010**, *55*, 6973.
[332] W. Zhou, J. Liu, T. Chen, K. S. Tan, X. Jia, Z. Luo, C. Cong, H. Yang, C. M. Li, T. Yu, *Phys. Chem. Chem. Phys.* **2011**, *13*, 14462.
[333] W. Shi, J. Zhu, D. H. Sim, Y. Y. Tay, Z. Lu, X. Zhang, Y. Sharma, M. Srinivasan, H. Zhang, H. H. Hng, Q. Yan, *J. Mater. Chem.* **2011**, *21*, 3422.
[334] B. Li, H. Cao, J. Shao, M. Qu, J. H. Warner, *J. Mater. Chem.* **2011**, *21*, 5069.
[335] T. Lu, Y. Zhang, H. Li, L. Pan, Y. Li, Z. Sun, *Electrochim. Acta* **2010**, *55*, 4170.
[336] X. Xia, J. Tu, Y. Mai, R. Chen, X. Wang, C. Gu, X. Zhao, *Chem. - Eur. J.* **2011**, *17*, 10898.
[337] Y. Guo, B. Chang, T. Wen, C. Zhao, H. Yin, Y. Zhou, Y. Wang, B. Yang, S. Zhang, *RSC Adv.* **2016**, *6*, 19394.
[338] J. W. Lee, A. S. Hall, J.-D. Kim, T. E. Mallouk, *Chem. Mater.* **2012**, *24*, 1158.
[339] Y. Hu, C. Guan, G. Feng, Q. Ke, X. Huang, J. Wang, *Adv. Funct. Mater.* **2015**, *25*, 7291.
[340] S.-G. Hwang, J.-E. Hong, G.-O. Kim, H. M. Jeong, K.-S. Ryu, *ECS Solid State Lett.* **2013**, *2*, M8.
[341] M. Lee, B.-H. Wee, J.-D. Hong, *Adv. Energy Mater.* **2015**, *5*, 1401890.
[342] G. Ye, Y. Gong, K. Keyshar, E. A. M. Husain, G. Brunetto, S. Yang, R. Vajtai, P. M. Ajayan, *Part. Part. Syst. Charact.* **2015**, *32*, 817.
[343] Y. Wang, C. X. Guo, J. Liu, T. Chen, H. Yang, C. M. Li, *Dalton Trans.* **2011**, *40*, 6388.
[344] J. Yang, G. Li, Z. Pan, M. Liu, Y. Hou, Y. Xu, H. Deng, L. Sheng, X. Zhao, Y. Qiu, Y. Zhang, *ACS Appl. Mater. Interfaces* **2015**, *7*, 22172.
[345] J. Hu, A. Ramadan, F. Luo, B. Qi, X. Deng, J. Chen, *J. Mater. Chem.* **2011**, *21*, 15009.
[346] Z. Wang, X. Zhang, Y. Li, Z. Liu, Z. Hao, *J. Mater. Chem. A* **2013**, *1*, 6393.
[347] S. Chen, J. Zhu, X. Wang, *J. Phys. Chem. C* **2010**, *114*, 11829.
[348] D. P. Dubal, R. Holze, P. Gomez-Romero, *Sci. Rep.* **2014**, *4*, 7349.
[349] H. Wang, H. S. Casalongue, Y. Liang, H. Dai, *J. Am. Chem. Soc.* **2010**, *132*, 7472.
[350] Y. Liu, R. Wang, X. Yan, *Sci. Rep.* **2015**, *5*, 11095.
[351] X.-C. Dong, H. Xu, X.-W. Wang, Y.-X. Huang, M. B. Chan-Park, H. Zhang, L.-H. Wang, W. Huang, P. Chen, *ACS Nano* **2012**, *6*, 3206.
[352] M. Liu, J. Sun, *J. Mater. Chem. A* **2014**, *2*, 12068.
[353] B. T. Dong, X. Zhang, X. Xu, G. X. Gao, S. J. Ding, J. Li, B. B. Li, *Carbon* **2014**, *80*, 222.
[354] G. H. Jeong, H.-M. Lee, H. Lee, C.-K. Kim, Y. Piao, J.-H. Lee, J.-H. Kim, S.-W. Kim, *RSC Adv.* **2014**, *4*, 51619.
[355] T. Brousse, D. Belanger, J. W. Long, *J. Electrochem. Soc.* **2015**, *162*, A5185.
[356] X. Lu, T. Liu, T. Zhai, G. Wang, M. Yu, S. Xie, Y. Ling, C. Liang, Y. Tong, Y. Li, *Adv. Energy Mater.* **2014**, *4*, 1300994.
[357] X. Lu, M. Yu, T. Zhai, G. Wang, S. Xie, T. Liu, C. Liang, Y. Tong, Y. Li, *Nano Lett.* **2013**, *13*, 2628.
[358] D. Choi, G. E. Blomgren, P. N. Kumta, *Adv. Mater.* **2006**, *18*, 1178.
[359] D. Choi, P. N. Kumta, *J. Electrochem. Soc.* **2006**, *153*, A2298.
[360] K.-H. Lee, Y.-W. Lee, A. R. Ko, G. Cao, K.-W. Park, *J. Am. Ceram. Soc.* **2013**, *96*, 37.
[361] M.-S. Balogun, W. Qiu, W. Wang, P. Fang, X. Lu, Y. Tong, *J. Mater. Chem. A* **2015**, *3*, 1364.
[362] X. Cong, C. Cheng, Y. Liao, Y. Ye, C. Dong, H. Sun, X. Ji, W. Zhang, P. Fang, L. Miao, J. Jiang, *J. Phys. Chem. C* **2015**, *119*, 20864.
[363] R. Ren, M. S. Faber, R. Dziedzic, Z. Wen, S. Jin, S. Mao, J. Chen, *Nanotechnology* **2015**, *26*, 494001.
[364] Y.-H. Dai, L.-B. Kong, K. Yan, M. Shi, T. Zhang, Y.-C. Luo, L. Kang, *RSC Adv.* **2016**, *6*, 7633.
[365] X.-Y. Yu, L. Yu, L. Shen, X. Song, H. Chen, X. W. Lou, *Adv. Funct. Mater.* **2014**, *24*, 7440.
[366] K.-J. Huang, L. Wang, Y.-J. Liu, Y.-M. Liu, H.-B. Wang, T. Gan, L.-L. Wang, *Int. J. Hydrogen Energy* **2013**, *38*, 14027.
[367] S. Ratha, C. S. Rout, *ACS Appl. Mater. Interfaces* **2013**, *5*, 11427.
[368] X. Meng, H. Sun, J. Zhu, H. Bi, Q. Han, X. Liu, X. Wang, *New J. Chem.* **2016**, *46*, 2843.

[369] P. Han, Y. Yue, X. Wang, W. Ma, S. Dong, K. Zhang, C. Zhang, G. Cui, *J. Mater. Chem.* **2012**, *22*, 24918.
[370] F. Tian, Y. Xie, H. Du, Y. Zhou, C. Xia, W. Wang, *RSC Adv.* **2014**, *4*, 41856.
[371] R. Wang, J. Lang, P. Zhang, Z. Lin, X. Yan, *Adv. Funct. Mater.* **2015**, *25*, 2270.
[372] C. Zhu, P. Yang, D. Chao, X. Wang, X. Zhang, S. Chen, B. K. Tay, H. Huang, H. Zhang, W. Mai, H. J. Fan, *Adv. Mater.* **2015**, *27*, 4566.
[373] J. Xu, S. Gai, F. He, N. Niu, P. Gao, Y. Chen, P. Yang, *J. Mater. Chem. A* **2014**, *2*, 1022.
[374] X. Dong, L. Wang, D. Wang, C. Li, J. Jin, *Langmuir* **2011**, *28*, 293.
[375] F. Wang, S. Xiao, Y. Hou, C. Hu, L. Liu, Y. Wu, *RSC Adv.* **2013**, *3*, 13059.
[376] J. H. Chae, K. C. Ng, G. Z. Chen, *Proc. Inst. Mech. Eng., Part A* **2010**, *224*, 479.
[377] H. L. Wang, *Pure Appl. Chem.* **2014**, *86*, 39.
[378] H. Wang, Y. Liang, T. Mirfakhrai, Z. Chen, H. Casalongue, H. Dai, *Nano Res.* **2011**, *4*, 729.
[379] Q. Cheng, J. Tang, J. Ma, H. Zhang, N. Shinya, L.-C. Qin, *Carbon* **2011**, *49*, 2917.
[380] B. Li, Y. Fu, H. Xia, X. Wang, *Mater. Lett.* **2014**, *122*, 193.
[381] J. Shen, C. Yang, X. Li, G. Wang, *ACS Appl. Mater. Interfaces* **2013**, *5*, 8467.
[382] T.-W. Lin, C.-S. Dai, K.-C. Hung, *Sci. Rep.* **2014**, *4*, 7274.
[383] Y. Cheng, H. Zhang, S. Lu, C. V. Varanasi, J. Liu, *Nanoscale* **2013**, *5*, 1067.
[384] Y. Meng, Y. Zhao, C. Hu, H. Cheng, Y. Hu, Z. Zhang, G. Shi, L. Qu, *Adv. Mater.* **2013**, *25*, 2326.
[385] P. Chen, J.-J. Yang, S.-S. Li, Z. Wang, T.-Y. Xiao, Y.-H. Qian, S.-H. Yu, *Nano Energy* **2013**, *2*, 249.
[386] Z. Dong, C. Jiang, H. Cheng, Y. Zhao, G. Shi, L. Jiang, L. Qu, *Adv. Mater.* **2012**, *24*, 1856.
[387] N. Jha, P. Ramesh, E. Bekyarova, M. E. Itkis, R. C. Haddon, *Adv. Energy Mater.* **2012**, *2*, 438.
[388] J. Lin, C. Zhang, Z. Yan, Y. Zhu, Z. Peng, R. H. Hauge, D. Natelson, J. M. Tour, *Nano Lett.* **2012**, *13*, 72.
[389] F. Du, D. Yu, L. Dai, S. Ganguli, V. Varshney, A. K. Roy, *Chem. Mater.* **2011**, *23*, 4810.
[390] H. Cheng, Z. Dong, C. Hu, Y. Zhao, Y. Hu, L. Qu, N. Chen, L. Dai, *Nanoscale* **2013**, *5*, 3428.
[391] X. Ding, Y. Zhao, C. Hu, Y. Hu, Z. Dong, N. Chen, Z. Zhang, L. Qu, *J. Mater. Chem. A* **2014**, *2*, 12355.
[392] M. Beidaghi, Y. Gogotsi, *Energy Environ. Sci.* **2014**, *7*, 867.
[393] D. Yu, K. Goh, H. Wang, L. Wei, W. Jiang, Q. Zhang, L. Dai, Y. Chen, *Nat. Nanotechnol.* **2014**, *9*, 555.
[394] Y. Xu, Z. Lin, X. Huang, Y. Liu, Y. Huang, X. Duan, *ACS Nano* **2013**, *7*, 4042.
[395] M. Liu, Y.-E. Miao, C. Zhang, W. W. Tjiu, Z. Yang, H. Peng, T. Liu, *Nanoscale* **2013**, *5*, 7312.
[396] Z. Zhang, F. Xiao, L. Qian, J. Xiao, S. Wang, Y. Liu, *Adv. Energy Mater.* **2014**, *4*, 1400064.
[397] L. Liu, Z. Niu, L. Zhang, W. Zhou, X. Chen, S. Xie, *Adv. Mater.* **2014**, *26*, 4855.
[398] B. D. McCloskey, *J. Phys. Chem. Lett.* **2015**, *6*, 3592.
[399] C. J. Jafta, F. Nkosi, L. le Roux, M. K. Mathe, M. Kebede, K. Makgopa, Y. Song, D. Tong, M. Oyama, N. Manyala, S. Chen, K. I. Ozoemena, *Electrochim. Acta* **2013**, *110*, 228.
[400] L. Ma, X. Shen, Z. Ji, G. Zhu, H. Zhou, *Chem. Eng. J.* **2014**, *252*, 95.
[401] G. He, J. Li, H. Chen, J. Shi, X. Sun, S. Chen, X. Wang, *Mater. Lett.* **2012**, *82*, 61.
[402] X. Wang, S. Liu, H. Wang, F. Tu, D. Fang, Y. Li, *J. Solid State Electrochem.* **2012**, *16*, 3593.
[403] Q. Wang, L. Jiao, H. Du, Y. Wang, H. Yuan, *J. Power Sources* **2014**, *245*, 101.
[404] T. Qi, J. Jiang, H. Chen, H. Wan, L. Miao, L. Zhang, *Electrochim. Acta* **2013**, *114*, 674.
[405] K. Qingqing, T. Chunhua, L. Yanqiong, L. Huajun, W. John, *Mater. Res. Express* **2014**, *1*, 025015.
[406] H. Wang, Z. Xu, H. Yi, H. Wei, Z. Guo, X. Wang, *Nano Energy* **2014**, *7*, 86.
[407] Z. Wang, C. Ma, H. Wang, Z. Liu, Z. Hao, *J. Alloys Compd.* **2013**, *552*, 486.
[408] S. P. Lim, N. M. Huang, H. N. Lim, *Ceram. Int.* **2013**, *39*, 6647.
[409] Y. Haldorai, W. Voit, J.-J. Shim, *Electrochim. Acta* **2014**, *120*, 65.
[410] C. Wang, J. Xu, M.-F. Yuen, J. Zhang, Y. Li, X. Chen, W. Zhang, *Adv. Funct. Mater.* **2014**, 6372.
[411] Y. Cai, Y. Wang, S. Deng, G. Chen, Q. Li, B. Han, R. Han, Y. Wang, *Ceram. Int.* **2014**, *40*, 4109.
[412] A. Ramadoss, S. J. Kim, *Carbon* **2013**, *63*, 434.
[413] H. Lee, M. Yanilmaz, O. Toprakci, K. Fu, X. Zhang, *Energy Environ. Sci.* **2014**, *7*, 3857.
[414] J. B. Goodenough, K.-S. Park, *J. Am. Chem. Soc.* **2013**, *135*, 1167.
[415] G. S. Pappas, S. Ferrari, C. Y. Wan, *Curr. Org. Chem.* **2015**, *19*, 1838.
[416] X. L. Wang, G. Q. Shi, *Energy Environ. Sci.* **2015**, *8*, 790.
[417] M. Srivastava, J. Singh, T. Kuila, R. K. Layek, N. H. Kim, J. H. Lee, *Nanoscale* **2015**, *7*, 4820.
[418] S. Wu, R. Xu, M. Lu, R. Ge, J. Iocozzia, C. Han, B. Jiang, Z. Lin, *Adv. Energy Mater.* **2015**, *5*, 1500400.
[419] B. Luo, L. Zhi, *Energy Environ. Sci.* **2015**, *8*, 456.
[420] Y. Shi, L. Wen, G. M. Zhou, J. Chen, S. F. Pei, K. Huang, H. M. Cheng, F. Li, *2D Mater.* **2015**, *2*, 024004.
[421] L. W. Ji, Z. Lin, M. Alcoutlabi, X. W. Zhang, *Energy Environ. Sci.* **2011**, *4*, 2682.
[422] J. Cai, Z. Li, P. K. Shen, *ACS Appl. Mater. Interfaces* **2012**, *4*, 4093.
[423] W. Wang, Y. Yang, S. Yang, Z. Guo, C. Feng, X. Tang, *Electrochim. Acta* **2015**, *155*, 297.
[424] P. Roy, S. K. Srivastava, *J. Mater. Chem. A* **2015**, *3*, 2454.
[425] X. Y. Zhu, D. J. Yang, J. J. Li, F. B. Su, *J. Nanosci. Nanotechnol.* **2015**, *15*, 15.
[426] M. Alcoutlabi, L. W. Ji, B. K. Guo, S. L. Li, Y. Li, S. Zhang, O. Toprakci, X. W. Zhang, *AATCC Rev.* **2011**, *11*, 45.
[427] L. W. Ji, Z. Lin, M. Alcoutlabi, O. Toprakci, Y. F. Yao, G. J. Xu, S. L. Li, X. W. Zhang, *RSC Adv.* **2012**, *2*, 192.
[428] L. W. Ji, O. Toprakci, M. Alcoutlabi, Y. F. Yao, Y. Li, S. Zhang, B. K. Guo, Z. Lin, X. W. Zhang, *ACS Appl. Mater. Interfaces* **2012**, *4*, 2672.
[429] D. Pan, S. Wang, B. Zhao, M. Wu, H. Zhang, Y. Wang, Z. Jiao, *Chem. Mater.* **2009**, *21*, 3136.
[430] G. Wang, X. Shen, J. Yao, J. Park, *Carbon* **2009**, *47*, 2049.
[431] E. Yoo, J. Kim, E. Hosono, H.-s. Zhou, T. Kudo, I. Honma, *Nano Lett.* **2008**, *8*, 2277.
[432] C. Wang, D. Li, C. O. Too, G. G. Wallace, *Chem. Mater.* **2009**, *21*, 2604.
[433] P. Guo, H. Song, X. Chen, *Electrochem. Commun.* **2009**, *11*, 1320.
[434] L. Ren, K. N. Hui, K. S. Hui, Y. Liu, X. Qi, J. Zhong, Y. Du, J. Yang, *Sci. Rep.* **2015**, *5*, 14229.
[435] A. L. M. Reddy, A. Srivastava, S. R. Gowda, H. Gullapalli, M. Dubey, P. M. Ajayan, *ACS Nano* **2010**, *4*, 6337.
[436] Z.-L. Wang, D. Xu, H.-G. Wang, Z. Wu, X.-B. Zhang, *ACS Nano* **2013**, *7*, 2422.
[437] G. Radhakrishnan, J. D. Cardema, P. M. Adams, H. I. Kim, B. Foran, *J. Electrochem. Soc.* **2012**, *159*, A752.
[438] L. D. Carr, M. T. Lusk, *Nat Nano* **2010**, *5*, 316.

[439] Y. Fang, Y. Lv, R. Che, H. Wu, X. Zhang, D. Gu, G. Zheng, D. Zhao, *J. Am. Chem. Soc.* **2013**, *135*, 1524.
[440] Z. Fan, J. Yan, G. Ning, T. Wei, L. Zhi, F. Wei, *Carbon* **2013**, *60*, 558.
[441] R. Mukherjee, A. V. Thomas, D. Datta, E. Singh, J. Li, O. Eksik, V. B. Shenoy, N. Koratkar, *Nat. Commun.* **2014**, *5*, 3710.
[442] Z.-S. Wu, W. Ren, L. Xu, F. Li, H.-M. Cheng, *ACS Nano* **2011**, *5*, 5463.
[443] X. Li, D. Geng, Y. Zhang, X. Meng, R. Li, X. Sun, *Electrochem. Commun.* **2011**, *13*, 822.
[444] H. Wang, C. Zhang, Z. Liu, L. Wang, P. Han, H. Xu, K. Zhang, S. Dong, J. Yao, G. Cui, *J. Mater. Chem.* **2011**, *21*, 5430.
[445] C. Zhang, N. Mahmood, H. Yin, F. Liu, Y. Hou, *Adv. Mater.* **2013**, *25*, 4932.
[446] Y. S. Yun, V.-D. Le, H. Kim, S.-J. Chang, S. J. Baek, S. Park, B. H. Kim, Y.-H. Kim, K. Kang, H.-J. Jin, *J. Power Sources* **2014**, *262*, 79.
[447] X. Ma, G. Ning, C. Qi, C. Xu, J. Gao, *ACS Appl. Mater. Interfaces* **2014**, *6*, 14415.
[448] L. Hu, M. Pasta, F. L. Mantia, L. Cui, S. Jeong, H. D. Deshazer, J. W. Choi, S. M. Han, Y. Cui, *Nano Lett.* **2010**, *10*, 708.
[449] F. Yao, F. Güneş, H. Q. Ta, S. M. Lee, S. J. Chae, K. Y. Sheem, C. S. Cojocaru, S. S. Xie, Y. H. Lee, *J. Am. Chem. Soc.* **2012**, *134*, 8646.
[450] S. Y. Jeong, S. Yang, S. Jeong, I. J. Kim, H. J. Jeong, J. T. Han, K.-J. Baeg, G.-W. Lee, *Small* **2015**, *11*, 2774.
[451] R. Mukherjee, A. V. Thomas, A. Krishnamurthy, N. Koratkar, *ACS Nano* **2012**, *6*, 7867.
[452] L. Shen, X. Zhang, H. Li, C. Yuan, G. Cao, *J. Phys. Chem. Lett.* **2011**, *2*, 3096.
[453] D. Choi, D. Wang, V. V. Viswanathan, I.-T. Bae, W. Wang, Z. Nie, J.-G. Zhang, G. L. Graff, J. Liu, Z. Yang, T. Duong, *Electrochem. Commun.* **2010**, *12*, 378.
[454] X. Xin, X. Zhou, J. Wu, X. Yao, Z. Liu, *ACS Nano* **2012**, *6*, 11035.
[455] S. Ding, J. S. Chen, D. Luan, F. Y. C. Boey, S. Madhavi, X. W. Lou, *Chem. Commun.* **2011**, *47*, 5780.
[456] S.-M. Paek, E. Yoo, I. Honma, *Nano Lett.* **2008**, *9*, 72.
[457] Z. Chen, M. Zhou, Y. Cao, X. Ai, H. Yang, J. Liu, *Adv. Energy Mater.* **2012**, *2*, 95.
[458] J. Zhang, L. Chang, F. X. Wang, D. Xie, Q. M. Su, G. H. Du, *Mater. Res. Bull.* **2015**, *68*, 120.
[459] H. Yang, Z. H. Hou, N. B. Zhou, B. H. He, J. G. Cao, Y. F. Kuang, *Ceram. Int.* **2014**, *40*, 13903.
[460] R. Tian, Y. Zhang, Z. Chen, H. Duan, B. Xu, Y. Guo, H. Kang, H. Li, H. Liu, *Sci. Rep.* **2016**, *6*, 19195.
[461] S. S. Chen, X. Qin, *Nano* **2015**, *10*, 1550081.
[462] L. Li, A. Kovalchuk, H. Fei, Z. Peng, Y. Li, N. D. Kim, C. Xiang, Y. Yang, G. Ruan, J. M. Tour, *Adv. Energy Mater.* **2015**, *5*, 1500171.
[463] Z.-S. Wu, W. Ren, L. Wen, L. Gao, J. Zhao, Z. Chen, G. Zhou, F. Li, H.-M. Cheng, *ACS Nano* **2010**, *4*, 3187.
[464] S. Yang, X. Feng, S. Ivanovici, K. Müllen, *Angew. Chem. Int. Ed.* **2010**, *49*, 8408.
[465] L. N. Wang, H. Wang, J. C. Wang, J. B. Bai, *Synth. React. Inorg., Met.-Org. Nano-Met. Chem.* **2015**, *45*, 614.
[466] X. Zhu, Y. Zhu, S. Murali, M. D. Stoller, R. S. Ruoff, *ACS Nano* **2011**, *5*, 3333.
[467] M. Zhang, B. Qu, D. Lei, Y. Chen, X. Yu, L. Chen, Q. Li, Y. Wang, T. Wang, *J. Mater. Chem.* **2012**, *22*, 3868.
[468] Y. K. Wang, L. C. Yang, R. Z. Hu, W. Sun, J. W. Liu, L. Z. Ouyang, B. Yuan, H. H. Wang, M. Zhu, *J. Power Sources* **2015**, *288*, 314.
[469] S. Yang, Y. Sun, L. Chen, Y. Hernandez, X. Feng, K. Müllen, *Sci. Rep.* **2012**, *2*, 427.
[470] Y. R. Ren, J. W. Wang, X. B. Huang, B. Yang, J. N. Ding, *RSC Adv.* **2015**, *5*, 59208.
[471] C. X. Guo, M. Wang, T. Chen, X. W. Lou, C. M. Li, *Adv. Energy Mater.* **2011**, *1*, 736.
[472] K. Wen, G. H. Chen, F. Jiang, X. Y. Zhou, J. Yang, *Int. J. Electrochem. Sci.* **2015**, *10*, 3859.
[473] C.-T. Hsieh, C.-Y. Lin, J.-Y. Lin, *Electrochim. Acta* **2011**, *56*, 8861.
[474] S. Zhang, L. X. Zhu, H. H. Song, X. H. Chen, J. S. Zhou, *Nano Energy* **2014**, *10*, 172.
[475] Q. Sun, Z. Wang, Z. Zhang, Q. Yu, Y. Qu, J. Zhang, Y. Yu, B. Xiang, *ACS Appl. Mater. Interfaces* **2016**, *8*, 6303.
[476] B. Wang, X.-L. Wu, C.-Y. Shu, Y.-G. Guo, C.-R. Wang, *J. Mater. Chem.* **2010**, *20*, 10661.
[477] J. Zhou, L. Ma, H. Song, B. Wu, X. Chen, *Electrochem. Commun.* **2011**, *13*, 1357.
[478] X. Y. Zhou, J. J. Shi, Y. Liu, Q. M. Su, J. Zhang, G. H. Du, *J. Alloys Compd.* **2014**, *615*, 390.
[479] Y. Huang, X.-l. Huang, J.-s. Lian, D. Xu, L.-m. Wang, X.-b. Zhang, *J. Mater. Chem.* **2012**, *22*, 2844.
[480] Y. Zou, Y. Wang, *Nanoscale* **2011**, *3*, 2615.
[481] X. H. Huang, P. Zhang, J. B. Wu, Y. Lin, R. Q. Guo, *Mater. Lett.* **2015**, *153*, 102.
[482] Z. J. Zhang, H. L. Zhao, Z. P. Zeng, C. H. Gao, J. Wang, Q. Xia, *Electrochim. Acta* **2015**, *155*, 85.
[483] Y. Sun, X. Hu, W. Luo, Y. Huang, *ACS Nano* **2011**, *5*, 7100.
[484] J. Zhu, T. Zhu, X. Zhou, Y. Zhang, X. W. Lou, X. Chen, H. Zhang, H. H. Hng, Q. Yan, *Nanoscale* **2011**, *3*, 1084.
[485] Y. R. Ren, H. M. Wei, X. B. Huang, J. N. Ding, *Int. J. Electrochem. Sci.* **2014**, *9*, 7784.
[486] G. Gao, H. B. Wu, B. Dong, S. Ding, X. W. Lou, *Adv. Sci.* **2015**, *2*, 1400014.
[487] W. Bai, H. Tong, Z. Gao, S. Yue, S. Xing, S. Dong, L. Shen, J. He, X. Zhang, Y. Liang, *J. Mater. Chem. A* **2015**, *3*, 21891.
[488] G. Wang, J. Bai, Y. Wang, Z. Ren, J. Bai, *Scr. Mater.* **2011**, *65*, 339.
[489] W. Yue, Z. Lin, S. Jiang, X. Yang, *J. Mater. Chem.* **2012**, *22*, 16318.
[490] K. Chang, W. Chen, *Chem. Commun.* **2011**, *47*, 4252.
[491] H. Hwang, H. Kim, J. Cho, *Nano Lett.* **2011**, *11*, 4826.
[492] J. Xiao, X. Wang, X.-Q. Yang, S. Xun, G. Liu, P. K. Koech, J. Liu, J. P. Lemmon, *Adv. Funct. Mater.* **2011**, *21*, 2840.
[493] L. Ji, H. L. Xin, T. R. Kuykendall, S.-L. Wu, H. Zheng, M. Rao, E. J. Cairns, V. Battaglia, Y. Zhang, *Phys. Chem. Chem. Phys.* **2012**, *14*, 6981.
[494] L. Zhuo, Y. Wu, L. Wang, Y. Yu, X. Zhang, F. Zhao, *RSC Adv.* **2012**, *2*, 5084.
[495] B. H. Qu, G. Ji, B. Ding, M. H. Lu, W. X. Chen, J. Y. Lee, *ChemElectroChem* **2015**, *2*, 1138.
[496] Y. C. Liu, H. Y. Kang, L. F. Jiao, C. C. Chen, K. Z. Cao, Y. J. Wang, H. T. Yuan, *Nanoscale* **2015**, *7*, 1325.
[497] Y. Gu, Y. Xu, Y. Wang, *ACS Appl. Mater. Interfaces* **2013**, *5*, 801.
[498] L. Fei, Q. Lin, B. Yuan, G. Chen, P. Xie, Y. Li, Y. Xu, S. Deng, S. Smirnov, H. Luo, *ACS Appl. Mater. Interfaces* **2013**, *5*, 5330.
[499] N. Mahmood, C. Zhang, J. Jiang, F. Liu, Y. Hou, *Chem. - Eur. J.* **2013**, *19*, 5183.
[500] Q. Pan, J. Xie, S. Liu, G. Cao, T. Zhu, X. Zhao, *RSC Adv.* **2013**, *3*, 3899.
[501] S. M. Lee, Y. N. Ko, S. H. Choi, J. H. Kim, Y. C. Kang, *Electrochim. Acta* **2015**, *167*, 287.
[502] L. Lai, J. Zhu, B. Li, Y. Zhen, Z. Shen, Q. Yan, J. Lin, *Electrochim. Acta* **2014**, *134*, 28.
[503] Y. Yue, P. Han, X. He, K. Zhang, Z. Liu, C. Zhang, S. Dong, L. Gu, G. Cui, *J. Mater. Chem.* **2012**, *22*, 4938.
[504] Y. Qiu, K. Yan, S. Yang, L. Jin, H. Deng, W. Li, *ACS Nano* **2010**, *4*, 6515.
[505] K. Zhang, H. Wang, X. He, Z. Liu, L. Wang, L. Gu, H. Xu, P. Han, S. Dong, C. Zhang, J. Yao, G. Cui, L. Chen, *J. Mater. Chem.* **2011**, *21*, 11916.

[506] A. Lu, X. Zhang, Y. Chen, Q. Xie, Q. Qi, Y. Ma, D.-L. Peng, *J. Power Sources* **2015**, *295*, 329.
[507] J. Yang, Y. Zhang, C. Sun, H. Liu, L. Li, W. Si, W. Huang, Q. Yan, X. Dong, *Nano Res.* **2016**, *9*, 612.
[508] Y. Lu, X. Wang, Y. Mai, J. Xiang, H. Zhang, L. Li, C. Gu, J. Tu, S. X. Mao, *J. Phys. Chem. C* **2012**, *116*, 22217.
[509] Y. Feng, H. Zhang, Y. Mu, W. Li, J. Sun, K. Wu, Y. Wang, *Chem. - Eur. J.* **2015**, *21*, 9229.
[510] J. K. Lee, K. B. Smith, C. M. Hayner, H. H. Kung, *Chem. Commun.* **2010**, *46*, 2025.
[511] K. Evanoff, A. Magasinski, J. Yang, G. Yushin, *Adv. Energy Mater.* **2011**, *1*, 495.
[512] L. Ji, H. Zheng, A. Ismach, Z. Tan, S. Xun, E. Lin, V. Battaglia, V. Srinivasan, Y. Zhang, *Nano Energy* **2012**, *1*, 164.
[513] H. W. Yue, S. Y. Wang, Z. B. Yang, Q. Li, S. M. Lin, D. Y. He, *Electrochim. Acta* **2015**, *174*, 688.
[514] S. Jing, H. Jiang, Y. Hu, J. Shen, C. Li, *Adv. Funct. Mater.* **2015**, *25*, 5395.
[515] B. Wang, X. Li, X. Zhang, B. Luo, Y. Zhang, L. Zhi, *Adv. Mater.* **2013**, *25*, 3560.
[516] G. Radhakrishnan, P. M. Adams, B. Foran, M. V. Quinzio, M. J. Brodie, *APL Mater.* **2013**, *1*, 062103.
[517] D.-J. Xue, S. Xin, Y. Yan, K.-C. Jiang, Y.-X. Yin, Y.-G. Guo, L.-J. Wan, *J. Am. Chem. Soc.* **2012**, *134*, 2512.
[518] D. Li, K. H. Seng, D. Q. Shi, Z. X. Chen, H. K. Liu, Z. P. Guo, *J. Mater. Chem. A* **2013**, *1*, 14115.
[519] L. Ji, Z. Tan, T. Kuykendall, E. J. An, Y. Fu, V. Battaglia, Y. Zhang, *Energy Environ. Sci.* **2011**, *4*, 3611.
[520] G. Wang, B. Wang, X. Wang, J. Park, S. Dou, H. Ahn, K. Kim, *J. Mater. Chem.* **2009**, *19*, 8378.
[521] W. W. Sun, Y. Wang, *Nanoscale* **2014**, *6*, 11528.
[522] Y. Zhao, X. F. Li, B. Yan, D. J. Li, S. Lawes, X. L. Sun, *J. Power Sources* **2015**, *274*, 869.
[523] S. Chen, P. Chen, M. Wu, D. Pan, Y. Wang, *Electrochem. Commun.* **2010**, *12*, 1302.
[524] A. Birrozzi, F. Maroni, R. Raccichini, R. Tossici, R. Marassi, F. Nobili, *J. Power Sources* **2015**, *294*, 248.
[525] Z. Yu, J. Song, M. L. Gordin, R. Yi, D. Tang, D. Wang, *Adv. Sci.* **2015**, *2*, 1400020.
[526] J. Zhu, K. Sun, D. Sim, C. Xu, H. Zhang, H. H. Hng, Q. Yan, *Chem. Commun.* **2011**, *47*, 10383.
[527] Q. Guo, Z. Zheng, H. Gao, J. Ma, X. Qin, *J. Power Sources* **2013**, *240*, 149.
[528] L. Li, A. Kovalchuk, J. Tour, *Nano Res.* **2014**, *7*, 1319.
[529] L. Lai, J. Zhu, Z. Li, D. Y. W. Yu, S. Jiang, X. Cai, Q. Yan, Y. M. Lam, Z. Shen, J. Lin, *Nano Energy* **2014**, *3*, 134.
[530] L. Pan, H. Zhao, W. Shen, X. Dong, J. Xu, *J. Mater. Chem. A* **2013**, *1*, 7159.
[531] J. Luo, J. Liu, Z. Zeng, C. F. Ng, L. Ma, H. Zhang, J. Lin, Z. Shen, H. J. Fan, *Nano Lett.* **2013**, *13*, 6136.
[532] B. Jin, G. Chen, X. Zhong, Y. Liu, K. Zhou, P. Sun, P. Lu, W. Zhang, J. Liang, *Ceram. Int.* **2014**, *40*, 10359.
[533] H. Zhang, L. Zhou, C. Yu, *RSC Adv.* **2014**, *4*, 495.
[534] J. Kan, Y. Wang, *Sci. Rep.* **2013**, *3*, 3502.
[535] S.-K. Park, A. Jin, S.-H. Yu, J. Ha, B. Jang, S. Bong, S. Woo, Y.-E. Sung, Y. Piao, *Electrochim. Acta* **2014**, *120*, 452.
[536] Y. Sun, X. Hu, W. Luo, F. Xia, Y. Huang, *Adv. Funct. Mater.* **2013**, *23*, 2436.
[537] T. Wu, F. Tu, S. Liu, S. Zhuang, G. Jin, C. Pan, *J. Mater. Sci.* **2014**, *49*, 1861.
[538] Y. J. Mai, S. J. Shi, D. Zhang, Y. Lu, C. D. Gu, J. P. Tu, *J. Power Sources* **2012**, *204*, 155.
[539] S. H. Choi, Y. N. Ko, J.-K. Lee, Y. C. Kang, *Sci. Rep.* **2014**, *4*, 5786.
[540] L. Ji, Z. Tan, T. R. Kuykendall, S. Aloni, S. Xun, E. Lin, V. Battaglia, Y. Zhang, *Phys. Chem. Chem. Phys.* **2011**, *13*, 7170.
[541] F. Zhang, T. Zhang, X. Yang, L. Zhang, K. Leng, Y. Huang, Y. Chen, *Energy Environ. Sci.* **2013**, *6*, 1623.
[542] X. Wang, X. Cao, L. Bourgeois, H. Guan, S. Chen, Y. Zhong, D.-M. Tang, H. Li, T. Zhai, L. Li, Y. Bando, D. Golberg, *Adv. Funct. Mater.* **2012**, *22*, 2682.
[543] M. Du, C. Xu, J. Sun, L. Gao, *Electrochim. Acta* **2012**, *80*, 302.
[544] K. Zhang, P. Han, L. Gu, L. Zhang, Z. Liu, Q. Kong, C. Zhang, S. Dong, Z. Zhang, J. Yao, H. Xu, G. Cui, L. Chen, *ACS Appl. Mater. Interfaces* **2012**, *4*, 658.
[545] X. Zhou, L.-J. Wan, Y.-G. Guo, *Adv. Mater.* **2013**, *25*, 2152.
[546] G. Zhou, D.-W. Wang, L.-C. Yin, N. Li, F. Li, H.-M. Cheng, *ACS Nano* **2012**, *6*, 3214.
[547] T. Hu, X. Sun, H. Sun, G. Xin, D. Shao, C. Liu, J. Lian, *Phys. Chem. Chem. Phys.* **2014**, *16*, 1060.
[548] Y. Liu, X. Wang, Y. Dong, Z. Wang, Z. Zhao, J. Qiu, *J. Mater. Chem. A* **2014**, *2*, 16832.
[549] N. Nitta, F. Wu, J. T. Lee, G. Yushin, *Mater. Today* **2015**, *18*, 252.
[550] X. Xu, W. Liu, Y. Kim, J. Cho, *Nano Today* **2014**, *9*, 604.
[551] C. Wu, J. Maier, Y. Yu, *Adv. Mater.* **2016**, *28*, 174.
[552] H. Wang, H. Feng, J. Li, *Small* **2014**, *10*, 2165.
[553] N. A. Kumar, M. A. Dar, R. Gul, J.-B. Baek, *Mater. Today* **2015**, *18*, 286.
[554] B. Luo, Y. Fang, B. Wang, J. Zhou, H. Song, L. Zhi, *Energy Environ. Sci.* **2012**, *5*, 5226.
[555] S. Liu, X. Lu, J. Xie, G. Cao, T. Zhu, X. Zhao, *ACS Appl. Mater. Interfaces* **2013**, *5*, 1588.
[556] K. Chang, W. Chen, *J. Mater. Chem.* **2011**, *21*, 17175.
[557] N. Mahmood, C. Zhang, Y. Hou, *Small* **2013**, *9*, 1321.
[558] X. Zhao, C. M. Hayner, M. C. Kung, H. H. Kung, *Adv. Energy Mater.* **2011**, *1*, 1079.
[559] J. Luo, X. Zhao, J. Wu, H. D. Jang, H. H. Kung, J. Huang, *J. Phys. Chem. Lett.* **2012**, *3*, 1824.
[560] R. Hu, W. Sun, Y. Chen, M. Zeng, M. Zhu, *J. Mater. Chem. A* **2014**, *2*, 9118.
[561] I. H. Son, J. Hwan Park, S. Kwon, S. Park, M. H. Rummeli, A. Bachmatiuk, H. J. Song, J. Ku, J. W. Choi, J.-M. Choi, S.-G. Doo, H. Chang, *Nat. Commun.* **2015**, *6*, 8393.
[562] S. Chen, P. Bao, X. Huang, B. Sun, G. Wang, *Nano Res.* **2014**, *7*, 85.
[563] M. Ko, S. Chae, S. Jeong, P. Oh, J. Cho, *ACS Nano* **2014**, *8*, 8591.
[564] C. Wang, Y. Li, Y.-S. Chui, Q.-H. Wu, X. Chen, W. Zhang, *Nanoscale* **2013**, *5*, 10599.
[565] J. Qin, C. He, N. Zhao, Z. Wang, C. Shi, E.-Z. Liu, J. Li, *ACS Nano* **2014**, *8*, 1728.
[566] C. Wu, J. Maier, Y. Yu, *Adv. Funct. Mater.* **2015**, *25*, 3488.
[567] X. Zheng, W. Lv, Y.-B. He, C. Zhang, W. Wei, Y. Tao, B. Li, Q.-H. Yang, *J. Nanomater.* **2014**, DOI: 10.1155/2014/974285.
[568] B. Luo, T. Qiu, D. Ye, L. Wang, L. Zhi, *Nano Energy* **2016**, *22*, 232.
[569] A. M. Tripathi, S. Mitra, *ChemElectroChem* **2014**, *1*, 1327.
[570] D. Li, K. H. Seng, D. Shi, Z. Chen, H. K. Liu, Z. Guo, *J. Mater. Chem. A* **2013**, *1*, 14115.
[571] F.-W. Yuan, H.-Y. Tuan, *Chem. Mater.* **2014**, *26*, 2172.
[572] S. Jin, N. Li, H. Cui, C. Wang, *ACS Appl. Mater. Interfaces* **2014**, *6*, 19397.
[573] Y. Zhang, J. Xie, T. Zhu, G. Cao, X. Zhao, S. Zhang, *J. Power Sources* **2014**, *247*, 204.
[574] W. Zhang, X. Hu, Y. Huang, *Meet. Abstr.* **2015**, *MA2015-01*, 620.
[575] S. Fang, L. Shen, H. Zheng, X. Zhang, *J. Mater. Chem. A* **2015**, *3*, 1498.
[576] N. Nitta, F. X. Wu, J. T. Lee, G. Yushin, *Mater. Today* **2015**, *18*, 252.
[577] L. Li, K. S. Lee, L. Lu, *Funct. Mater. Lett.* **2014**, *7*, 1430002.
[578] H. T. Tan, X. H. Rui, W. P. Sun, Q. Y. Yan, T. M. Lim, *Nanoscale* **2015**, *7*, 14595.

[579] S. T. Myung, K. Amine, Y. K. Sun, *J. Power Sources* **2015**, *283*, 219.
[580] J. H. Kim, N. P. W. Pieczonka, L. Yang, *ChemPhysChem* **2014**, *15*, 1940.
[581] S. B. Chikkannanavar, D. M. Bernardi, L. Y. Liu, *J. Power Sources* **2014**, *248*, 91.
[582] G. Kucinskis, G. Bajars, J. Kleperis, *J. Power Sources* **2013**, *240*, 66.
[583] L. Chen, M. Zhang, W. Wei, *J. Nanomater.* **2013**, DOI: 10.1155/2013/940389.
[584] F. Fathollahi, M. Javanbakht, H. Omidvar, M. Ghaemi, *J. Alloys Compd.* **2015**, *627*, 146.
[585] H. X. Wu, Q. J. Liu, S. W. Guo, *Nano-Micro Lett.* **2014**, *6*, 316.
[586] X. L. Ma, G. X. Chen, Q. Liu, G. P. Zeng, T. Wu, *J. Nanomater.* **2015**, DOI: 10.1155/2015/301731.
[587] Y. Ding, Y. Jiang, F. Xu, J. Yin, H. Ren, Q. Zhuo, Z. Long, P. Zhang, *Electrochem. Commun.* **2010**, *12*, 10.
[588] X. Zhou, F. Wang, Y. Zhu, Z. Liu, *J. Mater. Chem.* **2011**, *21*, 3353.
[589] S.-M. Bak, K.-W. Nam, C.-W. Lee, K.-H. Kim, H.-C. Jung, X.-Q. Yang, K.-B. Kim, *J. Mater. Chem.* **2011**, *21*, 17309.
[590] M. H. Pyun, Y. J. Park, *J. Alloys Compd.* **2015**, *643*, S90.
[591] Q. S. Ge, D. F. Wang, F. L. Li, D. Chen, G. X. Ping, M. Q. Fan, L. S. Qin, L. Q. Bai, G. L. Tian, C. J. Lv, K. Y. Shu, *Russ. J. Electrochem.* **2015**, *51*, 125.
[592] L. Jaber-Ansari, K. P. Puntambekar, S. Kim, M. Aykol, L. Luo, J. Wu, B. D. Myers, H. Iddir, J. T. Russell, S. J. Saldaña, R. Kumar, M. M. Thackeray, L. A. Curtiss, V. P. Dravid, C. Wolverton, M. C. Hersam, *Adv. Energy Mater.* **2015**, *5*, 1500646.
[593] K. Wang, Y. Wang, C. Wang, Y. Xia, *Electrochim. Acta* **2014**, *146*, 8.
[594] J. Zong, X. Liu, *Electrochim. Acta* **2014**, *116*, 9.
[595] R. Cheruku, S. B. D, G. Govindaraj, L. Vijayan, *AIP Conf. Proc.* **2015**, *1665*, 050136.
[596] X. Rui, D. Sim, K. Wong, J. Zhu, W. Liu, C. Xu, H. Tan, N. Xiao, H. H. Hng, T. M. Lim, Q. Yan, *J. Power Sources* **2012**, *214*, 171.
[597] L. M. Zhu, J. Yang, X. Y. Cao, *Int. J. Electrochem. Sci.* **2015**, *10*, 6509.
[598] K. Cui, Y. Li, *RSC Adv.* **2016**, *6*, 8431.
[599] H.-K. Roh, H.-K. Kim, K. C. Roh, K.-B. Kim, *RSC Adv.* **2014**, *4*, 31672.
[600] L.-L. Zhang, S. Duan, X.-L. Yang, G. Peng, G. Liang, Y.-H. Huang, Y. Jiang, S.-B. Ni, M. Li, *ACS Appl. Mater. Interfaces* **2013**, *5*, 12304.
[601] J. Yang, L. Hu, J. Zheng, D. He, L. Tian, S. Mu, F. Pan, *J. Mater. Chem. A* **2015**, *3*, 9601.
[602] H. Zhu, X. Wu, L. Zan, Y. Zhang, *ACS Appl. Mater. Interfaces* **2014**, *6*, 11724.
[603] J. Yang, X. Kang, D. He, A. Zheng, M. Pan, S. Mu, *J. Mater. Chem. A* **2015**, *3*, 16567.
[604] H. Zhu, H. He, X. Xin, X. Ma, L. Zan, Y. Zhang, *Electrochim. Acta* **2015**, *155*, 116.
[605] H. Gong, Y. Zhu, L. Wang, D. Wei, J. Liang, Y. Qian, *J. Power Sources* **2014**, *246*, 192.
[606] Y. Zhao, C. Wu, J. Li, L. Guan, *J. Mater. Chem. A* **2013**, *1*, 3856.
[607] H. Gwon, H.-S. Kim, K. U. Lee, D.-H. Seo, Y. C. Park, Y.-S. Lee, B. T. Ahn, K. Kang, *Energy Environ. Sci.* **2011**, *4*, 1277.
[608] H. Liu, W. Yang, *Energy Environ. Sci.* **2011**, *4*, 4000.
[609] Y. Yin, Y. Hu, P. Wu, H. Zhang, C. Cai, *Chem. Commun.* **2012**, *48*, 2137.
[610] Q. Fan, L. X. Lei, X. Y. Xu, G. Yin, Y. M. Sun, *J. Power Sources* **2014**, *257*, 65.
[611] X. Zhao, C. M. Hayner, M. C. Kung, H. H. Kung, *Chem. Commun.* **2012**, *48*, 9909.
[612] J. Liu, Y. Wan, W. Liu, Z. Ma, S. Ji, J. Wang, Y. Zhou, P. Hodgson, Y. Li, *J. Mater. Chem. A* **2013**, *1*, 1969.
[613] R. G. Ma, Z. G. Lu, C. D. Wang, H. E. Wang, S. L. Yang, L. J. Xi, J. C. Y. Chung, *Nanoscale* **2013**, *5*, 6338.
[614] C. Venkateswara Rao, A. Leela Mohana Reddy, Y. Ishikawa, P. M. Ajayan, *ACS Appl. Mater. Interfaces* **2011**, *3*, 2966.
[615] R. Ma, Z. Lu, C. Wang, H.-E. Wang, S. Yang, L. Xi, J. C. Y. Chung, *Nanoscale* **2013**, *5*, 6338.
[616] W. Guo, Y.-X. Yin, S. Xin, Y.-G. Guo, L.-J. Wan, *Energy Environ. Sci.* **2012**, *5*, 5221.
[617] M. Q. Sun, H. Li, J. Wang, G. C. Wang, *Carbon* **2015**, *94*, 864.
[618] Y. Ma, H. Chang, M. Zhang, Y. Chen, *Adv. Mater.* **2015**, *27*, 5296.
[619] H. Kim, K.-Y. Park, J. Hong, K. Kang, *Sci. Rep.* **2014**, *4*, 5278.
[620] T. Zhou, Y. Zheng, H. Gao, S. Min, S. Li, H. K. Liu, Z. Guo, *Adv. Sci.* **2015**, *2*, 1500027.
[621] K. Zhao, F. Liu, C. Niu, W. Xu, Y. Dong, L. Zhang, S. Xie, M. Yan, Q. Wei, D. Zhao, L. Mai, *Adv. Sci.* **2015**, *2*, 1500154.
[622] B. Z. Jang, C. Liu, D. Neff, Z. Yu, M. C. Wang, W. Xiong, A. Zhamu, *Nano Lett.* **2011**, *11*, 3785.
[623] N. Li, Z. Chen, W. Ren, F. Li, H.-M. Cheng, *Proc. Natl. Acad. Sci.* **2012**, *109*, 17360.
[624] P. G. Bruce, S. A. Freunberger, L. J. Hardwick, J.-M. Tarascon, *Nat. Mater.* **2012**, *11*, 19.
[625] X. Ji, K. T. Lee, L. F. Nazar, *Nat. Mater.* **2009**, *8*, 500.
[626] X. Li, Y. Cao, W. Qi, L. V. Saraf, J. Xiao, Z. Nie, J. Mietek, J.-G. Zhang, B. Schwenzer, J. Liu, *J. Mater. Chem.* **2011**, *21*, 16603.
[627] L. Ji, M. Rao, S. Aloni, L. Wang, E. J. Cairns, Y. Zhang, *Energy Environ. Sci.* **2011**, *4*, 5053.
[628] L. Xiao, Y. Cao, J. Xiao, B. Schwenzer, M. H. Engelhard, L. V. Saraf, Z. Nie, G. J. Exarhos, J. Liu, *Adv. Mater.* **2012**, *24*, 1176.
[629] A. Manthiram, Y. Fu, Y.-S. Su, *Acc. Chem. Res.* **2012**, *46*, 1125.
[630] S. Evers, L. F. Nazar, *Acc. Chem. Res.* **2012**, *46*, 1135.
[631] A. Rosenman, E. Markevich, G. Salitra, D. Aurbach, A. Garsuch, F. F. Chesneau, *Adv. Energy Mater.* **2015**, *5*, 1500212.
[632] A. Manthiram, Y. Z. Fu, Y. S. Su, *Acc. Chem. Res.* **2013**, *46*, 1125.
[633] A. Manthiram, S. H. Chung, C. X. Zu, *Adv. Mater.* **2015**, *27*, 1980.
[634] X. Fang, H. S. Peng, *Small* **2015**, *11*, 1488.
[635] L. Chen, L. L. Shaw, *J. Power Sources* **2014**, *267*, 770.
[636] S. S. Zhang, *J. Power Sources* **2013**, *231*, 153.
[637] M. Wild, L. O'Neill, T. Zhang, R. Purkayastha, G. Minton, M. Marinescu, G. J. Offer, *Energy Environ. Sci.* **2015**, *8*, 3477.
[638] L. Ma, K. E. Hendrickson, S. Y. Wei, L. A. Archer, *Nano Today* **2015**, *10*, 315.
[639] Z. Lin, C. D. Liang, *J. Mater. Chem. A* **2015**, *3*, 936.
[640] R. J. Chen, T. Zhao, F. Wu, *Chem. Commun.* **2015**, *51*, 18.
[641] M. Hagen, D. Hanselmann, K. Ahlbrecht, R. Maca, D. Gerber, J. Tubke, *Adv. Energy Mater.* **2015**, *5*, 1401986.
[642] S. Zhang, K. Ueno, K. Dokko, M. Watanabe, *Adv. Energy Mater.* **2015**, *5*, 1500117.
[643] Y. Son, J. S. Lee, Y. Son, J. H. Jang, J. Cho, *Adv. Energy Mater.* **2015**, *5*, 1500110.
[644] J. W. Wang, C. C. Lv, Y. L. Zhang, L. Deng, Z. Q. Peng, *Electrochim. Acta* **2015**, *165*, 136.
[645] X. H. Zhao, D. S. Kim, H. J. Ahn, K. W. Kim, K. K. Cho, J. H. Ahn, *Mater. Res. Bull.* **2014**, *58*, 204.
[646] B. Ding, C. Z. Yuan, L. F. Shen, G. Y. Xu, P. Nie, X. G. Zhang, *Chem.- Eur. J.* **2013**, *19*, 1013.
[647] G. C. Li, H. K. Jing, H. H. Li, L. Liu, Y. P. Wang, C. C. Yuan, H. B. Jiang, L. Chen, *Ionics* **2015**, *21*, 2161.
[648] B. Ding, Z. Chang, G. Y. Xu, P. Nie, J. Wang, J. Pan, H. Dou, X. G. Zhang, *ACS Appl. Mater. Interfaces* **2015**, *7*, 11165.
[649] X. Zhao, H. J. Ahn, K. W. Kim, K. K. Cho, J. H. Ahn, *J. Phys. Chem. C* **2015**, *119*, 7996.

[650] L. Ji, M. Rao, H. Zheng, L. Zhang, Y. Li, W. Duan, J. Guo, E. J. Cairns, Y. Zhang, *J. Am. Chem. Soc.* **2011**, *133*, 18522.
[651] X.-G. Sun, X. Wang, R. T. Mayes, S. Dai, *ChemSusChem* **2012**, *5*, 2079.
[652] J. H. Shin, E. J. Cairns, *J. Power Sources* **2008**, *177*, 537.
[653] C. Liao, B. K. Guo, X. G. Sun, S. Dai, *ChemSusChem* **2015**, *8*, 353.
[654] M. Barghamadi, A. S. Best, A. I. Bhatt, A. F. Hollenkamp, P. J. Mahon, M. Musameh, T. Ruther, *J. Power Sources* **2015**, *295*, 212.
[655] N. Azimi, Z. Xue, L. B. Hua, C. Takoudis, S. S. Zhang, Z. C. Zhang, *Electrochim. Acta* **2015**, *154*, 205.
[656] F. X. Wu, J. T. Lee, N. Nitta, H. Kim, O. Borodin, G. Yushin, *Adv. Mater.* **2015**, *27*, 101.
[657] M. K. Song, Y. G. Zhang, E. J. Cairns, *AIChE J.* **2015**, *61*, 2749.
[658] Y. Chen, S. T. Lu, X. H. Wu, J. Liu, *J. Phys. Chem. C* **2015**, *119*, 10288.
[659] B. Li, S. M. Li, J. H. Liu, J. J. Xu, *RSC Adv.* **2015**, *5*, 40310.
[660] H. Sohn, M. L. Gordin, T. Xu, S. R. Chen, D. Lv, J. X. Song, A. Manivannan, D. H. Wang, *ACS Appl. Mater. Interfaces* **2014**, *6*, 7596.
[661] Y. Zhao, Y. Zhang, Z. Bakenova, Z. Bakenov, *Front. Energy Res.* **2015**, *3*, 2.
[662] Z. Li, Y. M. Huang, L. X. Yuan, Z. X. Hao, Y. H. Huang, *Carbon* **2015**, *92*, 41.
[663] X. Gu, S. Zhang, Y. Hou, *Chin. J. Chem.* **2016**, *34*, 13.
[664] Y. Cao, X. Li, I. A. Aksay, J. Lemmon, Z. Nie, Z. Yang, J. Liu, *Phys. Chem. Chem. Phys.* **2011**, *13*, 7660.
[665] H. Wang, Y. Yang, Y. Liang, J. T. Robinson, Y. Li, A. Jackson, Y. Cui, H. Dai, *Nano Lett.* **2011**, *11*, 2644.
[666] F.-f. Zhang, X.-b. Zhang, Y.-h. Dong, L.-m. Wang, *J. Mater. Chem.* **2012**, *22*, 11452.
[667] N. Li, M. Zheng, H. Lu, Z. Hu, C. Shen, X. Chang, G. Ji, J. Cao, Y. Shi, *Chem. Commun.* **2012**, *48*, 4106.
[668] L. Yin, J. Wang, F. Lin, J. Yang, Y. Nuli, *Energy Environ. Sci.* **2012**, *5*, 6966.
[669] Z.-K. Wei, J.-J. Chen, L.-L. Qin, A.-W. Nemage, M.-S. Zheng, Q.-F. Dong, *J. Electrochem. Soc.* **2012**, *159*, A1236.
[670] L. Yin, J. Wang, X. Yu, C. W. Monroe, Y. NuLi, J. Yang, *Chem. Commun.* **2012**, *48*, 7868.
[671] H. Sun, G.-L. Xu, Y.-F. Xu, S.-G. Sun, X. Zhang, Y. Qiu, S. Yang, *Nano Res.* **2012**, *5*, 726.
[672] J. X. Zhu, D. Yang, Z. Y. Yin, Q. Y. Yan, H. Zhang, *Small* **2014**, *10*, 3480.
[673] H. Kim, H. D. Lim, J. Kim, K. Kang, *J. Mater. Chem. A* **2014**, *2*, 33.
[674] Y. Zhao, Z. Bakenova, Y. G. Zhang, H. F. Peng, H. X. Xie, Z. Bakenov, *Ionics* **2015**, *21*, 1925.
[675] G. Babu, L. M. R. Arava, *RSC Adv.* **2015**, *5*, 47621.
[676] H. Kim, H.-D. Lim, J. Kim, K. Kang, *J. Mater. Chem. A* **2014**, *2*, 33.
[677] M. Yu, R. Li, M. Wu, G. Shi, *Energy Storage Mater.* **2015**, *1*, 51.
[678] S. Wu, R. Ge, M. Lu, R. Xu, Z. Zhang, *Nano Energy* **2015**, *15*, 379.
[679] Y. L. Cao, X. L. Li, I. A. Aksay, J. Lemmon, Z. M. Nie, Z. G. Yang, J. Liu, *Phys. Chem. Chem. Phys.* **2011**, *13*, 7660.
[680] M.-S. Park, J.-S. Yu, K. J. Kim, G. Jeong, J.-H. Kim, Y.-N. Jo, U. Hwang, S. Kang, T. Woo, Y.-J. Kim, *Phys. Chem. Chem. Phys.* **2012**, *14*, 6796.
[681] L. Q. Lu, J. L. Lu, Y. Wang, *J. Mater. Chem. A* **2013**, *1*, 9173.
[682] T. Lin, Y. Tang, Y. Wang, H. Bi, Z. Liu, F. Huang, X. Xie, M. Jiang, *Energy Environ. Sci.* **2013**, *6*, 1283.
[683] G. Zhou, L.-C. Yin, D.-W. Wang, L. Li, S. Pei, I. R. Gentle, F. Li, H.-M. Cheng, *ACS Nano* **2013**, *7*, 5367.
[684] C. Zu, A. Manthiram, *Adv. Energy Mater.* **2013**, *3*, 1008.
[685] L. Fei, X. Li, W. Bi, Z. Zhuo, W. Wei, L. Sun, W. Lu, X. Wu, K. Xie, C. Wu, H. L. W. Chan, Y. Wang, *Adv. Mater.* **2015**, *27*, 5936.
[686] X. Yang, L. Zhang, F. Zhang, Y. Huang, Y. Chen, *ACS Nano* **2014**, *8*, 5208.
[687] Z. Wang, Y. Dong, H. Li, Z. Zhao, H. Bin Wu, C. Hao, S. Liu, J. Qiu, X. W. Lou, *Nat. Commun.* **2014**, *5*, 5002.
[688] H. Ting-Zheng, P. Hong-Jie, H. Jia-Qi, Z. Qiang, L. Bo, *2D Mater.* **2015**, *2*, 014011.
[689] X. Gu, C.-J. Tong, C. Lai, J. Qiu, X. Huang, W. Yang, B. Wen, L.-m. Liu, Y. Hou, S. Zhang, *J. Mater. Chem. A* **2015**, *3*, 16670.
[690] X. Yu, J. Zhao, R. Lv, Q. Liang, C. Zhan, Y. Bai, Z.-H. Huang, W. Shen, F. Kang, *J. Mater. Chem. A* **2015**, *3*, 18400.
[691] Y. Xie, Z. Meng, T. Cai, W.-Q. Han, *ACS Appl. Mater. Interfaces* **2015**, *7*, 25202.
[692] Y. Qiu, W. Li, W. Zhao, G. Li, Y. Hou, M. Liu, L. Zhou, F. Ye, H. Li, Z. Wei, S. Yang, W. Duan, Y. Ye, J. Guo, Y. Zhang, *Nano Lett.* **2014**, *14*, 4821.
[693] J. Song, Z. Yu, M. L. Gordin, D. Wang, *Nano Lett.* **2016**, *16*, 864.
[694] J.-Q. Huang, X.-F. Liu, Q. Zhang, C.-M. Chen, M.-Q. Zhao, S.-M. Zhang, W. Zhu, W.-Z. Qian, F. Wei, *Nano Energy* **2013**, *2*, 314.
[695] B. Ding, C. Yuan, L. Shen, G. Xu, P. Nie, Q. Lai, X. Zhang, *J. Mater. Chem. A* **2013**, *1*, 1096.
[696] H. Li, M. Q. Sun, T. Zhang, Y. Q. Fang, G. C. Wang, *J. Mater. Chem. A* **2014**, *2*, 18345.
[697] Y. You, W. C. Zeng, Y. X. Yin, J. Zhang, C. P. Yang, Y. W. Zhu, Y. G. Guo, *J. Mater. Chem. A* **2015**, *3*, 4799.
[698] H.-J. Peng, J. Liang, L. Zhu, J.-Q. Huang, X.-B. Cheng, X. Guo, W. Ding, W. Zhu, Q. Zhang, *ACS Nano* **2014**, *8*, 11280.
[699] C. Tang, B.-Q. Li, Q. Zhang, L. Zhu, H.-F. Wang, J.-L. Shi, F. Wei, *Adv. Funct. Mater.* **2016**, *26*, 577.
[700] J.-L. Shi, H.-J. Peng, L. Zhu, W. Zhu, Q. Zhang, *Carbon* **2015**, *92*, 96.
[701] J.-L. Shi, C. Tang, H.-J. Peng, L. Zhu, X.-B. Cheng, J.-Q. Huang, W. Zhu, Q. Zhang, *Small* **2015**, *11*, 5243.
[702] C. Zhao, C. Yu, M. Zhang, J. Yang, S. Liu, M. Li, X. Han, Y. Dong, J. Qiu, *J. Mater. Chem. A* **2015**, *3*, 21842.
[703] Z. Peng, W. Fang, H. Zhao, J. Fang, H. Cheng, T. N. L. Doan, J. Xu, P. Chen, *J. Power Sources* **2015**, *282*, 70.
[704] C. Wu, L. Fu, J. Maier, Y. Yu, *J. Mater. Chem. A* **2015**, *3*, 9438.
[705] L. Zhu, H.-J. Peng, J. Liang, J.-Q. Huang, C.-M. Chen, X. Guo, W. Zhu, P. Li, Q. Zhang, *Nano Energy* **2015**, *11*, 746.
[706] K. Jin, X. Zhou, Z. Liu, *Nanomaterials* **2015**, *5*, 1481.
[707] S. Liu, K. Xie, Z. Chen, Y. Li, X. Hong, J. Xu, L. Zhou, J. Yuan, C. Zheng, *J. Mater. Chem. A* **2015**, *3*, 11395.
[708] J. Shan, Y. Liu, Y. Su, P. Liu, X. Zhuang, D. Wu, F. Zhang, X. Feng, *J. Mater. Chem. A* **2016**, *4*, 314.
[709] Y. Dong, S. Liu, Z. Wang, Y. Liu, Z. Zhao, J. Qiu, *Nanoscale* **2015**, *7*, 7569.
[710] S. Niu, W. Lv, C. Zhang, F. Li, L. Tang, Y. He, B. Li, Q.-H. Yang, F. Kang, *J. Mater. Chem. A* **2015**, *3*, 20218.
[711] L. Zhang, L. Ji, P.-A. Glans, Y. Zhang, J. Zhu, J. Guo, *Phys. Chem. Chem. Phys.* **2012**, *14*, 13670.
[712] M. Liu, F. Ye, W. Li, H. Li, Y. Zhang, *Nano Res.* **2016**, *9*, 94.
[713] S. Yuan, J. L. Bao, L. Wang, Y. Xia, D. G. Truhlar, Y. Wang, *Adv. Energy Mater.* **2016**, *6*, 1501733.
[714] J. Song, M. L. Gordin, T. Xu, S. Chen, Z. Yu, H. Sohn, J. Lu, Y. Ren, Y. Duan, D. Wang, *Angew. Chem. Int. Ed.* **2015**, *54*, 4325.
[715] J. Song, T. Xu, M. L. Gordin, P. Zhu, D. Lv, Y.-B. Jiang, Y. Chen, Y. Duan, D. Wang, *Adv. Funct. Mater.* **2014**, *24*, 1243.
[716] S. S. Zhang, *Inorg. Chem. Front.* **2015**, *2*, 1059.
[717] C. Wang, K. Su, W. Wan, H. Guo, H. Zhou, J. Chen, X. Zhang, Y. Huang, *J. Mater. Chem. A* **2014**, *2*, 5018.
[718] G. Zhou, E. Paek, G. S. Hwang, A. Manthiram, *Nat. Commun.* **2015**, *6*, 7760.

[719] X. Liang, C. Hart, Q. Pang, A. Garsuch, T. Weiss, L. F. Nazar, *Nat. Commun.* **2015**, *6*, 6682.
[720] X. Liang, C. Y. Kwok, F. Lodi-Marzano, Q. Pang, M. Cuisinier, H. Huang, C. J. Hart, D. Houtarde, K. Kaup, H. Sommer, T. Brezesinski, J. Janek, L. F. Nazar, *Adv. Energy Mater.* **2016**, *6*, 1501636.
[721] J.-Q. Huang, X.-F. Liu, Q. Zhang, C.-M. Chen, M.-Q. Zhao, S.-M. Zhang, W. Zhu, W.-Z. Qian, F. Wei, *Nano Energy* **2013**, *2*, 314.
[722] Y. You, W. Zeng, Y.-X. Yin, J. Zhang, C.-P. Yang, Y. Zhu, Y.-G. Guo, *J. Mater. Chem. A* **2015**, *3*, 4799.
[723] M.-Q. Zhao, Q. Zhang, J.-Q. Huang, G.-L. Tian, J.-Q. Nie, H.-J. Peng, F. Wei, *Nat. Commun.* **2014**, *5*, 4410.
[724] G. Zhou, L. Li, C. Ma, S. Wang, Y. Shi, N. Koratkar, W. Ren, F. Li, H.-M. Cheng, *Nano Energy* **2015**, *11*, 356.
[725] H. Li, X. Yang, X. Wang, M. Liu, F. Ye, J. Wang, Y. Qiu, W. Li, Y. Zhang, *Nano Energy* **2015**, *12*, 468.
[726] Q. Zhang, S. Tan, X. Kong, Y. Xiao, L. Fu, *J. Materiomics* **2015**, *1*, 333.
[727] W. Qian, Q. Gao, K. Yang, W. Tian, Y. Tan, C. Yang, H. Zhang, Z. Li, L. Zhu, *Energy Technol.* **2016**, *4*, 625.
[728] S. Lu, Y. Chen, X. Wu, Z. Wang, Y. Li, *Sci. Rep.* **2014**, *4*, 4629.
[729] G. Zhou, Y. Zhao, A. Manthiram, *Adv. Energy Mater.* **2015**, *5*, 1402263.
[730] R. Chen, T. Zhao, J. Lu, F. Wu, L. Li, J. Chen, G. Tan, Y. Ye, K. Amine, *Nano Lett.* **2013**, *13*, 4642.
[731] H.-J. Peng, J.-Q. Huang, M.-Q. Zhao, Q. Zhang, X.-B. Cheng, X.-Y. Liu, W.-Z. Qian, F. Wei, *Adv. Funct. Mater.* **2014**, *24*, 2772.
[732] M. A. Pope, I. A. Aksay, *Adv. Energy Mater.* **2015**, *5*, 1500124.
[733] X. G. Li, M. M. Rao, H. B. Lin, D. R. Chen, Y. L. Liu, S. Z. Liu, Y. H. Liao, L. D. Xing, M. Q. Xu, W. S. Li, *J. Mater. Chem. A* **2015**, *3*, 18098.
[734] J. R. He, Y. F. Chen, P. J. Li, F. Fu, Z. G. Wang, W. L. Zhang, *J. Mater. Chem. A* **2015**, *3*, 18605.
[735] S. K. Liu, K. Xie, Y. J. Li, Z. X. Chen, X. B. Hong, L. J. Zhou, J. F. Yuan, C. M. Zheng, *RSC Adv.* **2015**, *5*, 5516.
[736] J. Ye, F. He, J. Nie, Y. L. Cao, H. X. Yang, X. P. Ai, *J. Mater. Chem. A* **2015**, *3*, 7406.
[737] M.-Q. Zhao, X.-F. Liu, Q. Zhang, G.-L. Tian, J.-Q. Huang, W. Zhu, F. Wei, *ACS Nano* **2012**, *6*, 10759.
[738] Y. Chen, S. Lu, X. Wu, J. Liu, *J. Phys. Chem. C* **2015**, *119*, 10288.
[739] S. Lu, Y. Cheng, X. Wu, J. Liu, *Nano Lett.* **2013**, *13*, 2485.
[740] H. Li, X. Yang, X. Wang, Y.-S. He, F. Ye, M. Liu, Y. Zhang, *Nanoscale* **2016**, *8*, 2395.
[741] S. Yuan, Z. Guo, L. Wang, S. Hu, Y. Wang, Y. Xia, *Adv. Sci.* **2015**, *2*, 1500071.
[742] C. Tang, Q. Zhang, M.-Q. Zhao, J.-Q. Huang, X.-B. Cheng, G.-L. Tian, H.-J. Peng, F. Wei, *Adv. Mater.* **2014**, *26*, 6100.
[743] X. Wang, Z. Zhang, Y. Qu, Y. Lai, J. Li, *J. Power Sources* **2014**, *256*, 361.
[744] M. Yu, R. Li, Y. Tong, Y. Li, C. Li, J.-D. Hong, G. Shi, *J. Mater. Chem. A* **2015**, *3*, 9609.
[745] M. Yu, A. Wang, F. Tian, H. Song, Y. Wang, C. Li, J.-D. Hong, G. Shi, *Nanoscale* **2015**, *7*, 5292.
[746] B. Li, S. Li, J. Liu, B. Wang, S. Yang, *Nano Lett.* **2015**, *15*, 3073.
[747] L. Zhang, H. Huang, H. Yin, Y. Xia, J. Luo, C. Liang, Y. Gan, X. Tao, W. Zhang, *J. Mater. Chem. A* **2015**, *3*, 16513.
[748] H. Wu, Y. Huang, M. Zong, H. Fu, X. Sun, *Electrochim. Acta* **2015**, *163*, 24.
[749] J.-Q. Huang, Q. Zhang, F. Wei, *Energy Storage Mater.* **2015**, *1*, 127.
[750] Z. Yunbo, M. Lixiao, N. Jing, X. Zhichang, H. Long, W. Bin, Z. Linjie, *2D Materials* **2015**, *2*, 024013.
[751] H.-J. Peng, D.-W. Wang, J.-Q. Huang, X.-B. Cheng, Z. Yuan, F. Wei, Q. Zhang, *Adv. Sci.* **2015**, *3*, 1500268.
[752] S. S. Zhang, J. A. Read, *J. Power Sources* **2012**, *200*, 77.
[753] X. Wang, Z. Wang, L. Chen, *J. Power Sources* **2013**, *242*, 65.
[754] J.-Q. Huang, T.-Z. Zhuang, Q. Zhang, H.-J. Peng, C.-M. Chen, F. Wei, *ACS Nano* **2015**, *9*, 3002.
[755] G. Zhou, S. Pei, L. Li, D.-W. Wang, S. Wang, K. Huang, L.-C. Yin, F. Li, H.-M. Cheng, *Adv. Mater.* **2014**, *26*, 625.
[756] G. Zhou, L. Li, D.-W. Wang, X.-y. Shan, S. Pei, F. Li, H.-M. Cheng, *Adv. Mater.* **2015**, *27*, 641.
[757] J. Zhu, C. Chen, Y. Lu, J. Zang, M. Jiang, D. Kim, X. Zhang, *Carbon* **2016**, *101*, 272.
[758] Z. Xiao, Z. Yang, L. Wang, H. Nie, M. e. Zhong, Q. Lai, X. Xu, L. Zhang, S. Huang, *Adv. Mater.* **2015**, *27*, 2891.
[759] H. Al Salem, G. Babu, C. V. Rao, L. M. R. Arava, *J. Am. Chem. Soc.* **2015**, *137*, 11542.
[760] X.-B. Cheng, H.-J. Peng, J.-Q. Huang, R. Zhang, C.-Z. Zhao, Q. Zhang, *ACS Nano* **2015**, *9*, 6373.
[761] P. Wei, M. Fan, H. Chen, D. Chen, C. Li, K. Shu, C. Lv, *Int. J. Hydrogen Energy* **2016**, *41*, 1819.
[762] C. Wan, W. Wu, C. Wu, J. Xu, L. Guan, *RSC Adv.* **2015**, *5*, 5102.
[763] X.-B. Cheng, R. Zhang, C.-Z. Zhao, F. Wei, J.-G. Zhang, Q. Zhang, *Adv. Sci.* **2015**, *3*, 1500213.
[764] W. Xu, J. Wang, F. Ding, X. Chen, E. Nasybulin, Y. Zhang, J.-G. Zhang, *Energy Environ. Sci.* **2014**, *7*, 513.
[765] J. Qian, W. A. Henderson, W. Xu, P. Bhattacharya, M. Engelhard, O. Borodin, J.-G. Zhang, *Nat. Commun.* **2015**, *6*, 7362.
[766] F. Ding, W. Xu, G. L. Graff, J. Zhang, M. L. Sushko, X. Chen, Y. Shao, M. H. Engelhard, Z. Nie, J. Xiao, X. Liu, P. V. Sushko, J. Liu, J.-G. Zhang, *J. Am. Chem. Soc.* **2013**, *135*, 4450.
[767] Y. Zhang, J. Qian, W. Xu, S. M. Russell, X. Chen, E. Nasybulin, P. Bhattacharya, M. H. Engelhard, D. Mei, R. Cao, F. Ding, A. V. Cresce, K. Xu, J.-G. Zhang, *Nano Lett.* **2014**, *14*, 6889.
[768] B. D. McCloskey, *J. Phys. Chem. Lett.* **2015**, *6*, 4581.
[769] A. C. Luntz, J. Voss, K. Reuter, *J. Phys. Chem. Lett.* **2015**, *6*, 4599.
[770] Y. Son, J.-S. Lee, Y. Son, J.-H. Jang, J. Cho, *Adv. Energy Mater.* **2015**, *5*, 1500110.
[771] R. Xu, J. Lu, K. Amine, *Adv. Energy Mater.* **2015**, *5*, 1500408.
[772] C. Wang, X. Wang, Y. Yang, A. Kushima, J. Chen, Y. Huang, J. Li, *Nano Lett.* **2015**, *15*, 1796.
[773] Y. Qiu, G. Rong, J. Yang, G. Li, S. Ma, X. Wang, Z. Pan, Y. Hou, M. Liu, F. Ye, W. Li, Z. W. Seh, X. Tao, H. Yao, N. Liu, R. Zhang, G. Zhou, J. Wang, S. Fan, Y. Cui, Y. Zhang, *Adv. Energy Mater.* **2015**, *5*, 1570128.
[774] K. Han, J. Shen, C. M. Hayner, H. Ye, M. C. Kung, H. H. Kung, *J. Power Sources* **2014**, *251*, 331.
[775] F. Wu, J. T. Lee, E. Zhao, B. Zhang, G. Yushin, *ACS Nano* **2016**, *10*, 1333.
[776] F. Wu, J. T. Lee, A. Magasinski, H. Kim, G. Yushin, *Part. Part. Syst. Charact.* **2014**, *31*, 639.
[777] H.-L. Wu, L. A. Huff, A. A. Gewirth, *ACS Appl. Mater. Interfaces* **2015**, *7*, 1709.
[778] N. A. Cañas, D. N. Fronczek, N. Wagner, A. Latz, K. A. Friedrich, *J. Phys. Chem. C* **2014**, *118*, 12106.
[779] L. Zielke, C. Barchasz, S. Waluś, F. Alloin, J. C. Leprêtre, A. Spettl, V. Schmidt, A. Hilger, I. Manke, J. Banhart, R. Zengerle, S. Thiele, *Sci. Rep.* **2015**, *5*, 10921.
[780] Y. Sun, G. Li, Y. Lai, D. Zeng, H. Cheng, *Sci. Rep.* **2016**, *6*, 22048.
[781] I. Villaluenga, K. H. Wujcik, W. Tong, D. Devaux, D. H. C. Wong, J. M. DeSimone, N. P. Balsara, *Proc. Natl. Acad. Sci.* **2016**, *113*, 52.
[782] S. S. Zhang, D. T. Tran, *Electrochim. Acta* **2013**, *114*, 296.

[783] M. Barghamadi, A. S. Best, A. I. Bhatt, A. F. Hollenkamp, M. Musameh, R. J. Rees, T. Ruther, *Energy Environ. Sci.* **2014**, *7*, 3902.
[784] Z. Lin, Z. Liu, W. Fu, N. J. Dudney, C. Liang, *Angew. Chem. Int. Ed.* **2013**, *52*, 7460.
[785] Y. Lu, Z. Tu, L. A. Archer, *Nat. Mater.* **2014**, *13*, 961.
[786] W. Xu, J. Xiao, D. Wang, J. Zhang, J.-G. Zhang, *J. Electrochem. Soc.* **2010**, *157*, A219.
[787] Y. Shao, S. Park, J. Xiao, J.-G. Zhang, Y. Wang, J. Liu, *ACS Catal.* **2012**, *2*, 844.
[788] Y. Shao, F. Ding, J. Xiao, J. Zhang, W. Xu, S. Park, J.-G. Zhang, Y. Wang, J. Liu, *Adv. Funct. Mater.* **2012**, *23*, 987.
[789] R. Padbury, X. Zhang, *J. Power Sources* **2011**, *196*, 4436.
[790] J. Christensen, P. Albertus, R. S. Sanchez-Carrera, T. Lohmann, B. Kozinsky, R. Liedtke, J. Ahmed, A. Kojic, *J. Electrochem. Soc.* **2012**, *159*, R1.
[791] M. Park, H. Sun, H. Lee, J. Lee, J. Cho, *Adv. Energy Mater.* **2012**, *2*, 780.
[792] G. Girishkumar, B. McCloskey, A. C. Luntz, S. Swanson, W. Wilcke, *J. Phys. Chem. Lett.* **2010**, *1*, 2193.
[793] Z. Ma, X. X. Yuan, L. Li, Z. F. Ma, D. P. Wilkinson, L. Zhang, J. J. Zhang, *Energy Environ. Sci.* **2015**, *8*, 2144.
[794] L. Grande, E. Paillard, J. Hassoun, J. B. Park, Y. J. Lee, Y. K. Sun, S. Passerini, B. Scrosati, *Adv. Mater.* **2015**, *27*, 784.
[795] L. Hui, W. Chuan, W. Feng, B. Ying, *Rare Met. Mater. Eng.* **2014**, *43*, 1525.
[796] B. D. McCloskey, C. M. Burke, J. E. Nichols, S. E. Renfrew, *Chem. Commun.* **2015**, *51*, 12701.
[797] Z. Y. Wen, C. Shen, Y. Lu, *ChemPlusChem* **2015**, *80*, 270.
[798] S. S. Zhang, D. Foster, J. Read, *J. Power Sources* **2010**, *195*, 1235.
[799] A. C. Luntz, B. D. McCloskey, *Chem. Rev.* **2014**, *114*, 11721.
[800] N. Feng, P. He, H. Zhou, *Adv. Energy Mater.* **2016**, *6*, 1502303.
[801] C. W. Sun, F. Li, C. Ma, Y. Wang, Y. L. Ren, W. Yang, Z. H. Ma, J. Q. Li, Y. J. Chen, Y. Kim, L. Q. Chen, *J. Mater. Chem. A* **2014**, *2*, 7188.
[802] D. F. Qiu, G. Bu, B. Zhao, Z. X. Lin, L. Pu, L. J. Pan, Y. Shi, *Mater. Lett.* **2015**, *141*, 43.
[803] Y. Li, J. Wang, X. Li, D. Geng, R. Li, X. Sun, *Chem. Commun.* **2011**, *47*, 9438.
[804] B. Sun, B. Wang, D. Su, L. Xiao, H. Ahn, G. Wang, *Carbon* **2012**, *50*, 727.
[805] Y. Wang, H. Zhou, *Energy Environ. Sci.* **2011**, *4*, 1704.
[806] E. Yoo, H. Zhou, *ACS Nano* **2011**, *5*, 3020.
[807] A. A. Franco, K.-H. Xue, *ECS J. Solid State Sci. Technol.* **2013**, *2*, M3084.
[808] J. Kang, O. L. Li, N. Saito, *J. Power Sources* **2014**, *261*, 156.
[809] J. Xiao, D. Mei, X. Li, W. Xu, D. Wang, G. L. Graff, W. D. Bennett, Z. Nie, L. V. Saraf, I. A. Aksay, J. Liu, J.-G. Zhang, *Nano Lett.* **2011**, *11*, 5071.
[810] Z.-L. Wang, D. Xu, J.-J. Xu, L.-L. Zhang, X.-B. Zhang, *Adv. Funct. Mater.* **2012**, *22*, 3699.
[811] T. Z. Haoran Jiang, Le Shi, P. Tan, L. An, *Journal of Physical Chemistry C* **2016**, *120*, 6612.
[812] E. Yoo, J. Nakamura, H. Zhou, *Energy Environ. Sci.* **2012**, *5*, 6928.
[813] Y. Li, J. Wang, X. Li, D. Geng, M. N. Banis, R. Li, X. Sun, *Electrochem. Commun.* **2012**, *18*, 12.
[814] C. Zhao, C. Yu, S. Liu, J. Yang, X. Fan, H. Huang, J. Qiu, *Adv. Funct. Mater.* **2015**, *25*, 6913.
[815] H. Huang, J. Zhu, W. Zhang, C. S. Tiwary, J. Zhang, X. Zhang, Q. Jiang, H. He, Y. Wu, W. Huang, P. M. Ajayan, Q. Yan, *Chem. Mater.* **2016**, *28*, 1737.
[816] Y. Yang, M. Shi, Q.-F. Zhou, Y.-S. Li, Z.-W. Fu, *Electrochem. Commun.* **2012**, *20*, 11.
[817] Y. S. Jeong, J. B. Park, H. G. Jung, J. Kirn, X. Y. Luo, J. Lu, L. Curtiss, K. Amine, Y. K. Sun, B. Scrosati, Y. J. Lee, *Nano Lett.* **2015**, *15*, 4261.
[818] X. Y. Zeng, C. H. You, L. M. Leng, D. Dang, X. C. Qiao, X. H. Li, Y. W. Li, S. J. Liao, R. R. Adzic, *J. Mater. Chem. A* **2015**, *3*, 11224.
[819] H.-G. Jung, Y. S. Jeong, J.-B. Park, Y.-K. Sun, B. Scrosati, Y. J. Lee, *ACS Nano* **2013**, *7*, 3532.
[820] E. Yilmaz, C. Yogi, K. Yamanaka, T. Ohta, H. R. Byon, *Nano Lett.* **2013**, *13*, 4679.
[821] L. Wang, X. Zhao, Y. Lu, M. Xu, D. Zhang, R. S. Ruoff, K. J. Stevenson, J. B. Goodenough, *J. Electrochem. Soc.* **2011**, *158*, A1379.
[822] H. Wang, Y. Yang, Y. Liang, G. Zheng, Y. Li, Y. Cui, H. Dai, *Energy Environ. Sci.* **2012**, *5*, 7931.
[823] R. S. Kalubarme, H. S. Jadhav, D. T. Ngo, G. E. Park, J. G. Fisher, Y. I. Choi, W. H. Ryu, C. J. Park, *Sci. Rep.* **2015**, *5*, 13266.
[824] Y. Yu, B. Zhang, Y.-B. He, Z.-D. Huang, S.-W. Oh, J.-K. Kim, *J. Mater. Chem. A* **2013**, *1*, 1163.
[825] Y. Yang, M. Shi, Y.-S. Li, Z.-W. Fu, *J. Electrochem. Soc.* **2012**, *159*, A1917.
[826] Y. Cao, Z. Wei, J. He, J. Zang, Q. Zhang, M. Zheng, Q. Dong, *Energy Environ. Sci.* **2012**, *5*, 9765.
[827] W. Zhang, Y. Zeng, C. Xu, H. Tan, W. Liu, J. Zhu, N. Xiao, H. H. Hng, H. Hoster, Y. Yazami, Q. Yan, *RSC Adv.* **2012**, *2*, 8508.
[828] W. Chen, Z. A. Zhang, W. Z. Bao, Y. Q. Lai, J. Li, Y. Q. Gan, J. J. Wang, *Electrochim. Acta* **2014**, *134*, 293.
[829] M. Wang, J. Huang, M. Wang, D. Zhang, W. Zhang, W. Li, J. Chen, *Electrochem. Commun.* **2013**, *34*, 299.
[830] Z. Zhang, Y. A. Chen, J. Bao, Z. J. Xie, J. P. Wei, Z. Zhou, *Part. Part. Syst. Charact.* **2015**, *32*, 680.
[831] J. Yin, J. M. Carlin, J. Kim, Z. Li, J. H. Park, B. Patel, S. Chakrapani, S. Lee, Y. L. Joo, *Adv. Energy Mater.* **2015**, *5*, 1401412.
[832] W.-B. Luo, S.-L. Chou, J.-Z. Wang, Y.-C. Zhai, H.-K. Liu, *Small* **2015**, *11*, 2817.
[833] C. Sun, F. Li, C. Ma, Y. Wang, Y. Ren, W. Yang, Z. Ma, J. Li, Y. Chen, Y. Kim, L. Chen, *J. Mater. Chem. A* **2014**, *2*, 7188.
[834] X. Guo, P. Liu, J. Han, Y. Ito, A. Hirata, T. Fujita, M. Chen, *Adv. Mater.* **2015**, *27*, 6137.
[835] K. P. C. Yao, Y. C. Lu, C. V. Amanchukwu, D. G. Kwabi, M. Risch, J. G. Zhou, A. Grimaud, P. T. Hammond, F. Barde, Y. Shao-Horn, *Phys. Chem. Chem. Phys.* **2014**, *16*, 2297.
[836] X. Guo, P. Liu, J. Han, Y. Ito, A. Hirata, T. Fujita, M. Chen, *Adv. Mater.* **2015**, *27*, 6137.
[837] H. Lv, R. Jiang, X. Zhang, J. Wang, Y. Li, *Int. J. Electrochem. Sci.* **2015**, *10*, 7622.
[838] B. Sun, X. Huang, S. Chen, P. Munroe, G. Wang, *Nano Lett.* **2014**, *14*, 3145.
[839] D. Y. Kim, M. Kim, D. W. Kim, J. Suk, O. O. Park, Y. Kang, *Carbon* **2015**, *93*, 625.
[840] M. Sevim, T. Şener, Ö. Metin, *Int. J. Hydrogen Energy* **2015**, *40*, 10876.
[841] J. G. Kim, Y. Kim, Y. Noh, W. B. Kim, *ChemSusChem* **2015**, *8*, 1752.
[842] Y. Chen, Q. Zhang, Z. Zhang, X. Zhou, Y. Zhong, M. Yang, Z. Xie, J. Wei, Z. Zhou, *J. Mater. Chem. A* **2015**, *3*, 17874.
[843] T. Liu, M. Leskes, W. Yu, A. J. Moore, L. Zhou, P. M. Bayley, G. Kim, C. P. Grey, *Science* **2015**, *350*, 530.
[844] J. Lu, Y. Jung Lee, X. Luo, K. Chun Lau, M. Asadi, H.-H. Wang, S. Brombosz, J. Wen, D. Zhai, Z. Chen, D. J. Miller, Y. Sub Jeong,

J.-B. Park, Z. Zak Fang, B. Kumar, A. Salehi-Khojin, Y.-K. Sun, L. A. Curtiss, K. Amine, *Nature* **2016**, *529*, 377.
[845] A. Manthiram, L. Li, *Adv. Energy Mater.* **2015**, *5*, 1401302.
[846] Y. Kato, S. Hori, T. Saito, K. Suzuki, M. Hirayama, A. Mitsui, M. Yonemura, H. Iba, R. Kanno, *Nat. Energy* **2016**, *1*, 16030.
[847] N. Yabuuchi, K. Kubota, M. Dahbi, S. Komaba, *Chem. Rev.* **2014**, *114*, 11636.
[848] M. D. Slater, D. Kim, E. Lee, C. S. Johnson, *Adv. Funct. Mater.* **2013**, *23*, 947.
[849] S.-W. Kim, D.-H. Seo, X. Ma, G. Ceder, K. Kang, *Adv. Energy Mater.* **2012**, *2*, 710.
[850] L. Ji, M. Gu, Y. Shao, X. Li, M. H. Engelhard, B. W. Arey, W. Wang, Z. Nie, J. Xiao, C. Wang, J.-G. Zhang, J. Liu, *Adv. Mater.* **2014**, *26*, 2901.
[851] H. L. Pan, Y. S. Hu, L. Q. Chen, *Energy Environ. Sci.* **2013**, *6*, 2338.
[852] L. P. Wang, L. H. Yu, X. Wang, M. Srinivasan, Z. C. J. Xu, *J. Mater. Chem. A* **2015**, *3*, 9353.
[853] Y. Liu, B. V. Merinov, W. A. Goddard, *Proc. Natl. Acad. Sci.* **2016**, *113*, 3735.
[854] N. Goubard-Bretesche, O. Crosnier, C. Payen, F. Favier, T. Brousse, *Electrochem. Commun.* **2015**, *57*, 61.
[855] R. Raccichini, A. Varzi, S. Passerini, B. Scrosati, *Nat. Mater.* **2015**, *14*, 271.
[856] A. Achour, R. L. Porto, M. A. Soussou, M. Islam, M. Boujtita, K. A. Aissa, L. Le Brizoual, A. Djouadi, T. Brousse, *J. Power Sources* **2015**, *300*, 525.
[857] V. Rebuttini, E. Fazio, S. Santangelo, F. Neri, G. Caputo, C. Martin, T. Brousse, F. Favier, N. Pinna, *Chem.- Eur. J.* **2015**, *21*, 12465.
[858] A. Ramos, I. Camean, N. Cuesta, A. B. Garcia, *Electrochim. Acta* **2015**, *178*, 392.
[859] P. E. Delannoy, B. Riou, T. Brousse, J. Le Bideau, D. Guyomard, B. Lestriez, *J. Power Sources* **2015**, *287*, 261.
[860] X. Y. Li, Y. M. Chen, L. M. Zhou, Y. W. Mai, H. T. Huang, *J. Mater. Chem. A* **2014**, *2*, 3875.
[861] J. D. Fang, S. Q. Wang, Z. T. Li, H. B. Chen, L. Xia, L. X. Ding, H. H. Wang, *J. Mater. Chem. A* **2016**, *4*, 1180.
[862] C. Wu, P. Kopold, Y. L. Ding, P. A. van Aken, J. Maier, Y. Yu, *ACS Nano* **2015**, *9*, 6610.
[863] H. S. Hou, C. E. Banks, M. J. Jing, Y. Zhang, X. B. Ji, *Adv. Mater.* **2015**, *27*, 7861.
[864] X. H. Rui, W. P. Sun, C. Wu, Y. Yu, Q. Y. Yan, *Adv. Mater.* **2015**, *27*, 6670.
[865] H. Y. Kang, Y. C. Liu, K. Z. Cao, Y. Zhao, L. F. Jiao, Y. J. Wang, H. T. Yuan, *J. Mater. Chem. A* **2015**, *3*, 17899.
[866] H. G. Wang, Z. Wu, F. L. Meng, D. L. Ma, X. L. Huang, L. M. Wang, X. B. Zhang, *ChemSusChem* **2013**, *6*, 56.
[867] Y. Yan, Y. X. Yin, S. Xin, J. Su, Y. G. Guo, L. J. Wan, *Electrochim. Acta* **2013**, *91*, 58.
[868] J. Sun, H.-W. Lee, M. Pasta, H. Yuan, G. Zheng, Y. Sun, Y. Li, Y. Cui, *Nat. Nano* **2015**, *10*, 980.
[869] J. Xiang, D. Dong, F. Wen, J. Zhao, X. Zhang, L. Wang, Z. Liu, *J. Alloys Compd.* **2016**, *660*, 11.
[870] H. A. Cha, H. M. Jeong, J. K. Kang, *J. Mater. Chem. A* **2014**, *2*, 5182.
[871] J. T. Xu, M. Wang, N. P. Wickramaratne, M. Jaroniec, S. X. Dou, L. M. Dai, *Adv. Mater.* **2015**, *27*, 2042.
[872] C. Ling, F. Mizuno, *Phys. Chem. Chem. Phys.* **2014**, *16*, 10419.
[873] H. Shen, D. Rao, X. Xi, Y. Liu, X. Shen, *RSC Adv.* **2015**, *5*, 17042.
[874] X. Q. Xie, D. W. Su, J. Q. Zhang, S. Q. Chen, A. K. Mondal, G. X. Wang, *Nanoscale* **2015**, *7*, 3164.
[875] X. Liu, Z. W. Li, H. L. Fei, M. D. Wei, *Dalton Trans.* **2015**, *44*, 18864.
[876] J. Zhang, Z. Zhang, X. X. Zhao, *RSC Adv.* **2015**, *5*, 104822.
[877] Q. Abbas, P. Ratajczak, P. Babuchowska, A. Le Comte, D. Belanger, T. Brousse, F. Beguin, *J. Electrochem. Soc.* **2015**, *162*, A5148.
[878] D. Kundu, E. Talaie, V. Duffort, L. F. Nazar, *Angew. Chem.-Int. Ed.* **2015**, *54*, 3431.
[879] S. P. Wu, R. Y. Ge, M. J. Lu, R. Xu, Z. Zhang, *Nano Energy* **2015**, *15*, 379.
[880] M. S. Balogun, Y. Luo, W. T. Qiu, P. Liu, Y. X. Tong, *Carbon* **2016**, *98*, 162.
[881] L. Wu, H. Y. Lu, L. F. Xiao, X. P. Ai, H. X. Yang, Y. L. Cao, *J. Power Sources* **2015**, *293*, 784.
[882] F. Zou, Y. M. Chen, K. W. Liu, Z. T. Yu, W. F. Liang, S. M. Bhaway, M. Gao, Y. Zhu, *Acs Nano* **2016**, *10*, 377.
[883] S. K. Das, B. Jache, H. Lahon, C. L. Bender, J. Janek, P. Adelhelm, *Chem. Commun.* **2016**, *52*, 1428.
[884] Y. Yan, Y.-X. Yin, Y.-G. Guo, L.-J. Wan, *Adv. Energy Mater.* **2014**, *4*, 1301584.
[885] M.-S. Balogun, Y. Luo, W. Qiu, P. Liu, Y. Tong, *Carbon* **2016**, *98*, 162.
[886] L. Hu, X. Zhu, Y. Du, Y. Li, X. Zhou, J. Bao, *Chem. Mater.* **2015**, *27*, 8138.
[887] D. Xie, D. H. Wang, W. J. Tang, X. H. Xia, Y. J. Zhang, X. L. Wang, C. D. Gu, J. P. Tu, *J. Power Sources* **2016**, *307*, 510.
[888] W. Deng, J. Qian, Y. Cao, X. Ai, H. Yang, *Small* **2016**, *12*, 583.
[889] S. Peng, X. Han, L. Li, Z. Zhu, F. Cheng, M. Srinivansan, S. Adams, S. Ramakrishna, *Small* **2016**, *12*, 1359.
[890] X. Fan, X. Chen, L. Dai, *Curr. Opin. Colloid Interface Sci.* **2015**, *20*, 429.
[891] H. Kang, Y. Liu, K. Cao, Y. Zhao, L. Jiao, Y. Wang, H. Yuan, *J. Mater. Chem. A* **2015**, *3*, 17899.
[892] S. Li, X. Cao, C. N. Schmidt, Q. Xu, E. Uchaker, Y. Pei, G. Cao, *J. Mater. Chem. A* **2016**, *4*, 4242.
[893] S. Qiu, X. Wu, L. Xiao, X. Ai, H. Yang, Y. Cao, *ACS Appl. Mater. Interfaces* **2016**, *8*, 1337.
[894] Y.-L. Ding, C. Wu, P. Kopold, P. A. van Aken, J. Maier, Y. Yu, *Small* **2015**, *11*, 6026.
[895] D. Larcher, J. M. Tarascon, *Nat. Chem.* **2015**, *7*, 19.
[896] T. S. Sahu, S. Mitra, *Sci. Rep.* **2015**, *5*, 12571.
[897] X. Q. Xie, S. Q. Chen, B. Sun, C. Y. Wang, G. X. Wang, *ChemSusChem* **2015**, *8*, 2948.
[898] Y. L. Ding, C. Wu, P. Kopold, P. A. van Aken, J. Maier, Y. Yu, *Small* **2015**, *11*, 6026.
[899] L. Y. Hu, X. S. Zhu, Y. C. Du, Y. F. Li, X. S. Zhou, J. C. Bao, *Chem. Mater.* **2015**, *27*, 8138.
[900] W. W. Xu, K. N. Zhao, L. Zhang, Z. Q. Xie, Z. Y. Cai, Y. Wang, *J. Alloys Compd.* **2016**, *654*, 357.
[901] X. L. Wang, G. Li, F. M. Hassan, J. D. Li, X. Y. Fan, R. Batmaz, X. C. Xiao, Z. W. Chen, *Nano Energy* **2015**, *15*, 746.
[902] X. J. Zhang, T. Q. Chen, D. Yan, W. Qin, B. W. Hu, Z. Sun, L. K. Pan, *Electrochim. Acta* **2015**, *180*, 616.
[903] W. Qin, T. Q. Chen, T. Lu, D. H. C. Chua, L. K. Pan, *J. Power Sources* **2016**, *302*, 202.
[904] T. T. Bao, H. Zhong, H. Y. Zheng, H. Zhan, Y. H. Zhou, *Mater. Lett.* **2015**, *158*, 21.
[905] W. Qin, T. Q. Chen, B. W. Hu, Z. Sun, L. K. Pan, *Electrochim. Acta* **2015**, *173*, 193.
[906] G. Pang, C. Z. Yuan, P. Nie, B. Ding, J. J. Zhu, X. G. Zhang, *Nanoscale* **2014**, *6*, 6328.
[907] J. M. Feng, L. Dong, Y. Han, X. F. Li, D. J. Li, *Int. J. Hydrogen Energy* **2016**, *41*, 355.
[908] Y. Fu, Q. Wei, X. Wang, G. Zhang, H. Shu, X. Yang, A. C. Tavares, S. Sun, *RSC Adv.* **2016**, *6*, 16624.
[909] Z. Jian, B. Zhao, P. Liu, F. Li, M. Zheng, M. Chen, Y. Shi, H. Zhou, *Chem. Commun.* **2014**, *50*, 1215.

[910] C. Wu, P. Kopold, Y.-L. Ding, P. A. van Aken, J. Maier, Y. Yu, *ACS Nano* **2015**, *9*, 6610.
[911] J. S. Cho, S. Y. Lee, Y. C. Kang, *Sci. Rep.* **2016**, *6*, 23338.
[912] Y. C. Lu, C. Ma, J. Alvarado, N. Dimov, Y. S. Meng, S. Okada, *J. Mater. Chem. A* **2015**, *3*, 16971.
[913] T. Wang, P. Hu, C. Zhang, H. Du, Z. Zhang, X. Wang, S. Chen, J. Xiong, G. Cui, *ACS Appl. Mater. Interfaces* **2016**, *8*, 7811.
[914] L. W. Ji, W. D. Zhou, V. Chabot, A. P. Yu, X. C. Xiao, *ACS Appl. Mater. Interfaces* **2015**, *7*, 24895.
[915] J. F. Huang, Z. W. Xu, L. Y. Cao, Q. L. Zhang, H. B. Ouyang, J. Y. Li, *Energy Technol.* **2015**, *3*, 1108.
[916] R. M. Sun, Q. L. Wei, Q. D. Li, W. Luo, Q. Y. An, J. Z. Sheng, D. Wang, W. Chen, L. Q. Mai, *ACS Appl. Mater. Interfaces* **2015**, *7*, 20902.
[917] Y. Yeo, J. W. Jung, K. Park, I. D. Kim, *Sci. Rep.* **2015**, *5*, 13862.
[918] C. Nithya, *ChemPlusChem* **2015**, *80*, 1000.
[919] X. S. Zhou, X. Liu, Y. Xu, Y. X. Liu, Z. H. Dai, J. C. Bao, *J. Phys. Chem. C* **2014**, *118*, 23527.
[920] D. W. Su, H. J. Ahn, G. X. Wang, *Chem. Commun.* **2013**, *49*, 3131.
[921] Y. Liu, Z. Cheng, H. Sun, H. Arandiyan, J. Li, M. Ahmad, *J. Power Sources* **2015**, *273*, 878.
[922] C. B. Zhu, P. Kopold, W. H. Li, P. A. van Aken, J. Maier, Y. Yu, *Adv. Sci.* **2015**, *2*, 1500200.
[923] J. Y. Xiang, D. D. Dong, F. S. Wen, J. Zhao, X. Y. Zhang, L. M. Wang, Z. Y. Liu, *J. Alloys Compd.* **2016**, *660*, 11.
[924] Y. X. Wang, S. L. Chou, D. Wexler, H. K. Liu, S. X. Dou, *Chem.-Eur. J.* **2014**, *20*, 9607.
[925] X. Q. Xie, Z. M. Ao, D. W. Su, J. Q. Zhang, G. X. Wang, *Adv. Funct. Mater.* **2015**, *25*, 1393.
[926] B. H. Qu, C. Z. Ma, G. Ji, C. H. Xu, J. Xu, Y. S. Meng, T. H. Wang, J. Y. Lee, *Adv. Mater.* **2014**, *26*, 3854.
[927] C. B. Zhu, P. Kopold, W. H. Li, P. A. van Aken, J. Maier, Y. Yu, *J. Mater. Chem. A* **2015**, *3*, 20487.
[928] Q. Zhou, L. Liu, G. X. Guo, Z. C. Yan, J. L. Tan, Z. F. Huang, X. Y. Chen, X. Y. Wang, *RSC Adv.* **2015**, *5*, 71644.
[929] B. Qu, C. Ma, G. Ji, C. Xu, J. Xu, Y. S. Meng, T. Wang, J. Y. Lee, *Adv. Mater.* **2014**, *26*, 3854.
[930] S. H. Choi, Y. N. Ko, J.-K. Lee, Y. C. Kang, *Adv. Funct. Mater.* **2015**, *25*, 1780.
[931] X. Xie, Z. Ao, D. Su, J. Zhang, G. Wang, *Adv. Funct. Mater.* **2015**, *25*, 1393.
[932] L. David, R. Bhandavat, G. Singh, *ACS Nano* **2014**, *8*, 1759.
[933] Y. X. Wang, Y. G. Lim, M. S. Park, S. L. Chou, J. H. Kim, H. K. Liu, S. X. Dou, Y. J. Kim, *J. Mater. Chem. A* **2014**, *2*, 529.
[934] A. Jahel, C. M. Ghimbeu, A. Darwiche, L. Vidal, S. Hajjar-Garreau, C. Vix-Guterl, L. Monconduit, *J. Mater. Chem. A* **2015**, *3*, 11960.
[935] T. F. Zhou, W. K. Pang, C. F. Zhang, J. P. Yang, Z. X. Chen, H. K. Liu, Z. P. Guo, *Acs Nano* **2014**, *8*, 8323.
[936] Y. Zheng, T. Zhou, C. Zhang, J. Mao, H. Liu, Z. P. Guo, *Angew. Chem.-Int. Ed.* **2016**, *128*, 3469.
[937] E. Lebegue, C. Benoit, T. Brousse, J. Gaubicher, C. Cougnon, *J. Electrochem. Soc.* **2015**, *162*, A2289.
[938] K. F. Li, D. W. Su, H. Liu, G. X. Wang, *Electrochim. Acta* **2015**, *177*, 304.
[939] J. Sun, H. W. Lee, M. Pasta, H. T. Yuan, G. Y. Zheng, Y. M. Sun, Y. Z. Li, Y. Cui, *Nat. Nanotechnol.* **2015**, *10*, 980.
[940] C. Zhang, X. Wang, Q. Liang, X. Liu, Q. Weng, J. Liu, Y. Yang, Z. Dai, K. Ding, Y. Bando, J. Tang, D. Golberg, *Nano Lett.* **2016**, *16*, 2054.
[941] G. Yang, H. Song, M. Wu, C. Wang, *J. Mater. Chem. A* **2015**, *3*, 18718.
[942] Z. Li, D. Young, K. Xiang, W. C. Carter, Y. M. Chiang, *Adv. Energy Mater.* **2013**, *3*, 290.
[943] X. Li, X. Zhu, J. Liang, Z. Hou, Y. Wang, N. Lin, Y. Zhu, Y. Qian, *J. Electrochem. Soc.* **2014**, *161*, A1181.
[944] G. D. Park, J. S. Cho, J.-K. Lee, Y. C. Kang, *Sci. Rep.* **2016**, *6*, 22432.
[945] L. Li, K. H. Seng, D. Li, Y. Xia, H. K. Liu, Z. Guo, *Nano Res.* **2014**, *7*, 1466.
[946] R. Sun, Q. Wei, Q. Li, W. Luo, Q. An, J. Sheng, D. Wang, W. Chen, L. Mai, *ACS Appl. Mater. Interfaces* **2015**, *7*, 20902.
[947] R. A. Shakoor, C. S. Park, A. A. Raja, J. Shin, R. Kahraman, *Phys. Chem. Chem. Phys.* **2016**, *18*, 3929.
[948] Y. H. Liu, T. Takasaki, K. Nishimura, S. Katsura, M. Yanagida, T. Sakai, *J. Electrochem. Soc.* **2014**, *161*, A1194.
[949] X. Li, X. H. Ma, D. Su, L. Liu, R. Chisnell, S. P. Ong, H. L. Chen, A. Toumar, J. C. Idrobo, Y. C. Lei, J. M. Bai, F. Wang, J. W. Lynn, Y. S. Lee, G. Ceder, *Nat. Mater.* **2014**, *13*, 586.
[950] A. M. Abakumov, A. A. Tsirlin, I. Bakaimi, G. Van Tendeloo, A. Lappas, *Chem. Mater.* **2014**, *26*, 3306.
[951] R. Tripathi, S. M. Wood, M. S. Islam, L. F. Nazar, *Energy Environ. Sci.* **2013**, *6*, 2257.
[952] W. Liu, H. Li, J. Y. Xie, Z. W. Fu, *ACS Appl. Mater. Interfaces* **2014**, *6*, 2209.
[953] H. L. Zhu, K. T. Lee, G. T. Hitz, X. G. Han, Y. Y. Li, J. Y. Wan, S. Lacey, A. V. Cresce, K. Xu, E. Wachsman, L. B. Hu, *ACS Appl. Mater. Interfaces* **2014**, *6*, 4242.
[954] V. Nguyen, Y. L. Liu, S. A. Hakim, S. Yang, A. R. Radwan, W. Chen, *Int. J. Electrochem. Sci.* **2015**, *10*, 10565.
[955] Y. L. Ruan, K. Wang, S. D. Song, X. Han, B. W. Cheng, *Electrochim. Acta* **2015**, *160*, 330.
[956] G. Ali, S. H. Oh, S. Y. Kim, J. Y. Kim, B. W. Cho, K. Y. Chung, *J. Mater. Chem. A* **2015**, *3*, 10258.
[957] M. W. Xu, L. Wang, X. Zhao, J. Song, H. Xie, Y. H. Lu, J. B. Goodenough, *Phys. Chem. Chem. Phys.* **2013**, *15*, 13032.
[958] Z. L. Chu, C. B. Yue, *Ceram. Int.* **2016**, *42*, 820.
[959] J. C. Chen, W. J. Li, J. Jiang, C. Wu, Y. Q. Liu, *RSC Adv.* **2016**, *6*, 13323.
[960] J. Z. Guo, X. L. Wu, F. Wan, J. Wang, X. H. Zhang, R. S. Wang, *Chem.- Eur. J.* **2015**, *21*, 17371.
[961] Y. Q. Shen, X. Y. Wang, H. Hu, M. L. Jiang, X. K. Yang, H. B. Shu, *J. Power Sources* **2015**, *283*, 204.
[962] H. Y. Jin, J. Dong, E. Uchaker, Q. F. Zhang, X. Z. Zhou, S. E. Hou, J. Y. Li, G. Z. Cao, *J. Mater. Chem. A* **2015**, *3*, 17563.
[963] Y. B. Niu, M. W. Xu, S. J. Bao, C. M. Li, *Chem. Commun.* **2015**, *51*, 13120.
[964] S. Y. Lim, H. Kim, J. Chung, J. H. Lee, B. G. Kim, J.-J. Choi, K. Y. Chung, W. Cho, S.-J. Kim, W. A. Goddard, Y. Jung, J. W. Choi, *Proc. Natl. Acad. Sci.* **2014**, *111*, 599.
[965] G. He, W. H. Kan, A. Manthiram, *Chem. Mater.* **2016**, *28*, 682.
[966] J. Fang, S. Wang, Z. Li, H. Chen, L. Xia, L. Ding, H. Wang, *J. Mater. Chem. A* **2016**, *4*, 1180.
[967] P. Hartmann, C. L. Bender, M. Vračar, A. K. Dürr, A. Garsuch, J. Janek, P. Adelhelm, *Nat. Mater.* **2013**, *12*, 228.
[968] C. Xia, R. Black, R. Fernandes, B. Adams, L. F. Nazar, *Nat Chem* **2015**, *7*, 496.
[969] J. Kim, H. Park, B. Lee, W. M. Seong, H.-D. Lim, Y. Bae, H. Kim, W. K. Kim, K. H. Ryu, K. Kang, *Nat. Commun.* **2016**, *7*, 10670.
[970] B. D. McCloskey, J. M. Garcia, A. C. Luntz, *J. Phys. Chem. Lett.* **2014**, *5*, 1230.
[971] H. Yadegari, Y. Li, M. N. Banis, X. Li, B. Wang, Q. Sun, R. Li, T.-K. Sham, X. Cui, X. Sun, *Energy Environ. Sci.* **2014**, *7*, 3747.
[972] S. K. Das, S. Lau, L. A. Archer, *J. Mater. Chem. A* **2014**, *2*, 12623.
[973] W.-J. Kwak, Z. Chen, C. S. Yoon, J.-K. Lee, K. Amine, Y.-K. Sun, *Nano Energy* **2015**, *12*, 123.
[974] P. Hartmann, C. L. Bender, M. Vracar, A. K. Durr, A. Garsuch, J. Janek, P. Adelhelm, *Nat. Mater.* **2013**, *12*, 228.

[975] W. Liu, Q. Sun, Y. Yang, J.-Y. Xie, Z.-W. Fu, *Chem. Commun.* **2013**, *49*, 1951.
[976] Y. Li, H. Yadegari, X. Li, M. N. Banis, R. Li, X. Sun, *Chem. Commun.* **2013**, *49*, 11731.
[977] S. Zhang, Z. Wen, K. Rui, C. Shen, Y. Lu, J. Yang, *J. Mater. Chem. A* **2015**, *3*, 2568.
[978] M. Prabu, P. Ramakrishnan, H. Nara, T. Momma, T. Osaka, S. Shanmugam, *ACS Appl. Mater. Interfaces* **2014**, *6*, 16545.
[979] Y. Li, M. Gong, Y. Liang, J. Feng, J.-E. Kim, H. Wang, G. Hong, B. Zhang, H. Dai, *Nat. Commun.* **2013**, *4*, 1805.
[980] Y. Li, H. Dai, *Chem. Soc. Rev.* **2014**, *43*, 5257.
[981] J.-S. Lee, S. Tai Kim, R. Cao, N.-S. Choi, M. Liu, K. T. Lee, J. Cho, *Adv. Energy Mater.* **2011**, *1*, 34.
[982] D. U. Lee, J.-Y. Choi, K. Feng, H. W. Park, Z. Chen, *Adv. Energy Mater.* **2014**, *4*, 1301389.
[983] L. Li, A. Manthiram, *Adv. Energy Mater.* **2016**, *6*, 1502054.
[984] Y. Xu, Y. Zhang, Z. Guo, J. Ren, Y. Wang, H. Peng, *Angew. Chem. Int. Ed.* **2015**, *54*, 15390.
[985] K. Wang, P. Pei, Z. Ma, H. Chen, H. Xu, D. Chen, X. Wang, *J. Mater. Chem. A* **2015**, *3*, 22648.
[986] J.-S. Lee, T. Lee, H.-K. Song, J. Cho, B.-S. Kim, *Energy Environ. Sci.* **2011**, *4*, 4148.
[987] K. Gong, F. Du, Z. Xia, M. Durstock, L. Dai, *Science* **2009**, *323*, 760.
[988] L. Qu, Y. Liu, J.-B. Baek, L. Dai, *ACS Nano* **2010**, *4*, 1321.
[989] Y. Zheng, Y. Jiao, M. Jaroniec, Y. Jin, S. Z. Qiao, *Small* **2012**, *8*, 3550.
[990] H.-W. Liang, Z.-Y. Wu, L.-F. Chen, C. Li, S.-H. Yu, *Nano Energy* **2015**, *11*, 366.
[991] D. Higgins, Z. Chen, D. U. Lee, Z. Chen, *J. Mater. Chem. A* **2013**, *1*, 2639.
[992] M. Prabu, P. Ramakrishnan, S. Shanmugam, *Electrochem. Commun.* **2014**, *41*, 59.
[993] D. U. Lee, H. W. Park, D. Higgins, L. Nazar, Z. Chen, *J. Electrochem. Soc.* **2013**, *160*, F910.
[994] S. K. Singh, V. M. Dhavale, S. Kurungot, *ACS Appl. Mater. Interfaces* **2015**, *7*, 21138.
[995] P. Ganesan, P. Ramakrishnan, M. Prabu, S. Shanmugam, *Electrochim. Acta* **2015**, *183*, 63.
[996] S. Chen, J. Duan, Y. Zheng, X. Chen, X. W. Du, M. Jaroniec, S.-Z. Qiao, *Energy Storage Mater.* **2015**, *1*, 17.
[997] J. Hu, L. Wang, L. Shi, H. Huang, *Electrochim. Acta* **2015**, *161*, 115.
[998] L. Li, S. Kim, W. Wang, M. Vijayakumar, Z. Nie, B. Chen, J. Zhang, G. Xia, J. Hu, G. Graff, J. Liu, Z. Yang, *Adv. Energy Mater.* **2011**, *1*, 394.
[999] B. Schwenzer, J. Zhang, S. Kim, L. Li, J. Liu, Z. Yang, *ChemSusChem* **2011**, *4*, 1388.
[1000] A. Weber, M. Mench, J. Meyers, P. Ross, J. Gostick, Q. Liu, *J. Appl. Electrochem.* **2011**, *41*, 1137.
[1001] A. Cunha, J. Martins, N. Rodrigues, F. P. Brito, *Int. J. Energy Res.* **2015**, *39*, 889.
[1002] K. J. Kim, M. S. Park, Y. J. Kim, J. H. Kim, S. X. Dou, M. Skyllas-Kazacos, *J. Mater. Chem. A* **2015**, *3*, 16913.
[1003] Q. Zheng, X. F. Li, Y. H. Cheng, G. L. Ning, F. Xing, H. M. Zhang, *Appl. Energy* **2014**, *132*, 254.
[1004] C. Ding, H. Zhang, X. Li, T. Liu, F. Xing, *J. Phys. Chem. Lett.* **2013**, *4*, 1281.
[1005] G. L. Soloveichik, *Chem. Rev.* **2015**, *115*, 11533.
[1006] T. N. L. Doan, T. K. A. Hoang, P. Chen, *RSC Adv.* **2015**, *5*, 72805.
[1007] H.-M. Tsai, S.-Y. Yang, C.-C. M. Ma, X. Xie, *Electroanalysis* **2011**, *23*, 2139.
[1008] M. Park, I. Y. Jeon, J. Ryu, J. B. Baek, J. Cho, *Adv. Energy Mater.* **2015**, *5*, 1401550.
[1009] L. Cao, Q. Q. Sun, Y. H. Gao, L. T. Liu, H. F. Shi, *Electrochim. Acta* **2015**, *158*, 24.
[1010] Z. González, C. Botas, P. Álvarez, S. Roldán, C. Blanco, R. Santamaría, M. Granda, R. Menéndez, *Carbon* **2012**, *50*, 828.
[1011] O. Di Blasi, N. Briguglio, C. Busacca, M. Ferraro, V. Antonucci, A. Di Blasi, *Appl. Energy* **2015**, *147*, 74.
[1012] M. Park, I.-Y. Jeon, J. Ryu, J.-B. Baek, J. Cho, *Adv. Energy Mater.* **2015**, *5*, 1401550.
[1013] X. Rui, M. O. Oo, D. H. Sim, S. c. Raghu, Q. Yan, T. M. Lim, M. Skyllas-Kazacos, *Electrochim. Acta* **2012**, *85*, 175.
[1014] C. Flox, J. Rubio-Garcia, R. Nafria, R. Zamani, M. Skoumal, T. Andreu, J. Arbiol, A. Cabot, J. R. Morante, *Carbon* **2012**, *50*, 2372.
[1015] P. Han, X. Wang, L. Zhang, T. Wang, J. Yao, C. Huang, L. Gu, G. Cui, *RSC Adv.* **2014**, *4*, 20379.
[1016] H.-M. Tsai, S.-J. Yang, C.-C. M. Ma, X. Xie, *Electrochim. Acta* **2012**, *77*, 232.
[1017] L. Shi, S. Q. Liu, Z. He, J. X. Shen, *Electrochim. Acta* **2014**, *138*, 93.
[1018] A. Ejigu, M. Edwards, D. A. Walsh, *ACS Catal.* **2015**, *5*, 7122.
[1019] J. Jin, X. Fu, Q. Liu, Y. Liu, Z. Wei, K. Niu, J. Zhang, *ACS Nano* **2013**, *7*, 4764.
[1020] P. Han, Y. Yue, Z. Liu, W. Xu, L. Zhang, H. Xu, S. Dong, G. Cui, *Energy Environ. Sci.* **2011**, *4*, 4710.
[1021] W. Li, Z. Zhang, Y. Tang, H. Bian, T.-W. Ng, W. Zhang, C.-S. Lee, *Adv. Sci.* **2015**, *3*, 1500276.
[1022] L. Cao, L. Kong, L. Kong, X. Zhang, H. Shi, *J. Power Sources* **2015**, *299*, 255.
[1023] L. Cao, Q. Sun, Y. Gao, L. Liu, H. Shi, *Electrochim. Acta* **2015**, *158*, 24.
[1024] W. Dai, Y. Shen, Z. Li, L. Yu, J. Xi, X. Qiu, *J. Mater. Chem. A* **2014**, *2*, 12423.
[1025] K. J. Lee, Y. H. Chu, *Vacuum* **2014**, *107*, 269.
[1026] S. Mao, G. Lu, J. Chen, *Nanoscale* **2015**, *7*, 6924.
[1027] H. Wang, X. Z. Yuan, G. M. Zeng, Y. Wu, Y. Liu, Q. Jiang, S. S. Gu, *Adv. Colloid Interface Sci.* **2015**, *221*, 41.
[1028] M. H. Yu, Y. C. Huang, C. Li, Y. X. Zeng, W. Wang, Y. Li, P. P. Fang, X. H. Lu, Y. X. Tong, *Adv. Funct. Mater.* **2015**, *25*, 324.
[1029] F. Xia, S. Kwon, W. W. Lee, Z. Liu, S. Kim, T. Song, K. J. Choi, U. Paik, W. I. Park, *Nano Lett.* **2015**, *15*, 6658.
[1030] A. Zhamu, G. Chen, C. Liu, D. Neff, Q. Fang, Z. Yu, W. Xiong, Y. Wang, X. Wang, B. Z. Jang, *Energy Environ. Sci.* **2012**, *5*, 5701.
[1031] W.-K. Shin, A. G. Kannan, D.-W. Kim, *ACS Appl. Mater. Interfaces* **2015**, *7*, 23700.
[1032] K. Yan, H.-W. Lee, T. Gao, G. Zheng, H. Yao, H. Wang, Z. Lu, Y. Zhou, Z. Liang, Z. Liu, S. Chu, Y. Cui, *Nano Lett.* **2014**, *14*, 6016.
[1033] G. Crabtree, *AIP Conf. Proc.* **2015**, *1652*, 112.
[1034] J. Muldoon, C. B. Bucur, T. Gregory, *Chem. Rev.* **2014**, *114*, 11683.
[1035] Y. Liu, L. Jiao, Q. Wu, Y. Zhao, K. Cao, H. Liu, Y. Wang, H. Yuan, *Nanoscale* **2013**, *5*, 9562.
[1036] Q. Chen, Y.-N. Nuli, W. Guo, J. Yang, J.-L. Wang, Y.-G. Guo, *Acta Phys. Chim. Sin.* **2013**, *29*, 2295.
[1037] C. J. Hsu, C. Y. Chou, C. H. Yang, T. C. Lee, J. K. Chang, *Chem. Commun.* **2016**, *52*, 1701.
[1038] Z. Zhao-Karger, X. Zhao, D. Wang, T. Diemant, R. J. Behm, M. Fichtner, *Adv. Energy Mater.* **2015**, *5*, 1401155.
[1039] R. Mori, *J. Electrochem. Soc.* **2015**, *162*, A288.
[1040] L. Ma, H. Zhuang, Y. Lu, S. S. Moganty, R. G. Hennig, L. A. Archer, *Adv. Energy Mater.* **2014**, *4*, 1400390.
[1041] M. A. Rahman, X. Wang, C. Wen, *J. Electrochem. Soc.* **2013**, *160*, A1759.
[1042] B. P. Vinayan, Z. Zhao-Karger, T. Diemant, V. S. K. Chakravadhanula, N. I. Schwarzburger, M. A. Cambaz, R. J. Behm, C. Kubel, M. Fichtner, *Nanoscale* **2016**, *8*, 3296.

[1043] P. Adelhelm, P. Hartmann, C. L. Bender, M. Busche, C. Eufinger, J. Janek, *Beilstein J. Nanotechnol.* **2015**, *6*, 1016.
[1044] Q. Zhao, Y. Hu, K. Zhang, J. Chen, *Inorg. Chem.* **2014**, *53*, 9000.
[1045] X. Lu, M. E. Bowden, V. L. Sprenkle, J. Liu, *Adv. Mater.* **2015**, *27*, 5915.
[1046] J. W. Choi, D. Aurbach, *Nat. Rev. Mater.* **2016**, *1*, 16013.
[1047] A. L. Lipson, B. Pan, S. H. Lapidus, C. Liao, J. T. Vaughey, B. J. Ingram, *Chem. Mater.* **2015**, *27*, 8442.
[1048] K. Chen, L. Chen, Y. Chen, H. Bai, L. Li, *J. Mater. Chem.* **2012**, *22*, 20968.
[1049] S. H. Lee, H. W. Kim, J. O. Hwang, W. J. Lee, J. Kwon, C. W. Bielawski, R. S. Ruoff, S. O. Kim, *Angew. Chem. Int. Ed.* **2010**, *49*, 10084.
[1050] C. Li, G. Shi, *Nanoscale* **2012**, *4*, 5549.
[1051] H. Wang, T. Maiyalagan, X. Wang, *ACS Catal.* **2012**, *2*, 781.
[1052] N. A. Kumar, J.-B. Baek, *Nanotechnology* **2015**, *26*, 492001.
[1053] A. Garcia-Gallastegui, D. Iruretagoyena, V. Gouvea, M. Mokhtar, A. M. Asiri, S. N. Basahel, S. A. Al-Thabaiti, A. O. Alyoubi, D. Chadwick, M. S. P. Shaffer, *Chem. Mater.* **2012**, *24*, 4531.
[1054] M. Zhou, T. Lin, F. Huang, Y. Zhong, Z. Wang, Y. Tang, H. Bi, D. Wan, J. Lin, *Adv. Funct. Mater.* **2012**, *23*, 2263.